Western Graduate&PostdoctoralStudies

Western University
Scholarship@Western

Electronic Thesis and Dissertation Repository

9-4-2015 12:00 AM

Reactions between Zinc Metallothionein and Carbonic Anhydrase

Tyler B. J. Pinter
The University of Western Ontario

Supervisor
Dr. Martin J. Stillman
The University of Western Ontario

Graduate Program in Chemistry
A thesis submitted in partial fulfillment of the requirements for the degree in Doctor of Philosophy
© Tyler B. J. Pinter 2015

Follow this and additional works at: https://ir.lib.uwo.ca/etd

Part of the Analytical Chemistry Commons, Biochemistry Commons, and the Inorganic Chemistry Commons

Recommended Citation

Pinter, Tyler B. J., "Reactions between Zinc Metallothionein and Carbonic Anhydrase" (2015). *Electronic Thesis and Dissertation Repository*. 3212.
https://ir.lib.uwo.ca/etd/3212

This Dissertation/Thesis is brought to you for free and open access by Scholarship@Western. It has been accepted for inclusion in Electronic Thesis and Dissertation Repository by an authorized administrator of Scholarship@Western. For more information, please contact wlswadmin@uwo.ca.

www.manaraa.com

REACTIONS BETWEEN ZINC METALLOTHIONEIN AND CARBONIC ANHYDRASE

(Thesis format: Integrated Article)

by

Tyler B. J. Pinter

Graduate Program in Chemistry

A thesis submitted in partial fulfillment
of the requirements for the degree of
Doctor of Philosophy

The School of Graduate and Postdoctoral Studies
The University of Western Ontario
London, Ontario, Canada

© Tyler Brian Joseph Pinter 2015

www.manaraa.com

Abstract

More than 25% of proteins require metal ion cofactors for structure or function. The interactions between metalloproteins have largely been overlooked, though these interactions ultimately govern metal localization and control metal ion homeostasis. Mammalian metallothionein (MT) is a small, cysteine-rich metalloprotein that binds numerous metal ions per protein strand. Up to seven divalent metals, such as zinc or cadmium, are wrapped into a clustered two-domain structure. This unusually high metal content places MT as an attractive candidate for studying interactions with other metal-binding proteins. This study investigates the metal transfer reactions between MTs and other metalloproteins, using carbonic anhydrase (CA) as a putative zinc-dependent enzyme.

This thesis presents electrospray ionization mass spectrometric (ESI-MS) data showing the competitive zinc metallation reactions between apoCA and various apoMTs. Modelling of the ESI-MS data was used to determine the reaction parameters and those parameters are shown to be reflected directly in the raw data. These results demonstrate how MT can act as a homeostatic buffer of metal ions, by binding them with different affinities. The kinetics of the metal transfers between zinc MTs and cadmium or zinc CA show that the rates of metal transfer between the two metalloproteins is directly dependent on the metal content of the MT. Further studies on the domain specific properties of MT using shortened MT domain fragment proteins showed that: (i) there was no significant degree of domain specificity in metal binding to apoMTs; (ii) the weakest bound metal ion is located within the N-terminal domain of the intact MT protein; (iii) the highest affinity binding site is located within the C-terminal domain; and, (iv) domain-domain interactions within the MT peptide strand modulate metal binding affinities. Taken together, these results support the homeostatic roles of metallothionein proteins while also challenging the current mechanisms for metal binding and release to apoenzymes.

Keywords

Metal homeostasis, zinc, cadmium, metallothionein, carbonic anhydrase, proteins, electrospray ionization mass spectrometry, chemical reaction modeling, chemical kinetics.

www.manaraa.com

Co-Authorship Statement

This thesis contains material from previously published manuscripts. Dr. Martin Stillman is a coauthor of all the published papers and supervised Tyler Pinter. For all chapters in which a portion has been published, Tyler Pinter wrote the first draft of the paper. Dr. Martin Stillman was involved in all levels of publication and had major roles in both editing and revising the published manuscripts.

For all Chapters, except Chapter 4, Tyler Pinter was solely responsible for acquiring all of the data, preparing the figures, and drafting the manuscripts with guidance and assistance from Dr. Martin Stillman.

Ms. Tiffany Jeen is kindly acknowledged for preliminary studies of the metal selectivity experiments between the isolated domain fragments (Chapter 4). Ms. Jeen was supervised by Tyler Pinter during her placement in the Stillman Group as an Undergraduate Inorganic Chemistry Exchange Student. For her contribution, Ms. Jeen is acknowledged in the published manuscript and is listed as a coauthor on relevant conference abstracts.

Mr. Gordon Irvine is gratefully acknowledged for assistance in interpreting the pH effects of the zinc and cadmium metallation data (Chapter 4), as well as with the preparation of related figures and the writing of relevant sections of the final manuscript. Tyler Pinter was responsible for all sample preparation, experimental design, and data acquisition and preparation of the manuscript for publication. For his contribution Mr. Gordon Irvine is listed as a coauthor on the associated manuscript.

www.manaraa.com

Acknowledgments

I thank my supervisor, Professor Martin Stillman, for taking a chance on me as a second year undergraduate even though I did not meet his minimum requirements to join the lab group at that time. Additionally, I thank him for his close guidance and support of my research goals, as well as for allowing me to present my research at several international conferences.

I also thank Stillman Bioinorganic Lab members past and present. Having been here for so long, there are too many of you to list but know that I am grateful for our shared time in the group. I must give special thanks to Dr. Thanh Ngu, Dr. Michael Tiedemann, and Dr. Duncan Sutherland who were each responsible for my training in one aspect or another: Dr. Ngu is acknowledged for training me in the use of the ESI-MS for kinetic experiments, and Dr. Sutherland and Dr. Tiedemann are equally recognized for training me in protein preparation and purification techniques. A special thank you to Dr. Sutherland for permitting me the use of his modelling spreadsheet, and to all lab members for helpful guidance and discussions on data interpretation.

Many thanks are given to the staff of the Electronic Shop for keeping our equipment up and running smoothly. I gratefully acknowledge Doug Hairsine for maintenance, training, and advice on the operation of the ESI-MS. I also thank the Department of Chemistry and its entire staff for their generous support on very many levels.

Lastly, I acknowledge my family and friends for their help and support. I owe an extra special thanks to Dr. Emily Simpson for editing my manuscripts and for her continued and unwavering support and assistance.

www.manaraa.com

Table of Contents

Abstract ii

Co-Authorship Statement iii

Acknowledgments iv

Table of Contents v

List of Figures x

List of Schemes xiv

List of Tables xiv

List of Appendices xv

List of Abbreviations and Definitions xvi

Chapter 1 1

1 Introduction 1

1.1 Zinc in biology 1

1.2 Zinc homeostasis, toxic metals, and MT 3

1.3 Structural properties of metallothioneins 5

1.4 Techniques for studying MTs 10

1.4.1 Ultraviolet absorption and circular dichroism spectroscopy 10

1.4.2 Electrospray ionization mass spectrometry 13

1.4.3 Competition experiments 16

1.5 Cooperativity and non-cooperativity of metal binding to MTs 19

1.5.1 Experimental evidence of metal binding cooperativity in MTs 21

1.6 Domain specificity 21

1.7 A history of MT metal binding constants 24

1.8 Scope of the thesis 25

1.9 References 27

www.manaraa.com

Chapter 2 35

2 The zinc balance: Competitive zinc metallation of carbonic anhydrase and metallothionein 1A 35

2.1 Introduction 35

2.2 Methods 38

2.2.1 Preparation of apoMT. 38

2.2.2 Preparation of apoCA. 38

2.2.3 ESI-MS procedures. 39

2.3 Results 39

2.3.1 Mass spectral data for the competition between apoMT and apoCA for added zinc 39

2.3.2 Modelling the competition reaction 41

2.3.3 Relative MT binding affinities are reflected in the raw data 45

2.4 Discussion 48

2.4.1 Spanning the ladder of MT binding constants 48

2.4.2 Trends in MT zinc binding affinities 50

2.4.3 Modelling reactions between CA and a competitor 52

2.5 References 55

Chapter 3 59

3 Putting the pieces into place: Properties of intact zinc metallothionein 1A determined from interaction of its isolated domains with carbonic anhydrase 59

3.1 Introduction 59

3.2 Methods 61

3.2.1 Purification of recombinant MT1A domain fragments. 61

3.2.2 Preparation of apometallothionein fragments. 62

3.2.3 Preparation of apocarbonic anhydrase. 62

3.2.4 Zinc and cadmium titrations. 63

www.manaraa.com

3.2.5 ESI-MS parameterizations. 63
3.3 Results 63
3.3.1 Competition for Zn^{2+} between apoCA and apo-αMT. 63
3.3.2 Competition for Zn^{2+} between apoCA and apo-βMT. 68
3.4 Discussion 72
3.4.1 Structural properties of MT 72
3.4.2 Past research on zinc binding properties of MTs 73
3.4.3 Competition between the apofragments and apoCA 76
3.4.4 Evidence for domain interactions in intact βα-MT that modulate zinc affinities 77
3.5 Conclusions 79
3.6 References 80
Chapter 4 85
4 Domain selection in metallothionein 1A: Affinity controlled mechanisms of zinc binding and cadmium exchange 85
4.1 Introduction 85
4.2 Methods 89
4.2.1 Purification of recombinant fragments. 89
4.2.2 Preparation of apofragments. 89
4.2.3 Zinc and cadmium titrations. 90
4.2.4 ESI-MS and CD parameterizations. 90
4.3 Results 91
4.3.1 Competitive zinc titration of MT fragments: ESI-MS Data. 92
4.3.2 Competitive zinc titration of MT fragments: Speciation profiles. 93
4.3.3 Competitive cadmium titrations of zinc-saturated fragments at pH 7.4. .. 95
4.3.4 Competitive cadmium titrations of zinc-saturated fragments at pH 5.8. .. 99
4.4 Discussion 101

www.manaraa.com

4.4.1 Extracting metal binding properties of MT using competitive titrations. 101

4.4.2 Comparison of pH 7.4 and pH 5.8 data. 103

4.4.3 Seven cadmium for seven zinc. 103

4.4.4 Modeling site selection mechanisms between the α and β domains. 104

4.4.5 Comparison of the experimental data and the models. 106

4.4.6 Potential for interdomain interactions and comparison to existing data. 109

4.5 Conclusions 110

4.6 References 111

Chapter 5 115

5 Kinetics of metal transfer reactions between zinc metallothioneins and carbonic anhydrase 115

5.1 Introduction 115

5.2 Methods 116

5.2.1 Purification of recombinant MT1A. 116

5.2.2 Preparation of zinc metallothionein. 117

5.2.3 Preparation of apocarbonic anhydrase and cadmium-carbonic anhydrase. 118

5.2.4 Reactions between Zn-MT and apoCA or Cd-CA and ESI-MS parameterization. 118

5.2.5 Data treatment and kinetic analyses. 119

5.3 Results 120

5.3.1 Kinetics of the reaction between Zn-MT and apoCA under MT-limiting conditions 120

5.3.2 Kinetics of the reaction between Zn_7-MT and Cd-CA 124

5.3.3 Kinetics of the reaction between partially metallated MTs and Cd-CA. 127

5.4 Discussion 130

5.4.1 Protein-protein interactions between metallothionein and other metal binding sites 130

www.manaraa.com

5.4.2 Metal binding to carbonic anhydrase 131

5.4.3 Are the zinc donation kinetics different for partially metallated MTs? .. 132

5.4.4 How readily does zinc saturated MT exchange with Cd-CA? 133

5.4.5 Are the metal exchange kinetics between Cd-CA and $Zn_{(3-5)}$-MTs faster or slower compared to those for Zn_7-MT? 134

5.4.6 The structure of CA and relevance to PPIs with MT 135

5.5 Conclusions 137

5.6 References 138

Chapter 6 140

6 Conclusion 140

6.1 The metal binding affinities of MT 140

6.2 Metal affinities from competition experiments 141

6.3 The location of the strong and weak affinity binding sites 142

6.4 Metal selectivity between separated α and β domains 143

6.5 Kinetics of the metal exchange reactions between MTs and CA 146

6.6 Final Word 147

6.7 References 148

Appendices 153

Curriculum Vitae 161

www.manaraa.com

List of Figures

Figure 1.1: Zinc-binding sites in proteins for structural or catalytic roles..... 2

Figure 1.2: The two-domain structure of Zn/Cd saturated mammalian MT..... 6

Figure 1.3: Possible structures of metal thiolate bonding formed for each of the two metallation pathways in MT for two to six metals bound. 9

Figure 1.4: Sample UV absorption spectra of MTs. 11

Figure 1.5: Example circular dichroism spectra of a cadmium titration of 15 µM apo-αMT1A..... 12

Figure 1.6: The electrospray ionization mass spectrometer..... 14

Figure 1.7: Speciation models of the competitive reactions between equal concentrations of B and C for substrate S. 18

Figure 1.8: Schematic representation of the two metallation pathways for MT..... 23

Figure 2.1: Deconvoluted ESI mass spectral data recorded for the equimolar competitive titration of apoCA and apo-rhMT at pH 6.8. 40

Figure 2.2: Experimentally determined zinc status of MT (A) and CA (B) during the stepwise competitive zinc metallation. 42

Figure 2.3: Simulation of the competitive zinc metallation of apoMT (A) in the presence of apoCA (B). 43

Figure 2.4: Calculated stability constants (A) and the experimental data reflecting those values (B). 46

Figure 2.5: ESI mass spectra based on experimental data (red) and data produced by simulating the titration using the best fit K_F values (black)..... 47

Figure 2.6: Modelled CA speciation profiles for the simulated competitive zinc titration between CA and a single zinc binding site. 53

www.manaraa.com

Figure 3.1: Deconvoluted ESI mass spectral data recorded during the competitive zinc titration between equimolar (30 µM) apo-αMT and apoCA at pH 7.0. 65

Figure 3.2: Extracted experimental speciation profiles from the competitive zinc titration of equimolar mixtures of apo-αMT (A) and apoCA (B) at pH 7.0. 66

Figure 3.3: Simulation of the competitive zinc metallation of apo-αMT (A) in the presence of apoCA (B). 67

Figure 3.4: Deconvoluted ESI mass spectral data recorded during the competitive zinc titration between equimolar (30 µM) apo-βMT and apoCA (a-CA) at pH 7.0. 69

Figure 3.5: Extracted experimental speciation profiles for the competitive zinc titrations of equimolar mixtures of apo-βMT (A) and apoCA (B) at pH 7.0. 70

Figure 3.6: Simulation of the competitive zinc metallation of apo-βMT (A) in the presence of apoCA (B). 71

Figure 3.7: Comparison of the calculated zinc affinity constants for zinc binding to αMT1A (black) and βMT1A (red)..... 78

Figure 4.1: (A) Protein structure, (B) metalloclusters of the β and α domains of zinc-saturated rh-MT1A. 86

Figure 4.2: Possible metal exchange pathways for MT. 87

Figure 4.3: Representative deconvoluted ESI mass spectral data recorded during the competitive zinc titrations at pH 7.4 (A-E) and pH 5.8 (F-J) of equimolar mixtures of β-MT and α-MT. 91

Figure 4.4: Extracted speciation profiles of recorded during the competitive zinc titrations of equimolar mixtures of apoα (A and C) and apoβ (B and D) MT at pH 7.4 (A and B) and pH 5.8 (C and D)..... 94

Figure 4.5: Representative ESI mass spectral data recorded during the competitive cadmium titration of an equimolar (31 µM) mixture of Zn4-αMT and Zn3-βMT at pH 7.4. 96

www.manaraa.com

Figure 4.6: Extracted speciation profiles recorded during the competitive cadmium titrations of an equimolar (31 μM) mixture of α (A and C) and β (B and D) Zn-MTs at pH 7.4. 97

Figure 4.7: ESI mass spectral data recorded during the competitive cadmium titration of an equimolar (34 μM) mixture of Zn4-αMT and Zn3-βMT at pH 5.8. 98

Figure 4.8: Extracted speciation profiles recorded during the competitive cadmium titrations of an equimolar (34 μM) mixture of Zn-αMT (A and C) and Zn-βMT (B and D) at pH 5.8. 99

Figure 4.9: CD spectroscopic data measured for the competitive cadmium titration starting from an equimolar (31 and 34 μM) mixture of Zn4-αMT and Zn3-βMT at (A) pH 7.4 and (B) pH 5.8. 100

Figure 4.10: Models of selectivity in binding of zinc and cadmium to MT. Shown are three possible mechanisms for binding of metals to MTs: (A) an α selective model, (B) a β selective model, and (C) a model in which there is no specific selectivity. 105

Figure 4.11: Experimental data for the zinc titrations at (A) pH 7.4 and (B) 5.8. 107

Figure 4.12: Experimental selectivity data for the cadmium titrations at (A) pH 7.4 and (B) 5.8. 108

Figure 5.1: Time dependence of the CA metallation by Zn-MT. 121

Figure 5.2: Time dependence of the MT demetallation by apoCA. 122

Figure 5.3: Time courses of the demetallation of (A) Zn-MT and the metallation of (B) apoCA extracted from the ESI mass spectral data. 123

Figure 5.4: Second order kinetic analysis of the zinc metallation of apoCA under MT limiting conditions. 124

Figure 5.5: Time course of the metal exchange between Zn_7-MT and Cd-CA. (A) MT and (B) CA. 125

Figure 5.6: Second order kinetic analysis of the reaction of Cd-CA with Zn_7-MT. 126

www.manaraa.com

Figure 5.7: Time dependence of the populations of metallothionein species for the reaction between partially metallated Zn-MT and Cd-CA. 128

Figure 5.8: Experimentally determined time courses of CA species extracted from the ESI mass spectral data of the reaction between an equimolar (30 µM) mixture of Cd-CA and $Zn_{(3-6)}$-MT. 129

Figure 5.9: Second order kinetic analysis of the reaction of Cd-CA with partially zinc metallated MT. 130

Figure 5.10: X-ray crystal structure of CA and metal binding residues that could facilitate metal transfers. 136

Figure 5.11: Manual docking of the crystal structures of CA and MT. 136

Figure 6.1: The “ladder” of zinc affinities in MTs. 142

Figure 6.2: The model of homeostatic control of zinc by MT. 144

Figure 6.3: Model of cadmium exchange with Zn-MT domain fragments. 145

www.manaraa.com

List of Schemes

Scheme 1.1: Sequential metallation reactions of MT. 8

Scheme 2.1: The sequential metallation reactions for the competitive titration of zinc to apoMT and apoCA. 44

Scheme 3.1: Competitive and sequential metallation reactions of apo-αMT and apoCA. 64

Scheme 3.2: Competitive and sequential metallation reactions of apo-βMT and apoCA. 68

Scheme 4.1: Competitive and sequential metallation reactions of apoβMT and apoαMT. 92

Scheme 4.2: Competitive and sequential cadmium replacement reactions of Zn_4-αMT and Zn_3-βMT. 95

List of Tables

Table 3.1: Comparison of reported average zinc affinity constant data of MTs. 75

www.manaraa.com

List of Appendices

Appendix A: Protein purification details 149

Appendix B: Supplementary figures for Chapter 2 153

Appendix C: Supplementary figures for Chapter 3 155

Appendix D: Permissions 159

www.manaraa.com

List of Abbreviations and Definitions

α-MT	α domain of metallothionein
β-MT	β domain of metallothionein
βα-MT	intact two-domain metallothionein
ε	molar extinction coefficient
AAS	atomic absorption spectroscopy
apoMT	metal-free metallothionein
apoCA	metal-free carbonic anhydrase
CA	Carbonic anhydrase
CD	circular dichroism
de novo	newly synthesized protein
DNA	deoxyribonucleic acid
ESI	electrospray ionization
holo-MT	metal-saturated metallothionein
in vitro	in an aqueous environment in a test tube
in vivo	in a biological or cellular environment
IPTG	isopropyl-β-D-thiogalactoside
K	equilibrium constant
k	rate constant
K_F	formation constant
LCMT	ligand-to-metal charge transfer
m/z	mass-to-charge ratio
MD	molecular dynamics

www.manaraa.com

MS	mass spectrometry
MT	metallothionein
MT1A	metallothionein isoform 1A
MTF-1	metal-responsive transcription factor
MWCO	molecular weight cut-off
NMR	nuclear magnetic resonance spectroscopy
PAR	4-(2-pyridylazo)resorcinol
PDA / PDC	2,6-pyridinedicarboxylic acid
pET	plasmid for expression by T7 RNA polymerase
PPI	protein-protein interactions
S	substrate or sulfur ligands
S-tag	recombinant fusion tag at N-terminus of protein
SEC	size-exclusion chromatography
TOF	time-of-flight
Tris	tris(hydroxymethyl)aminomethane buffer
5F-BAPTA	1,2-bis(2-amino-5-fluorophenoxy)ethane-N,N,N′,N′-tetraacetic acid

www.manaraa.com

Chapter 1

1 Introduction

Metallothioneins (MTs) are metalloproteins that bind multiple metals and are found in all forms of Life. Using the large number of cysteine residues, relative to their small size, MTs bind numerous metal ions *in vitro* and *in vivo* including, but not limited to: zinc, cadmium, copper, nickel, mercury, and arsenic. The ability to accommodate a large and varied number of heavy metals is a unique property of this polymorphous family of metalloproteins. Determining the metal binding stoichiometries of members of the MT family has been a significant focus since MT was first discovered in 1957 by Margoshes and Vallee while they were studying cadmium binding proteins in equine kidney. These stoichiometries, which have been referred to as the "magic numbers of MT," depend on the metal identity and preferred metal binding geometry, as well as the amino acid sequence composition and number of metal binding residues of the MT in question. The formation of protein-metal clusters involving bridging and terminal thiols is supported by the wrapping of the peptide backbone, which stabilizes and protects the metal clusters. The structural properties of the MT, and specifically the metalloclusters, govern the available chemistries and therefore, the *in vivo* activities of these ubiquitous proteins.

1.1 Zinc in biology

Many metals are essential for all life and play important roles in cellular development, cell signaling, and proper cellular function.[1, 2] The most common metal ion cofactor is zinc, where approximately 10% of all genes encoding for proteins contain at least one zinc binding site (determined from meta-analysis of the sequenced human genome).[3] Examples of zinc binding proteins are shown, along with an expanded view of the zinc coordinating ligands, in Figure 1.1. These zinc-binding proteins include zinc-dependent enzymes, zinc finger proteins, and other zinc-responsive elements such as cytokines and growth and transcription factors.

Owing to its involvement in numerous critical roles, zinc deficiency is common.[4] An estimated 15-25% of the world's population is considered zinc deficient[5] and the 2008

www.manaraa.com

Copenhagen Consensus ranked supplying zinc and vitamin A to the over 100 million significantly malnourished children as the highest priority for cost-effective improvement of overall global well-being.[6, 7] Depending on the severity of deficiency, numerous health complications can arise including: impaired immune function, growth retardation, sensory dysfunction, infertility, and neuronal, motor, and psychological disorders.[5, 8-13] Zinc also plays roles in aging[14] and has been implicated in numerous diseases including cancer,[15-17] diabetes,[18-20] and neurodegenerative[21-23] and cardiovascular diseases.[24-26] Understanding the physiochemical relationships between this metal and its biological targets is an active area of interest worldwide.[27-31]

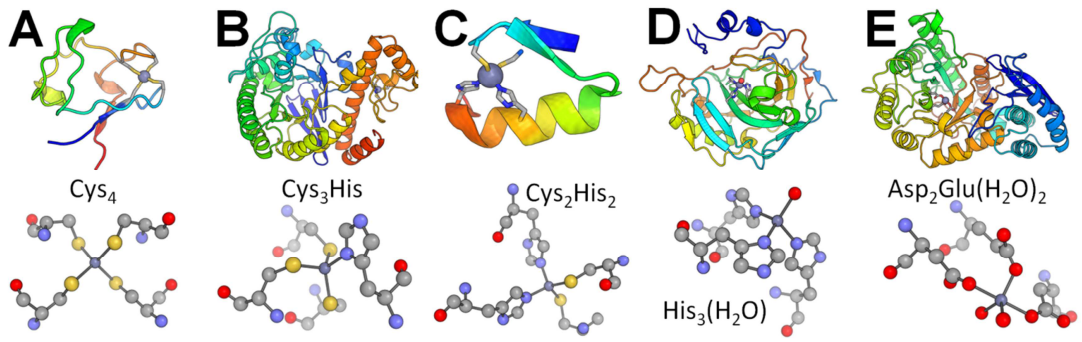

Figure 1.1: Zinc-binding sites in proteins for structural or catalytic roles. (A) Zinc-substituted rubredoxin (1IRN[32]), structural. (B) tRNA-guanine transglycosylase (1PUD[33]), structural. (C) Zinc finger domain of Xenopus protein Xfin (1ZNF[34]), structural. (D) Human carbonic anhydrase (2CBA[35]), catalytic. (E) Enolase (4ENL[36]), catalytic. The zinc binding ligands are shown below the protein structure.

Zinc enzymes catalyze many physiologically important reactions.[37] Carbonic anhydrase, for example, uses its active site containing one zinc ion to activate a coordinated water molecule in order to carry out hydration of CO_2, forming bicarbonate in muscle tissues.[38] The bicarbonate is later converted back to exhalable CO_2 in the lungs, forging the basis of respiration. Carboxypeptidase uses zinc-activated water to catalyze protein degradation.[39] The zinc-enzyme alcohol dehydrogenase catalyzes the interconversion of alcohols and aldehydes, which are important metabolites.[40, 41] Instead of participating directly in catalytic reaction, other proteins use one or more zinc ions for structural roles.

www.manaraa.com

Zinc fingers are domains of DNA-binding proteins commonly found in DNA transcription factors, whose folded structure is held together through the coordination of zinc ions. In these structural motifs, combinations of Cys and His residues bind to the zinc ion tetrahedrally resulting in a fold that resembles an outstretched finger.[34] DNA sequence specificity of zinc-fingers is accomplished through matching of favourable electrostatic and polar contacts between the DNA bases and surface exposed protein amino acid side chains that interact in the major groove of the DNA double helix.[42]

1.2 Zinc homeostasis, toxic metals, and MT

Despite the ubiquity of zinc in biological systems, free zinc concentrations are tightly regulated within a narrow range using a complex series of metal-specific sensors, importers, exporters, chaperones, and storage sites.[43-46] Normally, these systems work together to maintain an acceptable homeostatic level of the metal within an optimal range by controlling the flux of metal import and export as well as delivery to metal storage sites and metal-dependent processes such as metal-dependent enzymes.[47] The intracellular levels of free zinc, for example, have been estimated to be as low as picomolar[48, 49] or even femtomolar concentrations.[44] When this careful balance of metal concentration is disrupted, there is potential for numerous health complications, depending on the severity of the imbalance.

It has been suggested that MT plays key roles in the metal ion homeostasis of the essential metals copper and zinc and interacts with many metalloproteins.[50] Not only can MT act as a metal chaperone, delivering zinc to apo-zinc-dependent enzymes, but more recent results have shown that the multiple zinc binding affinities permit the zinc sensing and buffering capabilities discussed above.[51-53] There are numerous reports that Zn_7-MT is able to transfer its zinc to zinc-dependent apoenzymes, such as sorbitol dehydrogenase,[54] mitochondrial aconitase,[55] alkaline phosphatase,[56] and carbonic anhydrase.[57-60] Zn_7-MT has also been shown to donate zinc to and remove zinc from the zinc finger domains of the transcription factors: Gal4,[61] p53,[62, 63] NF-κB,[64] Sp1,[65] TFIIIA,[66, 67] and TTK.[68] Owing to the high metal binding affinities involved in both the donor MT and acceptor enzymes and the fast rates of these metal transfers, these metal delivery reactions are proposed to occur through direct protein-protein interactions

www.manaraa.com

between the apoenzymes and Zn_7-MT.[60] Further evidence in support of MT's metallochaperone function is the induction of MTs when cells are exposed to metals.[69-72] These studies, coupled with the prevalence of MT in all cell types, have been used to support the proposed homeostatic roles as functions of Zn-MTs. However, there are few detailed mechanistic studies regarding these metal transfers, which are governed by the relative metal affinities between donor and acceptor.

Studies of MT knockout mice fed zinc-deficient diets showed delayed and abnormal growth patterns due to the lack of a buffered supply of zinc from Zn-MTs.[73] The MT knockout mice also showed a greater sensitivity to the toxic effects of increased zinc levels[74] due to the lack of an inducible zinc-responsive metal binding element (apoMT). Taken together, these results show how MT protects against harmful effects of both zinc deficiency and zinc excess by acting as a reservoir of available zinc in times of deficiency and as a sink for excess zinc during excess.

The other most commonly proposed function of MT is the detoxification of toxic metals such as cadmium,[75] and, potentially, arsenic,[76] lead,[77] and mercury.[78, 79] The large number of soft cysteinyl sulfur ligands allows MT to coordinate to soft toxic metals, in most cases with binding affinities greater than the less toxic zinc.[80] This higher affinity for more toxic metals permits metal exchange with Zn-MTs, leading to the release of free zinc, which, as described above, induces production of apoMT. This feedback process ensures a rapid response to toxic metal sequestration and also that the homeostatic levels of zinc are quickly restored.

A major benefit of sequestration of toxic metals by MT is that binding to the of MT prevents the toxic metals from potentially interfering with more critical metal binding processes, for which the binding affinities are lower than in MT. Highlighting these roles, it was reported that MT knockout mice were hypersensitive to cadmium, despite the fact that they accumulated only a small amount of cadmium compared to normal mice at the same exposure levels.[81-83] The MT null mice were not protected from the toxic effects due to the lack of a safe site for cadmium sequestration. Wild-type mice treated with increasing doses of cadmium also developed higher tolerances to cadmium toxicity, due

www.manaraa.com

to the higher levels of induced MT protein.[84] These results are especially significant as chronic cadmium exposure for humans is relatively common in the workplace, from foods grown in cadmium-rich soil or fertilized with phosphate sources containing cadmium, and significantly, from inhaled cigarette smoke.[85, 86] Cadmium is retained by the body and excreted very slowly with an estimated time in the human body on the order of decades,[87] where it is accumulated primarily in the kidneys as Cd-MT,[88] eventually leading to serious kidney damage and the disruption of proper kidney function.

1.3 Structural properties of metallothioneins

In humans, there are four known MT isoforms: MT1, MT2, MT3, and MT4.[89, 90] The MT1 and MT2 isoforms are constitutively expressed in all cells at low levels, with enhanced expression in the kidneys, liver, pancreas, and intestines. MT3 and MT4 are expressed only in specialized tissues of the brain and skin, respectively.[91] Sequence substitutions between the isoforms, as well as a small sequence insertion for MT3, generate very subtle differences in metal binding properties.[92] In fact, the properties of MT1 and MT2 have long been regarded as synonymous despite the differences in the amino acid sequence. Invariably, in all mammalian MTs, the cysteines are perfectly conserved in repeating Cys-Cys, Cys-X-Cys, and Cys-X-X-Cys motifs.[93] The large number of cysteine residues (20) relative to the total size of 60-70 residues permits the flexible coordination of different stoichiometric ratios and identities of metal ions. This facile flexibility in accommodating different metal coordination geometries is a fundamental property of MTs and allows for homeostatic control through the buffering of essential metals, acting as a metal donor to metalloenzymes when saturated and a metal acceptor from lower affinity zinc sites when unsaturated.

Mammalian MTs bind up to seven zinc or cadmium ions in tetrahedral geometries in two distinct domains, as shown in Figure 1.2. The N-terminal β-domain binds three divalent metals coordinated with nine cysteines and the C-terminal α domain binds four divalent metals with 11 cysteines. The single X-ray structure of an intact two-domain mammalian MT shows that, in the solid state, the two-domains form a dumbbell-like structure where the domains are separated by a short, flexible linker region.[94, 95]

www.manaraa.com

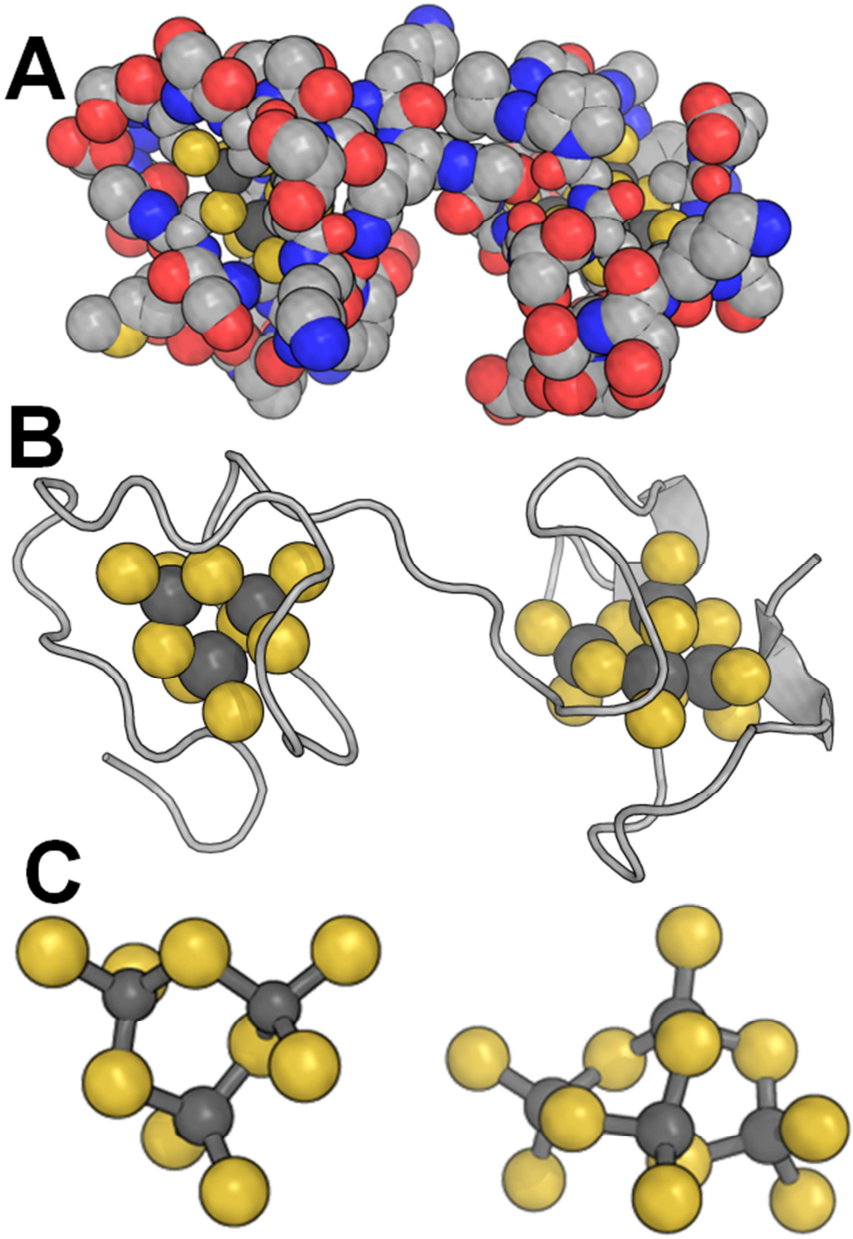

Figure 1.2: The two-domain structure of Zn/Cd saturated mammalian MT. (4MT2[96]) M_3S_9 β-domain on the left and the M_4S_{11} α domain on the right. (A) Space-filling model. (B) Dumbbell-like organization of the two-domains connected by the short peptide interdomain linker. (C) Bonding structure within each of the metal clusters. The protein backbone is shown as a light gray ribbon, the metals are shown as dark gray spheres, and the sulfur atoms as yellow spheres.

www.manaraa.com

The binding modes of the metals (M), that is the interaction of the metals with the thiols (S), are different in each domain. The β-domain M_3S_9 cluster is comprised of a six membered ring of alternating M and bridging S, the remaining six S are terminally bound, two per metal. The addition of one extra metal ion and two sulfur ligands in the α domain forms an M_4S_{11} adamantane-like cluster. Compared to the β-cluster, the additional metal in the α-cluster bridges two of the terminal sulfurs, resulting in a total of 5 bridging and 6 terminal S. The difference in the ligand to metal ratio, 3 and 2.75 for the β- and α-clusters, respectively, has been suggested to play important roles in domain-specific properties, such as metal binding cooperativity, metal transfer reactions, and domain interactions,[97] as it could be argued that the decreased ligand number decreases the overall affinity (K_F) for the 3 metals in the β-domain cluster.

To date, very few MT protein structures have been solved considering the ubiquitous nature of MT proteins.[98] Owing to their small size and high fluxtionality, MT proteins are difficult to crystallize. Solving the NMR solution structures of partially metallated MTs has also been hindered by this flexibility. In fact, the only structures that are currently available are of the metal-saturated forms with zinc and cadmium; significantly, there are no experimentally determined structures available of partially metallated MTs.

In the absence of metals, the apoMT peptide strand has been predicted from molecular dynamics (MD) calculations,[99] and supported experimentally,[100] to exist as a globular random coil, with no well-defined secondary structural elements. The "folding" of the MT protein into the two-domain structure is metal-induced, where reorganization of the peptide strand backbone and side-chains results from the formation of metal-binding sites to accommodate the metals, greatly reducing fluxtionality.[101, 102] The lack of motion of coordinating cysteinyl thiols has been reported from MD calculations.[103]

In forming metal-saturated MT from apoMT, the protein passes through distinct intermediate metallation states as shown in Scheme 1.1. The first added divalent metal binds to four of the exposed thiols, where the lability of the metal and flexibility of the peptide drives the reorganization to the most thermodynamically preferred occupancy (i.e., the most stable four from a pool of 20 available cysteines for $(M^{II})_1$-MT).

www.manaraa.com

$$\text{Apo-}H_{20}\text{-}\beta\alpha MT + M^{2+} \rightleftharpoons M_1\text{-}H_{18}\text{-}\beta\alpha MT + 2H^+$$
$$M_1\text{-}H_{18}\text{-}\beta\alpha MT + M^{2+} \rightleftharpoons M_2\text{-}H_{16}\text{-}\beta\alpha MT + 2H^+$$
$$M_2\text{-}H_{16}\text{-}\beta\alpha MT + M^{2+} \rightleftharpoons M_3\text{-}H_{14}\text{-}\beta\alpha MT + 2H^+$$
$$M_3\text{-}H_{14}\text{-}\beta\alpha MT + M^{2+} \rightleftharpoons M_4\text{-}H_{12}\text{-}\beta\alpha MT + 2H^+$$
$$M_4\text{-}H_{12}\text{-}\beta\alpha MT + M^{2+} \rightleftharpoons M_5\text{-}H_{10}\text{-}\beta\alpha MT + 2H^+$$
$$M_5\text{-}H_{10}\text{-}\beta\alpha MT + M^{2+} \rightleftharpoons M_6\text{-}H_8\text{-}\beta\alpha MT + 2H^+$$
$$M_6\text{-}H_8\text{-}\beta\alpha MT + M^{2+} \rightleftharpoons M_7\text{-}H_6\text{-}\beta\alpha MT + 2H^+$$
$$\text{SUM: } \text{Apo-}H_{20}\text{-}\beta\alpha MT + 7M^{2+} \rightleftharpoons M_7\text{-}H_6\text{-}\beta\alpha MT + 14H^+$$

Scheme 1.1: Sequential metallation reactions of MT.

The second metal to bind can occur via two pathways: (i) the metal binds to four free thiols in a beaded fashion with no bridging interactions to the first $M^{II}S_4$ site, or (ii) the metal shares a single bridging S with the $M^{II}S_4$ already present, forming an $(M^{II})_2S_7$ cluster. The third and fourth divalent metals have similar binding pathway options: (i) the beaded pathway, with three or four beaded $(M^{II})S_4$ independent binding sites (leaving 8 and 4 free thiols, respectively), or (ii) the clustered pathway, forming a three metal $(M^{II})_3S_9$ or four metal $(M^{II})_4S_{11}$ cluster (leaving 11 or 9 free thiols). This trend continues for the rest of the metallation steps, as shown in Figure 1.3, where the beaded pathway maximizes the number of terminal thiols (minimizing the number of bridging) and the cluster pathway maximizes the number of bridging thiols (by minimizing the number of terminal). Both pathways converge in the formation the metal saturated $(M^{II})_7$-MT where all the thiols are required to support the seven divalent metals.

Interestingly, the three and four metal clusters are the most efficient (lowest ligand to metal ratios), geometrically favoured combinations for tetrahedral metal ligand binding and are also the same cluster motifs found in the β- and α domains, respectively. There is experimental evidence in support of both pathways, as will be discussed in more detail in Section 1.4. Adoption of the specific metal binding pathway leads to determination of the metal binding mechanism: cooperative or non-cooperative metal binding.

www.manaraa.com

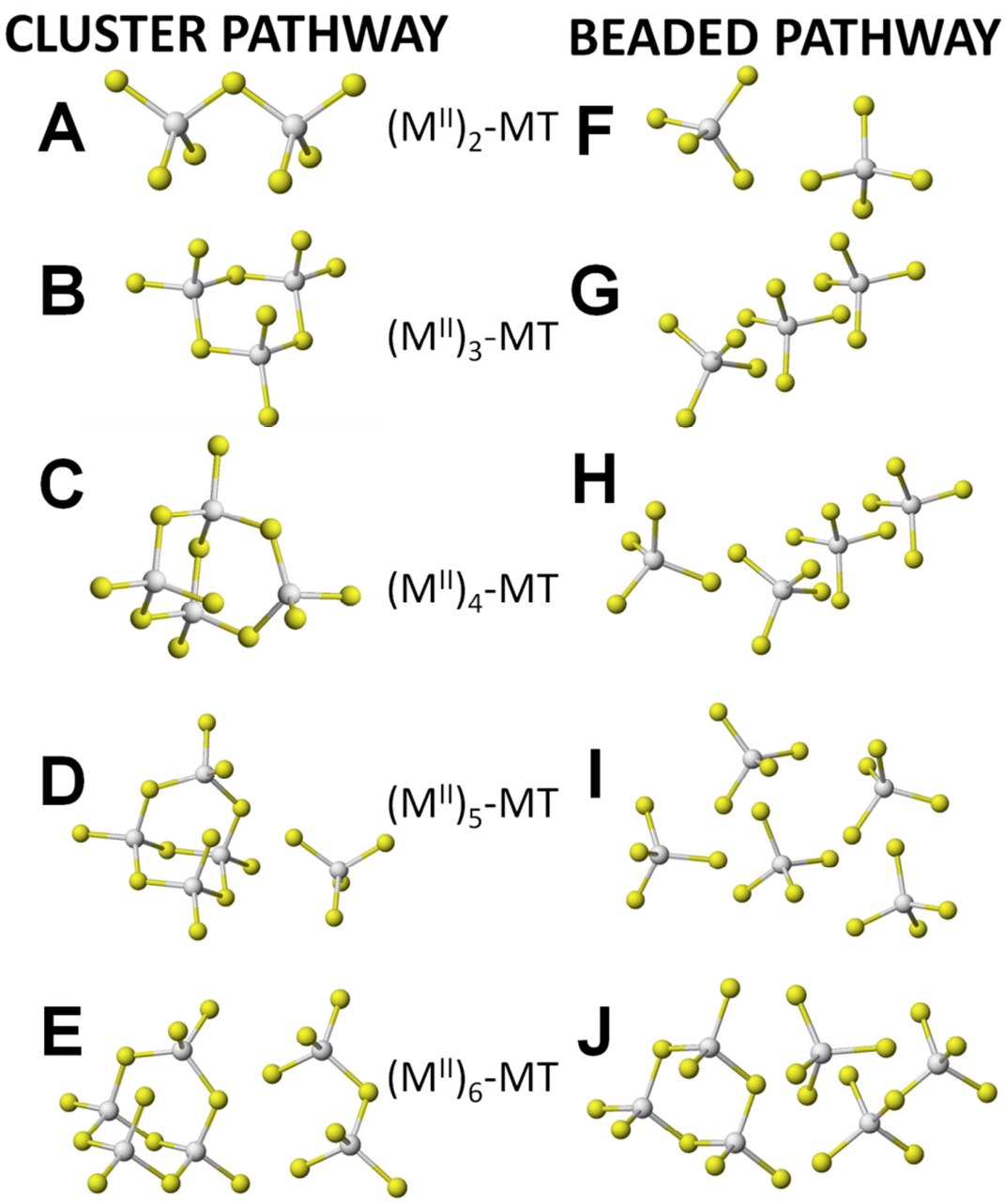

Figure 1.3: Possible structures of metal thiolate bonding formed for each of the two metallation pathways in MT for two to six metals bound. (A-E) Clustered products, where the number of geometrically favoured bridging thiols is maximized. (F-J) Beaded products, where the number of terminal thiols is maximized.

www.manaraa.com

1.4 Techniques for studying MTs

The properties of MTs have been studied using numerous experimental techniques. The most commonly used of these include: ultraviolet (UV) absorption spectroscopy, circular dichroism (CD) spectroscopy, electrospray ionization mass spectrometry (ESI-MS), nuclear magnetic resonance spectroscopy (^{1}H and $^{111/113}$Cd NMR), and X-ray absorption spectroscopies. This section will provide a brief overview of each of the techniques used in this thesis: UV and CD spectroscopies and ESI-MS. The information that can be determined from these techniques (as used for the data discussed throughout the thesis), as well as their respective limitations will also be described.

1.4.1 Ultraviolet absorption and circular dichroism spectroscopy

As discussed in Section 1.3, the absence of aromatic amino acids and lack of well-defined secondary structural elements (α-helices or β-sheets) severely limits the available spectroscopic signatures that can be used to study MTs. Perhaps the most useful absorptions are the ligand-to-metal charge transfer (LMCT) absorption bands between the thiolate sulfur and coordinated metal. The wavelength of the LMCT is metal-dependent, as it arises from the electronic transitions of Sn → Mπ*; therefore, the energy gap depends on the orbital energy of, predominantly, the π* of the metal.[104] UV and CD spectroscopic data measured in the LMCT region(s) of the MT-metal complexes are excellent probes with which to determine the geometries and stoichiometries of metal binding as well some information on the metal binding affinities.

The wavelengths of the LMCT bands of d^{10} metals bound to MT are longer than 225 nm. These transitions are especially useful in studying MTs because, for most metals, these transitions are completely clear and resolved from the amide n – π* absorptions of the protein backbone (~220 nm). The absence of aromatic amino acids clears the absorption spectrum region that is common in most other proteins (250-290 nm). Therefore, for apoMTs, the region of the UV spectrum λ > 225 nm is devoid of any significant spectral features, as shown in the spectra of apoMT shown in Figure 1.4 (black line). Metal binding to the protein can be followed by measuring the change in the LMCT band intensity as a function of added metal. The LMCT band of zinc occurs at approximately

www.manaraa.com

225 nm and for cadmium it is approximately centered on 250 nm, Figure 1.4 red and green lines, respectively. Since each metal possesses a different LMCT absorption maximum, it is possible to also measure the change in the relative intensity of these two LMCT bands as a function of added metals to monitor metal exchange reactions. These metal competition reactions, where MT loaded with one metal is challenged by addition of another metal, can be used to estimate the relative order of binding affinities of each metal for MT.

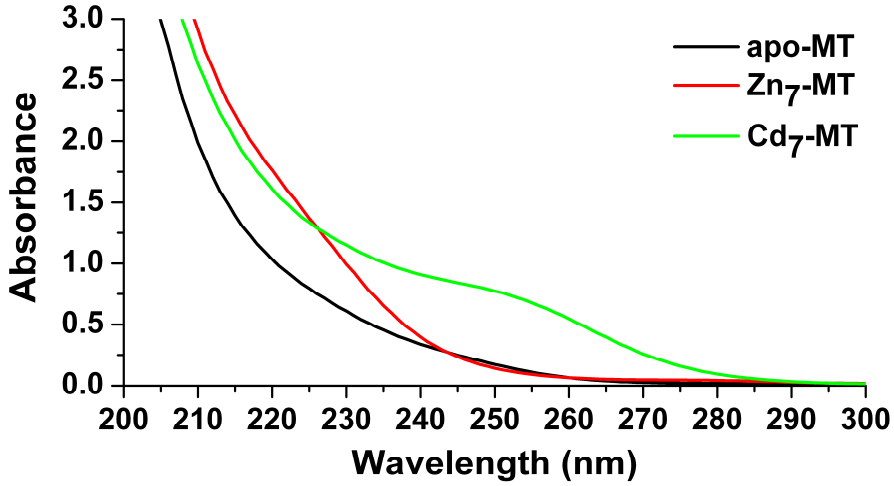

Figure 1.4: **Sample UV absorption spectra of MTs.** The LMCT band of zinc appears as a shoulder near 230nm on the protein backbone 220 nm absorption and the cadmium LMCT band as a shoulder centred at 250 nm. Lines: apo-βαMT1A (black), Zn_7-βαMT1A (red), and Cd_7-βαMT1A (green). Conditions: ~10 µM protein in 10 mM Tris buffer pH 7.4 measured at room temperature on a Varian Cary 50.

Circular dichroism (CD) spectroscopy has also been widely applied to the study of MTs. CD spectra measure the difference in the absorption of left-handed and right-handed circularly polarized light of optically active molecules. All proteins possess CD spectral signals in the UV region as all amino acids are chiral at the alpha carbon (excluding glycine) – these signals are sensitive to conformational changes. Organization of the chiral centres into repeating segments of secondary structure in the protein generates spectral signatures representative of α-helices, β-sheets, and random coils in the far UV region (190-220 nm).

www.manaraa.com

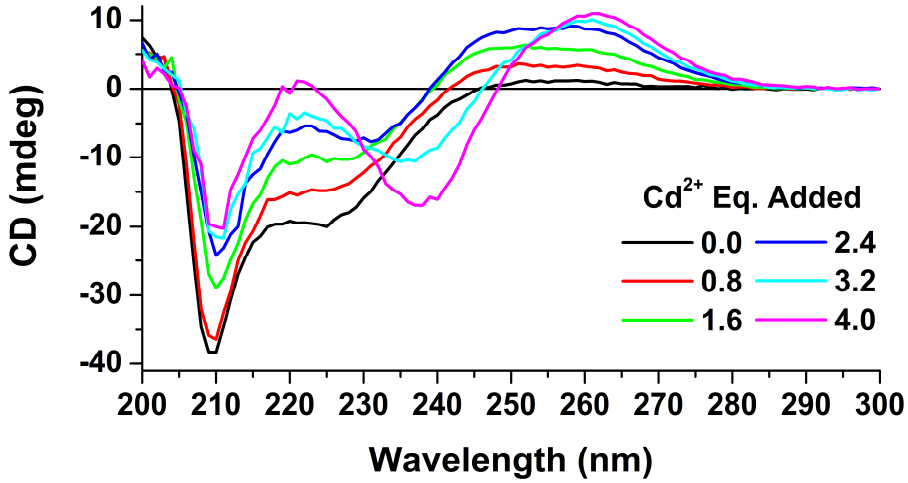

Figure 1.5: Example circular dichroism spectra of a cadmium titration of 15 µM apo-αMT1A. The first two equivalents of added cadmium build peaks at 255 nm and 220 nm. These bands are the result of the formation of beaded $(CdS_4)^{2-}$ structures. The derivative signal (260 nm peak, 240 nm trough) forms when clustering begins as required to support more than two bound Cd^{2+}. Data originally measured by Rigby-Duncan, K.E.[105] and replotted with permission.

The far UV peptide region of the CD spectra of metal-free apoMTs is monophasic and strongly negative at wavelengths < 220 nm, a result of the random coil nature of the peptide. Metal binding to MT results in folding of the MT peptide around the metal(s) into specific chiral structures. The LMCT UV absorption bands of MT are strongly dichroic due to the peptide-induced asymmetry of the metal binding sites and CD signals at λ > 220 nm are exclusively from metal binding to the protein. Many detailed spectroscopic analyses have been carried out on the metallation reactions of MT with numerous metals. Cd-binding to MT, for example, generates a strong derivative signal between 240-260 nm.[106-108] The origin of this derivative CD signal is a result of the asymmetric overlap of the dipole moments of the bridging thiolate ligands in the cluster, known as exciton splitting or coupling. The shape and intensity of the cadmium CD band is dependent on the stoichiometry of bound metals and the structure of the binding site(s).[109] Addition of cadmium to apoMT (Figure 1.5) has been interpreted as being due to the cadmium bound as separate $(CdS_4)^{2-}$ beads before coalescing into the clustered structure.[110]

www.manaraa.com

The major drawback to using many spectroscopic techniques to determine metal binding properties of MTs is that only the aggregate average signals are detected. In fact, based mostly on information from these techniques, the binding of metals to MTs was long considered to be homogeneous. This meant that for a single addition of metal ions, that exact number was bound in solution. The UV and CD spectra were therefore considered to directly report on the MT solution speciation. However, results from ESI-MS experiments showed that binding of metals, at least to some MTs, resulted in significant heterogeneity in solution speciation.[111] Thus, spectroscopic techniques lack the sensitivity required to resolve multiple speciation, such as the presence of various metallation states of MT, even though there are subtle differences in the clustered and beaded UV and CD spectra.

1.4.2 Electrospray ionization mass spectrometry

ESI-MS measures the mass to charge ratio (*m/z*) of ionized gas-phase analytes, providing both qualitative and quantitative information about the species in solution. ESI-MS has been used in numerous studies of MT metal binding. ESI-MS is especially well suited to the study of the metallation properties of MTs as it permits identification of the metals bound and their stoichiometries. Since ESI-MS is a key technique used for all work in this thesis, this section provides a more detailed description of the instrumentation and the advantages of its application to studying MTs.

A schematic diagram of a typical ESI mass spectrometer is shown in Figure 1.6A. All mass spectrometers contain: a sample inlet ionization source (a), ion optics (b), a mass analyzer and an ion detector (c), a data analyzer (d), and a vacuum pump system (e).[112] The ionization source converts analyte molecules into gas-phase ions. These ions are directed into the mass spectrometer and collected and focused with the ion optics. The collected ions are separated based on their *m/z* ratios by the mass analyzer. Finally, they are detected by the ion detector and counted and displayed by the data analyzer. The vacuum system is necessary for the ions to be analyzed without interference, due to collisions with atmospheric gases.

www.manaraa.com

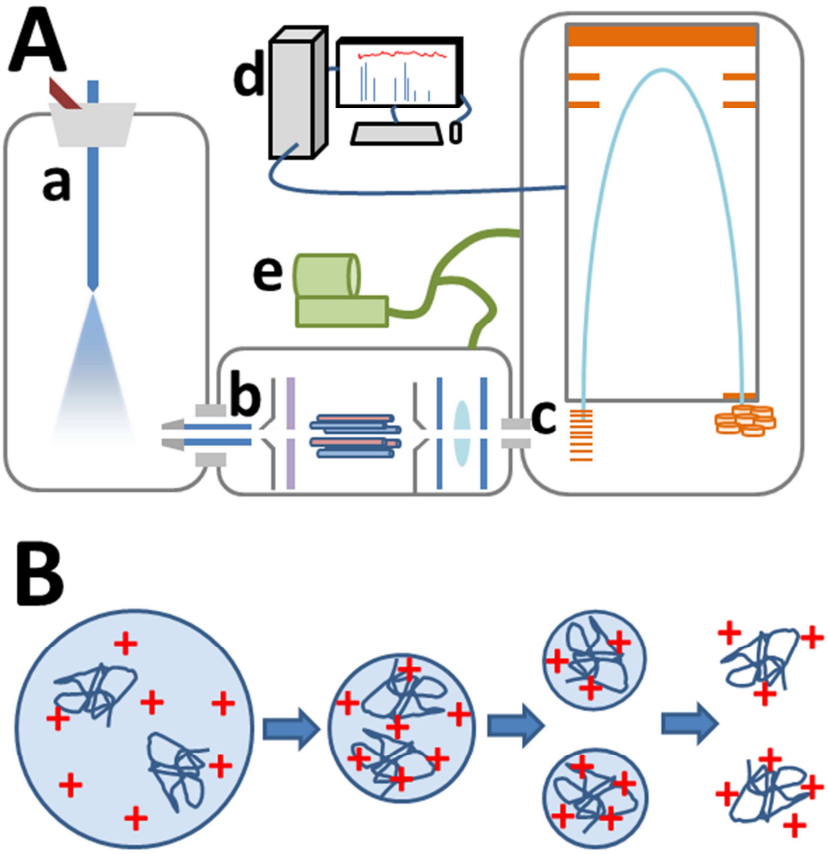

Figure 1.6: The electrospray ionization mass spectrometer. (A) Schematic of an electrospray ionization time-of-flight mass spectrometer (ESI-TOF-MS): (a) ESI ion source, (b) ion optics, (c) TOF mass analyzer and ion detector, (d) data analysis system, and (e) vacuum pump system. (B) Simplified illustration of the charged residue model for the production of gas-phase molecular ions in the electrospray process.

Several ionization methods are used in mass spectrometry. These can be separated into two categories: hard and soft ionization methods. Hard ionization sources, such as electron impact, result in significant fragmentation of analyte molecules and are not suited to the study of large biomolecules. Soft ionization sources, such as ESI and matrix-assisted laser desorption / ionization (MALDI), do not significantly fragment analyte molecules during the ionization process. Soft ionization methods are well-suited to the study of proteins due to their ability to detect mass changes from the parent protein species as a result of post-translational modifications, associated cofactors, and complex

www.manaraa.com

formation.[113] For example, the predictable and detectable mass changes in the mass spectra of protein-metal complexes can reveal the stoichiometry of the resulting complex.

Figure 1.6A shows a schematic of a typical ESI ion source commonly used in mass spectrometers. The sample solution containing the dissolved analyte is infused through a metal capillary charged to several thousand volts. A fine mist of charged droplets exits the capillary and the electrostatic field results in the formation of a Taylor cone. Evaporation of the solvent from the charged droplets decreases the droplet size while the charge remains the same, increasing the charge density. Fission of the droplet occurs when the charge density of the droplet surpasses the Rayleigh limit, when the repulsive Columbic forces become greater than the surface tension. Evaporative-fission events continue until very small droplets are produced. Production of the charged gas-phase analytes are thought to occur through different mechanisms depending on the analytes.

In the Charge Residue Model, the droplets continue to evaporate to dryness, leaving charged gas-phase analytes adducted with the remaining ions (Figure 1.6B).[114] A distribution of charges per analyte molecule are possible, depending on the size of the analyte molecule, solution composition, and electrospray conditions, resulting in the formation of multiple "charge states," usually from different numbers of adducted protons, forming $[M + nH]^{n+}$ species.[115] The charge state distribution of a protein can therefore provide conformational information, as unfolding of the protein increases the volume and exposes a greater number of protonatable basic sites, both of which increase the average and maximum supported charge. Charged analytes are separated by the mass analyzer, detected by the ion detector, and displayed by the data analyzer.

The ESI-MS technique has many advantages for the study of MTs, including: (i) small volumes (25 µL per measurement) of dilute (< 50 µM) samples, (ii) direct solution phase sample injection, (iii) the ability to monitor reactions in real time, (iv) identification of individual and multiple speciation from the unique *m/z* ratios, and (v) conformational/folding information from the charge state distributions. The soft ionization of ESI does not fragment or otherwise disrupt the metal binding sites, therefore, it is possible to quantitatively determine the stoichiometry of the metallation

www.manaraa.com

reaction for each metal with MT(s), in solution.[116] Quantitative analysis assumes that each species ionizes in a similar fashion, which is not true for all species. However, in 1993, Feneslau *et al*. showed that the concentrations of each of the M_n-MT species can be reliably estimated from the mass spectral data.[117]

The most significant disadvantage in ESI is the potential for ions other than protons to adduct in the electrospray process. Sodium and potassium, for example, also form adducts with proteins in the ESI process. Therefore, special care has to be taken to avoid contamination and salts containing these ions, including common buffers used in physiological studies.

1.4.3 Competition experiments

Competition experiment techniques can be used for studying the multiple metal binding affinities of MTs. In a competition experiment, two species compete for a common substrate (S) under equilibrium conditions:

$$B + S \rightleftharpoons BS$$

$$K_B = \frac{[BS]}{[B][S]} \qquad (1)$$

$$C + S \rightleftharpoons CS$$

$$K_C = \frac{[CS]}{[C][S]} \qquad (2)$$

This set of two competing reactions is described by the combination of their individual equilibrium reactions, eq 1 and eq 2. By having the species compete at equal concentration, the terms from the binding affinity equations become simplified. For example, the distribution of a substrate S after addition to an equimolar mixture of apoB and apoC will follow the most thermodynamically preferred occupancy, with the substrate preferentially occupying the higher affinity site. Thus, the ratio of the affinity

www.manaraa.com

constants between apoA and apoB is reflected in the substrate occupancy (or *vice versa*), as shown in eq 3.

$$\frac{K_B}{K_c} = \frac{[BS]}{[B]} \bullet \frac{[C]}{[CS]} \qquad (3)$$

Figure 1.7 shows how the substrate occupancy distribution between two competing species changes as a function of equilibrium constants. These curves are based on computational simulations of eq 3 and show the competitive formation of BS and CS from an equimolar mixture of B and C. Figure 1.7 show five different scenarios for the equilibrium constant (K) ratios: (A) when the equilibrium constants favour CS formation by 0.5 log units [$\log(K_B) = \log(K_C) - 0.5$], (B) when neither BS nor CS are favoured (identical equilibrium constants), and where the formation of BS is favoured over CS by (C) 0.5, (D) 1.0, and (E) 1.5 log units.

In a simplistic model, it might be assumed that the reaction with the largest K receives all or the majority of the reaction flux. However, when coupled reversible reactions are in equilibrium, how large (or small) of a difference in K between competing reactions is significant? The curves in Figure 1.7 permit visualization of the abstract competition reactions between two competing ligands with different binding affinities. Panel 3D, for example, shows that when competing species differ in K by one order of magnitude, there is significant preference for the preferred reaction (formation of BS); however, formation of the non-dominant product (CS) is also, significantly, non-zero.

In these one-to-one competition models, it is possible to determine the approximate ratio of the equilibrium constants from the speciation data.[118] For example, by measuring and plotting the competitive formation of substrate S binding to B and C, it is possible to determine the relative ratios of the equilibrium constants that describe the reactions forming BS and CS. If, in a separate experiment, the equilibrium constant of B or C is determined (or known) then that value and the ratios from the competition experiments can be used to assign a K-value for the unknown reaction.

www.manaraa.com

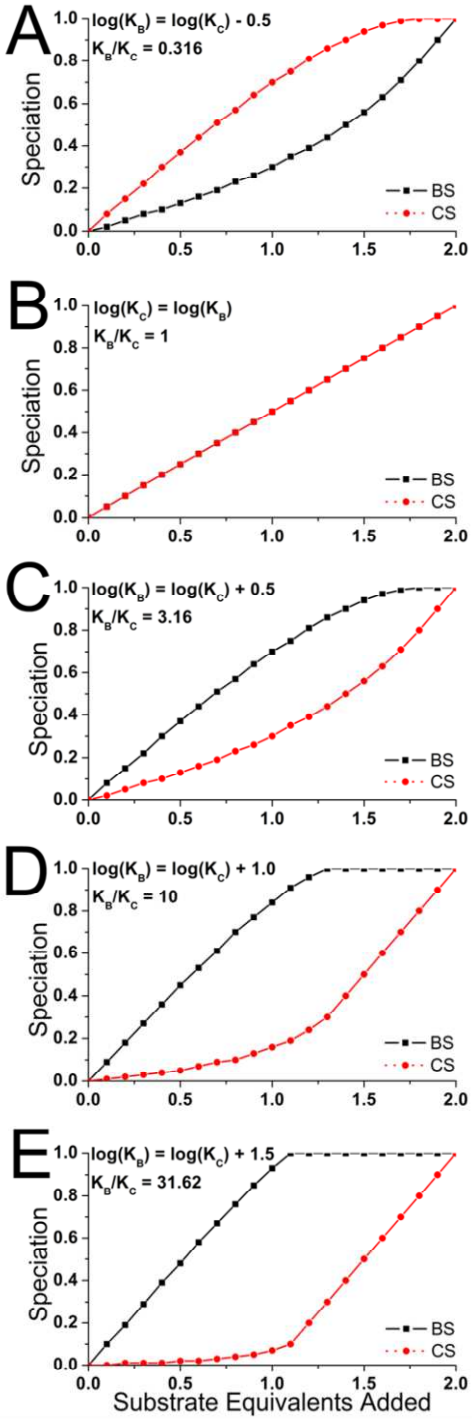

Figure 1.7: Speciation models of the competitive reactions between equal concentrations of B and C for substrate S. The curves show the competitive formation of the substrate bound species BS (black squares) and CS (red circles) as a function of added S.

www.manaraa.com

In the ESI-MS experiments used in this thesis, equal concentrations of MTs compete against each other or against the zinc-dependent enzyme carbonic anhydrase (CA) for added zinc or cadmium. The competitive formation of the metal-bound products was then measured and plotted as a function of added metal. This provides the relative K ratios of the reactions that govern the formation of those products. Addition of the known zinc binding constant (K_F) of CA from published experiments allows for the determination of the real K_F of zinc binding to MT. In this way, the MT binding affinities are locked onto the known value of CA.

1.5 Cooperativity and non-cooperativity of metal binding to MTs

The concept of metal binding cooperativity to MTs is significantly different from the traditional biochemical view of cooperativity, such as the binding of oxygen to the four domains of hemoglobin. Due to the lack of preformed binding sites, metal-induced folding of the protein strand, and numerous possible intermediate structures, the simple model of traditional biochemical cooperativity becomes much more complex when discussing the cooperativity of MT metal binding. However, the overall thermodynamic driving force remains the same. A multistep process is cooperative when the successive reactions become more thermodynamically favourable rather than less favourable, as expected theoretically.[119] In the case of oxygen binding to tetrameric hemoglobin, for example, binding of one molecule of oxygen in one of the four domains triggers a conformational change in the other three domains that increases their oxygen binding affinities and promotes the formation of fully oxygenated $(O_2)_4$-hemoglobin.[120] Thus, only deoxy- and fully oxygenated hemoglobin states are predominant, resulting in a fully cooperative mechanism.

In the cooperative mechanism of the reactions shown in Scheme 1.1, the successive K values increase, that is $K_{i+1} > K_i$, promoting the formation of the fully metal saturated product. In this mechanism, the only species that are present in solution at equilibrium are the fully metallated end point of the reaction, which is formed from any amount of added metal, and the fully unsaturated apoMT. Since the reaction equilibrium constants increase for cooperative systems, the intermediate metallation states are thermodynamically

www.manaraa.com

unfavoured and formation of saturated MT is promoted over partial metallation states. For example, if zinc binding to mammalian MT was fully cooperative, addition of 3 equiv of Zn to a solution of apoMT would result in the formation of ~3/7 Zn_7MT leaving ~4/7 apoMT with little to no intermediate metallation states.

The biophysical rationale for cooperativity in MTs is justified by the preferential clustering (over beading) of metals formed from metal templated folding and formation of transiently empty metal binding sites. Thus, reorganization of the apopeptide upon binding of one zinc ion preforms subsequent zinc binding sites, likely near the first binding site, promoting clustering. These reactions – metal binding leading to formation of a new metal binding site – cascade, one after another, which drives the reaction to completion and forming the fully metal-saturated MTs.

In contrast, in a non-cooperative process, the successive K values decrease such that $K_{i+1} < K_i$, following the theoretically expected trend. This means that, for example, for the set of successive reactions shown in Scheme 1.1, the reactions become less favoured with each additional metallation step. In this mechanism, all of the intermediate metallation states are formed statistically and the distribution of Zn_n-MT species will depend on the mole equivalents of zinc added. For example, if zinc binding to MT was fully non-cooperative, addition of 3 equiv of Zn to a solution of apoMT would result in formation of an approximately normal distribution of Zn_{1-5}-MT, where the average zinc load would equal Zn_3-MT. The actual speciation distribution that would be centered on Zn_3-MT would depend on the ratios of the K values for the reactions describing the formation of Zn_3-MT from Zn_2-MT and the reaction of Zn_3-MT forming Zn_4-MT.

The structural implications of non-cooperativity in the metallation reactions of MTs result in the preferential formation of $(M^{II}S_4)^{2-}$ beads over clusters. As each metal is added, there is no significant change to subsequent metallation reactions, with the exception that there are four fewer free thiols available to form the next beaded binding site. Thus, in a non-cooperative pathway, subsequent reactions become less favoured largely due to there being less open coordination sites. In fact, as was shown for arsenic metallation of MTs[121] (noting that arsenic binds in a trigonal pyramidal geometry,

www.manaraa.com

forming ($As^{III}S_3$)-beads and does not form clusters), the decrease in reaction rate constants was approximately linear with remaining open metal binding sites.[122, 123] A further corollary of non-cooperative binding is that cluster formation involving bridging thiols occurs only for the 6th and 7th divalent metals bound (Figure 1.3).

1.5.1 Experimental evidence of metal binding cooperativity in MTs

Numerous studies have suggested that zinc and cadmium bind to MTs in a cooperative fashion,[111] though more recent results from ESI-MS experiments, specifically on MT1[116, 124] and MT3,[125] have suggested the operation of a non-cooperative metal binding mechanism. There has been considerable debate on whether the binding of zinc and cadmium to mammalian MT was cooperative or non-cooperative. Results from CD, UV, NMR, and other experimental techniques have suggested that cadmium and zinc binding to MTs was cooperative and domain-specific. Analysis of optical spectral data led to the conclusion that the first four metals bound cooperatively to apoMT and were located specifically in the α domain.[126] For the intact 20 cysteine protein, this implies that only the apo [$(SH)_9\beta$-$(SH)_{11}\alpha$-MT] and $(M^{II})_4$ [$(SH)_9\beta$-$(M^{II})_4S_{11}$-αMT] species would be stable for up to four equivalents of divalent metals added. However, these experimental techniques provide the average metallation state of the solution species and are unable to resolve multiple metallation states. Recently, ESI-MS techniques have been applied to the study of metallation reactions of MT. As described above, ESI-MS is able to identify the stoichiometry of bound metals, including multiple metallation states, in addition to structural and other quantitative and qualitative information, demonstrating the power of this technique for studying the multiple metal binding events in MTs.

1.6 Domain specificity

MT domain properties have been well studied, yet the question remains: why did the two-domain structure seen in most MTs evolve? Surely, this feature is intricately tied to the exact *in vivo* functions of MT proteins, especially considering the prevalence of the MT protein family and their high sequence conservation. The metal binding site organization in MTs is unique compared to other metalloproteins and chaperones. The spatial separation of the two metal clusters is an interesting arrangement that shares properties

www.manaraa.com

with both metal storage proteins and metal chaperone proteins, a fact that has likely contributed to the debate over the exact *in vivo* functions of MT proteins that has been ongoing for more than five decades.

A common feature in nearly all MTs throughout life is the presence of two very distinct non-symmetric binding site environments. In wheat metallothionein E_C, for example, domain II possesses a Zn_3Cys_9 cluster (that resembles the β-domain of mammalian MT) as well as an additional $ZnCys_2His_2$ binding site, while domain I has a Zn_2Cys_6 cluster.[127] Each of the three zinc binding sites in the wheat E_C proteins binds the respective zinc with different affinities and it is probable that each site serves a unique *in vivo* function. Though the Zn_3Cys_9 β-domain cluster and the Zn_4Cys_{11} α domain cluster are more similar in mammalian MTs, the different metal:ligand ratios, cluster geometries, and solvent accessibility could possibly generate domain-specific properties.

Traditionally, the α domain, with the higher number of thiols, has been reported as having the highest affinity binding sites.[128] In fact, $^{111/113}$Cd and ^{1}H NMR studies have suggested that the first four divalent metals added to apoMT bind exclusively to the α domain, in a cooperative manner, while the β-domain non-cooperatively binds from five to seven equivalents of added metal.[129] These results are supported by experiments where four equivalents of cadmium were added to MT and the MT was digested with the non-specific protease subtilisin.[128] The subtilisin digested the β-domain faster than the α domain under these conditions, which was thought to be due to decreased enzyme accessibility to the α domain peptide backbone as a result of the cadmium being located in the α domain. It is not known, however, if metal rearrangements occurred during the digestion process or subsequent analyses. More recent experiments have used cysteine modifiers to label free cysteines and determine metal binding location within the MT peptide strand.[130, 131] These experiments also suggest that the first four metals bind exclusively to the α domain. Again, it is not known if these reactions are selective only for free cysteines or if the modifier causes metal rearrangement from displacement following Cys reactions with the modifier. Furthermore, the reaction rates of the modifiers for the cysteines may simply be disproportionate between the domains, mimicking the results that would be expected for a domain-specific mechanism.

www.manaraa.com

Metal exchange experiments, in which cadmium is added to Zn-MTs, have suggested that the α domain also cooperatively exchanges its bound zinc for cadmium before the β-domain does. These results led to the proposal that each domain had a higher propensity or metal selectivity, with higher cadmium selectivity in the α domain and higher zinc in the β-domain. A notable result is that the X-ray crystal structure for the mixed metal Cd_5Zn_2-MT2 from rat, shows specifically a Cd_4 α-cluster and a Cd_1,Zn_2 β-cluster.[94, 95]

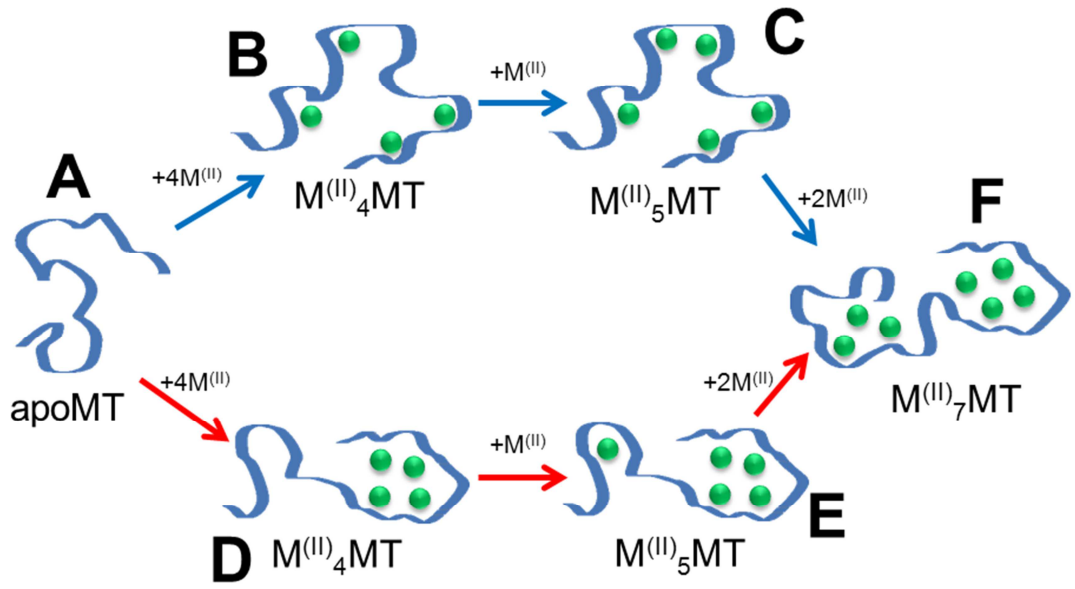

Figure 1.8: Schematic representation of the two metallation pathways for MT. The paths start with apoMT (A) and end with $M^{(II)}_7$MT (F). The blue path (A-B-C-F) shows the beaded non-specific pathway and the red path (A-D-E-F) shows the clustered α domain-specific pathway.

There are two potential pathways for metal binding and metal exchange reactions of MTs, as shown in Figure 1.8. These are the domain-specific pathway and the non-specific, or random, pathway. For metal binding and/or exchange to occur in a domain-specific fashion, the thermodynamics of the set of reactions that describe metal binding to MTs must skew significantly in favour of the more specific domain. If metal binding to apoMT was α domain-specific, for example, then the reactions that describe metal binding to the α domain would have equilibrium constants that were significantly larger than those that describe β-domain metallation. As shown in the models of competition

www.manaraa.com

reactions in Section 1.4.3, the binding constant difference would have to be larger than one log unit in order to generate those levels of selectivity. This means that the reaction that describes the formation of the metal saturated Zn_4-αMT from Zn_3-αMT (adding one zinc to a system where there are no free thiols and very limited flexibility) would outcompete the reaction that describes the formation of Zn_1-βMT from Zn_0-βMT (where there are nine free thiols that can be organized to form the most thermodynamically stable Zn_1Cys_4-βMT binding site).

Domain specificity describes two separate but related properties of MTs. The first is the addition (or removal) of a single metal type to the MT protein, as is described in detail in Section 1.3. The second is the exchange of one metal (Cd) for another metal (Zn) in metallated MTs. If it is a single metal, what is the impact of "domain specificity" on the metal binding and donation? That is, are metals bound with higher affinities in one domain and weaker affinities in another? What about the mixed metal situation and domain specificity, for example Cd/Zn-MT or Cu/Zn-MT? Are the metals preferentially segregated in mixed metal MT species where only one metal occupies one of the domains? The implications of domain specificity on metal binding to MTs will be discussed, in relation to the results shown in Chapters 2-5, in Chapter 6.

1.7 A history of MT metal binding constants

Despite the long history of stoichiometric and structural studies of MTs, as well as numerous investigations of the reactions of MTs with other biological metal centres, only a relatively small number of studies have been aimed at assigning numerical values to the metal binding affinities of MTs. These values are critical to the understanding of MT function, as the values of the various metal binding (and, in reverse, metal release/donation) formation constants determine *in vivo* metal distributions with respect to other metal sources and sinks. For example, metal binding sites with higher zinc affinity than MT, such as those found in zinc-dependent enzymes ($K_{enzyme} > K_{(Zn)7MT}$), will acquire zinc from Zn-MT. Weaker zinc interactions, between zinc and non-specific zinc binding sites for example ($K_{zincsite} < K_{(Zn)nMT}$, n = 0-7), are stripped of zinc by unsaturated MT species with higher zinc affinities.

www.manaraa.com

The first available estimations of metal binding affinities assumed that all seven divalent metal binding sites were equivalent, determining the average (across all seven binding sites) zinc and cadmium binding affinities as approximately ($\log(K_F)$) 10^{12} and 10^{16} at pH 7, respectively.[132] These estimations were based on pH titrations of rabbit Zn_7- and Cd_7-MT monitored through the disappearance of the LMCT bands as a function of pH and the values extrapolated to pH 7.0.[133]

Through competition with numerous small molecular zinc binding agents, the average values for the seven zinc affinities have been reported for a number of MT isoforms. These reported averages range, depending on the experimental conditions and technique, from ($\log(K_F)$) 10^{11} to 10^{13} for zinc binding to MT. The most recent and significant development in determining the metal binding affinities of the zinc binding sites in MTs was the assignment of four distinct binding affinities instead of an average affinity for all seven sites.[52] This report had suggested that the first four zinc bound with the same high affinity, while the fifth, sixth, and seventh zinc were bound with significantly decreasing affinities. An important result from that study was that the seventh zinc was bound with an exceptionally weak affinity relative to the others, which had not been reported previously. A follow-up study by another research group showed that this exceptionally weak affinity site was not present under their conditions,[134, 135] but that they could generate the same result by subjecting the protein to much lower pH in the demetallation procedure for apoMT preparation.[136] Knowledge of four independent zinc binding affinities to the seven sites of Zn-MT suggested that, with high enough resolution, and from a suitably designed experiment, the first four binding affinities could be determined independently as well.

1.8 Scope of the thesis

The majority of MT research has focused primarily on the properties of the metal saturated Zn_7- and Cd_7-MTs. Less is known about the partially metallated $(M^{II})_n$-MT (where n = 0-6). These partially metallated species are critical partners in the *in vivo* reactions that occur for the proposed functions of MT. Metal donation and metal acquisition in the homeostatic zinc buffering role of MTs generates and fills open zinc binding sites, respectively. Therefore, in order to be able to more accurately describe the

www.manaraa.com

metallation properties of MTs, more knowledge of these partially metallated species is required. The research presented in this thesis focuses primarily on the properties of partially metallated MT species, with in-depth analyses of the domain-specific properties.

This thesis contains six chapters and an appendix. This first chapter provides a description of important and relevant concepts of MT research with an emphasis on past experimental results, leading up to the state of MT research at the commencement of this research. The second chapter describes competitive zinc metallation reactions of intact βα-MT1A with apocarbonic anhydrase (apoCA) using ESI-MS. These experiments reveal the individual binding affinities for each of the seven bound zinc. Chapter 3 continues with the competitive zinc metallation reactions of separated α domain and β-domain fragments of MT1A competing against apoCA to determine the binding affinity constants for each of the two-domains in isolation. Furthermore, chapter 3 relates the results for the separated domain binding affinities to the intact βα-MT1A in order to determine the roles of domain-domain interactions in the intact MT protein.

Chapter 4 investigates the domain specificity of zinc binding to apoMT and the cadmium exchange of Zn-MT through competition between the two-domains using the separated β-domain and α domain fragments, this time competing against each other.

Chapter 5 describes progress toward kinetic and thermodynamic analysis of metal binding and exchange with carbonic anhydrase. Various combinations of MT species (Zn-MT, Cd-MT, and apoMT) were added to CA in different metallated states (apoCA, Zn-CA, and Cd-CA) to probe the kinetics and thermodynamics of CA metal binding and exchange. This chapter also addresses the protective nature of MT through the rescuing of Cd-poisoned enzymes and toxic metal sequestration.

Finally, Chapter 6 draws together the results from the previous chapters in order to comment on the progress made toward our understanding of the metal binding, release and exchange properties of MT.

www.manaraa.com

1.9 References

1. Fraga, C. G. (2005) Relevance, essentiality and toxicity of trace elements in human health, *Mol. Asp. Med. 26*, 235-244.
2. Bertini, I., and Sigel, A. (2001) *Handbook on metalloproteins*, CRC Press, Boca Raton.
3. Andreini, C., Banci, L., Bertini, I., and Rosato, A. (2006) Counting the zinc-proteins encoded in the human genome, *J. Proteome Res. 5*, 196-201.
4. Hambidge, M. (2000) Human zinc deficiency, *J. Nutr. 130*, 1344S-1349S.
5. Prasad, A. S. (2013) Discovery of human zinc deficiency: its impact on human health and disease, *Adv Nutr. 4*, 176-190.
6. Horton, S., Alderman, H., and Rivera, J. (2008) Copenhagen consensus 2008 challenge paper: hunger and malnutrition, *Copenhagen Consensus*.
7. Bhagwati, J., Bourguignon, F., Kydland, F. E., Mundell, R., North, D. C., Schelling, T., Smith, V. L., and Stokey, N. (2008) Copenhagen Consensus 2008 Results
8. Prasad, A. S. (1988) Zinc in growth and development and spectrum of human zinc deficiency, *J. Am. Coll. Nutr. 7*, 377-384.
9. Keen, C. L., and Gershwin, M. E. (1990) Zinc deficiency and immune function, *Annu. Rev. Nutr. 10*, 415-431.
10. Caldamone, A. A., Freytag, M. K., Cockett, A. T., and Cockett, T. (1979) Seminal zinc and male infertility, *Urology 13*, 280-281.
11. Shambaugh Jr, G. E. (1986) Zinc for tinnitus, imbalance, and hearing loss in the elderly, *Otol. Neurotol. 7*, 476-477.
12. Sandstead, H. H. (1985) Zinc: essentiality for brain development and function, *Nutr. Rev. 43*, 129-137.
13. Black, M. M. (2003) The evidence linking zinc deficiency with children's cognitive and motor functioning, *J. Nutr. 133*, 1473S-1476S.
14. Mocchegiani, E., Muzzioli, M., and Giacconi, R. (2000) Zinc and immunoresistance to infection in aging: new biological tools, *Trends Pharmacol. Sci. 21*, 205-208.
15. Ho, E. (2004) Zinc deficiency, DNA damage and cancer risk, *J. Nutr. Biochem. 15*, 572-578.
16. Prasad, A. S., and Kucuk, O. (2002) Zinc in cancer prevention, *Cancer Metastasis Rev. 21*, 291-295.
17. Franklin, R. B., and Costello, L. C. (2007) Zinc as an anti-tumor agent in prostate cancer and in other cancers, *Arch. Biochem. Biophys. 463*, 211-217.
18. Kinlaw, W. B., Levine, A. S., Morley, J. E., Silvis, S. E., and McClain, C. J. (1983) Abnormal zinc metabolism in type II diabetes mellitus, *Am. J. Med. 75*, 273-277.
19. Chausmer, A. B. (1998) Zinc, insulin and diabetes, *J. Am. Coll. Nutr. 17*, 109-115.
20. Niewoehner, C., Allen, J. I., Boosalis, M., Levine, A. S., and Morley, J. E. (1986) Role of zinc supplementation in type II diabetes mellitus, *Am. J. Med. 81*, 63-68.
21. Mocchegiani, E., Bertoni-Freddari, C., Marcellini, F., and Malavolta, M. (2005) Brain, aging and neurodegeneration: role of zinc ion availability, *Prog. Neurobiol. 75*, 367-390.
22. Cuajungco, M. P., and Lees, G. J. (1997) Zinc metabolism in the brain: relevance to human neurodegenerative disorders, *Neurobiol. Dis. 4*, 137-169.
23. Frederickson, C. J., Koh, J.-Y., and Bush, A. I. (2005) The neurobiology of zinc in health and disease, *Nat. Rev. Neurosci. 6*, 449-462.
24. Little, P. J., Bhattacharya, R., Moreyra, A. E., and Korichneva, I. L. (2010) Zinc and cardiovascular disease, *Nutrition 26*, 1050-1057.

www.manaraa.com

25. Leone, N., Courbon, D., Ducimetiere, P., and Zureik, M. (2006) Zinc, copper, and magnesium and risks for all-cause, cancer, and cardiovascular mortality, *Epidemiology 17*, 308-314.
26. Song, Y., Wang, J., Li, X.-k., and Cai, L. (2005) Zinc and the diabetic heart, *Biometals 18*, 325-332.
27. Maywald, M., and Rink, L. (2015) Zinc homeostasis and immunosenescence, *J. Trace Elem. Med. Biol. 29*, 24-30.
28. Braymer, J. J., and Giedroc, D. P. (2014) Recent developments in copper and zinc homeostasis in bacterial pathogens, *Curr. Opin. Chem. Biol. 19*, 59-66.
29. Fukada, T., Yamasaki, S., Nishida, K., Murakami, M., and Hirano, T. (2011) Zinc homeostasis and signaling in health and diseases, *J. Biol. Inorg. Chem. 16*, 1123-1134.
30. Choi, S., and Bird, A. J. (2014) Zinc'ing sensibly: controlling zinc homeostasis at the transcriptional level, *Metallomics 6*, 1198-1215.
31. Haase, H., and Rink, L. (2014) Multiple impacts of zinc on immune function, *Metallomics 6*, 1175-1180.
32. Dauter, Z., Wilson, K. S., Sieker, L. C., Moulis, J.-M., and Meyer, J. (1996) Zinc-and iron-rubredoxins from Clostridium pasteurianum at atomic resolution: a high-precision model of a ZnS4 coordination unit in a protein, *Proc. Natl. Acad. Sci. U. S. A. 93*, 8836-8840.
33. Romier, C., Reuter, K., Suck, D., and Ficner, R. (1996) Crystal structure of tRNA-guanine transglycosylase: RNA modification by base exchange, *EMBO J. 15*, 2850.
34. Lee, M. S., Gippert, G. P., Soman, K. V., Case, D. A., and Wright, P. E. (1989) Three-dimensional solution structure of a single zinc finger DNA-binding domain, *Science 245*, 635-637.
35. Håkansson, K., Carlsson, M., Svensson, L. A., and Liljas, A. (1992) Structure of native and apo carbonic anhydrase II and structure of some of its anion-ligand complexes, *J. Mol. Biol. 227*, 1192-1204.
36. Lebioda, L., and Stec, B. (1989) Crystal structure of holoenolase refined at 1.9 Å resolution: Trigonal-bipyramidal geometry of the cation binding site, *J. Am. Chem. Soc. 111*, 8511-8513.
37. Vallee, B. L., and Galdes, A. (1984) The metallobiochemistry of zinc enzymes, *Adv. Enzymol. Relat. Areas Mol. Biol. 56*, 283-430.
38. Maren, T. H. (1967) Carbonic anhydrase: chemistry, physiology, and inhibition, *Physiol. Rev. 47*, 595-781.
39. Lindskog, S. (1997) Structure and mechanism of carbonic anhydrase, *Pharmacol. Ther. 74*, 1-20.
40. Silverstein, E., and Boyer, P. (1964) Equilibrium reaction rates and the mechanisms of liver and yeast alcohol dehydrogenase, *J. Biol. Chem. 239*, 3908-3914.
41. Cook, P. F., Oppenheimer, N. J., and Cleland, W. (1981) Secondary deuterium and nitrogen-15 isotope effects in enzyme-catalyzed reactions. Chemical mechanism of liver alcohol dehydrogenase, *Biochemistry 20*, 1817-1825.
42. Pavletich, N. P., and Pabo, C. O. (1991) Zinc finger-DNA recognition: crystal structure of a Zif268-DNA complex at 2.1 A, *Science 252*, 809-817.
43. Waldron, K. J., Rutherford, J. C., Ford, D., and Robinson, N. J. (2009) Metalloproteins and metal sensing, *Nature 460*, 823-830.
44. Outten, C. E., and O'Halloran, T. V. (2001) Femtomolar sensitivity of metalloregulatory proteins controlling zinc homeostasis, *Science 292*, 2488-2492.

www.manaraa.com

45. Krężel, A., and Maret, W. (2006) Zinc-buffering capacity of a eukaryotic cell at physiological pZn, *J. Biol. Inorg. Chem. 11*, 1049-1062.
46. Maret, W., and Li, Y. (2009) Coordination dynamics of zinc in proteins, *Chem. Rev. 109*, 4682-4707.
47. Colvin, R. A., Holmes, W. R., Fontaine, C. P., and Maret, W. (2010) Cytosolic zinc buffering and muffling: their role in intracellular zinc homeostasis, *Metallomics 2*, 306-317.
48. Bozym, R. A., Thompson, R. B., Stoddard, A. K., and Fierke, C. A. (2006) Measuring picomolar intracellular exchangeable zinc in PC-12 cells using a ratiometric fluorescence biosensor, *ACS Chem. Biol. 1*, 103-111.
49. Vinkenborg, J. L., Nicolson, T. J., Bellomo, E. A., Koay, M. S., Rutter, G. A., and Merkx, M. (2009) Genetically encoded FRET sensors to monitor intracellular Zn2+ homeostasis, *Nat. Meth. 6*, 737-740.
50. Zalewska, M., Trefon, J., and Milnerowicz, H. (2014) The role of metallothionein interactions with other proteins, *Proteomics 14*, 1343-1356.
51. Pinter, T. B., and Stillman, M. J. (2014) The Zinc Balance: Competitive Zinc Metalation of Carbonic Anhydrase and Metallothionein 1A, *Biochemistry 53*, 6276-6285.
52. Krężel, A., and Maret, W. (2007) Dual nanomolar and picomolar Zn (II) binding properties of metallothionein, *J. Am. Chem. Soc. 129*, 10911-10921.
53. Summers, K. L., Sutherland, D. E. K., and Stillman, M. J. (2013) Single-domain metallothioneins: Evidence of the onset of clustered metal binding domains in Zn-rhMT 1a, *Biochemistry 52*, 2461-2471.
54. Jiang, L.-J., Maret, W., and Vallee, B. L. (1998) The glutathione redox couple modulates zinc transfer from metallothionein to zinc-depleted sorbitol dehydrogenase, *Proc. Natl. Acad. Sci. U. S. A. 95*, 3483-3488.
55. Feng, W., Cai, J., Pierce, W. M., Franklin, R. B., Maret, W., Benz, F. W., and Kang, Y. J. (2005) Metallothionein transfers zinc to mitochondrial aconitase through a direct interaction in mouse hearts, *Biochem. Biophys. Res. Commun. 332*, 853-858.
56. Udom, A. O., and Brady, F. O. (1980) Reactivation in vitro of zinc-requiring apo-enzymes by rat liver zinc-thionein, *Biochem. J. 187*, 329-335.
57. Mason, A. Z., Moeller, R., Thrippleton, K. A., and Lloyd, D. (2007) Use of stable isotopically enriched proteins and directly coupled high-performance liquid chromatography inductively coupled plasma mass spectrometry for quantitatively monitoring the transfer of metals between proteins, *Anal. Biochem. 369*, 87-104.
58. Jacob, C., Maret, W., and Vallee, B. L. (1998) Control of zinc transfer between thionein, metallothionein, and zinc proteins, *Proc. Natl. Acad. Sci. U. S. A. 95*, 3489-3494.
59. Zaia, J., Fabris, D., Wei, D., Karpel, R. L., and Fenselau, C. (1998) Monitoring metal ion flux in reactions of metallothionein and drug-modified metallothionein by electrospray mass spectrometry, *Protein Sci. 7*, 2398-2404.
60. Ejnik, J., Muñoz, A., Gan, T., Shaw III, C. F., and Petering, D. (1999) Interprotein metal ion exchange between cadmium-carbonic anhydrase and apo-or zinc-metallothionein, *J. Biol. Inorg. Chem. 4*, 784-790.
61. Maret, W., Larsen, K. S., and Vallee, B. L. (1997) Coordination dynamics of biological zinc “clusters” in metallothioneins and in the DNA-binding domain of the transcription factor Gal4, *Proc. Natl. Acad. Sci. U. S. A. 94*, 2233-2237.
62. Méplan, C., Richard, M.-J., and Hainaut, P. (2000) Metalloregulation of the tumor suppressor protein p53: zinc mediates the renaturation of p53 after exposure to metal chelators in vitro and in intact cells, *Oncogene 19*, 5227-5236.

www.manaraa.com

63. Ostrakhovitch, E. A., Olsson, P.-E., Jiang, S., and Cherian, M. G. (2006) Interaction of metallothionein with tumor suppressor p53 protein, *FEBS Lett. 580*, 1235-1238.
64. Abdel-Mageed, A. B., and Agrawal, K. C. (1998) Activation of nuclear factor κB: potential role in metallothionein-mediated mitogenic response, *Cancer Res. 58*, 2335-2338.
65. Posewitz, M. C., and Wilcox, D. E. (1995) Properties of the Sp1 zinc finger 3 peptide: coordination chemistry, redox reactions, and metal binding competition with metallothionein, *Chem. Res. Toxicol. 8*, 1020-1028.
66. Huang, M., Shaw III, C. F., and Petering, D. H. (2004) Interprotein metal exchange between transcription factor IIIa and apo-metallothionein, *J. Inorg. Biochem. 98*, 639-648.
67. Zeng, J., Vallee, B. L., and Kägi, J. (1991) Zinc transfer from transcription factor IIIA fingers to thionein clusters, *Proc. Natl. Acad. Sci. U. S. A. 88*, 9984-9988.
68. Roesijadi, G., Bogumil, R., Vasák, M., and Kägi, J. H. (1998) Modulation of DNA binding of a tramtrack zinc finger peptide by the metallothionein-thionein conjugate pair, *J. Biol. Chem. 273*, 17425-17432.
69. Ecker, D. J., Butt, T., Sternberg, E., Neeper, M., Debouck, C., Gorman, J., and Crooke, S. (1986) Yeast metallothionein function in metal ion detoxification, *J. Biol. Chem. 261*, 16895-16900.
70. Stuart, G. W., Searle, P. F., Chen, H. Y., Brinster, R. L., and Palmiter, R. D. (1984) A 12-base-pair DNA motif that is repeated several times in metallothionein gene promoters confers metal regulation to a heterologous gene, *Proc. Natl. Acad. Sci. U. S. A. 81*, 7318-7322.
71. Bonneton, F., Théodore, L., Silar, P., Maroni, G., and Wegnez, M. (1996) Response of Drosophila metallothionein promoters to metallic, heat shock and oxidative stresses, *FEBS Lett. 380*, 33-38.
72. Andrews, G. K. (2000) Regulation of metallothionein gene expression by oxidative stress and metal ions, *Biochem. Pharmacol. 59*, 95-104.
73. Kelly, E. J., Quaife, C. J., Froelick, G. J., and Palmiter, R. D. (1996) Metallothionein I and II protect against zinc deficiency and zinc toxicity in mice, *J. Nutr. 126*, 1782.
74. Cai, L., Li, X.-K., Song, Y., and Cherian, M. G. (2005) Essentiality, toxicology and chelation therapy of zinc and copper, *Curr. Med. Chem. 12*, 2753-2763.
75. Leber, A. P., and Miya, T. S. (1976) A mechanism for cadmium-and zinc-induced tolerance to cadmium toxicity: Involvement of metallothionein, *Toxicol. Appl. Pharmacol. 37*, 403-414.
76. Albores, A., Koropatnick, J., Cherian, M. G., and Zelazowski, A. J. (1992) Arsenic induces and enhances rat hepatic metallothionein production in vivo, *Chem-Biol. Interact. 85*, 127-140.
77. Qu, W., Diwan, B. A., Liu, J., Goyer, R. A., Dawson, T., Horton, J. L., Cherian, M. G., and Waalkes, M. P. (2002) The metallothionein-null phenotype is associated with heightened sensitivity to lead toxicity and an inability to form inclusion bodies, *Am. J. Pathol. 160*, 1047-1056.
78. Funk, A. E., Day, F. A., and Brady, F. O. (1987) Displacement of zinc and copper from copper-induced metallothionein by cadmium and by mercury: in vivo and ex vivo studies, *Comp. Biochem. Physiol. C Pharmacol. Toxicol. Endocrinol. 86*, 1-6.
79. Piotrowski, J., Trojanowska, B., Wiśniewska-Knypl, J., and Bolanowska, W. (1974) Mercury binding in the kidney and liver of rats repeatedly exposed to mercuric chloride: Induction of metallothionein by mercury and cadmium, *Toxicol. Appl. Pharmacol. 27*, 11-19.

www.manaraa.com

80. Nielson, K. B., Atkin, C., and Winge, D. (1985) Distinct metal-binding configurations in metallothionein, *J. Biol. Chem. 260*, 5342-5350.
81. Chan, H. M., Zhu, L.-F., Zhong, R., Grant, D., Goyer, R., and Cherian, M. (1993) Nephrotoxicity in rats following liver transplantation from cadmium-exposed rats, *Toxicol. Appl. Pharmacol. 123*, 89-96.
82. Masters, B. A., Kelly, E. J., Quaife, C. J., Brinster, R. L., and Palmiter, R. D. (1994) Targeted disruption of metallothionein I and II genes increases sensitivity to cadmium, *Proc. Natl. Acad. Sci. U. S. A. 91*, 584-588.
83. Liu, J., Liu, Y., Habeebu, S. S., and Klaassen, C. D. (1998) Susceptibility of MT-null mice to chronic CdCl2-induced nephrotoxicity indicates that renal injury is not mediated by the CdMT complex, *Toxicol. Sci. 46*, 197-203.
84. Park, J. D., Liu, Y., and Klaassen, C. D. (2001) Protective effect of metallothionein against the toxicity of cadmium and other metals, *Toxicology 163*, 93-100.
85. Satarug, S., and Moore, M. R. (2004) Adverse health effects of chronic exposure to low-level cadmium in foodstuffs and cigarette smoke, *Environ. Health Perspect. 112*, 1099.
86. Pinot, F., Kreps, S. E., Bachelet, M., Hainaut, P., Bakonyi, M., and Polla, B. S. (2000) Cadmium in the environment: sources, mechanisms of biotoxicity, and biomarkers, *Rev. Environ. Health 15*, 299-324.
87. Suwazono, Y., Kido, T., Nakagawa, H., Nishijo, M., Honda, R., Kobayashi, E., Dochi, M., and Nogawa, K. (2009) Biological half-life of cadmium in the urine of inhabitants after cessation of cadmium exposure, *Biomarkers 14*, 77-81.
88. Klaassen, C. D., Liu, J., and Diwan, B. A. (2009) Metallothionein protection of cadmium toxicity, *Toxicol. Appl. Pharmacol. 238*, 215-220.
89. Li, Y., and Maret, W. (2008) Human metallothionein metallomics, *J. Anal. At. Spectrom. 23*, 1055-1062.
90. Cherian, M. G., Jayasurya, A., and Bay, B.-H. (2003) Metallothioneins in human tumors and potential roles in carcinogenesis, *Mutat. Res., Fundam. Mol. Mech. Mutagen. 533*, 201-209.
91. Thirumoorthy, N., Shyam Sunder, A., Manisenthil Kumar, K. T., Senthil Kumar, M., Ganesh, G. N. K., and Chatterjee, M. (2011) A review of metallothionein isoforms and their role in pathophysiology, *World J. Surg. Oncol. 9*, 1-7.
92. Romero-Isart, N., and Vašák, M. (2002) Advances in the structure and chemistry of metallothioneins, *J. Inorg. Biochem. 88*, 388-396.
93. Vašák, M., and Hasler, D. W. (2000) Metallothioneins: new functional and structural insights, *Curr. Opin. Chem. Biol. 4*, 177-183.
94. Furey, W., Robbins, A., Clancy, L., Winge, D., Wang, B., and Stout, C. (1986) Crystal structure of Cd, Zn metallothionein, *Science 231*, 704-710.
95. Robbins, A., McRee, D., Williamson, M., Collett, S., Xuong, N., Furey, W., Wang, B., and Stout, C. (1991) Refined crystal structure of Cd, Zn metallothionein at 2.0 Å resolution, *J. Mol. Biol. 221*, 1269-1293.
96. Braun, W., Vasak, M., Robbins, A., Stout, C., Wagner, G., Kägi, J., and Wüthrich, K. (1992) Comparison of the NMR solution structure and the X-ray crystal structure of rat metallothionein-2, *Proc. Natl. Acad. Sci. U. S. A. 89*, 10124-10128.
97. Jiang, L.-J., Vašák, M., Vallee, B. L., and Maret, W. (2000) Zinc transfer potentials of the α-and β-clusters of metallothionein are affected by domain interactions in the whole molecule, *Proc. Natl. Acad. Sci. U. S. A. 97*, 2503-2508.

www.manaraa.com

98. Blindauer, C. A., and Leszczyszyn, O. I. (2010) Metallothioneins: Unparalleled diversity in structures and functions for metal ion homeostasis and more, *Nat. Prod. Rep. 27*, 720-741.
99. Summers, K. L., Mahrok, A. K., Dryden, M. D., and Stillman, M. J. (2012) Structural properties of metal-free apometallothioneins, *Biochem. Biophys. Res. Commun. 425*, 485-492.
100. Hong, S.-H., Hao, Q., and Maret, W. (2005) Domain-specific fluorescence resonance energy transfer (FRET) sensors of metallothionein/thionein, *Protein Eng., Des. Sel. 18*, 255-263.
101. Ejnik, J., Robinson, J., Zhu, J., Försterling, H., Shaw, C. F., and Petering, D. H. (2002) Folding pathway of apo-metallothionein induced by Zn^{2+}, Cd^{2+} and Co^{2+}, *J. Inorg. Biochem. 88*, 144-152.
102. Duncan, K. E. R., and Stillman, M. J. (2006) Metal-dependent protein folding: metallation of metallothionein, *J. Inorg. Biochem. 100*, 2101-2107.
103. Rigby, K. E., Chan, J., Mackie, J., and Stillman, M. J. (2006) Molecular dynamics study on the folding and metallation of the individual domains of metallothionein, *Proteins: Struct., Funct., Bioinf. 62*, 159-172.
104. Vasak, M., Kaegi, J. H., and Hill, H. A. O. (1981) Zinc (II), cadmium (II), and mercury (II) thiolate transitions in metallothionein, *Biochemistry 20*, 2852-2856.
105. Duncan, R., Kelly, E., and Stillman, M. J. (2007) Evidence for noncooperative metal binding to the α domain of human metallothionein, *FEBS J. 274*, 2253-2261.
106. Stillman, M. J., and Szymanska, J. A. (1984) Absorption, circular dichroism, magnetic circular dichroism and emission study of rat kidney Cd, Cu-metallothionein, *Biophys. Chem. 19*, 163-169.
107. Stillman, M. J., and Zelazowski, A. (1988) Domain specificity in metal binding to metallothionein. A circular dichroism and magnetic circular dichroism study of cadmium and zinc binding at temperature extremes, *J. Biol. Chem. 263*, 6128-6133.
108. Weser, U., Rupp, H., Donay, F., Linnemann, F., Voelter, W., Voetsch, W., and Jung, G. (1973) Characterization of Cd, Zn-thionein (metallothionein) isolated from rat and chicken liver, *Eur. J. Biochem. 39*, 127-140.
109. Willner, H., Vasak, M., and Kaegi, J. H. (1987) Cadmium-thiolate clusters in metallothionein: spectrophotometric and spectropolarimetric features, *Biochemistry 26*, 6287-6292.
110. Freisinger, E., and Vašák, M. (2013) Cadmium in metallothioneins, In *Cadmium: From Toxicity to Essentiality*, pp 339-371, Springer.
111. Gehrig, P. M., You, C., Dallinger, R., Gruber, C., Brouwer, M., Kägi, J. H. R., and Hunziker, P. E. (2000) Electrospray ionization mass spectrometry of zinc, cadmium, and copper metallothioneins: evidence for metal-binding cooperativity, *Protein Sci. 9*, 395-402.
112. Fenn, J. B., Mann, M., Meng, C. K., Wong, S. F., and Whitehouse, C. M. (1989) Electrospray ionization for mass spectrometry of large biomolecules, *Science 246*, 64-71.
113. Loo, J. A. (2000) Electrospray ionization mass spectrometry: a technology for studying noncovalent macromolecular complexes, *Int. J. Mass Spectrom. 200*, 175-186.
114. Felitsyn, N., Peschke, M., and Kebarle, P. (2002) Origin and number of charges observed on multiply-protonated native proteins produced by ESI, *Int. J. Mass Spectrom. 219*, 39-62.
115. Kebarle, P., and Verkerk, U. H. (2009) Electrospray: from ions in solution to ions in the gas phase, what we know now, *Mass Spectrom. Rev. 28*, 898-917.

www.manaraa.com

116. Sutherland, D. E., and Stillman, M. J. (2008) Noncooperative cadmium (II) binding to human metallothionein 1a, *Biochem. Biophys. Res. Commun. 372*, 840-844.
117. Yu, X., Wojciechowski, M., and Fenselau, C. (1993) Assessment of metals in reconstituted metallothioneins by electrospray mass spectrometry, *Anal. Chem. 65*, 1355-1359.
118. Heinz, U., Kiefer, M., Tholey, A., and Adolph, H.-W. (2005) On the competition for available zinc, *J. Biol. Chem. 280*, 3197-3207.
119. Perutz, M. F. (1989) Mechanisms of cooperativity and allosteric regulation in proteins, *Q. Rev. Biophys. 22*, 139-237.
120. Lee, A., and Karplus, M. (1983) Structure-specific model of hemoglobin cooperativity, *Proc. Natl. Acad. Sci. U. S. A. 80*, 7055-7059.
121. Ngu, T. T., and Stillman, M. J. (2006) Arsenic binding to human metallothionein, *J. Am. Chem. Soc. 128*, 12473-12483.
122. Ngu, T. T., Easton, A., and Stillman, M. J. (2008) Kinetic analysis of arsenic-metalation of human metallothionein: Significance of the two-domain structure, *J. Am. Chem. Soc. 130*, 17016-17028.
123. Ngu, T. T., Lee, J. A., Pinter, T. B., and Stillman, M. J. (2010) Arsenic-metalation of triple-domain human metallothioneins: Support for the evolutionary advantage and interdomain metalation of multiple-metal-binding domains, *J. Inorg. Biochem. 104*, 232-244.
124. Sutherland, D. E., Summers, K. L., and Stillman, M. J. (2012) Noncooperative metalation of metallothionein 1a and its isolated domains with zinc, *Biochemistry 51*, 6690-6700.
125. Palumaa, P., Eriste, E., Njunkova, O., Pokras, L., Jörnvall, H., and Sillard, R. (2002) Brain-specific metallothionein-3 has higher metal-binding capacity than ubiquitous metallothioneins and binds metals noncooperatively, *Biochemistry 41*, 6158-6163.
126. Byrd, J., and Winge, D. R. (1986) Cooperative cluster formation in metallothionein, *Arch. Biochem. Biophys. 250*, 233-237.
127. Loebus, J., Peroza, E. A., Blüthgen, N., Fox, T., Meyer-Klaucke, W., Zerbe, O., and Freisinger, E. (2011) Protein and metal cluster structure of the wheat metallothionein domain γ-Ec-1: the second part of the puzzle, *J. Biol. Inorg. Chem. 16*, 683-694.
128. Stillman, M., Cai, W., and Zelazowski, A. (1987) Cadmium binding to metallothioneins. Domain specificity in reactions of alpha and beta fragments, apometallothionein, and zinc metallothionein with Cd^{2+}, *J. Biol. Chem. 262*, 4538-4548.
129. Good, M., Hollenstein, R., Sadler, P. J., and Vasak, M. (1988) Cadmium-113 NMR studies on metal-thiolate cluster formation in rabbit cadmium (II) metallothionein: evidence for a pH dependence, *Biochemistry 27*, 7163-7166.
130. Chen, S.-H., Russell, W. K., and Russell, D. H. (2013) Combining chemical labeling, bottom-up and top-down ion-mobility mass spectrometry to identify metal-binding sites of partially metalated metallothionein, *Anal. Chem. 85*, 3229-3237.
131. Chen, S.-H., Chen, L., and Russell, D. H. (2014) Metal-induced conformational changes of human metallothionein-2A: A combined theoretical and experimental study of metal-free and partially metalated intermediates, *J. Am. Chem. Soc. 136*, 9499-9508.
132. Vasak, M., and Kägi, J. (1983) Spectroscopic properties of metallothionein, *Met. Ions Biol. Syst. 15*, 213-273.
133. Kägi, J. H. R. (1993) Evolution, structure, and chemical activity of class I metallothioneins: An overview, In *Metallothionein* (Suzuki, K. T., Imura, N., and Kimura, M., Eds.), pp 29-55, Birkhäuser Verlag, Basel Switzerland.

www.manaraa.com

134. Margoshes, M., and Vallee, B. L. (1957) A cadmium protein from equine kidney cortex, *J. Am. Chem. Soc. 79*, 4813-4814.
135. Capdevila, M., and Atrian, S. (2011) Metallothionein protein evolution: a miniassay, *J. Biol. Inorg. Chem. 16*, 977-989.
136. Namdarghanbari, M. A., Meeusen, J., Bachowski, G., Giebel, N., Johnson, J., and Petering, D. H. (2010) Reaction of the zinc sensor FluoZin-3 with Zn 7-metallothionein: inquiry into the existence of a proposed weak binding site, *J. Inorg. Biochem. 104*, 224-231.

www.manaraa.com

Chapter 2

2 The zinc balance: Competitive zinc metallation of carbonic anhydrase and metallothionein 1A*

2.1 Introduction

Zinc is the most abundant metal cofactor found in metal-dependent enzymes with nearly a quarter of identified metalloproteins containing one or more zinc ions.[1, 2] Despite this ubiquity, free zinc levels are tightly controlled.[3, 4] The homeostatic intracellular concentration of free zinc is buffered within a narrow range using myriad zinc specific sensors, importers, exporters, and chaperones.[5-7] These complex systems work together to not only maintain control of the transport and storage of zinc,[8, 9] but also to deliver and insert zinc ions into newly synthesized zinc enzymes.[10-12] When this careful balance of zinc is disturbed, a large number of health complications arise.[13-15] Zinc is also a transcription cofactor and has important roles in cell signaling, development, and proper cellular function.[16, 17]

Metallothionein (MT) is a ubiquitous family of metal-binding proteins that are critical to the homeostatic control of cellular zinc (and other metal) levels. MT has been implicated in toxic metal detoxification, oxidative stress response, and essential metal homeostasis.[18, 19] It is capable of binding multiple metals using the relatively high number of cysteine residues for its small size. There are four known human MT isoforms: the more common MT1 and MT2 are predominantly expressed in the liver and kidneys, but are also expressed in numerous tissues and cell types; MT3 and MT4 are minor isoforms specifically expressed in specialized tissues such as the brain and epithelial cells respectively.[20] Numerous MT1 subisoforms have also been identified. MT1 and MT2 are associated with binding both zinc and cadmium *in vivo*.

---

*A version of this chapter has been published:

Reproduced with permission from: T.B.J. Pinter, and M.J. Stillman. *Biochemistry* 53 (2014): 6276-6285. Copyright 2014 American Chemical Society.

www.manaraa.com

Human MTs bind up to seven zinc ions in tetrahedral ($ZnS_{4(CYS)}$) clusters using 20 cysteines. The fully zinc-saturated Zn_7hMT1A binds the zinc in two distinct domains.[21] The N-terminal beta domain binds three zinc ions using nine cysteines and the C-terminal alpha domain binds four zinc ions using 11 cysteines. There are numerous studies on the structure and properties of fully saturated MT's but little information on the important partially metallated species.[22-24] Of particular interest is the relevance of these species to the donation of zinc from MT to zinc-dependent apoenzymes.

MT has been identified as a key player in zinc homeostasis and interacts with numerous metalloproteins.[25] Critical to the *in vivo* functions of MT species is the zinc occupancy of the available metal binding sites. The ability of MT to act as both a zinc donor and acceptor depends on the intracellular zinc (and MT) concentration in the cell. Zn_7MT has been shown to act as a zinc donor to numerous zinc-dependent enzymes, while apoMT is capable of removing and accepting zinc from holo-Zn enzymes.[26, 27]

With respect to the role of MT in donating Zn to enzymes, very little has been reported on the mechanistic detail of these important reactions. However, the property of MT acting as a zinc chaperone in the acquisition of free metals and the subsequent release of zinc to metalloenzymes has been previously investigated.[28-33] Carbonic anhydrase has been shown to accept donation of a single zinc ion from zinc-saturated MTs at rates and concentrations that support *in vivo* zinc donation as a function of MT.[32] These studies have shown that fully saturated Zn-MT is capable of donating zinc to the apoenzymes, but the important mechanistic details are not understood.

Carbonic anhydrase (CA), the first discovered metalloenzyme, binds a single zinc ion in its active site using three histidine ligands. CA binds zinc relatively strongly[34] with an apparent stability constant ($\log(K_F)$) of approximately 11.4 at pH 7.[35] Following *de novo* protein synthesis, apocarbonic anhydrase must acquire and insert the enzymatically necessary zinc ion into the active site. However, the estimated femtomolar[4] to picomolar[36] pool of "free zinc" is an inadequate zinc source for metalloenzymes to metallate within a suitable time frame[37] and thus, the majority of the zinc must be acquired from zinc chaperones, of which Zn-MT is one example. *In vivo*, numerous zinc

www.manaraa.com

sources, chaperones, and enzymes will be in constant competition for the limited amount of zinc within the cell. The range of zinc binding stability constants reported for zinc importers and exporters provides an approximation of the relative range over which zinc is buffered within the cytoplasm. Though exact values are currently not known, there is evidence that zinc importation starts at picomolar concentrations.[38] Exportation of excess zinc is complicated by cellular processes that are designed to protect the cell from metal toxicity, but significant cellular disruptions arise when cells are treated with zinc above 30-100 μM.[39] The K_F values for MT1A zinc binding, as determined by MT-MT competition, apparently fall within the buffering range of functional cells.[40, 41]

Studies by numerous groups have shown that Zn_7MT transfers a single zinc ion to CA.[26-28] Zn_7MT and apoMT have been shown to exchange metals with cadmium substituted CA, hypothesized through a protein-protein interaction.[42] However, little is known about the interactions between the apo or partially metallated MT and the apoCA. Since MT exists in a number of partially metallated states,[43] a complete understanding of these interactions is critical to determine the exact mechanistic details of the vitally important metallation reaction of CA.

Recently, the Stillman group has reported data[44, 45] addressing possible binding motifs for the partially metallated recombinant human MT1A (rhMT1A), but no experimental data have been reported that specifically describe the mechanism for zinc transfers from these partially metallated MTs. The conclusion from the binding motif studies was that a beaded five zinc structure formed initially; further zinc resulted in the development of a clustered two-domain structure containing the full complement of seven zinc ions. The consequence of this result was that the last two zinc ions bound with lower binding constants, and it was suggested that these two zinc ions would be accessible for donation to apoenzymes.[46]

In this Chapter, the zinc titration of rhMT1A in the presence of carbonic anhydrase is reported. Apocarbonic anhydrase, which remains folded following loss of zinc,[47] acts as a putative model for understanding the homeostatic control of zinc with respect to the metallation of zinc enzymes. The metallation status of CA and rhMT1A during a

www.manaraa.com

competitive titration with zinc is reported and the relative stability constants for each of the seven independent MT-bound zinc ions is determined with respect to the single zinc stability constant for CA. The data indicate that CA outcompetes rhMT1A for the three weakest bound zinc ions and shows little competition for the first four zinc bound by rhMT1A. Finally, the homeostatic control of zinc concentrations is discussed in relation to the suitability of MTs to act as a zinc reservoir for apo zinc-dependent enzymes.

2.2 Methods

2.2.1 Preparation of apoMT.

The rhMT1A was expressed and purified following previously reported methods, and detailed in Appendix A.[48] The MT sequence used in this study is based on the recombinant human MT1A sequence that consists of 72 residues: MGKAAAACSC ATGGSCTCTG SCKCKECKCN SCKKAAAACC SCCPMSCAKC AQGCVCKGAS EKCSCCKKAA AA. The corresponding DNA sequence was inserted as an N-terminal S-tag (for protein stability purposes) fusion protein into a pET29a plasmid and expressed in BL21(DE3) *E. coli* cells as Cd_7MT. All solutions were rigorously evacuated and argon-saturated to impede cysteine oxidation. Following protein purification, the S-tag was removed with a Thrombin CleanCleave Kit (Sigma). Concentrated HCl was used to adjust the pH to 2.7 before apoMT was separated from the cadmium using SEC on GE Sephadex G-25 size exclusion media using 5 mM formic acid pH 2.7 buffer as the eluent. The deoxygenated apoMT was simultaneously concentrated and buffer exchanged to pH 7.0 using Millipore Amicon Ultra-4 centrifuge filter units under argon (3 kDa MWCO).

2.2.2 Preparation of apoCA.

Bovine CA (Sigma) was first purified on a Sephadex G-50 gel filtration column with 5 mM pH 7.4 ammonium formate buffer as the eluent. The fractions containing only pure carbonic anhydrase 2 were pooled, and concentrated with 10 kDa MWCO Amicon centrifuge filter units. The zinc was removed from the CA through modification of methods previously reported.[49] An equal amount of 50 mM 2,6-pyridinedicarboxylic acid pH 6 (PDA) was added to the concentrated CA and spun down in the filter unit. The PDA zinc wash was repeated 6 times. To remove PDA from apoCA prior to MS experiments,

www.manaraa.com

the protein was exhaustively buffer exchanged to 5 mM ammonium formate pH 7.4 until neither PDA nor zinc were detected in the filtrate.

2.2.3 ESI-MS procedures.

Stock apo-rhMT1A concentrations were determined by remetallation of a small fraction of protein with Cd^{2+}; formation of Cd_7MT was monitored through the 250 nm thiolate-to-cadmium charge transfer band, $\varepsilon_{(250)}$ = 89,000 $M^{-1}cm^{-1}$. Stock apoCA concentrations were determined using $\varepsilon_{(280)}$ = 45,000 $M^{-1}cm^{-1}$. Zinc acetate stock (10 mM) was prepared in deionized water; all molar equivalents of zinc were determined through atomic absorption spectroscopy. Equal concentrations of both stock apoproteins were mixed in a vial and equivalents of zinc were added under argon atmosphere and allowed to equilibrate for a minimum of 3 min between addition and data collection; separate samples were left for up to 1 h (data not shown), and there was no change in zinc distribution with longer incubation times. ESI mass spectral data were collected on a Bruker Micro-TOF II (Bruker Daltonics, Toronto, ON) operated in the positive ion mode calibrated with NaI. Settings: scan = 500-4000 m/z; rolling average = 2; nebulizer = 2 bar; dry gas = 80°C @ 6.0 L/min; capillary = 4000 V; end plate offset = -500 V; capillary exit = 175 V; Skimmer 1 = 30.0 V; Skimmer 2 = 23.5 V; Hexapole RF = 800 V. The spectra were collected for a minimum of 2 min and deconvoluted using Maximum Entropy of the Bruker Compass DataAnalysis software package. All titrations were performed in at least triplicate to ensure accuracy and reproducibility of results.

2.3 Results

2.3.1 Mass spectral data for the competition between apoMT and apoCA for added zinc

Figure 2.1 shows a selection of the deconvoluted mass spectral data recorded during a competitive zinc titration to a solution containing equal concentrations of apo-rhMT1A and apoCA. The deconvoluted data shown here were calculated from the charge state spectra in Figure B-1 (Appendix B). Figure 2.1 shows the formation of the fully metallated Zn_7MT and ZnCA (F) as a function of six representative steps of the titration (A – E).

www.manaraa.com

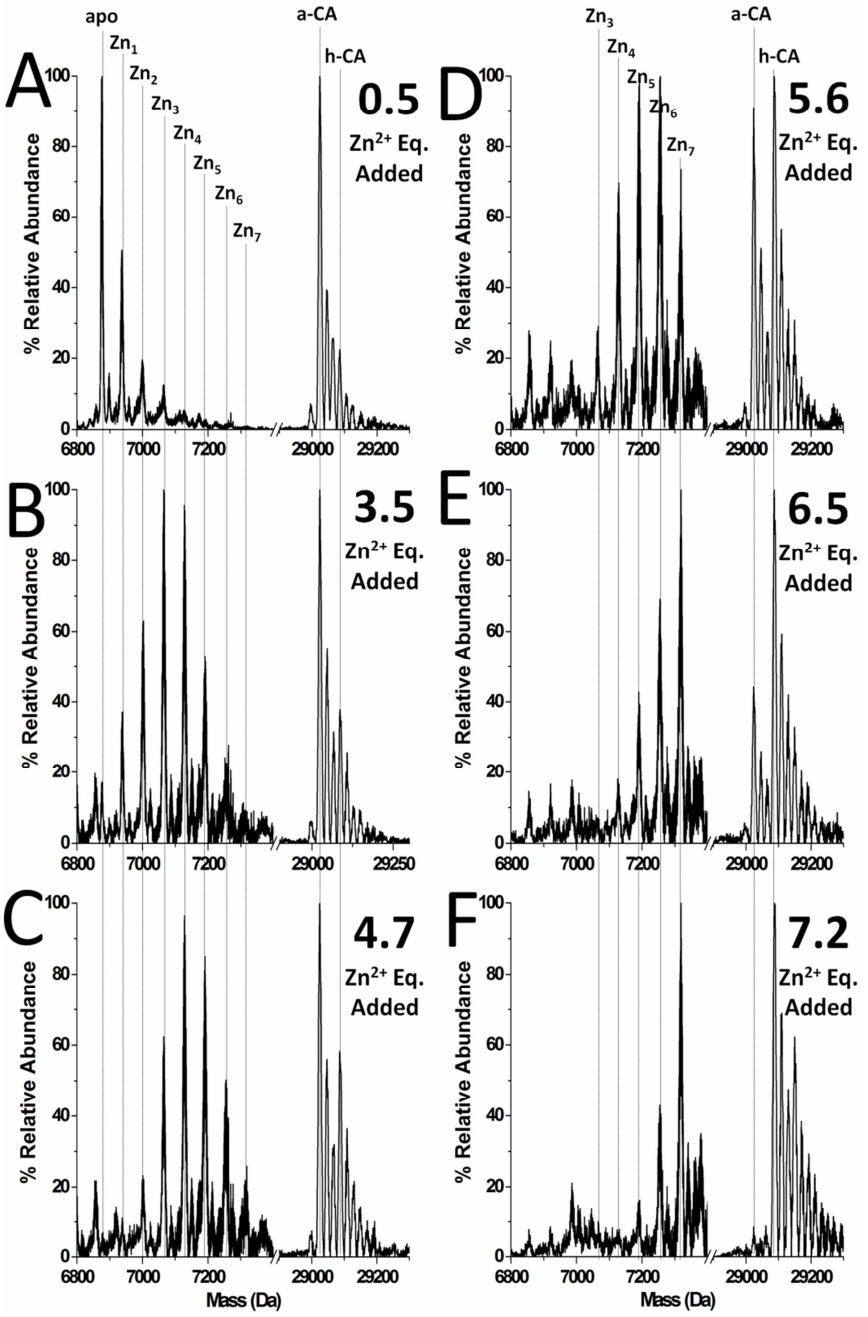

Figure 2.1: Deconvoluted ESI mass spectral data recorded for the equimolar competitive titration of apoCA and apo-rhMT at pH 6.8. The apo-proteins were mixed to a final concentration of 30 µM under argon and zinc (1 mM in diH_2O) and were aliquoted to the combined protein solutions. The zinc speciation of the MT and CA is highlighted with vertical gray lines. The mass range for each species has been normalized to 100% relative abundance.

www.manaraa.com

The abundance of each species was plotted relative to the most abundant species of the protein: apoMT and apoCA in Figure 2.1A, and Zn_7MT and holoCA in Figure 2.1F. Zinc equivalents were determined from the concentration of the two proteins and AAS measurements of the zinc solution. These equivalents refer to a ratio such that one zinc equivalent would fill a single zinc binding site. Therefore, eight zinc equivalents (seven for MT and one for CA) are required to fill all the sites, completing the titration.

The relative concentrations of each metallated species were plotted in Figure 2.2 as a function of the equivalents of zinc added stepwise. The individual zinc metallated species were extracted from the mass spectral data. Figure 2.2A shows the experimental data for the eight rhMT1A species (apoMT to Zn_7MT). Figure 2.2B shows the corresponding experimental data for apoCA and ZnCA, as a function of the equivalents of zinc added. The CA was 50% metallated when 6 equiv of zinc was added. The change in the zinc binding efficiency of apoCA is shown in Figure 2.2C as the first derivative (d[apoCA]/d[Zn Added]) of the metallation of the apoCA line shown in Figure 2.2B. The significance of the data representations in Figure 2.2C will be discussed in Section 2.4.

2.3.2 Modelling the competition reaction

In order to determine the zinc binding affinity for each of the rhMT1A species, the metallation state at each specific zinc loading was simulated from a model that minimized the root mean square difference between the experimental and a theoretical data set determined by the 8 binding constants. The model was based on seven sequential bimolecular reactions that resulted in the formation of Zn_7MT from apoMT and the competitive reaction of apoCA forming ZnCA. The relative concentrations of each species depend on the relative binding constants (K_{MT1-7} and K_{CA1}).

www.manaraa.com

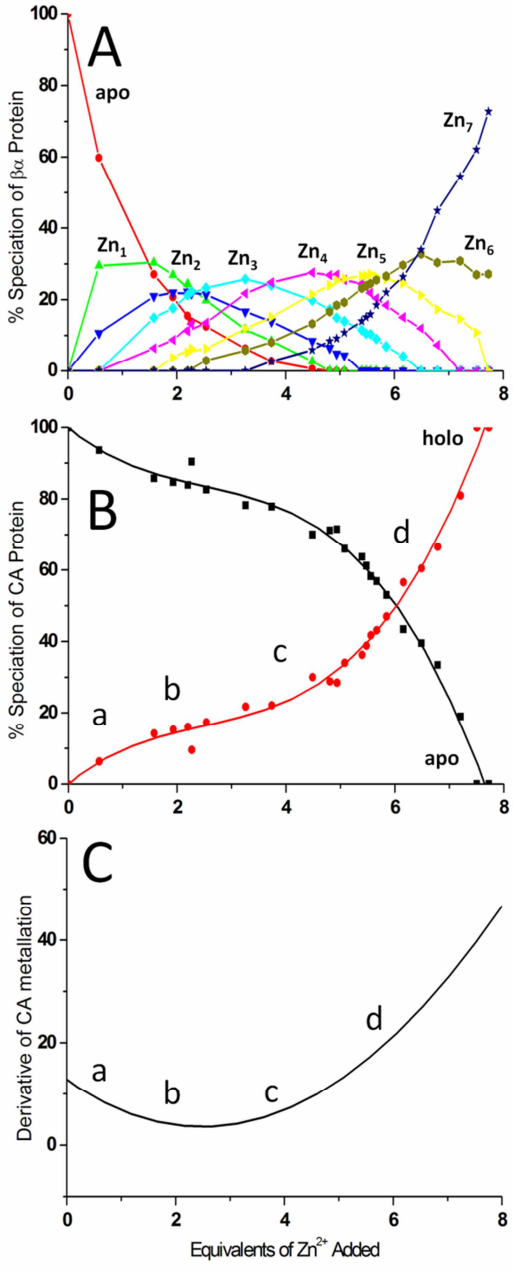

Figure 2.2: Experimentally determined zinc status of MT (A) and CA (B) during the stepwise competitive zinc metallation. Based on the ESI mass spectral data partially shown in Figure 2.1. Panel C shows the metallation efficiency of CA calculated as the first derivative (d[apoCA]/d[Zn^{2+} added]).

www.manaraa.com

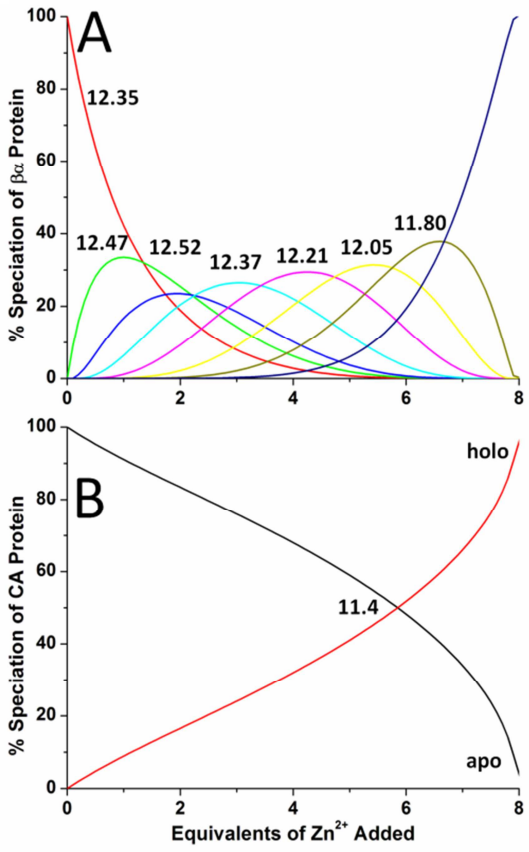

Figure 2.3: Simulation of the competitive zinc metallation of apoMT (A) in the presence of apoCA (B). The simulation uses $\log_{10}(K_F)$ values for the MT of 12.35, 12.47, 12.52, 12.37, 12.21, 12.05, and 11.80 for the seven sequential metallation events in the formation of Zn_7MT. These values were derived from extraction of the competition speciation of the MT versus the known $\log_{10}(K_F)$ of CA of 11.4.

Figure 2.3 shows a fit of the apo-rhMT1A and apoCA ESI mass spectral data using seven consecutive equilibrium binding constants for the apoMT coupled to the single metallation equilibrium for the apoCA. The simulated competition reaction used the following criteria: (i) the log K_F of CA is 11.4 under the conditions of the experiments,[35] and (ii) all reactions were coupled and reversible such that zinc could freely redistribute to the preferred occupancy. This model was used to simulate the speciation profiles shown in Figure 2.2 to allow direct assessment of the accuracy of the fits. The seven K_F values for MT zinc binding, determined by the model, which most closely fit the experimental data, were $\log[K_{F(1\text{-}7\ Zn)}]$: 12.35, 12.47, 12.52, 12.37, 12.21, 12.05, and 11.8.

www.manaraa.com

$$\text{Apo-}\beta\alpha\text{-rhMT} + Zn^{2+} \overset{K_1}{\rightleftharpoons} Zn_1\text{-}\beta\alpha\text{-rhMT} \quad \log(K_1) = 12.35$$

$$Zn_1\text{-}\beta\alpha\text{-rhMT} + Zn^{2+} \overset{K_2}{\rightleftharpoons} Zn_2\text{-}\beta\alpha\text{-rhMT} \quad \log(K_2) = 12.47$$

$$Zn_2\text{-}\beta\alpha\text{-rhMT} + Zn^{2+} \overset{K_3}{\rightleftharpoons} Zn_3\text{-}\beta\alpha\text{-rhMT} \quad \log(K_3) = 12.52$$

$$Zn_3\text{-}\beta\alpha\text{-rhMT} + Zn^{2+} \overset{K_4}{\rightleftharpoons} Zn_4\text{-}\beta\alpha\text{-rhMT} \quad \log(K_4) = 12.37$$

$$Zn_4\text{-}\beta\alpha\text{-rhMT} + Zn^{2+} \overset{K_5}{\rightleftharpoons} Zn_5\text{-}\beta\alpha\text{-rhMT} \quad \log(K_5) = 12.21$$

$$Zn_5\text{-}\beta\alpha\text{-rhMT} + Zn^{2+} \overset{K_6}{\rightleftharpoons} Zn_6\text{-}\beta\alpha\text{-rhMT} \quad \log(K_6) = 12.05$$

$$Zn_6\text{-}\beta\alpha\text{-rhMT} + Zn^{2+} \overset{K_7}{\rightleftharpoons} Zn_7\text{-}\beta\alpha\text{-rhMT} \quad \log(K_7) = 11.80$$

$$\text{ApoCA} + Zn^{2+} \overset{K_{CA}}{\rightleftharpoons} \text{holo-CA} \quad \log(K_{CA}) = 11.4$$

Scheme 2.1: The sequential metallation reactions for the competitive titration of zinc to apoMT and apoCA. The apparent stability constants for each sequential zinc addition to MT are indicated by $\log(K_n)$ (n = 1-7) and the apparent stability constant for zinc binding to apoCA is indicated by $\log(K_{CA})$.The seven $\log K_F$ values for MT are plotted in Figure 2.4A as a function of the MT zinc loading in order to compare the magnitudes of the zinc binding constants. While the first two constants are below the value of K_{MT3}, the values of K_{MT3} to K_{MT7} follow the expected linear decrease that results from the statistical reduction of available zinc binding sites.

In Figure 2.3A the stepwise metallation of rhMT1A proceeds through 6 distinct intermediates between apoMT and Zn_7MT. Figure 2.3B shows the simulated metallation of apoCA as a function of increasing concentration of zinc. There is very close alignment between the simulated data in Figure 2.3A and the experimental data in Figure 2.2A for the metallation of MT and between the simulated data of Figure 2.3B and the experimental data from Figure 2.2B for the metallation of CA. Figure B-2 (Appendix B) shows the overlaid model and experimental traces for assessment of the quality of the fit.

www.manaraa.com

Because the set of eight K values is determined in a single calculation, we have confidence that the K values determined in the model represent accurate values under the conditions of the experiment. It should be noted that the individual values of each Kn (n = 1-7) impact the quality of the fit for all other species since the equilibrium equations are coupled and successive while also being in competition with each other and the CA. The experimental error on all reported K values by the model is on the order of ±0.3 log units. An overlay of each individual species fit and experimental data is shown in Figure A-2 for comparison. It should be noted that since the model minimized the error and provided a fit for all 10 speciation traces (apo to Zn_7MT and apo and holoCA) simultaneously that not all the model traces exactly match the data; Zn_5- and Zn_6MT, for example, show some deviation between the model and experimental data.

2.3.3 Relative MT binding affinities are reflected in the raw data

Figure 2.4B shows the superimposition of the change in binding efficiency of apoCA as a function of the total zinc load inverted from Figure 2.2C (line) and the binding constants calculated for the seven zinc rhMT1A species (points) relative to the first K. This figure shows how the experimental data reflect directly the calculated K values for both MT and CA. The importance of this figure is that the precise trend in the value of K values that were calculated in the model from the raw experimental data of the metallation of CA is observed. These data are particularly important in confirming the increase in K_2 and K_3 for the metallation of MT.

Figure 2.5 shows the experimental (red) mass spectral data at representative zinc additions compared with the simulated (black) mass spectral data predicted by the model shown in Figure 2.3. Figure 2.5A-G show the experimentally determined relative abundance of seven zinc containing MT species from the full data set. Figure 2.5H-N show the predicted mass spectral data based on the model used in Figure 2.3 at these same zinc loadings. Figure 2.5 O-U show the experimental and predicted mass spectral data at the same zinc loading values for CA. Only the apo and holo species profiles are shown because CA binds a single zinc.

www.manaraa.com

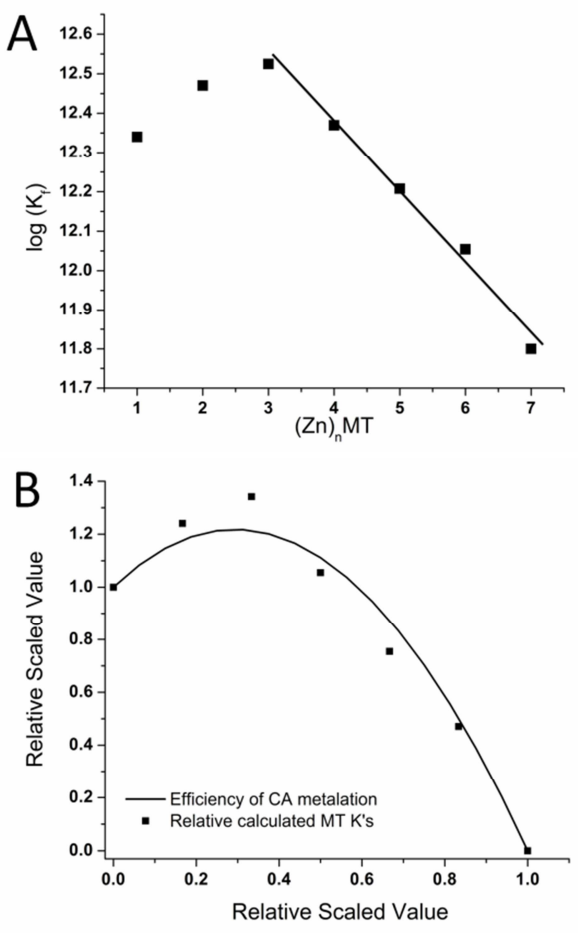

Figure 2.4: Calculated stability constants (A) and the experimental data reflecting those values (B). (A) The calculated fitted K values of MT that best fit the data shown in Figure 2.2 to produce Figure 2.3 based on the competitive metallation of apoMT in the presence of CA. The solid line shows the linear trend of decreasing K values as the MT metallates. (B) Superimposition of the relative metallation efficiency of apoCA (solid line) plotted against the calculated log(K_F) values (points). The two data sets were scaled such that the initial values (metallation efficiency and first MT zinc binding K) were 1.

www.manaraa.com

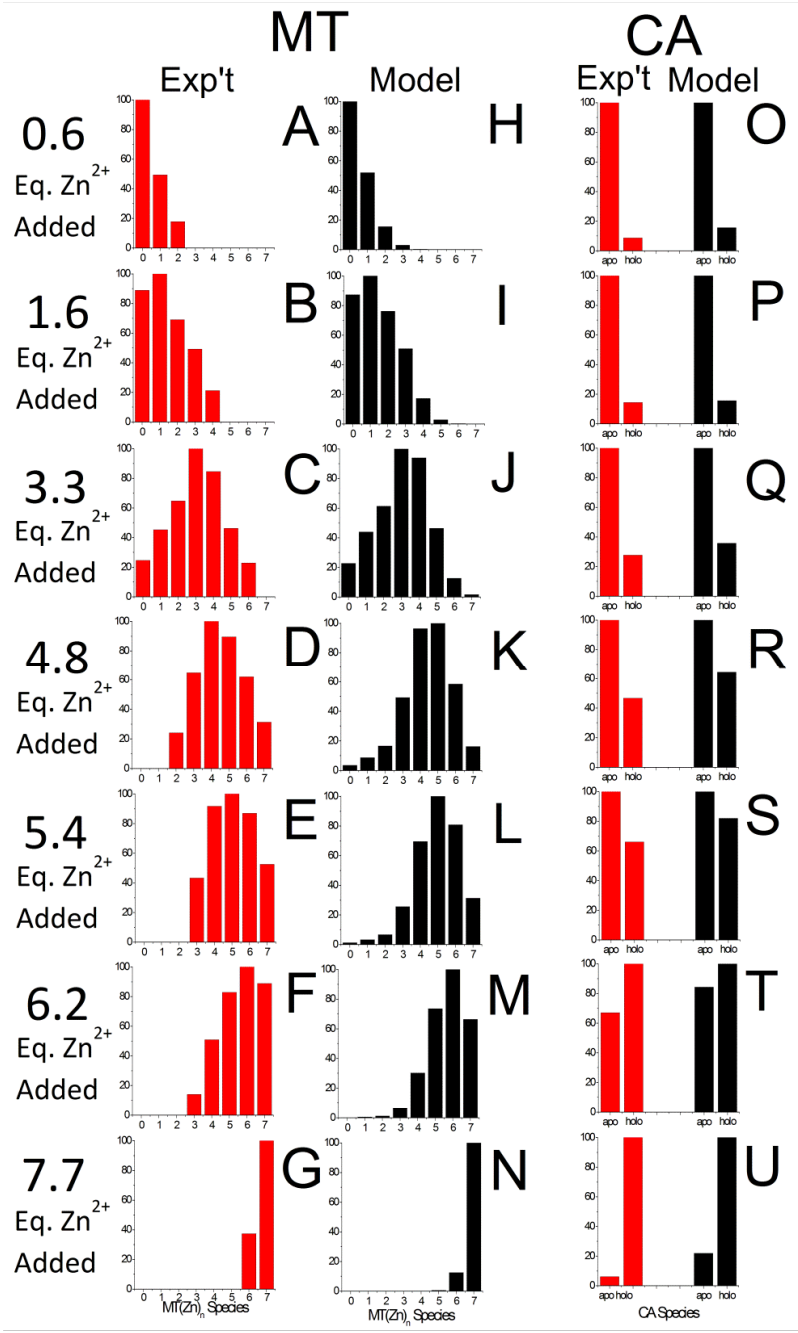

Figure 2.5: ESI mass spectra based on experimental data (red) and data produced by simulating the titration using the best fit K_F values (black). A-G show the experimental mass spectral data collected for all Zn_nMT (n = 0-7) species during the competitive titration of apoCA and apoMT. H-N show the predicted ESI mass spectral data for the same species generated from the simulated titration. O-U show both the experimental and predicted ESI mass spectral data for apo and holoCA species.

www.manaraa.com

2.4 Discussion

2.4.1 Spanning the ladder of MT binding constants

MT is a metallochaperone with the proposed role of supplying zinc to apoenzymes. While numerous studies have discussed the metallation of CA, even including interactions with Zn_7MT, no studies have previously addressed the mechanism for a potential role of zinc buffering between MT and the apoenzyme could be found in the literature. Results from both the Stillman lab and Maret *et al*., indicate that a ladder of binding constants exists for the binding of zinc to metallothionein.[44, 50]

Previous results showed that MT1A possesses seven independent sequentially decreasing zinc binding affinities from zinc competition experiments between the full rhMT1A protein and individual N-terminal β and C-terminal α domains. The previous work used a much simpler modeling procedure and manually set the span of the seven K values to extend over the data reported by Maret and co-workers[50] as a best estimate for the K values. In this current report, the modeling of the K values is locked to the known value of carbonic anhydrase metallation. The model mathematically minimized the errors on the values of K so the model best fits the data. In this way, this current set of K values has both confirmed the existence of the seven independent zinc binding affinities and calibrated their values to accommodate the known value of CA.

To place the metallation of CA within this ladder, an experiment in which both aporhMT1A and apoCA could compete for zinc as it was added in a stepwise manner was designed. The competition experiment is unique in that it is able to leverage the difference in the relative binding affinities for such high affinity sites.[51] In the presence of a competitive zinc binding site, such as that found in CA, the two proteins will redistribute zinc to form the thermodynamically preferred zinc distribution that will be governed by the relative magnitudes of the eight equilibrium constants. These data show how apoCA metallates with a sequence directly related to the relative binding constants of the seven individual sites in MT. This establishes the buffering properties afforded by MT for zinc.

www.manaraa.com

Figure 2.1A shows how the initial zinc binds in a distributed fashion to the rhMT1A and, to a minor extent, to the CA. The important observation is the change that takes place when a further three zinc equivalents are added and the data in Figure 2.1B recorded. At this point during the titration, the Zn_3 and Zn_4MT species dominate the distribution of zinc metallation, whereas, in contrast, the ZnCA fraction has increased only slightly. These data clearly and unambiguously show that MT is binding a greater fraction of the added zinc than is CA. This can only occur under the equimolar conditions of the competition experiment, if the relative binding constants favor MT zinc binding. Addition of a further 2 equiv (to 5.6 total added; Figure 2.1D) results in both MT and CA binding significant fractions of the added zinc. This means that the binding site affinities in MT must be more similar to the binding site affinity of CA. The major change in zinc binding to CA occurs with the addition to 6.5 equiv (Figure 2.1E). Now approximately 70% of the CA is metallated.

Figure 2.2A clearly shows the stepwise metallation proceeds as reported previously for zinc binding, in that each individual species (meaning Zn_1, to Zn_5) forms and then is replaced with approximately the same fractional composition of about 30% maximum. At each point in the titration, the data here show the distribution of species simply by constructing a fractional distribution. For example, at the 4.0 zinc added point, the slice through the data shows that the relative concentrations are: $Zn_4 > Zn_3 > Zn_5 > Zn_2 > Zn_6 > Zn_1 > Zn_7 >$ apoMT.

Figure 2.2B shows that the binding of zinc to apoCA takes place nonlinearly as a function of zinc added. In the region from 0 to 5 zinc added, the data show that zinc binding to CA is dependent directly on the relative binding constant for the individual sites in MT. This means that, for example, the small fraction of the initial addition of zinc is bound by CA when Zn_1MT is forming. However, when Zn_3MT forms at about three zinc added, CA metallation is depressed so that between three and almost five zinc added only about 5% of the CA metallates, due to the increase in competition from the MT. The CA metallation trends, therefore, mirror the span of the seven MT binding affinities: when the binding affinity for CA is closer to that of a single site in MT, CA metallates, but when the binding affinity of CA is much less than MT, MT metallates.

www.manaraa.com

The sensitivity of apoCA metallation to the presence of the seven competing MT sites can be expressed by taking the derivative of the metallation status of apoCA as a function of the number of added zinc (Figure 2.2C). From points a to b, the binding affinity difference increases between apoCA and the MT species and CA metallation becomes less efficient with respect to MT metallation ($Zn_{1\text{-}3}$MT bind while CA essentially stops binding zinc). In the b-c region, CA metallation is essentially zero (less than 10% change over 3 equiv of zinc added), in contrast to MT metallation of $Zn_{2\text{-}4}$MT. However, the c-d region shows the onset of apoCA metallation; now CA is competing more efficiently against the formation of $Zn_{6\text{-}7}$MT. The unusual region is the pivot point between b-c and c-d because at this point there is a distinct reduction in the binding affinity of the competitive species (Zn_nMT). This pivot point is interpreted to represent the threshold in the binding affinities of the MT species with respect to apoCA. This is demonstrated in Figure 2.2C because if the binding affinities for every MT site were the same, the derivative (d[apoCA]/d[Zn Added]) would be constant for a competitor with the same binding affinity.

2.4.2 Trends in MT zinc binding affinities

The binding affinity data calculated for Figure 2.3 introduced an interesting trend. Whereas the sequence of binding affinities for MT to was expected to diminish, as noted above, the fits required that K_1 and K_2 should be lower than K_3. The effect of this can be seen in Figure 2.2B, as described above, where apoCA metallates proportionally with a greater fraction than at the higher zinc-added points. The seven calculated equilibrium constant values determined for each zinc addition from the competitive titration experiments shown in Figures 2.1-2.5 are shown in Scheme 2.1 (note that the value of $\log(K_{CA})$ was taken from the literature as 11.4).[35]

The unexpected increase in zinc affinity for the first two binding constants (where K_1 (apoMT) < K_2 (Zn_1MT) < K_3 (Zn_2MT)) could possibly arise from the much greater fluxional nature of the apoMT strand and therefore lack of structured zinc binding sites as compared to the partially metallated (and therefore structured) Zn_1- and Zn_2MT species. The binding of the first and second metal must rearrange the peptide backbone to accommodate metal binding. This rearrangement facilitates the subsequent metallation

www.manaraa.com

events (Zn_1- to Zn_2 and Zn_2- to Zn_3MT) in a manner not previously observed due to the fact that multiple species are metallating simultaneously as shown in the modeling and especially the deconvoluted and raw ESI mass spectral data. Once three zinc ions have been incorporated by the MT strand, this effect is no longer observed, since the entire strand now must now possess some organized structure.

The change in structure from the charge state distribution following metallation of the apoMT has been previously discussed. For example, this same trend was observed in arsenic binding to MT[52] and may be connected with the globular conformation of apoMT suggested from the ESI mass spectral data.[53] This arsenic work showed that the kinetics of arsenic binding was mostly controlled by the rate of the on reaction (k_{on}), as the rate of the off reaction (k_{off}) for each As_xMT species was presumed to be similar. Since the equilibrium binding constant (K) equals the ratio of (k_{on} / k_{off}) and since the k_{off} values were presumed similar, those kinetic parameters reflect directly the equilibrium binding of arsenic to MT. While the values and magnitudes are certainly not comparable, and even though it involves a different metal, these arsenic data highlight the surprising similarity in the trends between these kinetic arsenic data and the zinc equilibrium data described here.

The values of the subsequent K_n (n = 3-7) follow the expected trend for distributed metallation in which the number of sites available diminishes sequentially so that the value of K_n also diminishes. Recent results have shown that even low zinc occupancy MT species (Zn_nMT where n = 0, 1 or 2) adopt structural characteristics that differ from the traditional view of apoMTs existing as a pure random coil.[54, 55]

The span of the seven stability constants, relative to the apoCA zinc binding constant, shows that MT zinc binding occurs throughout the range of zinc enzyme stability constants, even at the start of the titration against much higher affinity MT binding sites. As the MT binds zinc sequentially into each site, the binding constants decrease to a point where the apoCA can begin to compete more efficiently with MT for the incoming zinc. CA then continues to compete with MT for the incoming zinc until it saturates, and MT binds the remaining incoming zinc until it too is saturated.

www.manaraa.com

2.4.3 Modelling reactions between CA and a competitor

To visualize the effects of the relative binding affinities on the zinc distribution the results of a computational simulation that demonstrates the major changes that take place in the fractional distribution of zinc as a function of the relative magnitudes of the binding affinities of an example metal chaperone (MT) and a metal-dependent enzyme (CA) have been included.

For simplicity, only a single site competitor was used. The effect of different ratios of the binding affinities was explored and the results are shown in Figure 2.6. The panels in Figure 2.6 examine the effect on the metallation of apoCA for five scenarios: (A) where $K_{comp} < K_{CA}$ by 0.5 log units; (B) where $K_{comp} = K_{CA}$; (C) where $K_{comp} > K_{CA}$ by 0.5 log units; (D) where $K_{comp} > K_{CA}$ by 1 log unit; and (E) where $K_{comp} > K_{CA}$ by 1.5 log units. What is important in this figure is that the trend in the metallation of apoCA for the set of values of binding affinities obtained from the fit reported in Figure 2.3 can be simulated. Figure 2.6D shows that competition with a competitor whose zinc binding affinity is approximately 10x stronger than CA results in inefficient metallation until over 50% of the zinc has been bound to the competitor. The trend in apoCA metallation, therefore, illustrates the situation at the different points in Figure 2.2B. Figure 2.6A shows metallation taking place efficiently because the competitor binding constant is modelled to be less than that of CA. Clearly, the amount of zinc that is available for an enzyme to acquire from MT is dependent on the relative zinc binding constants. An enzyme with a high zinc binding constant, has a much larger zinc pool available than those enzymes that bind zinc more weakly. The series of binding constants represent, in sequence from high to low, the increase in the availability of zinc to a zinc acceptor.

The efficiency in metallation of the apoCA, meaning the fraction of the added zinc that apoCA binds, confirms the presence of the multiple binding affinities of the seven MT sites. This effect is directly dependent on the intricate equilibrium chemistry that takes place when eight possible binding sites vie for the zinc that is added in a stepwise manner. That the binding affinity of apoCA is smaller than the last zinc bound to the MT sets up the buffering action controlled by the seven sites of MT.

www.manaraa.com

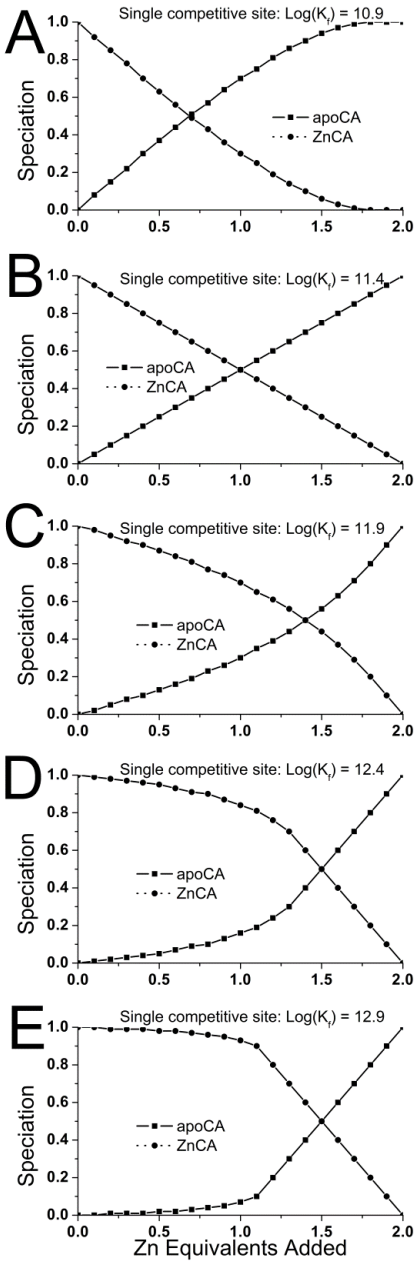

Figure 2.6: Modelled CA speciation profiles for the simulated competitive zinc titration between CA and a single zinc binding site. The competitor has been modelled with zinc affinity increasing by 0.5 log units A (10.9) to E (12.9). The simulated titration requires 2 equiv of zinc to complete. The zinc occupancy of the CA depends on the relative difference in the zinc binding affinity from the competitor. These model traces highlight the sensitivity of this modelling for interpreting speciation and determining relative zinc affinities. Log(K_{CA}) was set to 11.4.

www.manaraa.com

When the cell is in a state of zinc excess, MT production is induced. It would be advantageous for the newly synthesized apoMT proteins to rapidly bind the weakly associated zinc that turn on zinc-specific transcription factors such as MTF-1. The first few zinc that are bound to MT, therefore, act as a deep sink of bound zinc. This deep sink is only accessible during times of extreme zinc deficiency. The rest of the zinc binding constants decrease approximately linearly. The more weakly bound zinc act as a shallow source of zinc, to be exchanged between other zinc sinks and enzymes. The proposal is that MT acts as both a zinc chaperone (one of many others) and a zinc sensor for the cell. When zinc levels are low and the cell is zinc-starved, MT binds all available zinc, which has two effects: to turn on zinc importers, and to cause upregulation of genes that code for zinc importation. The facility of zinc-loaded MT to donate occurs when the cell is zinc-loaded and the most predominant MT species have >6 zinc bound. These species supply the weakly bound zinc to zinc-dependent apoenzymes; the most weakly bound zinc ion is also likely constantly exchanging with weak zinc binding sites, highlighting the role of zinc buffering. If the cell contains zinc in excess of the MT binding capabilities, these "free" zinc are bound by non-specific zinc sites, sequestered into zinc vesicles, and/or bound by and exported by zinc exporters,[56, 57] which have lower zinc binding constants. Thus MT is able to act as a zinc buffer, maintaining the appropriate cellular concentration of zinc by utilizing the range of the zinc binding constants.

In conclusion, in this Chapter, the precise metallation status of both apoCA and apoMT during zinc metallation was shown. By using a competitive metallation strategy, the relative stability constants for each of the seven independent, sequential binding reactions for zinc binding to apoMT was calculated. The experimental data indicate that CA out-competes MT only for the three weakest bound zinc ions – these are the last zinc to bind to the MT. The fractional zinc occupancies in terms of the speciation for each of the 10 species that coexist during the titration were reported and modeled by simulations involving 8 competitive bimolecular reactions. The change in fractional zinc metallation of the apoCA as a function of zinc added to the mixture of apoCA and apoMT was shown to mirror the relative values of the binding affinities for the seven MT sites. These data provide a detailed and sensitive indication of the buffering role of Zn-MT both in providing a zinc sink and in delivering zinc to a zinc-dependent enzyme.

www.manaraa.com

2.5 References

1. Andreini, C., Bertini, I., Cavallaro, G., Holliday, G., and Thornton, J. (2008) Metal ions in biological catalysis: from enzyme databases to general principles, *J. Biol. Inorg. Chem. 13*, 1205-1218.
2. Andreini, C., Cavallaro, G., Lorenzini, S., and Rosato, A. (2013) MetalPDB: a database of metal sites in biological macromolecular structures, *Nucleic Acids Res. 41*, D312-D319.
3. Krężel, A., and Maret, W. (2006) Zinc-buffering capacity of a eukaryotic cell at physiological pZn, *J. Biol. Inorg. Chem. 11*, 1049-1062.
4. Outten, C. E., O'Halloran, and V., T. (2001) Femtomolar Sensitivity of Metalloregulatory Proteins Controlling Zinc Homeostasis, *Science 292*, 2488-2492.
5. Laity, J. H., and Andrews, G. K. (2007) Understanding the mechanisms of zinc-sensing by metal-response element binding transcription factor-1 (MTF-1), *Arch. Biochem. Biophys. 463*, 201-210.
6. McMahon, R. J., and Cousins, R. J. (1998) Mammalian Zinc Transporters, *J. Nutr. 128*, 667-670.
7. Robinson, N., and Pohl, E. (2013) Zinc Sensors in Bacteria, In *Encyclopedia of Metalloproteins* (Kretsinger, R., Uversky, V., and Permyakov, E., Eds.), pp 2499-2506, Springer New York.
8. Cousins, R. J., Liuzzi, J. P., and Lichten, L. A. (2006) Mammalian Zinc Transport, Trafficking, and Signals, *J. Biol. Chem. 281*, 24085-24089.
9. Eide, D. J. (2006) Zinc transporters and the cellular trafficking of zinc, *Biochim. Biophys. Acta, Mol. Cell Res. 1763*, 711-722.
10. Colvin, R. A., Holmes, W. R., Fontaine, C. P., and Maret, W. (2010) Cytosolic zinc buffering and muffling: their role in intracellular zinc homeostasis, *Metallomics 2*, 306-317.
11. Tottey, S., Harvie, D. R., and Robinson, N. J. (2005) Understanding How Cells Allocate Metals Using Metal Sensors and Metallochaperones, *Acc. Chem. Res. 38*, 775-783.
12. Waldron, K. J., Rutherford, J. C., Ford, D., and Robinson, N. J. (2009) Metalloproteins and metal sensing, *Nature 460*, 823-830.
13. Kulkarni, P. P., She, Y. M., Smith, S. D., Roberts, E. A., and Sarkar, B. (2006) Proteomics of Metal Transport and Metal-Associated Diseases, *Chem.--Eur. J. 12*, 2410-2422.
14. Nelson, N. (1999) Metal ion transporters and homeostasis, *EMBO J. 18*, 4361-4371.
15. Taylor, K. M., Vichova, P., Jordan, N., Hiscox, S., Hendley, R., and Nicholson, R. I. (2008) ZIP7-Mediated Intracellular Zinc Transport Contributes to Aberrant Growth Factor Signaling in Antihormone-Resistant Breast Cancer Cells, *Endocrinology 149*, 4912-4920.
16. Fukada, T., Yamasaki, S., Nishida, K., Murakami, M., and Hirano, T. (2011) Zinc homeostasis and signaling in health and diseases, *J. Biol. Inorg. Chem. 16*, 1123-1134.
17. Yamasaki, S., Sakata-Sogawa, K., Hasegawa, A., Suzuki, T., Kabu, K., Sato, E., Kurosaki, T., Yamashita, S., Tokunaga, M., and Nishida, K. (2007) Zinc is a novel intracellular second messenger, *J. Cell Biol. 177*, 637-645.
18. Kang, Y. J. (2006) Metallothionein redox cycle and function, *Exp. Biol. Med. 231*, 1459-1467.
19. Maret, W., and Vallee, B. L. (1998) Thiolate ligands in metallothionein confer redox activity on zinc clusters, *Proc. Natl. Acad. Sci. U. S. A. 95*, 3478-3482.
20. Thirumoorthy, N., Shyam Sunder, A., Manisenthil Kumar, K., Senthil Kumar, M., Ganesh, G., and Chatterjee, M. (2011) A review of metallothionein isoforms and their role in pathophysiology, *World J. Surg. Oncol. 9*, 54.

www.manaraa.com

21. Robbins, A., McRee, D., Williamson, M., Collett, S., Xuong, N., Furey, W., Wang, B., and Stout, C. (1991) Refined crystal structure of Cd, Zn metallothionein at 2.0 Åresolution, *J. Mol. Biol. 221*, 1269-1293.
22. Coyle, P., Philcox, J., Carey, L., and Rofe, A. (2002) Metallothionein: the multipurpose protein, *Cell. Mol. Life Sci. 59*, 627-647.
23. Meloni, G., Sonois, V., Delaine, T., Guilloreau, L., Gillet, A., Teissié, J., Faller, P., and Vašák, M. (2008) Metal swap between Zn7-metallothionein-3 and amyloid-β–Cu protects against amyloid-β toxicity, *Nat. Chem. Biol. 4*, 366-372.
24. Petering, D. H., Zhu, J., Krezoski, S., Meeusen, J., Kiekenbush, C., Krull, S., Specher, T., and Dughish, M. (2006) Apo-Metallothionein Emerging as a Major Player in the Cellular Activities of Metallothionein, *Exp. Biol. Med. 231*, 1528-1534.
25. Zalewska, M., Trefon, J., and Milnerowicz, H. (2014) The role of metallothionein interactions with other proteins, *Proteomics 14*, 1343-1356.
26. Mason, A. Z., Moeller, R., Thrippleton, K. A., and Lloyd, D. (2007) Use of stable isotopically enriched proteins and directly coupled high-performance liquid chromatography inductively coupled plasma mass spectrometry for quantitatively monitoring the transfer of metals between proteins, *Anal. Biochem. 369*, 87-104.
27. Zaia, J., Fabris, D., Wei, D., Karpel, R. L., and Fenselau, C. (1998) Monitoring metal ion flux in reactions of metallothionein and drug-modified metallothionein by electrospray mass spectrometry, *Protein Sci. 7*, 2398-2404.
28. Jacob, C., Maret, W., and Vallee, B. L. (1998) Control of zinc transfer between thionein, metallothionein, and zinc proteins, *Proc. Natl. Acad. Sci. U. S. A. 95*, 3489-3494.
29. Jiang, L.-J., Maret, W., and Vallee, B. L. (1998) The glutathione redox couple modulates zinc transfer from metallothionein to zinc-depleted sorbitol dehydrogenase, *Proc. Natl. Acad. Sci. U. S. A. 95*, 3483-3488.
30. Feng, W., Cai, J., Pierce, W. M., Franklin, R. B., Maret, W., Benz, F. W., and Kang, Y. J. (2005) Metallothionein transfers zinc to mitochondrial aconitase through a direct interaction in mouse hearts, *Biochem. Biophys. Res. Commun. 332*, 853-858.
31. Leszczyszyn, O. I., and Blindauer, C. A. (2010) Zinc transfer from the embryo-specific metallothionein EC from wheat: a case study, *Phys. Chem. Chem. Phys. 12*, 13408-13418.
32. Li, T.-Y., Kraker, A. J., Shaw, C. F., and Petering, D. H. (1980) Ligand substitution reactions of metallothioneins with EDTA and apo-carbonic anhydrase, *Proc. Natl. Acad. Sci. U. S. A. 77*, 6334-6338.
33. Udom, A. O., and Brady, F. O. (1980) Reactivation *in vitro* of zinc-requiring apo-enzymes by rat liver zinc-thionein, *Biochem. J 187*, 329-335.
34. Lindskog, S., and Malmström, B. G. (1962) Metal binding and catalytic activity in bovine carbonic anhydrase, *J. Biol. Chem. 237*, 1129-1137.
35. Kiefer, L. L., Krebs, J. F., Paterno, S. A., and Fierke, C. A. (1993) Engineering a cysteine ligand into the zinc binding site of human carbonic anhydrase II, *Biochemistry 32*, 9896-9900.
36. Palmiter, R. D., and Findley, S. D. (1995) Cloning and functional characterization of a mammalian zinc transporter that confers resistance to zinc, *EMBO J. 14*, 639.
37. Wommer, S., Rival, S., Heinz, U., Galleni, M., Frère, J.-M., Franceschini, N., Amicosante, G., Rasmussen, B., Bauer, R., and Adolph, H.-W. (2002) Substrate-activated zinc binding of metallo-β-lactamases Physiological importance of the mononuclear enzymes, *J. Biol. Chem. 277*, 24142-24147.

www.manaraa.com

38. Antala, S., and Dempski, R. E. (2012) The Human ZIP4 Transporter Has Two Distinct Binding Affinities and Mediates Transport of Multiple Transition Metals, *Biochemistry 51*, 963-973.
39. Sharif, R., Thomas, P., Zalewski, P., and Fenech, M. (2012) Zinc deficiency or excess within the physiological range increases genome instability and cytotoxicity, respectively, in human oral keratinocyte cells, *Genes and Nutrition 7*, 139-154.
40. Krężel, A., and Maret, W. (2007) Dual Nanomolar and Picomolar Zn(II) Binding Properties of Metallothionein, *J. Am. Chem. Soc. 129*, 10911-10921.
41. Namdarghanbari, M. A., Meeusen, J., Bachowski, G., Giebel, N., Johnson, J., and Petering, D. H. (2010) Reaction of the zinc sensor FluoZin-3 with Zn_7-metallothionein: Inquiry into the existence of a proposed weak binding site, *J. Inorg. Biochem. 104*, 224-231.
42. Ejnik, J., Muñoz, A., Gan, T., Shaw III, C. F., and Petering, D. (1999) Interprotein metal ion exchange between cadmium-carbonic anhydrase and apo-or zinc-metallothionein, *J. Biol. Inorg. Chem. 4*, 784-790.
43. Petering, D. H., Zhu, J., Kreżoski, S., Meeusen, J., Kiekenbush, C., Krull, S., Specher, T., and Dughish, M. (2006) Apo-metallothionein emerging as a major player in the cellular activities of metallothionein, *Exp. Biol. Med. 231*, 1528-1534.
44. Summers, K. L., Sutherland, D. E. K., and Stillman, M. J. (2013) Single-domain metallothioneins: Evidence of the onset of clustered metal binding domains in Zn-rhMT 1a, *Biochemistry 52*, 2461-2471.
45. Sutherland, D. E. K., Summers, K. L., and Stillman, M. J. (2012) Noncooperative Metalation of Metallothionein 1a and Its Isolated Domains with Zinc, *Biochemistry 51*, 6690-6700.
46. Sutherland, D. E., and Stillman, M. J. (2014) Challenging conventional wisdom: single domain metallothioneins, *Metallomics*.
47. Avvaru, B. S., Busby, S. A., Chalmers, M. J., Griffin, P. R., Venkatakrishnan, B., Agbandje-McKenna, M., Silverman, D. N., and McKenna, R. (2009) Apo-human carbonic anhydrase II revisited: Implications of the loss of a metal in protein structure, stability, and solvent network, *Biochemistry 48*, 7365-7372.
48. Chan, J., Huang, Z., Watt, I., Kille, P., and Stillman, M. (2008) Metallobiological Necklaces: Mass Spectrometric and Molecular Modeling Study of Metallation in Concatenated Domains of Metallothionein, *Chem.--Eur. J. 14*, 7579-7593.
49. Hunt, J. B., Rhee, M.-J., and Storm, C. B. (1977) A rapid and convenient preparation of apocarbonic anhydrase, *Anal. Biochem. 79*, 614-617.
50. Krężel, A., and Maret, W. (2008) Thionein/metallothionein control Zn (II) availability and the activity of enzymes, *J. Biol. Inorg. Chem. 13*, 401-409.
51. Hein, U., Kiefer, M., Tholey, A., and Adolph, H.-W. (2005) On the competition for available zinc, *J. Biol. Chem. 280*, 3197-3207.
52. Ngu, T. T., Easton, A., and Stillman, M. J. (2008) Kinetic Analysis of Arsenic−Metalation of Human Metallothionein: Significance of the Two-Domain Structure, *J. Am. Chem. Soc. 130*, 17016-17028.
53. Irvine, G. W., and Stillman, M. J. (2013) Topographical analysis of As-induced folding of α-MT1a, *Biochem. Biophys. Res. Commun. 441*, 208-213.
54. Hong, S.-H., and Maret, W. (2003) A fluorescence resonance energy transfer sensor for the β-domain of metallothionein, *Proc. Natl. Acad. Sci. U. S. A. 100*, 2255-2260.

www.manaraa.com

55. Irvine, G. W., Summers, K. L., and Stillman, M. J. (2013) Cysteine accessibility during As3+ metalation of the α- and β-domains of recombinant human MT1a, *Biochem. Biophys. Res. Commun. 433*, 477-483.
56. Palmiter, R. D., Cole, T. B., and Findley, S. D. (1996) ZnT-2, a mammalian protein that confers resistance to zinc by facilitating vesicular sequestration, *EMBO J. 15*, 1784.
57. Rink, L., and Haase, H. (2007) Zinc homeostasis and immunity, *Trends Immunol. 28*, 1-4.

www.manaraa.com

Chapter 3

3 Putting the pieces into place: Properties of intact zinc metallothionein 1A determined from interaction of its isolated domains with carbonic anhydrase*

3.1 Introduction

Metallothionein is a cysteine-rich family of proteins that are involved in the homeostatic control of essential metals and the detoxification of toxic heavy metals.[1] These essential roles are underscored by the prevalence of metallothioneins throughout all forms of Life.[2, 3] Numerous studies have shown that mammalian metallothioneins (MTs) bind a wide variety of metals, with the most well studied and biologically relevant being the essential metals zinc(II) and copper(I) and toxic cadmium(II).[4-7]

MTs bind up to seven divalent metal cations using its complement of 20 cysteines. For saturated $(M^{II})_7$-βαMT, the coordinated metals are clustered into two distinct domains: an N-terminal β domain that uses nine Cys to bind three metals; and, a C-terminal α domain that binds four metals with 11 Cys. The structures of these metalloclusters were elucidated using ^{113}Cd NMR[8] and X-ray crystallographic[9] techniques.[10] The structures of Zn_7- and Cd_7-MT show that the two-domains are separated by a small variable length (depending on the species and isoform) linker region. No NMR or X-ray structures are available for unsaturated MTs due to increased fluxtionality of the protein.

There has been much discussion regarding the domain properties of metal-saturated MTs. For example, the binding mechanism of cadmium and zinc to apoMT has traditionally been reported to involve a domain-specific mechanism where the first four metals bind to the α domain cooperatively. The two-domain structure adopted by metal-saturated MTs has also been suggested to be an important factor in the MT-protein interactions that are a

* A version of this Chapter is in press:

Reproduced with permission from: T.B.J. Pinter, and M.J. Stillman. *Biochem. J.* (2015) , in press, DOI: 10.1042/BJ20150676. Copyright 2015 Portland Press.

www.manaraa.com

necessary element of the metal homeostatic roles of MTs.[11] The evolutionary advantages of the MT domains have also been investigated.[2, 12-14]

Less is known about the domain properties of partially metallated MTs, though they do exist *in vivo*, as demonstrated by multiple studies.[15-19] The proposed functions of MT require either accessible cysteines (for metal exchange), free cysteines (to be used for redox chemistry by forming disulfides in response to oxidative cellular stress), or open coordination sites (from the synthesis of the upregulation of MTs in response to acute metal toxicity).[20, 21] The structures adopted during metallation, and the properties of the intermediate metallation states (Zn_{3-6}-βαMT for zinc), dictate the type of chemistries that occur *in vivo*. The zinc binding affinities of Zn_{5-7}-βαMT, for example, permit zinc donation to zinc dependent apo-enzymes.[22, 23] On the other hand, the first three zinc bind to MT with higher affinity forming Zn_{1-3}-βαMT, which is well suited for zinc storage.

Carbonic anhydrase, the enzyme that catalyzes the hydration of carbon dioxide to form carbonic acid driving respiration, binds a single zinc ion in its active site.[24] This zinc ion is solely catalytic, with no significant change in protein structure upon removal of the zinc.[25] Previous work on the interaction of MT with CA demonstrated that zinc-saturated MTs donate a single zinc ion to apoCA.[23, 26-28] Other reports have shown that apo- and Zn_7-MT are able to exchange with CdCA, through protein-protein interactions (PPIs), rescuing the enzymatic function of cadmium-poisoned CA.[29]

We recently reported on zinc competition reactions between apoCA and apoMT1A demonstrating that the last two zinc bound to MT (Zn_6- and Zn_7-MT1A) had binding affinities that were low enough to permit competitive zinc binding by apoCA, and therefore other cellular zinc binding sites.[30] This report also provided evidence in support of our current model of MT zinc exchange where the two-domain Zn_7-βαMT is able to donate two zinc ions from the metal-saturated clustered domains to form Zn_5-βαMT, a structure using all 20 Cys in terminal coordination of the five zinc ions.[31, 32] However, despite the clarity in the values of the seven MT zinc binding affinities, assigning the location of the cysteines that bound the zinc within the sequence was not possible so the actual domain that donated the first zinc was unknown. We also hypothesized that the

www.manaraa.com

suppression of the first two MT zinc binding affinities (relative to the linear trend set by the remaining five log(K_F)'s) was due to tangling of the apoMT strand, by which we mean the unscrambling of the cysteine ligands from the apoMT bundle required to form the tetrahedral coordination. By separating the domains, we challenge the significance of the presence of 20 cysteines in the intact protein with respect to zinc donation to metal-dependent enzymes.

In this current report, we relate the zinc binding properties of the domain fragments, determined from competition between the apo-fragments and apoCA, to the domain-effects of zinc binding and zinc donation in the intact protein. We show the metal distribution between each apo-fragment and apoCA as a function of added zinc to solutions containing equimolar concentrations of the apo-fragment and apoCA. Using modeling procedures that have been previously described, we calculated the zinc affinity constants for the four zinc binding events in the αMT fragment and the three for the βMT fragment. The data show that the αMT fragment outcompetes the apoCA for added zinc until it is nearly saturated. The apoCA is able to effectively compete with the βMT fragment after $Zn_1\beta$ has formed. These results suggest that the highest affinity zinc binding sites are more localized in the α domain, and the weaker affinity zinc binding sites in the β-domain. This suggests that the first zinc donated to CA is from the β-domain in the intact two-domain protein.

3.2 Methods

3.2.1 Purification of recombinant MT1A domain fragments.

The amino acid sequences for the separated domains used for this study were based on human MT1A. The β-MT domain sequence comprised 38 residues: MGKAAAACSC ATGGSCTCTG SCKCKECKCN SCKKAAAA, and the α-MT domain fragment sequence comprised 41 residues: MGKAAAAC CSCCPMSCAK CAQGCVCKGA SEKCSCCKKA AAA. We do note here that these sequences include additional residues in the form of polyA's to the N and C-termini compared to the native MT1A, which model the connecting linker region of the intact peptide and also do not significantly alter metal binding properties. Recombinant MT fragments were prepared following methods

www.manaraa.com

that have been described in detail elsewhere, and in Appendix A.[33] In brief, pET29a plasmids, containing DNA sequences corresponding to the sequences for the isolated domains, were transformed into BL21(DE3) *Escherichia coli*. The recombinant fragments were overexpressed in 4 L of cultured lysogeny broth (Miller) supplemented with cadmium. The cadmium-saturated MT fragments were isolated from disrupted (Constant Systems, UK) cellular lysate with SP anion exchange columns (GE Healthcare, USA). The S-tag was removed from the domain fragments using thrombin CleanCleave kits (Sigma). Purified MT fragments were concentrated using a pressurized cell concentrator fitted with a 3K MWCO membrane and stored in aliquots at -20°C until use. All purified protein solutions were thoroughly evacuated and argon-saturated in attempt to impede cysteine oxidation.

3.2.2 Preparation of apometallothionein fragments.

Aliquots of purified MT fragments were thawed under vacuum and acidified to pH 2.7 with concentrated formic acid to protonate cysteines and release bound cadmium. Protein was then separated from the freed cadmium on G-25 size exclusion media equilibrated with argon-saturated, dilute formic acid (pH 2.7). Eluted metal-free protein was concentrated and buffer exchanged with 5 mM ammonium formate (pH 7.0) using Millipore Amicon Ultra-4 centrifugal filter units (3 kDa MWCO) under argon. Small fractions of the final, pH adjusted apo fragments were remetallated with cadmium and UV-visible absorption spectroscopy (Cary 50, Varian Canada) was used to determine final stock protein concentrations; ε_{250nm} = 36,000 $M^{-1}cm^{-1}$ and 45,000 $M^{-1}cm^{-1}$ for Cd_3-βMT and Cd_4-αMT, respectively.

3.2.3 Preparation of apocarbonic anhydrase.

The removal of zinc from carbonic anhydrase followed modification of previous methods.[34] 10 mg of bovine carbonic anhydrase II (Sigma) was dissolved in 4 mL of 50 mM 2,6-pyridinedicarboxylic acid (Sigma), pH 6.0 (PDC) and equilibrated on ice for 15 min. Millipore Amicon Ultra-4 filters (10k MWCO) were used to separate zinc-PDC from protein and fresh PDC was added back to the protein solution. In total, the protein was treated with 6 aliquots of fresh PDC chelating buffer to remove all of the zinc bound

www.manaraa.com

to carbonic anhydrase. To remove PDC, the apo-protein solution was buffer exchanged to argon-saturated, 5 mM ammonium formate, pH 7.0 until no PDA was detected in the filtrate. The concentration of the apoCA was determined immediately prior to MS experiments using UV-visible absorption spectroscopy (ε_{280nm} = 54,000 $M^{-1}cm^{-1}$).[35, 36]

3.2.4 Zinc and cadmium titrations.

5 mM zinc acetate (Fisher Scientific) was prepared in deionized water. In separate experiments, equal concentrations of either apo-βMT or apo-αMT were mixed with apoCA in acid washed vials. Equivalents of zinc were then added to the mixed protein solutions under argon atmosphere. These solutions were equilibrated on ice for 3-5 minutes before ESI measurement. No change in speciation was observed with longer equilibration times (up to 120 min data not shown). The stepwise addition of the zinc continued until each protein was zinc saturated. Titrations were repeated in triplicate. The zinc content of the apo-proteins, stock zinc solution and titration endpoints were verified using atomic absorption spectroscopy (AA 240, Varian, Canada).

3.2.5 ESI-MS parameterizations.

The ESI mass spectral data were collected on a Bruker Micro-TOF II (Bruker Daltonics, Toronto, ON) operated in the positive ion mode calibrated with NaI as an external calibrant. The settings used were: scan = 500 - 4000 m/z; rolling average = 2; nebulizer = 2 Bar; dry gas = 85°C @ 6.0 L/min; capillary = 4000 V; end plate offset = -500 V; capillary exit = 175 V; Skimmer 1 = 30.0 V; Skimmer 2 = 23.5 V; Hexapole RF = 800 V. The spectra were collected for a minimum of 2 minutes and deconvoluted using the Maximum Entropy algorithm of the Bruker Compass DataAnalysis software package.

3.3 Results

3.3.1 Competition for Zn^{2+} between apoCA and apo-αMT.

Figure 3.1 shows a selection of the deconvoluted mass spectral data recorded during the titration of Zn^{2+} into a solution of apoCA and apo-αMT. This figure show the stepwise formation of zinc saturated αMT and ZnCA (Figure 3.1F) over six steps of the titration (Figure 3.1A-F). The species have been plotted relative to the most abundant species in

www.manaraa.com

the solution for each protein: apo-αMT and apoCA in Figure 3.1A and Zn_4-αMT and holo-CA in Figure 3.1F. The mole equivalents of zinc added (indicated in each panel of the figure) were determined from the amount of added zinc based on the concentrations of the two proteins in solution, and verified by AAS measurements. These mole equivalents are stated as the amount of zinc required to saturate a single zinc binding site, thus 5 equivalents are required to complete the titration for the four zinc binding sites in αMT and the one zinc binding site in CA. A very small fraction of the MT did oxidize by the end of the titration, but this did not impact the results of the fitting.

$$apo\alpha MT + Zn^{2+} \overset{K_{1\alpha}}{\rightleftharpoons} Zn_1\alpha MT$$
$$Zn_1\alpha MT + Zn^{2+} \overset{K_{2\alpha}}{\rightleftharpoons} Zn_2\alpha MT$$
$$Zn_2\alpha MT + Zn^{2+} \overset{K_{3\alpha}}{\rightleftharpoons} Zn_3\alpha MT$$
$$Zn_3\alpha MT + Zn^{2+} \overset{K_{4\alpha}}{\rightleftharpoons} Zn_4\alpha MT$$
$$vs.$$
$$apoCA + Zn^{2+} \overset{K_{CA}}{\rightleftharpoons} holoCA$$

Scheme 3.1: Competitive and sequential metallation reactions of apo-αMT and apoCA.

Figure 3.2 shows the relative populations of each of the zinc species during the stepwise zinc titration that were extracted from the deconvoluted ESI mass spectral data. Figure 3.2A shows that apo-αMT metallates non-cooperatively with zinc under the conditions of the experiment as previously described at higher pH.[37] Each of the five αMT species (apo to Zn_4) dominates the species distribution for the amount of zinc added to the solution as expected for non-cooperative binding Zn_1-αMT dominates at one equivalent of added zinc, Zn_2-αMT at two equivalents of added zinc, etc. Figure 3.2B shows the corresponding apoCA and holo-CA population data that were measured simultaneously with the αMT data and also plotted as a function of added zinc. The apoCA begins to compete effectively for incoming zinc only after Zn_3-αMT has formed. No significant amount of holo-CA (Zn_1-CA) was detected earlier in the titration (Figure 3.1A-C). The CA was 50% metallated after approximately 4.2 equivalents of zinc had been added.

www.manaraa.com

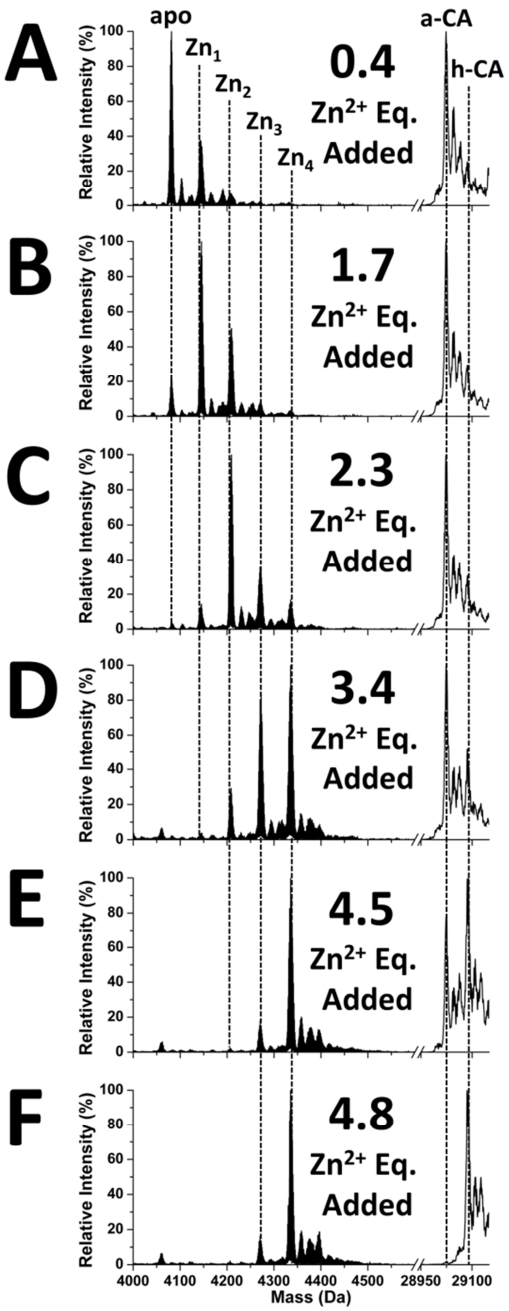

Figure 3.1: Deconvoluted ESI mass spectral data recorded during the competitive zinc titration between equimolar (30 µM) apo-αMT and apoCA at pH 7.0. Equivalents of zinc acetate stock (5 mM in diH_2O) were added into the mixed protein solutions and equilibrated for 3 min prior to measurement. Each of the αMT and CA (a = apo-, h = Zn-CA) species are highlighted with dashed lines. The separate mass ranges for each protein have been individually normalized to 100% abundance.

www.manaraa.com

We have previously described a modeling procedure that simulates these population distributions based on the zinc binding affinities within and between competing species.[30, 31, 38] Here, the affinity constants of the αMT fragment were determined in a similar manner, by minimization of the root mean square difference between the experimental data (Figure 3.2) and a theoretical data set. This theoretically calculated data set was based on the four competitive, sequential, reversible, bimolecular reactions that describe the formation of Zn_4-αMT from apo-αMT and with the competitive reaction that describes the formation of holo-CA from apoCA (Scheme 3.1). In these models, zinc distribution is determined by the thermodynamically preferred occupancy based on the relative values of the individual binding affinities.

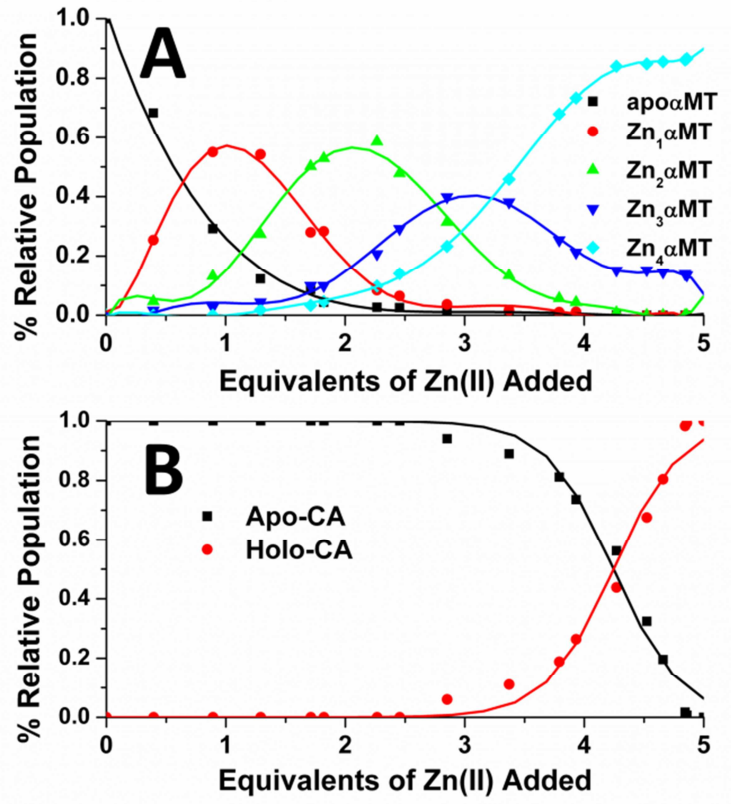

Figure 3.2: Extracted experimental speciation profiles from the competitive zinc titration of equimolar mixtures of apo-αMT (A) and apoCA (B) at pH 7.0. The fraction of each species has been plotted according to the stoichiometry of the zinc added. An equivalent means zinc added for one metal binding site. The lines have been added as guides with no theoretical significance.

www.manaraa.com

Figure 3.3 shows the population curves calculated for the model of the stepwise competitive zinc titration of apo-αMT and apoCA. This is the model that best fit the experimental data set shown in Figure 3.2. To facilitate evaluation of the accuracy of the model, an overlay of experimental data points and predicted modeled speciation is shown in Figure C-1 (Appendix C). These population distributions are based on the four zinc affinity constants of αMT (Figure 3.3A) coupled to the single zinc affinity constant of CA (Figure 3.3B). The relative magnitudes of the affinities are thus anchored to the known value for CA of $\log_{10}(K_F) = 11.4$ at pH 7.[39] The four αMT zinc affinity constants that best fit the experimental data were $\log_{10}(K_{F(\alpha,\ 1\text{-}4)})$: 13.5, 13.2, 12.7, and 12.6. Since the affinities are linked, the quality of the fit for each of the four calculated zinc affinities depends on all of the other values. Because the model is minimized and all of the affinities simultaneously determined in a single step, we are confident in our assessment and estimate the error for each value at < ±0.2 log units.

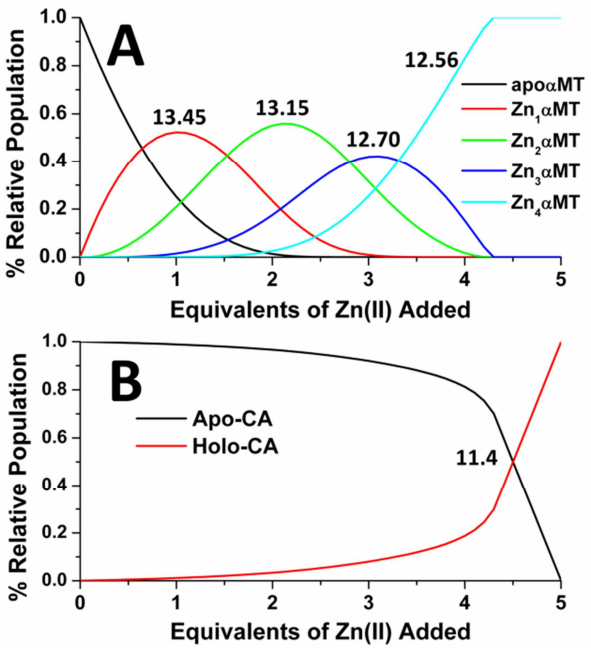

Figure 3.3: Simulation of the competitive zinc metallation of apo-αMT (A) in the presence of apoCA (B). This simulation uses $\log_{10}K_F$ of 13.5, 13.2, 12.7, and 12.6 for the αMT affinity constants. These affinity constants were determined by minimization of the RMSD between the simulated data and the experimental data and the relative affinities anchored to the known zinc affinity constant of CA (11.4).[39]

www.manaraa.com

3.3.2 Competition for Zn^{2+} between apoCA and apo-βMT.

Figure 3.4 shows representative deconvoluted ESI mass spectral data measured during the stepwise competitive zinc titration of a solution of apo-βMT and apoCA. This figure shows the eventual formation of zinc-saturated Zn_3-βMT and holo-CA (Figure 3.4F) as a function of six of the steps of the zinc titrated into an equimolar solution of apo-βMT and apoCA (Figure 3.4A). Here, four equivalents of zinc (three to saturate apo-βMT and one for apoCA) are required to complete the titration. Again, as with the α-MT, a small amount of the β-MT oxidized due to micromolar amounts of dissolved oxygen.

The relative population distributions for each of the species present during the zinc competition between apo-βMT and apoCA were extracted from the ESI mass spectral data and are shown in Figure 3.5, which shows that zinc binds to apo-βMT also non-cooperatively (Zn_1-βMT dominates at one equivalent of added zinc, Zn_2-βMT at two equivalents, etc.). Figure 3.5B shows that the apoCA competes effectively with Zn_2- and Zn_3-βMT. Therefore, less of the incoming zinc binds proportionally to the βMT fragment, and as a result Zn_2- and Zn_3-βMT metallate later in the titration. The shape of the metallation curve for apoCA is neither linear, sigmodal, nor exponential, as a function of added zinc. This is significant as the trend in metallation as a function of added Zn^{2+} is dependent on the relative values of the three binding affinities of the competing species as a function of the amount of added zinc. The apoCA was 50% metallated at approximately 2.5 equivalents of added zinc.

$$apo\beta MT + Zn^{2+} \overset{K_{1\beta}}{\rightleftharpoons} Zn_1\beta MT$$
$$Zn_1\beta MT + Zn^{2+} \overset{K_{2\beta}}{\rightleftharpoons} Zn_2\beta MT$$
$$Zn_2\beta MT + Zn^{2+} \overset{K_{3\beta}}{\rightleftharpoons} Zn_3\beta MT$$
$$vs.$$
$$apoCA + Zn^{2+} \overset{K_{CA}}{\rightleftharpoons} holoCA$$

Scheme 3.2: Competitive and sequential metallation reactions of apo-βMT and apoCA.

www.manaraa.com

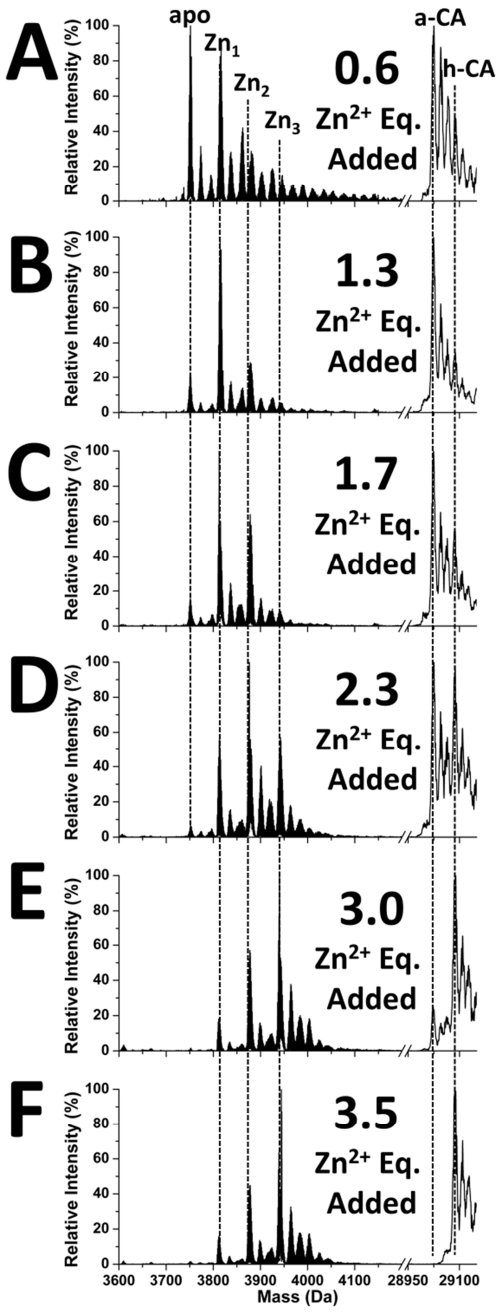

Figure 3.4: Deconvoluted ESI mass spectral data recorded during the competitive zinc titration between equimolar (30 µM) apo-βMT and apoCA (a-CA) at pH 7.0. Equivalents of zinc acetate stock (5 mM in diH_2O) were added into the mixed protein solutions and equilibrated for 3 min prior to measurement. Each of the βMT and CA (a = apo-, h = Zn-CA) species are highlighted with dashed lines. The separate mass ranges for each protein have been individually normalized to 100% abundance.

www.manaraa.com

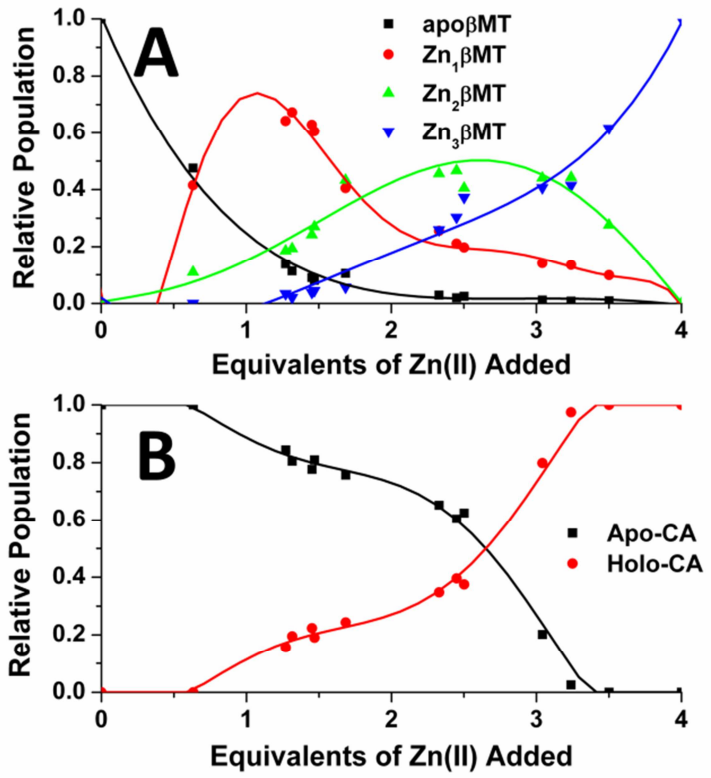

Figure 3.5: Extracted experimental speciation profiles for the competitive zinc titrations of equimolar mixtures of apo-βMT (A) and apoCA (B) at pH 7.0. The fractional presence of each species has been plotted according to the stoichiometry of the zinc added. An equivalent means one metal binding site. The lines have been added as guides with no theoretical significance.

We also modeled the competition between the apo-βMT and apoCA for zinc using the same procedure as described for apo-αMT with apoCA above. Figure 3.6 shows the relative population distributions calculated from the best fitting model of the reaction. The model was also based on minimization of the RMSD between the data in Figure 3.4 and a theoretical dataset created by modeling the three reactions that describe formation of Zn_3-βMT from apo-βMT competing against apoCA (Scheme 3.2). Here, the βMT zinc affinity constants that best reproduced the experimental data were $\log_{10}K_{F(\beta,\ 1\text{-}3)}$): 12.2, 11.7, and 11.4 (± 0.2). The values of these three zinc affinities demonstrate why apoCA ($\log_{10}K_F$ = 11.4) competes with Zn_2- and, much more effectively, with Zn_3-βMT, for the added zinc.

www.manaraa.com

The experimental data for the apo-βMT vs. apoCA zinc competition (Figure 3.5) were more accurately reproduced by the model for the βMT speciation. We have provided an overlay of the modeled population curves and the experimental data points for this best fit for assessment of the model in the supplementary information (Figure C-2, Appendix C). We do note that this model less accurately reproduces the CA population curves. This may be due to the simplicity of the model and the nature of the sequential, linked reactions. We have also included a fit that weighted the apoCA trend more heavily and used a more flexible convergence criterion. The CA metallation data for the alternate model were predicted more accurately, but at the cost of worse fitting to the βMT species (Figures C-3 and C-4, Appendix C).

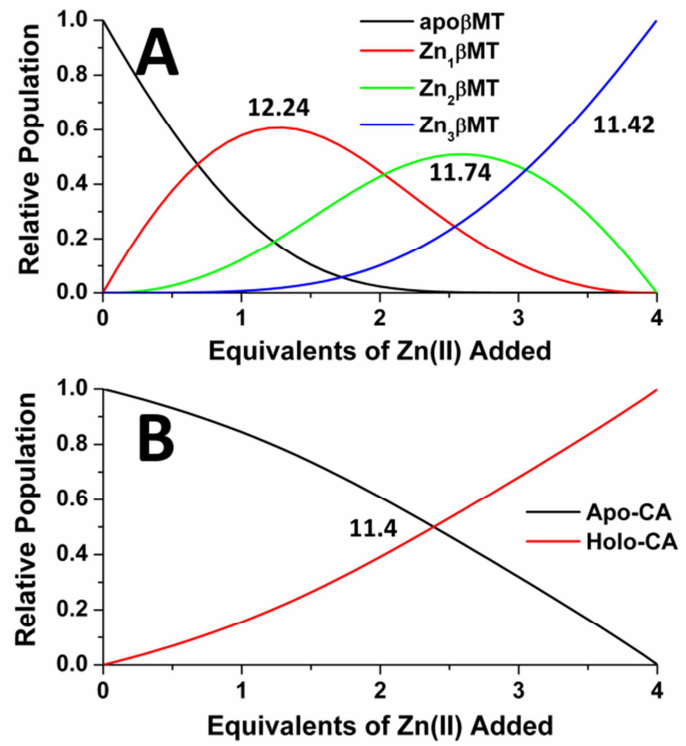

Figure 3.6: Simulation of the competitive zinc metallation of apo-βMT (A) in the presence of apoCA (B). This simulation uses $\log_{10}K_F$ of 12.2, 11.7, and 11.4 for the βMT affinity constants. These affinity constants were determined by minimization of the RMSD between the simulated data and the experimental data with the relative affinities anchored to the known zinc affinity constant of CA (11.4).[39]

www.manaraa.com

3.4 Discussion

3.4.1 Structural properties of MT

To place the significance of these results into perspective, it is necessary to briefly review what is currently known about the structural properties of MTs. In the absence of metals, apoMT shows no well-defined structure; it exists as a globular, bundled structure shown through molecular dynamics calculations,[40] FRET experiments,[41] and the fact that apoMT runs similarly to Zn-MT on Sephadex.[42] With the introduction of metals, this "bundled" peptide chain has to undergo significant structural reorganization to facilitate tetrahedral metal coordination with the four cysteinyl thiolates.[41, 43, 44] Regardless of which thiols initially bind to the incoming metal, the fluxtionality of the MT peptide strand, coupled with the lability of the coordinated metals, ensures that the most favourable thermodynamic product is formed. The complexity of the series of rearrangements that takes place as each metal is added can be understood when one considers the sequence and the folding required for four cysteinyl thiols to bind tetrahedrally to just a single Zn^{2+}. For divalent metals, saturation leads to a further complication with the formation of a combination of bridging and terminal cysteines in the two clustered domains. In the absence of cooperativity (as shown here in the ESI data) the successive formation constants decrease and the separated domains appear late in the titration, after all terminal cysteines have been exhausted in the formation of five $[Zn(Cys)_4]^{2-}$ units. The thiolate sulfurs have to bridge to support the two additional metals. The formation of the clusters results in the protein coalescing into the two-domain structure.[45]

The bonding network within the clusters is different for the Zn_4-αMT and Zn_3-βMT fragments. Zn_3-βMT uses nice cysteines (three bridging and six terminally) while Zn_4-αMT has 11 cysteines (five bridging and six terminal). The ligand:metal ratios are 3.0 and 2.75 for βMT and αMT, respectively. There is only limited definitive information available on the structures formed for unsaturated or partially metallated species (Zn_{1-6}-βαMTs). The binding of cadmium to apoMT has been reported to occur in a domain-specific manner, where the first four equivalents of cadmium added bind exclusively to the α domain, cooperatively.[46, 47] As zinc and cadmium have long been considered

www.manaraa.com

isomorphous in their properties, these data have been widely applied to describe the zinc binding characteristics of MTs, even though there are few studies that have used specifically zinc. In one such study, zinc binding to the apoMT2 isoform was monitored using ESI, which suggested that zinc binding was largely cooperative.[48] We propose that the difference between those data and the data in this report is due to fundamental differences in the experimental design. In the former, the zinc was added to apoMT2 at low pH and the pH was adjusted back to pH 7. In the experiments presented in this report, the zinc was added directly to the apoMT1 at pH7. There could also be different pH dependencies for cooperativity between the isoforms.

3.4.2 Past research on zinc binding properties of MTs

The zinc binding properties of MTs have been investigated since MT was first discovered,[49] though not until more recently have the average zinc binding affinities of MT been reported (Table 3.1). Both MT1 and MT2 bind cadmium and zinc with high affinities. Proton titrations of the separated zinc saturated domain fragments of MT2 showed average zinc affinities for the β fragment as $\log_{10}K_F$ = 11.3 (average apparent).[50] This value is comparable to the average of the three modeled βMT zinc affinities reported here (average $\log_{10}K_F$ = 11.9). Though 0.6 log units seems a large discrepancy, we consider the approximate agreement as verification of our methodology, especially considering that the data are for different isoforms, have been determined using vastly different methodologies, and falls within one order of magnitude of other apparent average affinities determined for MTs. Average affinities for the seven zinc binding sites have also been reported: $\log_{10}K_F$ = 12.9 from proton titrations of MT2[51], 11.5 and 10.8, from competition experiments between the chelator 5F-BAPTA and MT2 and MT3, respectively.[52] MT2 has also been shown to transfer only a single zinc to apo-SDH which has a zinc affinity (K_D = 6 pM) similar, but slightly less than that of CA (K_D = 4 pM).[53]

Previous work using the MT2 isoform suggested that the highest affinity binding constants (for the first four zinc added) bound zinc with approximately the same high affinity, and that the last three were each bound with lower, sequentially decreasing affinities, and also suggested one very low affinity with $\log_{10}(K)$ of > 8.[54] The very low

www.manaraa.com

binding affinity was later shown to be an artifact of the apoMT preparation procedure, rather than a fundamental property of MTs.[55] Our studies on domain-domain competition between the individual domains and with the intact MT1A protein revealed that the first four zinc bound also with differing affinity, expanding the "ladder" of K's from four to seven, one for each metal bound to apo-βαMT.[31, 56] We followed with a report on the competitive zinc titration between the full rhMT1A protein and apoCA where we determined values for each of those seven independent zinc affinity constants, and simultaneously confirmed the lack of any very low zinc binding affinity as had been suggested (or else the CA would have outcompeted the very weak site entirely).[30] The seven affinity constants span a range of zinc affinities that appear to permit MT to both homeostatically control the delivery of zinc to apo-enzymes and to lock away zinc in thermodynamically inaccessible pools, properties that are dependent on the intracellular concentrations of zinc, MTs, and other zinc binding proteins. However, questions regarding the domain properties with respect to the both the zinc storage (for the first bound, high affinity sites) and zinc donation (for the last, most weakly bound low affinity sites), remained. Particularly, it was not clear which section of the peptide exhibited the highest or lowest affinities.

The transfer of zinc from MT to apoCA has been shown to follow a PPI mechanism from the bimolecular reactions reported by Petering and coworkers.[57, 58] However, there is no definitive structural information showing possible exchange location. The dumbbell-shape of Zn_7-βαMT includes two crevices that expose on the surface the α and β metalloclusters that could permit metal donation from either domain. Robbins and Stout also reported on the solvent accessibility of the sulfurs in the two domains of the crystal structure, finding that the four sulfurs bound to one zinc in the β domain had the highest solvent accessibility (than all other metals), which may be key to the more efficient competitive metal transfer from the β-domain to the apoCA in the PPI.[59]

The competition experiment, where two species compete for a common metal exploits differences in affinities.[60] The zinc occupies the binding site of the most thermodynamically preferred coordination mode. These experiments provide the relative affinities of the competing species directly with no analysis, as the values are apparent

www.manaraa.com

from the observed speciation. We modeled the effects of competitor strength on zinc distribution between two competing species in our previous report.[30] In this current report, we have modeled the zinc affinity constants of the individual domain fragments. These models were based on ESI mass spectral data measured during competitive zinc titrations between apoCA and metal free MT domain fragments. The modeling of the complete competition reaction, with stepwise binding of zinc to both proteins (MT and CA), locks the modeled domain zinc affinities to the known value for CA. Our current models provide strong evidence that this method of modeling as originally demonstrated for the intact βαMT protein is an accurate means of calculating the ladder of binding affinities (the seven independent K_F's for zinc binding to βαMT).[61-63]

Table 3.1: Comparison of reported average zinc affinity constant data of MTs.

Isoform	Domain	Method	pH	Reported avg. ($log_{10}(K_F)$)	Ref.
MT1	βα	NTA Competition	7.4	11.33	[64]
	βα	H_2KTMS_2 Competition		11.10	
MT2	β	Proton Titration	7.0	11.30	[50]
MT2	βα	Competition with 8-hydroxy-quinoline-5-sulfonic acid	7.0	12.85	[51]
MT2	βα	Zinc titrations and competition with FluoZin-3 and RhodZin-3	7.4	11.56	[65]
MT2	βα	Competition with PAR	7.4	12.50	[66]
MT2	βα	H_2KTSM_2 competition	7.4	11.23	[64]
MT1 and MT2 average	βα	NTA + H_2KTSM_2 + Proton Competition Results Averaged	7.4	11.24	[64]
	β			11.22	
	α			11.25	
MT2	βα	5F-BAPTA competition	8.0	11.49	[52]
MT3	βα			10.79	
rhMT1A	βα	Competition between apoMT strands	9.2	12.77	[31]
	β			12.45	
	α			12.24	
rhMT1A	βα	Competition with apoCA	7.0	12.30	[30]
rhMT1A	β	Competition with apoCA	7.0	11.93	This work
	α			13.11	
	β + α	Sum of fragments		12.88	

www.manaraa.com

3.4.3 Competition between the apofragments and apoCA

Figure 3.1 demonstrates that the αMT fragment outcompetes the apoCA for the added zinc. Figure 3.1A-C, where apo-αMT, Zn_1-αMT and Zn_2-αMT dominate, show no detectable amount of zinc binding to the apoCA. It is not until after the formation of the weaker bound Zn_3- and Zn_4-αMT species are formed does the CA begin to metallate (Figure 3.1D-F). In fact, by the point in the titration where CA is only ~50% metallated, the αMT fragment is essentially filled. These results demonstrate experimentally and conclusively that the αMT fragment affinity constants are all greater than that of CA.

The relative concentrations of each of the Zn_n-MT species can be estimated from the ESI-MS data, as was first shown by Fenselau.[67] We have used similar methodologies in the past to study the kinetics of arsenic binding to various MTs.[12, 13, 68, 69] We normalize each protein only against itself as the intensities of the ESI-MS peaks have been shown to remain approximately the same for different metallation states of the same protein/isoform at the same pH.[70] There are numerous other examples of thermodynamic properties determined from similar ESI-based experiments from other research groups, even specifically for MT. The Palumma group determined copper binding affinities of various copper binding proteins, including MT with ESI-MS.[71, 72] The Russel group used peak intensities to determine relative cadmium binding constants of MT2.[73] And, finally, the Blindauer group[74, 75] and Freisinger group[76, 77] used ESI-MS data (including peak intensities) to characterize metal binding and modifications to MTs.

Each Zn_n-αMT (n = 0 - 4) species develops and dominates the MT speciation in turn as a function of the amount of added zinc as shown in the extracted speciation profiles in Figure 3.2A. The non-cooperative filling of the α domain is demonstrated by the presence of the dominating species at each equivalent of zinc added (Zn_1-αMT dominates at 1 eq, Zn_2-αMT at 2 eq, etc.). The αMT fragment saturates when only slightly more than four equivalents of zinc are added due to the lack of competition by the apoCA. This is reflected in the results for the apoCA metallation in Figure 3.2B where no appreciable amount of apoCA metallates until a significant fraction of Zn_4-αMT has formed.

www.manaraa.com

The fact that the αMT fragment outcompetes apoCA for zinc binding lies in stark contrast with the results of the apo-βMT fragment metallation (Figure 3.4 and Figure 3.5). The data for the zinc competition between the apo-βMT fragment and apoCA indicate that the βMT zinc affinities span a range over which apoCA can compete efficiently.

Figure 3.4A-B shows that the first metal binds almost exclusively in the βMT fragment, with no significant amount of zinc detected bound to CA. Then, as the βMT fragment fills, the CA competes with the lower affinity Zn_2- and Zn_3-βMT species (Figure 3.4C-E). The CA is also saturated before the βMT fragment (Figure 3.4F). This trend becomes more apparent when the populations of the species during the titration are plotted (Figure 3.5). The appearance of Zn_2- and Zn_3-βMT is shifted to later in the titration due to the CA binding zinc between 1-3 equivalents of added zinc.

The binding of zinc to apoCA during the competition with βMT (Figure 3.5B) occurs nonlinearly and mirrors the span of the zinc affinities of the βMT fragment. This is because populating the apoCA depends upon the affinity of the species against which it is competing. Between 0 and 1 equivalents of zinc added, the apoCA is competing with the highest affinity Zn_1-βMT, and very little zinc is bound by apoCA. This indicates that Zn_1-βMT has an affinity that is beyond the reach of apoCA. Then between 1.25 and 2.25 equivalents of zinc added, the apoCA binds a greater fraction of added zinc as it competes with the more favorable Zn_2-βMT affinity. Finally, from 2.25 to 3.25 eq of zinc added, the apoCA metallates sharply, when it is competing mostly against formation of the weakest affinity Zn_3-βMT.

3.4.4 Evidence for domain interactions in intact βα-MT that modulate zinc affinities

The values determined for the zinc affinities of the αMT (Figure 3.3) and βMT (Figure 3.6) fragments are shown in Figure 3.7. The binding affinities decrease linearly as a function of binding sites. We have included the calculated data for the intact protein on the same axis (pink triangles) previously reported for comparison. The seven binding constants of the intact βαMT show that the first two zinc binding affinities are

www.manaraa.com

significantly depressed relative to the linear trend. We had interpreted this to indicate the tangling of the apo-peptide within the globular bundle and the resulting scrambling of the set of cysteine ligands required to form the terminally bound zinc ions. The zinc affinities of the fragments do not show this same depression. We suggest that this is due to the shorter chain lengths becoming less bundled and the cysteines are thus more easily reorganized to form the metal binding sites in the apo-proteins. Therefore, the formation of the "binding sites" upon zinc addition requires a lesser degree of structural reorganization.

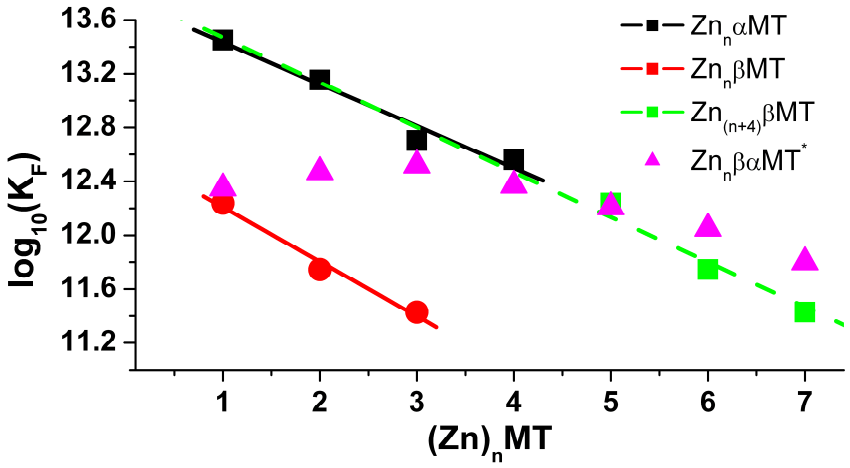

Figure 3.7: Comparison of the calculated zinc affinity constants for zinc binding to αMT1A (black) and βMT1A (red). The symbols show the calculated binding constants and the lines show linear fits to each set. The green dashed line shows the linear fit for the β fragment affinities shifted by four to illustrate the expected linear trend for connected fragments. *Affinity data for the zinc binding to the intact βαMT replotted from ref[30] (pink triangles).

The significant result of the binding constant data reported here is that only the first two zinc binding affinities are modulated by domain-domain interactions when the two fragments are linked together in the intact βαMT. We have shown that the βMT binding affinity constants shifted by four sites to simulate linking of the isolated β and the α fragments (green squares) overlap the affinity constants of the intact protein. Surprisingly, the linear trends between the α domain (solid black line) and the α + shifted

www.manaraa.com

β (dashed green line) are practically co-linear. This linearity spans the range of the intact βαMT protein.

The difference between the trend for the sum of the individual α and β fragments (4 + 3 sites) and the intact βαMT (7 sites) shows that the intact protein chain length (and number of cysteines) influences the resulting metal binding properties. Our quantitative data show that this change is not as previously discussed, namely due to the linker between the two formed clusters for the saturated intact protein. The difference is due to the effects of strand unbundling and cysteine scrambling for the first two metals bound only. However, fully metallated Zn_7-βαMT, which absolutely has the metals separated into the two (α-4 sites + β-3 sites) distinct domains, likely donates the weakest bound zinc from the β domain. Formation of $(Zn_4S_{11})(Zn_2S_9)$-βαMT (α-4 sites + β-2 sites) following a zinc donation event, likely leads to reorganization of the cysteine ligands where the zinc ions are bound by cysteine ligands across the length of the peptide (αβ-6 sites, i.e. there are additional rearrangement options for the longer intact MT compared to the shorter domain fragments) and not into specific domains, as inferred from the stabilization of the intact protein data vs. the separated fragment domains.

3.5 Conclusions

In this Chapter, we have shown the precise metallation status of MT1A fragments competing with CA for available zinc. The ESI mass spectral data show that apoCA competes effectively only with the weakest bound zinc, Zn_4-αMT and Zn_{2-3}-βMT. We have calculated relative zinc affinity constants for each of the zinc binding events in both fragments and locked these affinities to the known affinity of CA. The affinities in both domains decrease linearly as a function of the number of remaining zinc binding sites.

Comparing the affinities of the separated domains with the intact MT1A protein, we suggest that in the apo-βαMT significant scrambling of the cysteines of the MT protein strand depresses the first two zinc affinities. Using the affinity data of the fragments, we propose that the zinc is donated from the N-terminal β cluster in Zn_7-βαMT. The stabilization of Zn_6-βαMT and Zn_7-βαMT, relative to the isolated domains, was

www.manaraa.com

suggested to be a result of increased plasticity in metal coordination due to the longer peptide chain and greater number of cysteine ligands. These data provide support for, and new details on, the homeostatic interactions of MT and zinc enzymes in regards to the zinc donation and binding properties of MT1A and other MTs in general.

3.6 References

1. Coyle, P., Philcox, J., Carey, L., and Rofe, A. (2002) Metallothionein: The multipurpose protein, *Cell. Mol. Life Sci. 59*, 627-647.
2. Capdevila, M., and Atrian, S. (2011) Metallothionein protein evolution: a miniassay, *J. Biol. Inorg. Chem. 16*, 977-989.
3. Blindauer, C. A., and Leszczyszyn, O. I. (2010) Metallothioneins: Unparalleled diversity in structures and functions for metal ion homeostasis and more, *Nat. Prod. Rep. 27*, 720-741.
4. Cobbett, C., and Goldsbrough, P. (2002) Phytochelatins and metallothioneins: Roles in heavy metal detoxification and homeostasis, *Annu. Rev. Plant Biol. 53*, 159-182.
5. Robinson, N. J. (2008) A bacterial copper metallothionein, *Nat. Chem. Biol. 4*, 582-583.
6. Meloni, G., Sonois, V., Delaine, T., Guilloreau, L., Gillet, A., Teissie, J., Faller, P., and Vasak, M. (2008) Metal swap between Zn_7-metallothionein-3 and amyloid-ß-Cu protects against amyloid-ß toxicity, *Nat. Chem. Biol. 4*, 366-372.
7. Blindauer, C. A. (2015) Advances in the molecular understanding of biological zinc transport, *Chem. Commun. 51*, 4544-4563.
8. Boulanger, Y., Armitage, I., Miklossy, K., and Winge, D. (1982) 113Cd NMR study of a metallothionein fragment. Evidence for a two-domain structure, *J. Biol. Chem. 257*, 13717-13719.
9. Robbins, A. H., McRee, D. E., Williamson, M., Collett, S. A., Xuong, N. H., Furey, W. F., Wang, B. C., and Stout, C. D. (1991) Refined crystal structure of Cd, Zn metallothionein at 2.0Å resolution, *J. Mol. Biol. 221*, 1269-1293.
10. Braun, W., Vasak, M., Robbins, A., Stout, C., Wagner, G., Kägi, J., and Wüthrich, K. (1992) Comparison of the NMR solution structure and the X-ray crystal structure of rat metallothionein-2, *Proc. Natl. Acad. Sci. U. S. A. 89*, 10124-10128.
11. Feng, W., Cai, J., Pierce, W. M., Franklin, R. B., Maret, W., Benz, F. W., and Kang, Y. J. (2005) Metallothionein transfers zinc to mitochondrial aconitase through a direct interaction in mouse hearts, *Biochem. Biophys. Res. Commun. 332*, 853-858.
12. Ngu, T. T., Easton, A., and Stillman, M. J. (2008) Kinetic analysis of arsenic-metalation of human metallothionein: Significance of the two-domain structure, *J. Am. Chem. Soc. 130*, 17016-17028.
13. Ngu, T. T., Lee, J. A., Pinter, T. B., and Stillman, M. J. (2010) Arsenic-metalation of triple-domain human metallothioneins: Support for the evolutionary advantage and interdomain metalation of multiple-metal-binding domains, *J. Inorg. Biochem. 104*, 232-244.
14. Mauro, J. M., and Pazirandeh, M. (2000) Construction and expression of functional multi-domain polypeptides in Escherichia coli: expression of the Neurospora crassa metallothionein gene, *Lett. Appl. Microbiol. 30*, 161-166.

www.manaraa.com

15. Petering, D. H., Zhu, J., Krezoski, S., Meeusen, J., Kiekenbush, C., Krull, S., Specher, T., and Dughish, M. (2006) Apo-metallothionein emerging as a major player in the cellular activities of metallothionein, *Exp. Biol. Med. 231*, 1528-1534.
16. Rana, U., Kothinti, R., Meeusen, J., Tabatabai, N. M., Krezoski, S., and Petering, D. H. (2008) Zinc binding ligands and cellular zinc trafficking: Apo-metallothionein, glutathione, TPEN, proteomic zinc, and Zn-Sp1, *J. Inorg. Biochem. 102*, 489-499.
17. Pattanaik, A., Shaw III, C. F., Petering, D. H., Garvey, J., and Kraker, A. J. (1994) Basal metallothionein in tumors: Widespread presence of apoprotein, *J. Inorg. Biochem. 54*, 91-105.
18. Apostolova, M., Bontchev, P., Nachev, C., and Sirakova, I. (1993) Apometallothionein in rat liver, *J. Chromatogr. B Biomed. Appl. 620*, 191-197.
19. Yang, Y., Maret, W., and Vallee, B. L. (2001) Differential fluorescence labeling of cysteinyl clusters uncovers high tissue levels of thionein, *Proc. Natl. Acad. Sci. U. S. A. 98*, 5556-5559.
20. Kang, Y. J. (2006) Metallothionein redox cycle and function, *Exp. Biol. Med. 231*, 1459-1467.
21. Maret, W., and Vallee, B. L. (1998) Thiolate ligands in metallothionein confer redox activity on zinc clusters, *Proc. Natl. Acad. Sci. U. S. A. 95*, 3478-3482.
22. Zalewska, M., Trefon, J., and Milnerowicz, H. (2014) The role of metallothionein interactions with other proteins, *Proteomics 14*, 1343-1356.
23. Udom, A. O., and Brady, F. O. (1980) Reactivation in vitro of zinc-requiring apo-enzymes by rat liver zinc-thionein, *Biochem. J. 187*, 329-335.
24. Lindskog, S., and Malmström, B. G. (1962) Metal binding and catalytic activity in bovine carbonic anhydrase, *J. Biol. Chem. 237*, 1129-1137.
25. Avvaru, B. S., Busby, S. A., Chalmers, M. J., Griffin, P. R., Venkatakrishnan, B., Agbandje-McKenna, M., Silverman, D. N., and McKenna, R. (2009) Apo-human carbonic anhydrase II revisited: Implications of the loss of a metal in protein structure, stability, and solvent network, *Biochemistry 48*, 7365-7372.
26. Zaia, J., Fabris, D., Wei, D., Karpel, R. L., and Fenselau, C. (1998) Monitoring metal ion flux in reactions of metallothionein and drug-modified metallothionein by electrospray mass spectrometry, *Protein Sci. 7*, 2398-2404.
27. Mason, A. Z., Moeller, R., Thrippleton, K. A., and Lloyd, D. (2007) Use of stable isotopically enriched proteins and directly coupled high-performance liquid chromatography inductively coupled plasma mass spectrometry for quantitatively monitoring the transfer of metals between proteins, *Anal. Biochem. 369*, 87-104.
28. Jacob, C., Maret, W., and Vallee, B. L. (1998) Control of zinc transfer between thionein, metallothionein, and zinc proteins, *Proc. Natl. Acad. Sci. U. S. A. 95*, 3489-3494.
29. Ejnik, J., Muñoz, A., Gan, T., Shaw III, C. F., and Petering, D. (1999) Interprotein metal ion exchange between cadmium-carbonic anhydrase and apo-or zinc-metallothionein, *J. Biol. Inorg. Chem. 4*, 784-790.
30. Pinter, T. B. J., and Stillman, M. J. (2014) The zinc balance: Competitive zinc metalation of carbonic anhydrase and metallothionein 1A, *Biochemistry 53*, 6276-6285.
31. Summers, K. L., Sutherland, D. E. K., and Stillman, M. J. (2013) Single-domain metallothioneins: Evidence of the onset of clustered metal binding domains in Zn-rhMT 1a, *Biochemistry 52*, 2461-2471.
32. Sutherland, D. E. K., and Stillman, M. J. (2008) Noncooperative cadmium(II) binding to human metallothionein 1a, *Biochem. Biophys. Res. Commun. 372*, 840-844.

www.manaraa.com

33. Merrifield, M. E., Huang, Z., Kille, P., and Stillman, M. J. (2002) Copper speciation in the α and β domains of recombinant human metallothionein by electrospray ionization mass spectrometry, *J. Inorg. Biochem. 88*, 153-172.
34. Hunt, J. B., Rhee, M.-J., and Storm, C. B. (1977) A rapid and convenient preparation of apocarbonic anhydrase, *Anal. Biochem. 79*, 614-617.
35. Coleman, J. E. (1967) Mechanism of action of carbonic anhydrase: Substrate, sulfonamide, and anion binding, *J. Biol. Chem. 242*, 5212-5219.
36. Chen, R. F., and Kernohan, J. C. (1967) Combination of bovine carbonic anhydrase with a fluorescent sulfonamide, *J. Biol. Chem. 242*, 5813-5823.
37. Sutherland, D. E., Summers, K. L., and Stillman, M. J. (2012) Noncooperative metalation of metallothionein 1a and its isolated domains with zinc, *Biochemistry 51*, 6690-6700.
38. Sutherland, D. E. K., Summers, K. L., and Stillman, M. J. (2012) Modeling the Zn^{2+} and Cd^{2+} metalation mechanism in mammalian metallothionein 1a, *Biochem. Biophys. Res. Commun. 426*, 601-607.
39. Kiefer, L. L., Krebs, J. F., Paterno, S. A., and Fierke, C. A. (1993) Engineering a cysteine ligand into the zinc binding site of human carbonic anhydrase II, *Biochemistry 32*, 9896-9900.
40. Rigby, K. E., Chan, J., Mackie, J., and Stillman, M. J. (2006) Molecular dynamics study on the folding and metallation of the individual domains of metallothionein, *Proteins: Struct., Funct., Bioinf. 62*, 159-172.
41. Hong, S.-H., and Maret, W. (2003) A fluorescence resonance energy transfer sensor for the β-domain of metallothionein, *Proc. Natl. Acad. Sci. U. S. A. 100*, 2255-2260.
42. Minkel, D. T., Poulsen, K., Wielgus, S., Shaw, C. F., 3rd, and Petering, D. H. (1980) On the sensitivity of metallothioneins to oxidation during isolation, *Biochem. J. 191*, 475-485.
43. Irvine, G. W., Summers, K. L., and Stillman, M. J. (2013) Cysteine accessibility during As^{3+} metalation of the α-and β-domains of recombinant human MT1a, *Biochem. Biophys. Res. Commun. 433*, 477-483.
44. Irvine, G. W., and Stillman, M. J. (2013) Topographical analysis of As-induced folding of α-MT1a, *Biochem. Biophys. Res. Commun. 441*, 208-213.
45. Sutherland, D. E. K., and Stillman, M. J. (2014) Challenging conventional wisdom: Single domain metallothioneins, *Metallomics 6*, 702-728.
46. Stillman, M. J., and Zelazowski, A. (1988) Domain specificity in metal binding to metallothionein. A circular dichroism and magnetic circular dichroism study of cadmium and zinc binding at temperature extremes, *J. Biol. Chem. 263*, 6128-6133.
47. Nielson, K. B., and Winge, D. (1983) Order of metal binding in metallothionein, *J. Biol. Chem. 258*, 13063-13069.
48. Gehrig, P. M., You, C., Dallinger, R., Gruber, C., Brouwer, M., KÄGI, J. H., and Hunziker, P. E. (2000) Electrospray ionization mass spectrometry of zinc, cadmium, and copper metallothioneins: evidence for metal-binding cooperativity, *Protein Sci. 9*, 395-402.
49. Margoshes, M., and Vallee, B. L. (1957) A cadmium protein from equine kidney cortex, *J. Am. Chem. Soc. 79*, 4813-4814.
50. Jiang, L.-J., Vašák, M., Vallee, B. L., and Maret, W. (2000) Zinc transfer potentials of the α- and β-clusters of metallothionein are affected by domain interactions in the whole molecule, *Proc. Natl. Acad. Sci. U. S. A. 97*, 2503-2508.
51. Kägi, J. H. R. (1993) Evolution, structure and chemical activity of class I metallothioneins: An overview, In *Metallothionein III : Biological Roles and Medical Implications* (Suzuki, K. T., Imura, N., and Kimura, M., Eds.), pp 29-55, Birkhäuser Verlag, Basel ; Boston.

www.manaraa.com

52. Hasler, D. W., Jensen, L. T., Zerbe, O., Winge, D. R., and Vašák, M. (2000) Effect of the two conserved prolines of human growth inhibitory factor (Metallothionein-3) on its biological activity and structure Eluctuation: Comparison with a mutant protein, *Biochemistry 39*, 14567-14575.
53. Jiang, L.-J., Maret, W., and Vallee, B. L. (1998) The glutathione redox couple modulates zinc transfer from metallothionein to zinc-depleted sorbitol dehydrogenase, *Proc. Natl. Acad. Sci. U. S. A. 95*, 3483-3488.
54. Krężel, A., and Maret, W. (2007) Dual nanomolar and picomolar Zn(II) binding properties of metallothionein, *J. Am. Chem. Soc. 129*, 10911-10921.
55. Namdarghanbari, M. A., Meeusen, J., Bachowski, G., Giebel, N., Johnson, J., and Petering, D. H. (2010) Reaction of the zinc sensor FluoZin-3 with Zn 7-metallothionein: inquiry into the existence of a proposed weak binding site, *J. Inorg. Biochem. 104*, 224-231.
56. Krężel, A., and Maret, W. (2008) Thionein/metallothionein control Zn(II) availability and the activity of enzymes, *J. Biol. Inorg. Chem. 13*, 401-409.
57. Li, T.-Y., Kraker, A. J., Shaw, C. F., and Petering, D. H. (1980) Ligand substitution reactions of metallothioneins with EDTA and apo-carbonic anhydrase, *Proc. Natl. Acad. Sci. U. S. A. 77*, 6334-6338.
58. Huang, M., Shaw III, C. F., and Petering, D. H. (2004) Interprotein metal exchange between transcription factor IIIa and apo-metallothionein, *J. Inorg. Biochem. 98*, 639-648.
59. Robbins, A. H., and Stout, C. D. (1991) Crystal structure of metallothionein In *Metallothioneins: Synthesis, Structure and Properties of Metallothioneins: Phytochelatins, and Metal-Thiolate Complexes* (Stillman, M. J., Shaw, C. F., and Suzuki, K. T., Eds.), pp 31 - 54, Wiley-VCH Verlag GmbH, New York.
60. Heinz, U., Kiefer, M., Tholey, A., and Adolph, H.-W. (2005) On the competition for available zinc, *J. Biol. Chem. 280*, 3197-3207.
61. Tottey, S., Harvie, D. R., and Robinson, N. J. (2005) Understanding how cells allocate metals using metal sensors and metallochaperones, *Acc. Chem. Res. 38*, 775-783.
62. Cousins, R. J., Liuzzi, J. P., and Lichten, L. A. (2006) Mammalian zinc transport, trafficking, and signals, *J. Biol. Chem. 281*, 24085-24089.
63. Eide, D. J. (2006) Zinc transporters and the cellular trafficking of zinc, *Biochim. Biophys. Acta, Mol. Cell Res. 1763*, 711-722.
64. Namdarghanbari, M. A., Meeusen, J., Bachowski, G., Giebel, N., Johnson, J., and Petering, D. H. (2010) Reaction of the Zinc Sensor FluoZin-3 with Zn(7)-metallothionein: Inquiry into the Existence of a Proposed Weak Binding Site, *J. Inorg. Biochem. 104*, 224-231.
65. Krężel, A., and Maret, W. (2007) Dual nanomolar and picomolar Zn (II) binding properties of metallothionein, *J. Am. Chem. Soc. 129*, 10911-10921.
66. Peroza, E. A., dos Santos Cabral, A., Wan, X., and Freisinger, E. (2013) Metal ion release from metallothioneins: proteolysis as an alternative to oxidation, *Metallomics 5*, 1204-1214.
67. Yu, X., Wojciechowski, M., and Fenselau, C. (1993) Assessment of metals in reconstituted metallothioneins by electrospray mass spectrometry, *Anal. Chem. 65*, 1355-1359.
68. Ngu, T. T., and Stillman, M. J. (2006) Arsenic Binding to Human Metallothionein, *J. Am. Chem. Soc. 128*, 12473-12483.

www.manaraa.com

69. Ngu, T. T., Lee, J. A., Rushton, M. K., and Stillman, M. J. (2009) Arsenic Metalation of Seaweed Fucus vesiculosus Metallothionein: The Importance of the Interdomain Linker in Metallothionein, *Biochemistry 48*, 8806-8816.
70. Pérez-Rafael, S., Atrian, S., Capdevila, M., and Palacios, Ò. (2011) Differential ESI-MS behaviour of highly similar metallothioneins, *Talanta 83*, 1057-1061.
71. Banci, L., Bertini, I., Ciofi-Baffoni, S., Kozyreva, T., Zovo, K., and Palumaa, P. (2010) Affinity gradients drive copper to cellular destinations, *Nature 465*, 645-648.
72. Chung, R. S., Howells, C., Eaton, E. D., Shabala, L., Zovo, K., Palumaa, P., Sillard, R., Woodhouse, A., Bennett, W. R., Ray, S., Vickers, J. C., and West, A. K. (2010) The Native Copper- and Zinc- Binding Protein Metallothionein Blocks Copper-Mediated Aβ Aggregation and Toxicity in Rat Cortical Neurons, *PLoS ONE 5*, e12030.
73. Chen, S.-H., Russell, W. K., and Russell, D. H. (2013) Combining Chemical Labeling, Bottom-Up and Top-Down Ion-Mobility Mass Spectrometry To Identify Metal-Binding Sites of Partially Metalated Metallothionein, *Anal. Chem. 85*, 3229-3237.
74. Leszczyszyn, O. I., Zeitoun-Ghandour, S., Sturzenbaum, S. R., and Blindauer, C. A. (2011) Tools for metal ion sorting: in vitro evidence for partitioning of zinc and cadmium in C. elegans metallothionein isoforms, *Chem. Commun. 47*, 448-450.
75. Leszczyszyn, O. I., and Blindauer, C. A. (2010) Zinc transfer from the embryo-specific metallothionein EC from wheat: a case study, *Phys. Chem. Chem. Phys. 12*, 13408-13418.
76. Peroza, E. A., Kaabi, A. A., Meyer-Klaucke, W., Wellenreuther, G., and Freisinger, E. (2009) The two distinctive metal ion binding domains of the wheat metallothionein Ec-1, *J. Inorg. Biochem. 103*, 342-353.
77. Peroza, E. A., and Freisinger, E. (2008) Tris is a non-innocent buffer during intein-mediated protein cleavage, *Protein Expr. Purif. 57*, 217-225.

www.manaraa.com

Chapter 4

4 Domain selection in metallothionein 1A: Affinity controlled mechanisms of zinc binding and cadmium exchange*

4.1 Introduction

Zinc is intricately involved in a myriad of essential biological processes, including enzymatic catalysis, respiration, protein folding, cell signaling, and tissue growth.[1-3] These functions are significantly disrupted in the presence of cadmium from common sources of chronic cadmium exposure or more rarely acute cadmium poisoning.[4] The effect of cadmium toxicity on organisms has been well documented,[5] though the details of the toxicological action at the molecular level are not fully understood.[6, 7] Cellular function is maintained only within a relatively narrow range of zinc concentrations[8] and even low cadmium levels disrupt this.[4] The family of metallothionein proteins is considered to be largely responsible for maintaining the homeostatic control of zinc levels. It has been widely proposed that metallothionein is also involved in the detoxification of cadmium.[9] Currently, this detoxification mechanism is thought to occur in a domain-selective fashion.[10]

Metallothioneins (MTs) are a superfamily of cysteine-rich, metal-binding proteins that are found in all forms of life.[11, 12] MTs bind biologically-relevant metals with relatively high binding affinities (K_F). *In vivo* functions of MTs include metal homeostasis and detoxification of toxic metals.[13, 14] MTs are generally characterized by their relatively small size (60-70 amino acids for human MTs), and high cysteine content, with up to one-third of the sequence comprised of Cys residues.[2] The redox properties of these thiols have also implicated MTs in the cellular response to oxidative stress.[15, 16]

---

* A version of this Chapter has been published:

Reproduced with permission from: T.B.J. Pinter, G.W. Irvine, and M.J. Stillman. *Biochemistry* 54 (2015): 5006-5016. Copyright 2015 American Chemical Society.

www.manaraa.com

There are four known isoforms (and numerous subisoforms) of human metallothionein: MT1, MT2, MT3 and MT4. The human MT1 and MT2 isoforms are involved in zinc homeostasis and heavy metal detoxification. MT3 and MT4 are expressed in specialized cells and tissues: MT3 in neuronal and glial brain cells, and MT4 in squamous epithelial cells.[17] All human MT isoforms have a high degree of sequence conservation and, for the divalent metal-saturated species, a two-domain metal cluster structure in which the domains are arranged in a dumbbell-like fashion.[18] It is important to note that structures have been determined only for the metal-saturated MTs, as the apo and partially metallated forms of MT are too fluxional, prohibiting NMR structural analysis and preventing crystallization. Significantly, this two-domain cluster structure is formed only when MT is nominally saturated with seven divalent metals.[19]

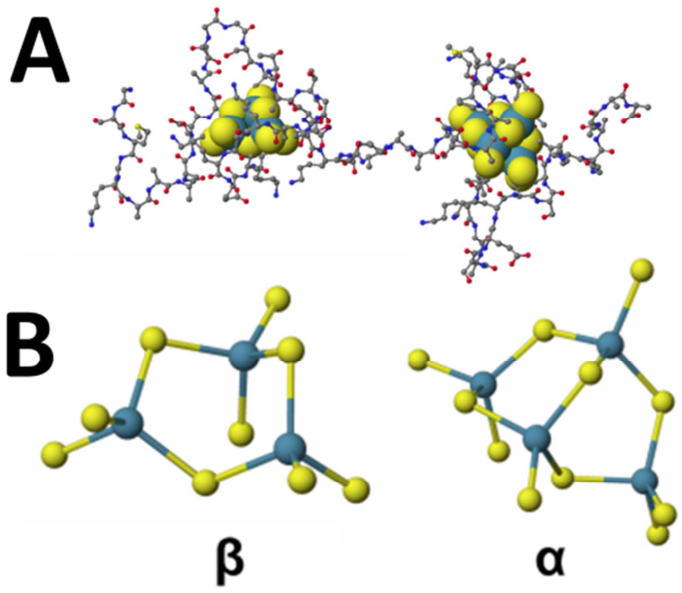

Figure 4.1: (A) Protein structure, (B) metalloclusters of the β and α domains of zinc-saturated rh-MT1A.

The structure of the metal cluster is dependent on both the stoichiometry of added metals and the preferred coordination number of the metal(s).[20, 21] For zinc- and cadmium-saturated human MT1A (Figure 4.1) the N-terminal β domain binds three metals using nine cysteine thiolates and the C-terminal α domain binds four metals using 11 cysteines; all of the metals are tetrahedrally coordinated through a combination of bridging and

www.manaraa.com

terminal thiolates (Figure 4.1B).[22] Past research has highlighted the significance of the metal-saturated, two-domain structure and its relevance to the metal binding and release properties. However, recent work by Chen et al.,[23] Krężel et al.,[24] and the Stillman group[25] has demonstrated the importance of intermediates in the metallation pathway from the metal-free apoMT to the fully metal-saturated holo-MT.

The mechanism for detoxification of cadmium by MT is currently reported to occur in a domain-specific manner (Figure 4.2, Pathway 2a).[26] This detoxification action can arise from the binding of Cd^{2+} by newly synthesized apoMT or via exchange into Zn-saturated MT. This mechanism was proposed from analyses of cadmium exchange of Zn-MTs studied spectroscopically in which the domain-specific exchange was used to explain the results that were thought to be related to equivalents of metals added and the "magic-numbers" of MT metal binding.[21] However, spectroscopic methods used in the past provide the average metal loading of the protein. The use of ESI-MS to study cadmium-zinc replacement in the intact MT protein has been reported previously.[27]

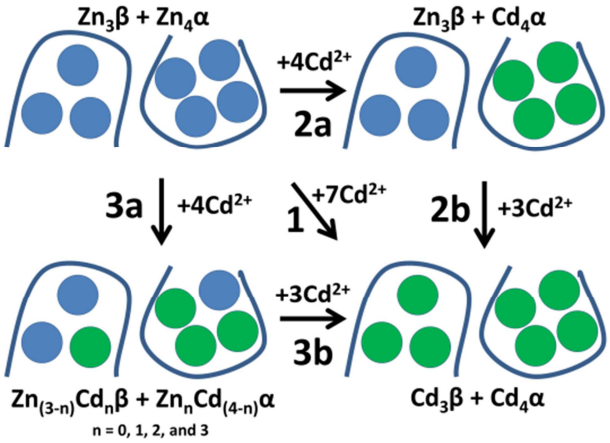

Figure 4.2: Possible metal exchange pathways for MT. The overall reaction is shown in Pathway 1 with the substitution of seven Zn^{2+} (blue) for seven Cd^{2+} (green). A domain specific model in which the majority of the zinc is substituted in one of the domains first as shown in Pathway 2. The random replacement model in which the metal exchange shows no significant metal preference between the domains and the metals are scrambled between the domains randomly as shown in Pathway 3.

www.manaraa.com

Much of the current knowledge regarding domain specificity in MTs is based on results obtained from partial digestion of the MT strand (leaving one of the domains intact)[28] or the cadmium titrations of apoMTs, studied by ^{113}Cd NMR.[29-31] Specifically, a pH dependence on the chemical shifts (and therefore the cadmium cluster formation) has been reported.[32] Significantly, these NMR studies report that binding of cadmium to the apoMT strand occurs cooperatively, with the first four added cadmium ions binding exclusively to the α domain, and that these are bound to the protein with the highest affinities.[33] Furthermore, it has been suggested that mixed Cd_4Zn_3-MT forms specifically Cd_4-α,Zn_3-β-MT in a highly domain selective manner.[31, 34] Other NMR experiments have demonstrated metal exchange,[35] which is related to strand fluxionality.[36] Finally, the Cd_5Zn_2 X-ray crystal structure, obtained from the addition of cadmium to Zn_7MT, showed that the two remaining zinc ions were located in the β domain.[37]

The binding of metals to MT is largely an affinity-driven process. The distribution of metals within the full MT protein, between the two-domains, as well as with competing MT strands, is reflected by those affinity constants ($K_{n,F}$, where n = 1-7); the higher affinity sites will be saturated earlier.[38] Previous studies have demonstrated that there are multiple binding constants for zinc and cadmium, with an average binding constant difference of $>10^3$ (K_F)[39] and have shown mixed Cd,Zn-MT species form *in vitro* and *in vivo*.[10, 35, 40-42]

A domain specific model (Figure 4.2, 2a) for cadmium displacement of zinc in Zn_7-MT would imply distorted binding affinity ratios (K_F^{Cd}/K_F^{Zn}) such that the α domain would have cadmium to zinc binding constant ratios all significantly higher than the β domain binding constant ratios to promote cadmium binding exclusively in the α domain. The random replacement model (Figure 4.2, 3a) for this same reaction would involve a random ordering of binding affinity ratios or a set of binding affinity ratios close enough that the distribution would not dominate the distribution of metal in a specific domain.

In this Chapter, we report the fragment and domain preferences when zinc and cadmium bind to the isolated α and β fragments of MT1A. Detailed competition studies using ESI mass spectrometry and CD spectroscopy were used to determine the fractional selectivity

www.manaraa.com

of the two fragments (and later domains) on a metal-by-metal basis. The high-resolution data allowed analysis of the fractional changes in binding site location selected as the metal binding domains formed. Our analysis is the first to show the stepwise preferences for both zinc and cadmium at physiologically relevant pH values. The data analysis provides detailed insight into the formation of the fully metallated protein and indicates that at pH 7.4 there is no significant trend to domain specificity for either zinc or cadmium. The ESI mass spectral data provide a quantitative domain selectivity index reflective of the K_F^{Cd}/K_F^{Zn} ratios for each of the seven metal exchange reactions.

4.2 Methods

4.2.1 Purification of recombinant fragments.

Preparation of isolated MT domain fragments followed previously reported methods (Appendix A).[43] The amino acid sequences for the isolated domains used in this study are based on the recombinant human MT1A sequence: the 38-residue β-MT domain fragment sequence (MGKAAAACSC ATGGSCTCTG SCKCKECKCN SCKKAAAA) and the 41-residue α-MT domain fragment sequence (MGKAAAAC CSCCPMSCAK CAQGCVCKGA SEKCSCCKKA AAA). Each of the corresponding DNA sequences was inserted as an N-terminal S-tag fusion protein into pET29a plasmids and individually expressed in *Escherichia coli* BL21(DE3) with cadmium-supplemented growth medium. Each protein was expressed and purified separately as the cadmium-saturated form. All purified protein solutions were evacuated and saturated with argon to impede cysteine oxidation.

4.2.2 Preparation of apofragments.

Cadmium was removed from the purified, isolated MT domains. The protein solutions were acidified to pH 2.7 before the released cadmium was separated from the apoproteins on GE Sephadex G-25 size exclusion media using formic acid in water (pH 2.7) as the eluent. The apoproteins were then concentrated and buffer exchanged with 5 mM ammonium formate (pH 7.4) using Millipore Amicon Ultra-4 centrifuge filter units (3 kDa MWCO). Protein concentrations of the final, pH-adjusted apoβMT and apoαMT solutions were determined by cadmium remetallation of small fractions of each protein

www.manaraa.com

monitored using UV-visible absorption (Cary 50, Varian Canada): ε_{250} values of 36,000 $M^{-1}cm^{-1}$ and 45,000 $M^{-1}cm^{-1}$ for Cd_3-βMT and Cd_4-αMT, respectively.

4.2.3 Zinc and cadmium titrations.

Stocks of 5 mM zinc acetate (Fisher Scientific) and 5 mM cadmium acetate (Acros Organics) were freshly prepared in deionized water, and the concentrations of zinc and cadmium were determined using atomic absorption spectroscopy (AA 240, Varian). *Caution: Cadmium acetate is a known carcinogen. Special care should be taken with its handling and disposal.* Equal concentrations of apoβMT and apoαMT were mixed in acid-washed vials, and the pH values of the resulting solutions were adjusted for the titration. Equivalents of zinc were then added under an argon atmosphere. Following each addition, the solution equilibrated on ice for 3-5 min before the acquisition of ESI data. Longer equilibration times showed no significant change in the speciation of spectral data (data not shown). Once both the fragments were saturated with zinc, cadmium equivalents were added following a similar procedure. The room-temperature circular dichroism (CD) spectra of the solutions were also measured following each cadmium addition. Cadmium was added until the fragments had both exchanged all zinc and were cadmium-saturated. The titrations were each repeated in triplicate.

4.2.4 ESI-MS and CD parameterizations.

A Bruker Micro-TOF II instrument (Bruker Daltonics, Toronto, ON) operated in positive ion mode was used to collect the data. NaI was used as an external calibrant. The following settings were used: scan, *m/z* 500-3000; rolling average, 2; nebulizer, 2 bar; dry gas, 80°C at a rate of 8.0 L/min; capillary, 4000 V; end plate offset, -500 V; capillary exit, 175 V; skimmer 1, 30.0 V; skimmer 2, 23.5 V; hexapole RF, 800 V. The spectra were collected for a minimum of 2 min and deconvoluted using the Maximum Entropy algorithm of the Bruker Compass DataAnalysis software package. A Jasco J810 spectropolarimeter was used to collect CD spectral data. The following scan parameters were used: step scan; range, 350−220 nm; data pitch, 1 nm; bandwidth, 0.5 nm; response, 1 s. Spectra were zeroed at 300 nm, and a three point fast Fourier transform filter was applied to smooth the data.

www.manaraa.com

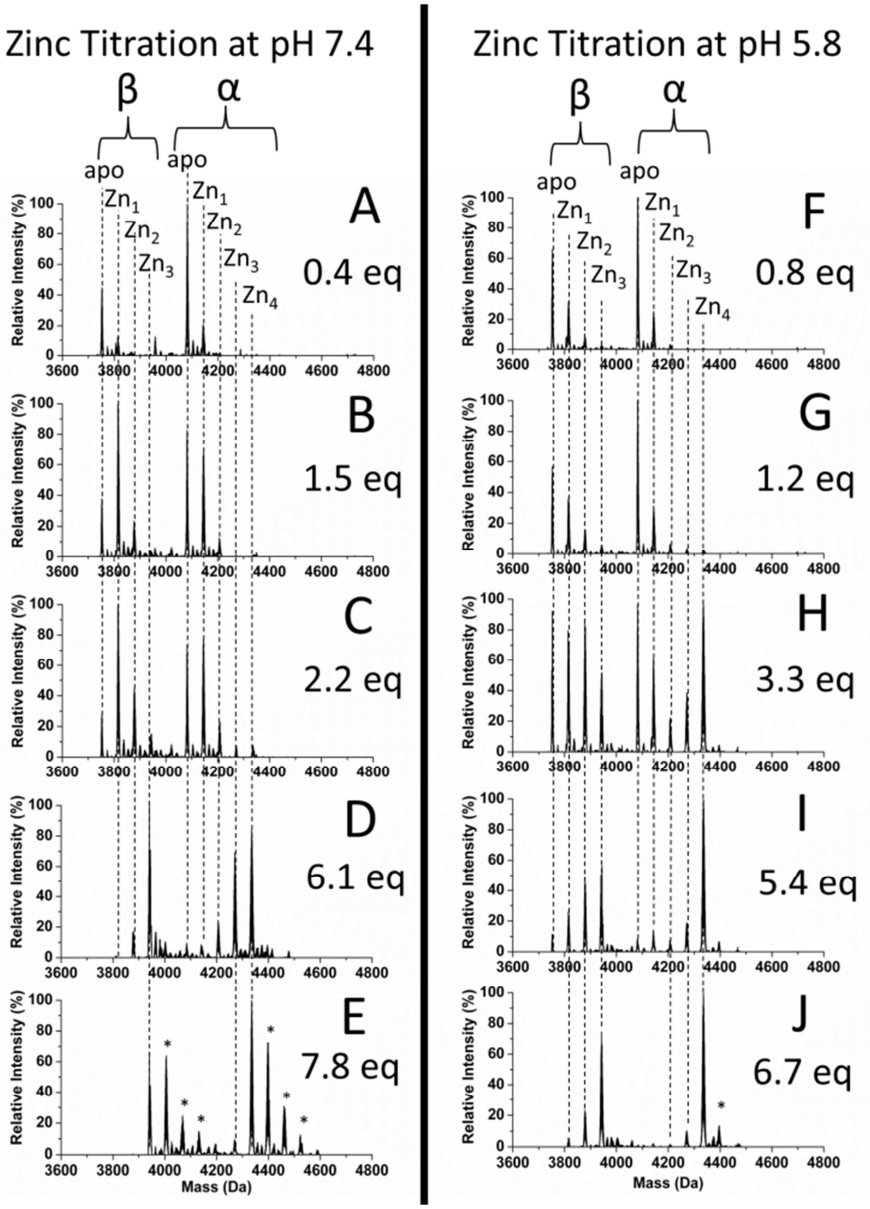

Figure 4.3: Representative deconvoluted ESI mass spectral data recorded during the competitive zinc titrations at pH 7.4 (A-E) and pH 5.8 (F-J) of equimolar mixtures of β-MT and α-MT. The important species are labeled with dashed lines. Asterisks indicate non-specific zinc adducts.

4.3 Results

The question we wish to answer concerns the binding location of the incoming metal during the isomorphous replacement of zinc by cadmium. To test which fragment the

www.manaraa.com

incoming metal occupies, we devised a series of competitive titrations in which the isolated α and β fragments of MT1A, used as a general model, could compete for incoming metals. Key to these competitive reactions is the fact that the two competing species are at equal concentrations. Subsequent metallation results in occupancy that will depend solely on the thermodynamically preferred distribution based on the relative magnitude of the formation constants. Thus, in all of the following experiments, the α and β fragments are always at equal concentrations and the metal occupancy will depend on the relative values of the seven formation constants ($K_{n,F}$, where n = 1-7) that govern the competitive reaction products.

4.3.1 Competitive zinc titration of MT fragments: ESI-MS Data.

In the process of initial metallation, the apoMT strand must rearrange the protein backbone to accommodate metal binding by the cysteine side chains. The relative abundancies in the ESI mass spectral data are representative of the relative concentrations of the species in solution, as demonstrated previously for zinc,[25] cadmium,[42] arsenic,[44] and bismuth[45] MTs. Figure 4.3 shows the mass spectral data for the competitive zinc titrations of equimolar α and β at pH 7.4 and 5.8 as a function of added zinc. Though we have previously reported a similar titration,[46] those results were measured at pH 9.2, significantly beyond the physiological range. As this report demonstrates, such a large pH discrepancy can have effects on the metal binding properties, especially the metal distributions of Zn_n-MT, which differ quite significantly at all of these three pH values because of the pH dependence of the metal binding reactions.

$$apo\beta MT + Zn^{2+} \underset{}{\overset{K_{1\beta}}{\rightleftharpoons}} Zn_1\beta MT$$
$$Zn_1\beta MT + Zn^{2+} \underset{}{\overset{K_{2\beta}}{\rightleftharpoons}} Zn_2\beta MT$$
$$Zn_2\beta MT + Zn^{2+} \underset{}{\overset{K_{3\beta}}{\rightleftharpoons}} Zn_3\beta MT$$

$$apo\alpha MT + Zn^{2+} \underset{}{\overset{K_{1\alpha}}{\rightleftharpoons}} Zn_1\alpha MT$$
$$Zn_1\alpha MT + Zn^{2+} \underset{}{\overset{K_{2\alpha}}{\rightleftharpoons}} Zn_2\alpha MT$$
$$Zn_2\alpha MT + Zn^{2+} \underset{}{\overset{K_{3\alpha}}{\rightleftharpoons}} Zn_3\alpha MT$$
$$Zn_3\alpha MT + Zn^{2+} \underset{}{\overset{K_{4\alpha}}{\rightleftharpoons}} Zn_4\alpha MT$$

Scheme 4.1: Competitive and sequential metallation reactions of apoβMT and apoαMT.

As zinc is added stepwise to the competing domain fragments, we observed the sequential addition of zinc to both fragments as shown in Scheme 4.1. Because the

www.manaraa.com

binding sites are in direct competition for the zinc ions, the zinc is bound in a sequence that correlates with the order of the zinc affinities between the α and β domain fragments. For example, at pH 7.4, Figure 4.3 (A-E) shows that the β fragment binds a greater fraction of the first equivalent of zinc. In Figure 4.3B, where a total of 1.5 equiv of zinc has been added, the β distribution is dominated by Zn_1-βMT with some formation of Zn_2-βMT. The α species at the same point in the titration show the apo α form being more dominant than Zn_1-αMT. These data indicate that, under the conditions of the experiment, the first zinc binding event takes place in the β domain. At pH 5.8, (Figure 4.3 F-J) the first zinc also binds to the β fragment. However, under these acidic conditions, the α fragment shows a higher degree of cooperativity compared to the binding at pH 7.4, and the order of subsequent zinc binding events is impacted. Though the α fragment begins to fill with zinc later in the titration, it saturates earlier than the β fragment. For example, in Figure 4.3I, where 5.4 equiv of zinc has been added, the α speciation is dominated by Zn_4- αMT, while the β fragment speciation shows significant apo-, Zn_1-, and Zn_2-βMT species. The competitive zinc titration data at pH 9.2 from ref[46] shows a degree of non-cooperativity even higher than that shown here at pH 7.4, though the data sets do look similar.

4.3.2 Competitive zinc titration of MT fragments: Speciation profiles.

To compare the titration data between the two-domains as well as to observe differences within the fragments as a function of pH, we extracted the ESI speciation profiles for the two fragments as shown in Figure 4.4. This Figure reveals information related to the overall binding properties of each of the two fragments. Panel A and B show the speciation of the α fragment and β fragment, respectively, as a function of added zinc. Zn_2-αMT and Zn_2-βMT are depressed relative to the other speciation traces. This indicates that the binding of the second and third zinc ions in αMT facilitates the next binding events. We interpret this to imply that structural reorganization of the peptide backbone occurs such that the subsequent metallation to Zn_4-αMT is promoted. Figure 4.4C, which shows the zinc speciation of the α fragment as a function of added zinc at pH 5.8, highlights how this effect is even more pronounced at lower pH. At pH 5.8, the

www.manaraa.com

titration is dominated by the formation of the fully metallated Zn_4-αMT; the intermediate metallation states are all suppressed and Zn_4-αMT appears earlier in the titration. This effect is not observed for the β fragment at pH 5.8, Figure 4.4D, indicating that the zinc metallation mechanism of the α fragment is more sensitive to acidic conditions.

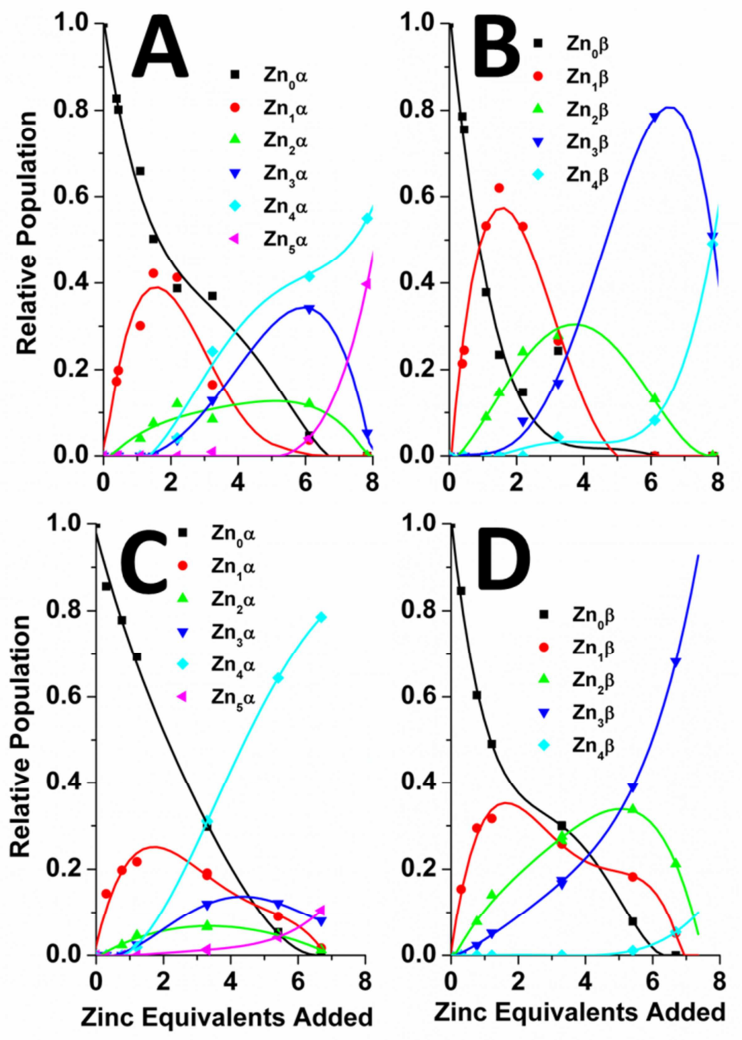

Figure 4.4: Extracted speciation profiles of recorded during the competitive zinc titrations of equimolar mixtures of apoα (A and C) and apoβ (B and D) MT at pH 7.4 (A and B) and pH 5.8 (C and D). Zinc was added stepwise to the solution of apo-fragments until both fragments were zinc-saturated. The species have been plotted according to the stoichiometry of added zinc. One equivalent means the amount of zinc to fill one binding site. Lines have been added as guides linking the data points.

www.manaraa.com

4.3.3 Competitive cadmium titrations of zinc-saturated fragments at pH 7.4.

Representative deconvoluted ESI mass spectral data for the competitive cadmium titration of zinc-saturated α-MT and β-MT fragments at pH 7.4 are shown in Figure 4.5. This figure, and the corresponding pH 5.8 titration data in Figure 4.7, reveals information about the location of cadmium exchange. Similar to how binding of zinc to the apo fragments depends on the zinc formation constants of the competitive reactions shown in Scheme 4.1, the site of the cadmium replacement depends on the relative magnitudes of the formation constants of the incoming cadmium and the outgoing zinc as shown in Scheme 4.2. This means that, starting with the first equivalent of added cadmium, the first zinc to exchange will depend on which site has the greatest K_F^{Cd}/K_F^{Zn} ratio. The Zn_6Cd_1-MT species that is most thermodynamically preferred will form.

The ESI mass spectral data in Figure 4.5 show that, for the cadmium exchange at pH 7.4, cadmium binds to both domains simultaneously. At all steps in the cadmium titration, the speciation of the metals is mixed between the fragments. For example, in Figure 5.5D, the expanded deconvoluted data for 4.2 equiv of added cadmium shows mixed metal β (Zn_3-, Zn_2Cd_1- $ZnCd_2$- and Cd_3-βMT) and mixed metal α (Zn_4-, Zn_3Cd_1-, Zn_2Cd_2-, $ZnCd_3$-, and Cd_4-αMT) metallation states.

$$Zn_3\beta MT + Cd^{2+} \underset{}{\overset{K_{1\beta}}{\rightleftharpoons}} Cd_1Zn_2\beta MT + Zn^{2+}$$
$$Cd_1Zn_2\beta MT + Cd^{2+} \underset{}{\overset{K_{2\beta}}{\rightleftharpoons}} Cd_2Zn_1\beta MT + Zn^{2+}$$
$$Cd_2Zn_1\beta MT + Cd^{2+} \underset{}{\overset{K_{3\beta}}{\rightleftharpoons}} Cd_3\beta MT + Zn^{2+}$$

$$Zn_4\alpha MT + Cd^{2+} \underset{}{\overset{K_{1\alpha}}{\rightleftharpoons}} Cd_1Zn_3\alpha MT + Zn^{2+}$$
$$Cd_1Zn_3\alpha MT + Cd^{2+} \underset{}{\overset{K_{2\alpha}}{\rightleftharpoons}} Cd_2Zn_2\alpha MT + Zn^{2+}$$
$$Cd_2Zn_2\alpha MT + Cd^{2+} \underset{}{\overset{K_{3\alpha}}{\rightleftharpoons}} Cd_3Zn_1\alpha MT + Zn^{2+}$$
$$Cd_3Zn_1\alpha MT + Cd^{2+} \underset{}{\overset{K_{4\alpha}}{\rightleftharpoons}} Cd_4\alpha MT + Zn^{2+}$$

Scheme 4.2: Competitive and sequential cadmium replacement reactions of Zn_4-αMT and Zn_3-βMT.

The model for the isomorphous replacement of zinc with cadmium (Scheme 4.2) follows a similar sequential mechanism as shown in Scheme 4.1. Each of the zinc ions is replaced in sequence from zinc-saturated Zn_7-MT to cadmium-saturated Cd_7-MT in a series of seven, sequential, bimolecular reversible reactions. In this model, the populations of the

www.manaraa.com

various MT species are dependent on the K_F^{Cd}/K_F^{Zn} ratios for each of the metal exchange reactions.

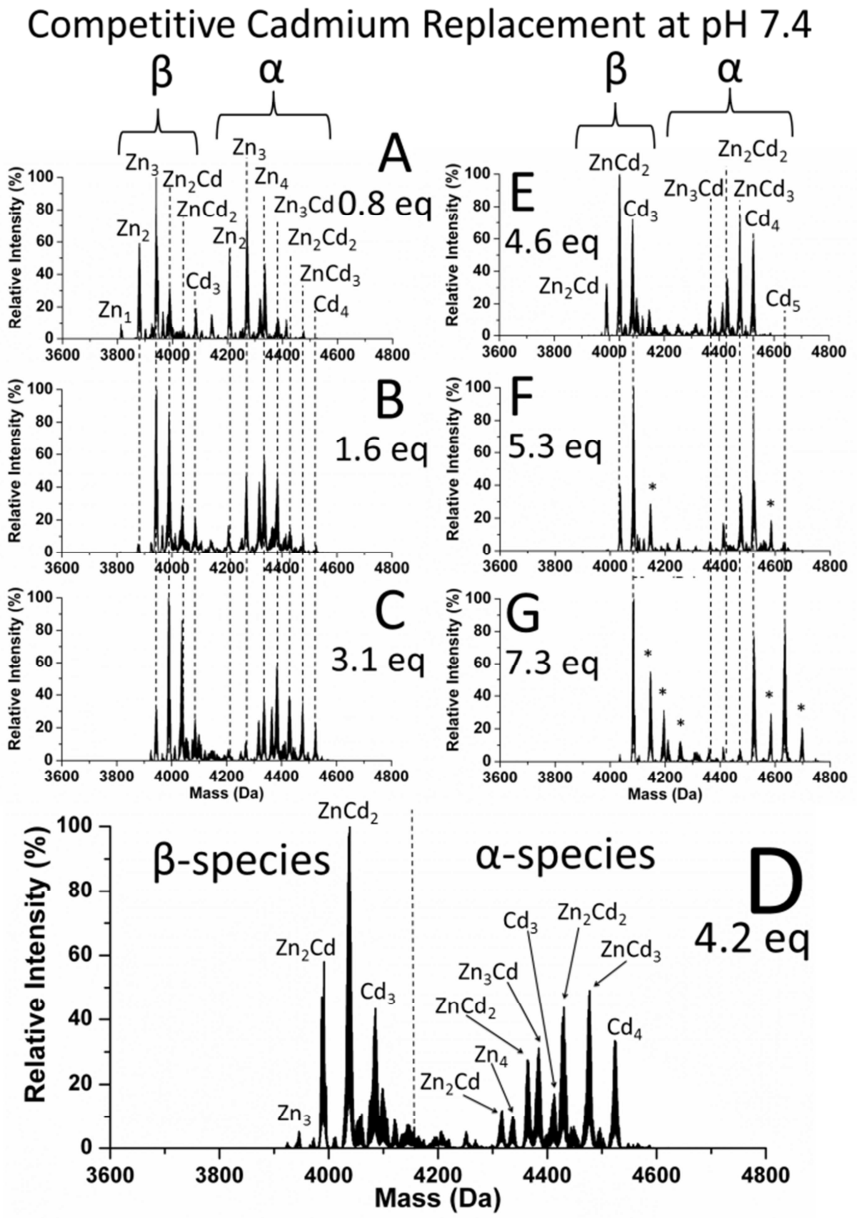

Figure 4.5: Representative ESI mass spectral data recorded during the competitive cadmium titration of an equimolar (31 µM) mixture of Zn4-αMT and Zn3-βMT at pH 7.4. The important species are labelled with dashed lines. Asterisks indicate non-specific zinc adducts. Panel D shows expanded spectral data after 4.2 equiv has been added.

www.manaraa.com

The extracted speciation profiles for the pH 7.4 cadmium competitive exchange shown in Figure 4.5 are plotted in Figure 4.6. Panels A and B show the amounts of zinc bound to the α and β fragments, respectively, as a function of mole equivalents of added cadmium. These top two panels highlight the incremental decrease in zinc loading of the initially zinc-saturated fragments between the two-domains (Zn_4-MT → Zn_3-MT → Zn_2-MT → Zn_1-MT → Zn_0-MT) as each zinc is substituted by the tighter binding cadmium ions. Panels C and D show the populations of increasing numbers of cadmium-bound species also as a function of added cadmium.

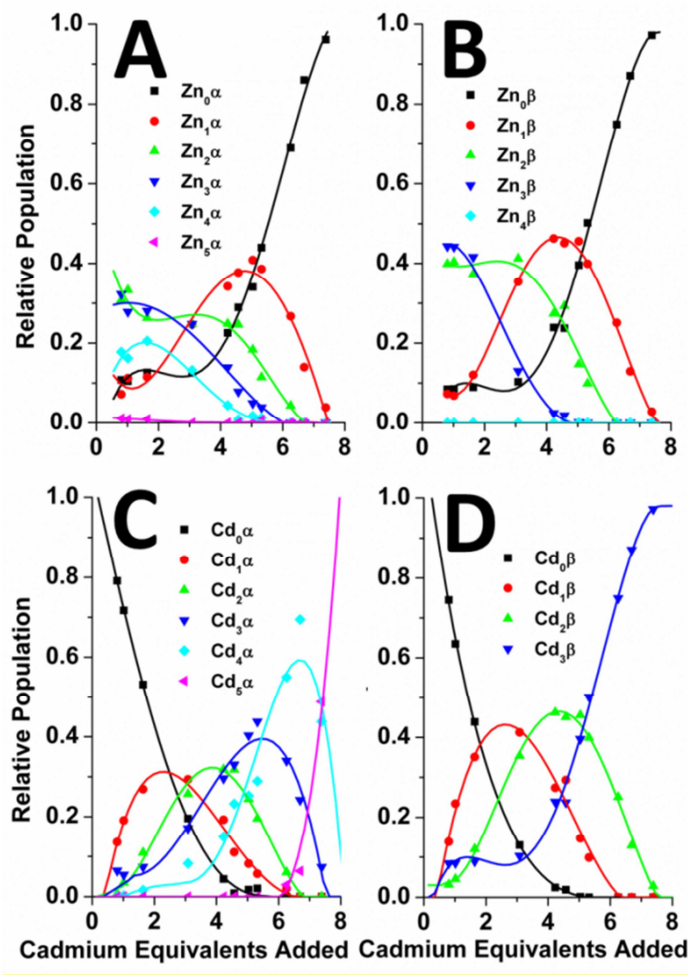

Figure 4.6: Extracted speciation profiles recorded during the competitive cadmium titrations of an equimolar (31 μM) mixture of α (A and C) and β (B and D) Zn-MTs at pH 7.4. The species have been plotted according to the stoichiometry of bound zinc (A and B) and cadmium (C and D). Lines have been added as guides linking the data points.

www.manaraa.com

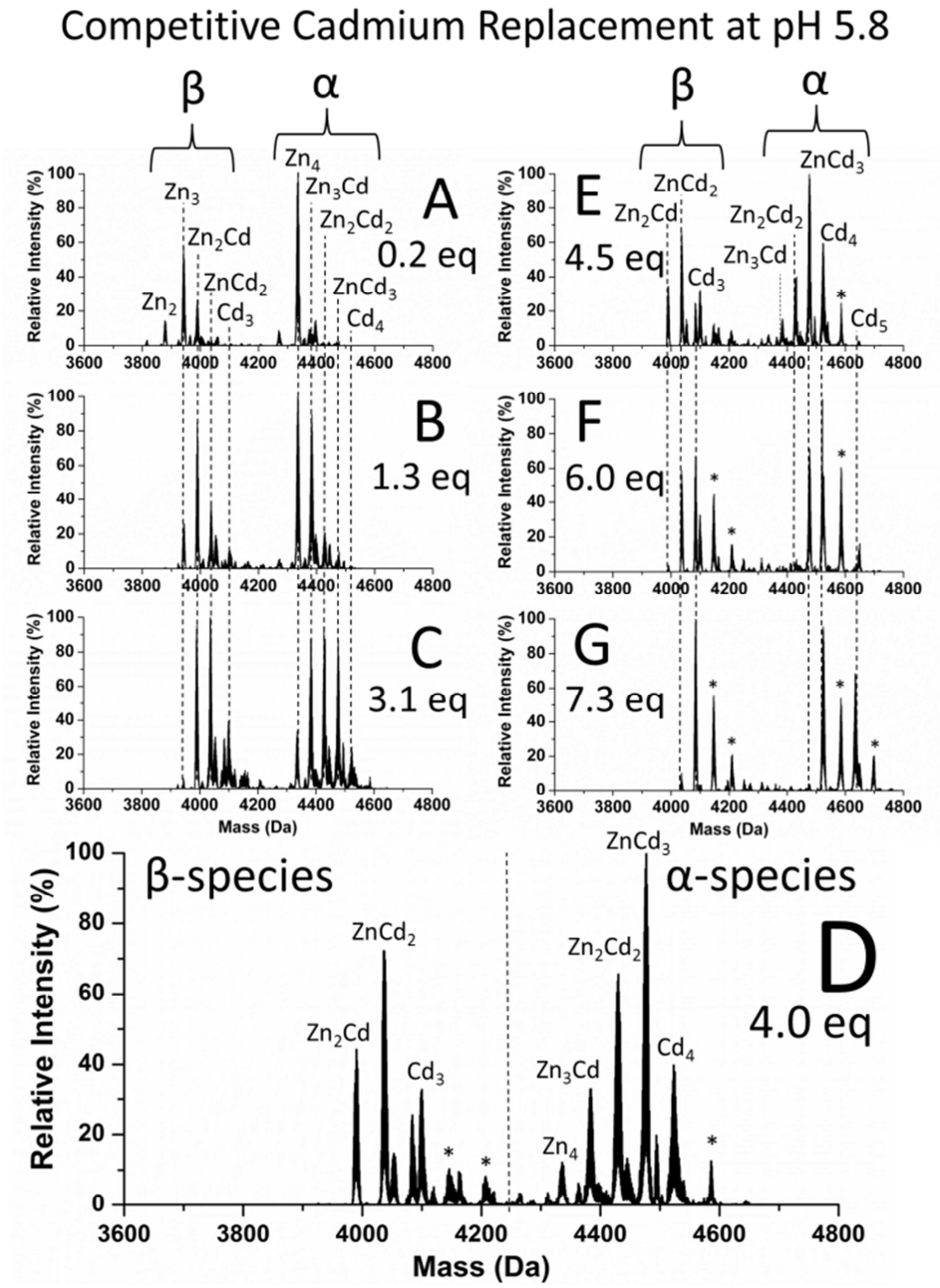

Figure 4.7: ESI mass spectral data recorded during the competitive cadmium titration of an equimolar (34 μM) mixture of Zn4-αMT and Zn3-βMT at pH 5.8. The important species are labelled with dashed lines. Panel D shows expanded spectral data after 4.0 equiv of Cd^{2+} has been added.

www.manaraa.com

4.3.4 Competitive cadmium titrations of zinc-saturated fragments at pH 5.8.

Figure 4.7 shows deconvoluted mass spectral data for the zinc-cadmium competitive exchange reaction at pH 5.8. As cadmium is added, the zinc is replaced in a sequential manner within each fragment. Figure 4.7B shows how the first cadmium exchange reaction largely takes place in the β fragment.

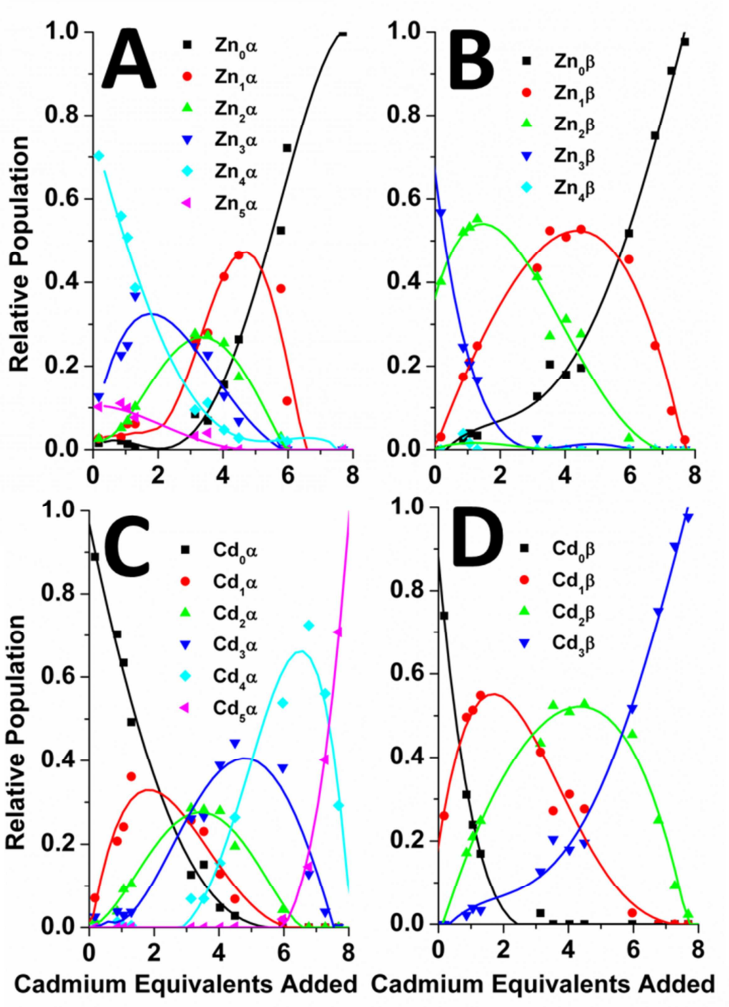

Figure 4.8: Extracted speciation profiles recorded during the competitive cadmium titrations of an equimolar (34 µM) mixture of Zn-αMT (A and C) and Zn-βMT (B and D) at pH 5.8. The species have been plotted according to the stoichiometry of bound zinc (A and B) and cadmium (C and D). Lines have been added as guides linking the data points.

www.manaraa.com

The extracted ESI mass spectral data speciation profiles for the pH 5.8 competitive cadmium titration are shown in Figure 4.8. Again, we compare the different experimental speciation profiles based on relative populations, the population peak intensity, and population peak location to reveal information about the relative site occupancy following displacement of zinc with cadmium in the two fragments.

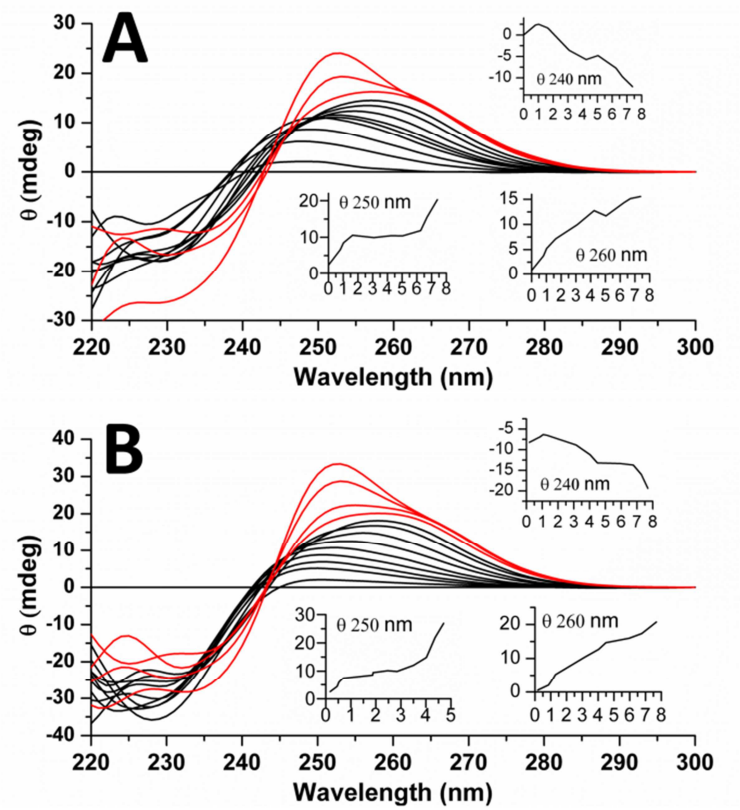

Figure 4.9: CD spectroscopic data measured for the competitive cadmium titration starting from an equimolar (31 and 34 μM) mixture of Zn4-αMT and Zn3-βMT at (A) pH 7.4 and (B) pH 5.8. The inset boxes show the change in ellipticity at 240, 250, and 260 nm as a function of equivalents of Cd^{2+} added. Red lines indicate solutions containing Cd_5-αMT based on ESI mass spectral data.

Circular Dichroism. The CD spectra that were simultaneously measured for each cadmium addition during the stepwise cadmium titrations are shown in Figure 4.9. At pH 7.4 (Figure 4.9A) there is an initial increase in the dichroism at 250 nm as the cadmium displaces a single zinc. A red shift to a 260 nm shoulder is indicative of the clustering to

www.manaraa.com

nominally cadmium-saturated Cd_3- βMT and Cd_4-αMT. Finally, the intensity maximum shifts back to 250 nm because of the formation of Cd_5-αMT at the end of the titration, as has been previously described.[47] The pH 5.8 data (Figure 4.9B) have similar spectral features. The key difference between the spectral profiles is the absence of the strongly isodichroic point at 250 nm in the pH 7.4 spectra. This is likely due to the fact that under acidic conditions, the formation of Cd_4-αMT clusters is preferred, meaning that the α fragment exchanges earlier in the titration at lower pH values.

4.4 Discussion

4.4.1 Extracting metal binding properties of MT using competitive titrations.

There has been considerable discussion regarding the metal binding constants associated with each metal that binds to MT.[16, 24, 25, 39, 48-52] Initial reports of binding of zinc to MT had suggested that all seven zinc ions were bound with approximately the same binding constant.[39] This model was refined by Maret and co-workers[24] when they determined four independent binding constants (where the four highest-affinity sites bound zinc with approximately the same K_F and the three remaining sites had sequentially decreasing affinities) and again by our group when we reported the values of all seven independent zinc binding constants, one for each of the zinc binding events.[25] As previous results have demonstrated, MTs bind zinc and cadmium with high affinities.[38] The fluxional nature of the apoMT strand, the metal-dependent folding that occurs during metallation, and the mobility of the metals between and within the protein all require careful and innovative experimental designs to assign independent affinity constants.

Competitive titrations have previously been used to study the metallation processes of MTs.[25, 27, 46, 48] In the formation of metal-saturated final products, the MTs pass through partially-metallated intermediates. For example, the formation of Zn_4-MT follows Zn_3-MT as an intermediate, which requires formation of Zn_2-MT, and so on back to apoMT, (Scheme 4.1). Similar schemes have been proposed for the zinc,[25] cadmium,[42] and arsenic[44] metallation mechanisms for MT.[49] Some of the proposed functions of MT are accessible only when the protein is not metal-saturated. For example, the homeostatic

www.manaraa.com

control of zinc requires both acquisition and donation of zinc,[53] necessitating the presence of unsaturated MTs *in vivo*; studies have shown the presence of these unsaturated MTs *in vivo*.[54] Differences in the zinc transfer potentials of the two-domains have also been discussed in relation to the importance of the domain structure of the intact MT protein.[52]

It is important to note that we are extrapolating information about the intact protein on the basis of results from titrations of the separated domains. Previous work has suggested that the two isolated domains possess properties that differ from those of the intact peptide.[52] Determining the metal distribution in the whole protein, however, is complicated by the lability of the metals, especially following chromatographic separations and/or chemical modifications common in other studies of domain specificity. Though the affinity constants of the separated domains are changed upon domain separation (because of increased fluxionality and options for domain reorganization in the larger intact protein strand), we expect that the properties governing metal distribution between the domains remain essentially unchanged, as has been demonstrated for metal-saturated MTs.[55] Assuming that the metallation reactions follow a purely domain-specific mechanism, it is likely that the separated domains would enhance this feature because the number of interdomain interactions between the separated domains and intact protein is reduced.[52] Evidence of interdomain interactions will be discussed further in Section 4.4.6. Arsenic binding studies showed that the trend in binding was maintained in the isolated domains relative to that of the intact protein.[44, 56]

At the MT protein concentrations used in this study, dimerization of the MT species, either in solution or in the ESI ionization process, is possible. However, we saw no evidence of dimer formation in the resulting ESI mass spectral data. We also note that at higher metal concentrations, such as the end of the cadmium titration of mixed Zn-MTs (where total $[Cd^{2+}] + [Zn^{2+}] \approx 500\ \mu M$), nonspecific metal binding may occur during the electrospray process that does not directly correspond to the solution phase metallation states. There were some nonspecific adducts formed towards the end of the zinc titration experiments, especially at higher pH (Figure 4.3E). Because of the fact that the cadmium added replaced the zinc bound stoichiometrically, we are confident that this effect was minimal for the conditions of the cadmium experiments.

www.manaraa.com

4.4.2 Comparison of pH 7.4 and pH 5.8 data.

Via substitution of zinc with cadmium in one MT species, the vertical panels in Figure 4.6 and 4.8 (zinc loss vs cadmium bound) should result in mirror images. Each cadmium binding event must correspond to a zinc loss. However, we see interesting speciation profiles for these competition reactions because both domain fragments are competing for the added cadmium and released zinc. For each metal substitution step, the concentration of free zinc in the solution changes, and 7 equiv of free zinc is released by the end of the titration. As shown in Scheme 4.2, the increases in free zinc concentration compete with cadmium binding, which leads to a redistribution of the zinc and cadmium among the two fragments governed by the thermodynamic minimum of the K_F^{Cd}/K_F^{Zn} ratio.

4.4.3 Seven cadmium for seven zinc.

One of the most discussed functions of MT is its ability to detoxify heavy metals. This occurs *in vivo* through the replacement of the zinc in Zn-MT with cadmium. *In vivo*, MTs predominantly exist as the zinc-bound form (Zn_n-MT, where n = 4-7) and not the apo form, and the binding of cadmium to MT is a result of the metal exchange. In this study, we used Zn-MT1A fragments as the starting point of the cadmium exchange competition, which may account for discrepancies between this work and previously published results that showed that the cadmium binding was cooperative and α domain-selective for experiments that used MT2A.[52] Cadmium binds with an affinity (K_F) higher than that of zinc; zinc binding and cadmium binding have long been considered isomorphous.

Past work has suggested that this exchange may occur in a domain-specific manner, where the first four added cadmiums are primarily localized to the α domain of the full MT. This mechanism was largely developed from data obtained through spectroscopic techniques such as UV-visible absorption, CD, MCD, NMR, and EPR and on the assumption that the MT metallation state was largely homogeneous. Except for NMR (whose signal intensity is resolved only for the metal saturated and nonfluxtional clusters and at millimolar concentrations), these techniques all provide the average metal load of all the concurrent species that exist. However, as shown by numerous ESI-MS studies, the metallation speciation of the MT strand is significantly heterogeneous, with a spread

www.manaraa.com

of speciation summing to the average metal loads. Our data unambiguously confirm and support this distributed heterogeneous binding mode (Figures 4.3, 4.5 and 4.7).

4.4.4 Modeling site selection mechanisms between the α and β domains.

Three models of metal selectivity between the domains (or, in the case of our competition experiments, the domain fragments) are shown in Figure 4.10. These models show the expected experimental results for a completely α (Panel A) or β (Panel B) selective mechanism, as well as for a mechanism in which there is no selectivity between the fragments (Panel C). Figure 4.10 provides the average metal loading (top panels) and domain selectivity (bottom panels) of those three models. The relative selectivity is defined as the difference in stepwise occupancy between the domains for each incoming metal. A value of +1 indicates the incoming metal bound specifically in the α domain, and a value of -1 indicates the incoming metal bound specifically in the β domain. A value of zero indicates the incoming metal was distributed evenly between both randomly, meaning no domain specificity.

The first model shows the domain occupancy with α selectivity where the first 4 equiv of added metal binds to only the α domain (Figure 4.10A). Once the α domain is filled with 4 equiv, the next 3 equiv fills the β domain. The final equivalent supermetallates the α domain to form $(Cd/Zn)_5$-αMT as has been previously described.[47] The modeled selectivity for the α domain over the β domain is based on the order of the binding constants that describe the reactions in the competition experiments (Scheme 4.1 and Scheme 4.2, and discussed above). In this model, the four sites with the highest affinities are located exclusively in the α domain.

The second model shows the effect on occupancy with β selectivity; the first 3 equiv of added metal binds to only the β domain (Figure 4.10B). Once the β domain is filled, the α domain binds the remaining incoming metals. Again, the modeled selectivity for the β domain over the α domain is due to the order of the binding constants that would generate this β selective model. In this model, the binding constants in the β domain have affinities higher than that of the α domain, and the binding is β-directed.

www.manaraa.com

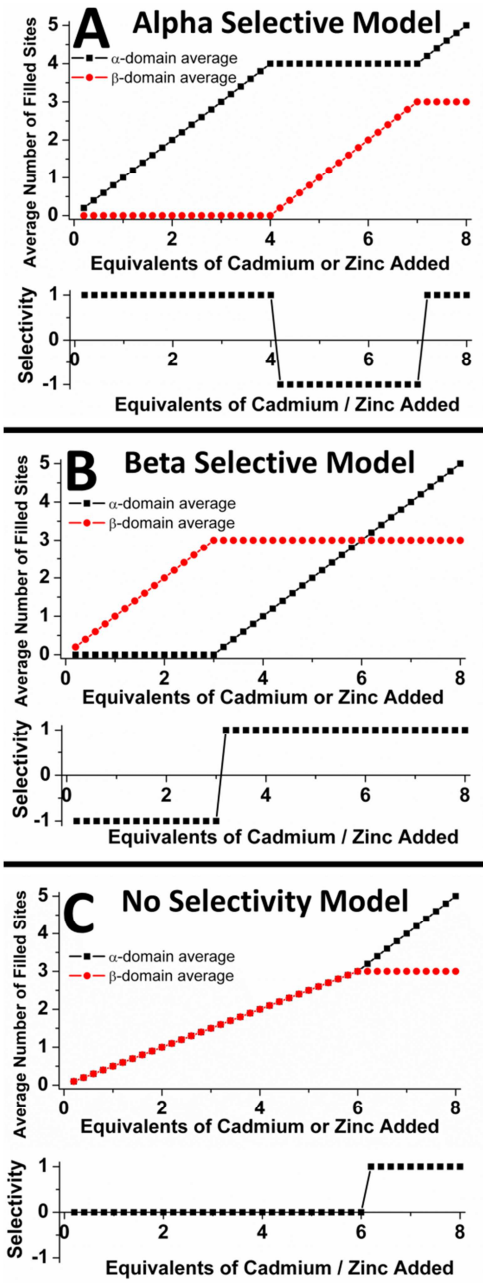

Figure 4.10: Models of selectivity in binding of zinc and cadmium to MT. Shown are three possible mechanisms for binding of metals to MTs: (A) an α selective model, (B) a β selective model, and (C) a model in which there is no specific selectivity. Top panels show the approximate speciation for the average metal loading in the α and β domains. Bottom panels show the domain selectivity during the course of the titration (+1 for α domain binding, -1 for β domain binding).

www.manaraa.com

In the final model, there is no specific selectivity between the domains, and it is clear that the first 6 equiv of added metal binds equally to both domains (Figure 4.10C). After the first 6 equiv has been added, the β domain is filled and the α domain binds the final equivalent to complete the titration. Once again, this model is based on the relative magnitudes of the binding constants at each point during the metal titrations. For this model, the first six binding constants are mixed between the two-domains and neither domain shows selectivity.

4.4.5 Comparison of the experimental data and the models.

Figure 4.11 shows the stepwise, metal-by-metal, selectivity calculated from the ESI-MS, as zinc was added to the mixed α and β fragments at (A) pH 7.4 and (B) 5.8. The dashed lines indicate the occupancy per addition if there was 100% selectivity for either the α fragment (+1) or the β fragment (-1). It is clear that, at pH 7.4, the more numerous cysteines in the α fragment bias the results such that there is a trend towards the α fragment. The conclusion is that there is no specific selectivity that cannot be ascribed to the greater numbers of cysteines in the α fragment (11 vs 9). At pH 5.8, however, there is evidence of weak α domain selectivity. Again, after the first zinc binds to the β fragment, the zinc ions bind to the α fragment until the α cluster is filled and the remaining zinc ions fill the β fragment. Our conclusion is that under acidic conditions, there is a weak selectivity. The α fragment binds a greater fraction of, but not all of, the added zinc.

We next turn to data recorded for the stepwise displacement of zinc by cadmium (Figure 4.12). This reaction has long been studied because of the toxicological implications of cadmium exposure, and the initial structural data came from cadmium-containing protein. In the experiments analyzed here, we are able to identify the fragment (and later the domain) selection that is the precursor to the domain specificity mentioned in the literature. The ESI-MS data provide far more detail than other techniques. Figure 4.12 provides the analysis of the mass spectral data to assess the fragment selection for each addition of cadmium. We note that for each cadmium added, a zinc is displaced, increasing $[Zn]_{free}$. At pH 7.4 Figure 4.12A), we see that the two-domains fill with cadmium evenly.

www.manaraa.com

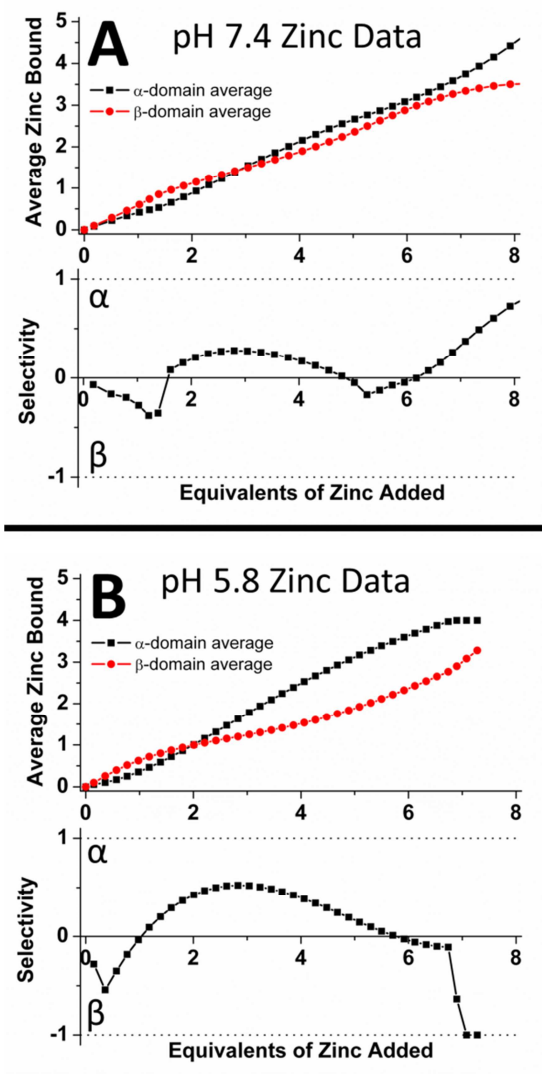

Figure 4.11: Experimental data for the zinc titrations at (A) pH 7.4 and (B) 5.8. Top panels show the calculated average zinc loading by each fragment over the stepwise titration shown in Figure 4.3-4.4. Bottom panels show the differential domain selectivity of each zinc addition (+1 for α domain binding, -1 for β domain binding).

The selectivity shows a pattern almost exactly the same as that for zinc. That is, the first cadmium displaces a zinc in the β cluster (we now talk about clusters because the two fragments are saturated with zinc so they exist as the two clustered species, Zn_4Cys_{11}- α -MT and Zn_3Cys_9-β-MT). There is, however, little evidence of more than minor selectivity for the α domain at pH 7.4. We conclude that, at pH 7.4, there is little domain specificity for cadmium displacing zinc.

www.manaraa.com

At pH 5.8 (Figure 4.12B), there is clearly an increase in the degree of selection of the α domain. The first cadmium still displaces the zinc in the β cluster, but then the α domain is preferred. Comparison with the theoretical simulations shows that the preference is nowhere near domain specific; rather, there is again a preference for the α domain.

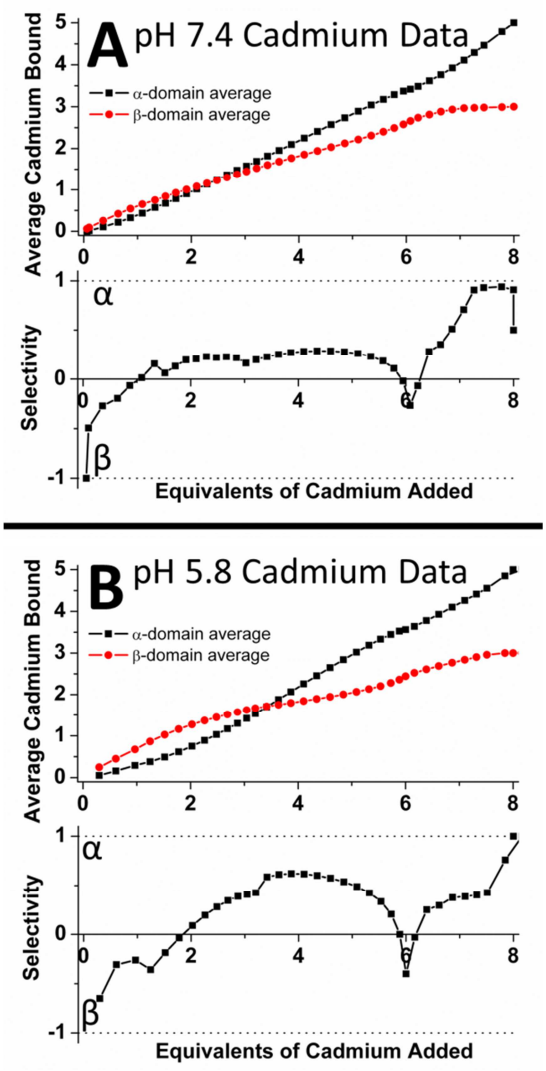

Figure 4.12: Experimental selectivity data for the cadmium titrations at (A) pH 7.4 and (B) 5.8. Top panels show the calculated average cadmium loading by each fragment over the stepwise titration shown in Figure 4.5-4.8. Bottom panels show the differential domain selectivity of each cadmium addition (+1 for α domain binding, -1 for β domain binding).

www.manaraa.com

4.4.6 Potential for interdomain interactions and comparison to existing data.

It is possible that the separated domains possess metal binding properties, including domain specificity, different from those in the intact protein, because the chain lengths and cysteine content are different. For example, we have previously described a model metallation pathway for the intact protein, based on the results of metal titrations to MTs at basic pH, where the first five metals added to apoMT bind in a beaded fashion, forming $(M^{II})Cys_4$ beads before clustering, following the addition of two additional metals to the two-domain protein.[46] By definition, this model meant that the metals bound initially in a non-domain specific fashion because, for example, the $(M^{II})_4(Cys)_{16}$-MT species uses 16 of the total 20 cysteines in the binding of the metals, more than occur in either domain. Because the domain structure is not formed at this point, we cannot determine if the metals bound in the early stages of the titration, $(M^{II})_{1\text{-}3}$-MTs, occurred in either the N-terminal or C-terminal region of the protein first. The data presented in this report of the separated domain fragments of MT1A extend the data in support of the model [at least for $(M^{II})_{1\text{-}2}$-MTs], showing that the metals are distributed between the fragments at all points in the titration. The results also hint at interactions between the domains in the intact MTs that may facilitate metal binding and change the metal binding properties.

These results contrast with those of other studies of domain selectivity,[32, 34, 35, 60] from most notably NMR experiments of metal titrations of MTs. However, data recently reported by Chen *et al.* showed, using NEM modification of intact MT2 studied by ESI-MS/MS, that the stable Cd_4-MT species had the cadmium bound exclusively to the α domain at pH 7.4.[57] An even more recent study by the same group suggested that other intermediate metallation states had cadmium bound to both domains, and suggested that the Cd_4-MT was due to metal rearrangements to form a thermodynamically stable product.[23]

This apparent discrepancy in the determination of the presence of domain selectivity may be due to methodological differences in the studies; for example, NEM (and other) modifications may influence the cadmium binding and "push" the cadmium toward α

www.manaraa.com

domain-selectivity, which could possibly arise from NEM reaction rate differences between the domains. Alternatively, connection of the domains in the intact protein may permit the reorganization of the bound metals from sites distant on the sequence that is more difficult for the separated domains to achieve. MT-MT metal transfers through direct protein-protein interactions have been reported for arsenic transfer between MT species,[58] which is significantly less labile than zinc or cadmium. Finally, the difference in the experimental data could simply be due to the different isoforms having different binding affinities for cadmium, as it has been suggested that different MTs do show different metal selectivity.[59] Clearly, a careful and direct comparison between the metal binding properties of MT1 and MT2, studied under the same conditions, using the same methodology is required.

4.5 Conclusions

It is becoming increasingly apparent that the traditional model of the two-domain structure of MTs is an insufficient descriptor of the functionality of MT species. It is also clear from many other experiments that the metals in MTs are labile and occupy those sites with the largest binding constants. Here, we have investigated the role of the two isolated domain fragments of MT1A in zinc acquisition and cadmium exchange using competitive metal titrations at two biologically relevant pHs. The data showed subtle cadmium bias for the α fragment at lower pH. All species showed mixed metallation states at all points in the competitive cadmium exchange titration, for both the α and β fragments.

The experimental data, supported by the models, unambiguously show that, under these conditions, neither zinc nor cadmium follows a domain-selective binding mechanism between either of the isolated domains. The binding affinity constants clearly span both fragments in their magnitude, resulting in a distribution of metals. This distribution is driven by the interplay of these binding affinities (K_F^{Cd}/K_F^{Zn}) that are close in magnitude, resulting in the non-specific site selection between the fragments.

www.manaraa.com

4.6 References

1. Berg, J. M., and Shi, Y. (1996) The galvanization of biology: A growing appreciation for the roles of zinc, *Science 271*, 1081-1085.
2. Capdevila, M., and Atrian, S. (2011) Metallothionein protein evolution: a miniassay, *J. Biol. Inorg. Chem. 16*, 977-989.
3. Blindauer, C. A. (2015) Advances in the molecular understanding of biological zinc transport, *Chem. Commun. 51*, 4544-4563.
4. Waisberg, M., Joseph, P., Hale, B., and Beyersmann, D. (2003) Molecular and cellular mechanisms of cadmium carcinogenesis, *Toxicology 192*, 95-117.
5. Shimoda, R., Nagamine, T., Takagi, H., Mori, M., and Waalkes, M. P. (2001) Induction of apoptosis in cells by cadmium: Quantitative negative correlation between basal or induced metallothionein concentration and apoptotic rate, *Toxicol. Sci. 64*, 208-215.
6. Waalkes, M. P. (2000) Cadmium carcinogenesis in review, *J. Inorg. Biochem. 79*, 241-244.
7. Bertin, G., and Averbeck, D. (2006) Cadmium: Cellular effects, modifications of biomolecules, modulation of DNA repair and genotoxic consequences (a review), *Biochimie 88*, 1549-1559.
8. Outten, C. E., and O'Halloran, T. V. (2001) Femtomolar sensitivity of metalloregulatory proteins controlling zinc homeostasis, *Science 292*, 2488-2492.
9. Coyle, P., Philcox, J., Carey, L., and Rofe, A. (2002) Metallothionein: The multipurpose protein, *Cell. Mol. Life Sci. 59*, 627-647.
10. Stillman, M., Cai, W., and Zelazowski, A. (1987) Cadmium binding to metallothioneins. Domain specificity in reactions of alpha and beta fragments, apometallothionein, and zinc metallothionein with Cd^{2+}, *J. Biol. Chem. 262*, 4538-4548.
11. Margoshes, M., and Vallee, B. L. (1957) A cadmium binding protein from equine kindney cortex, *J. Am. Chem. Soc. 79*, 4813-4814.
12. Capdevila, M., Bofill, R., Palacios, Ò., and Atrian, S. (2012) State-of-the-art of metallothioneins at the beginning of the 21st century, *Coord. Chem. Rev. 256*, 46-62.
13. Klaassen, C. D., Liu, J., and Choudhuri, S. (1999) Metallothionein: An intracellular protein to protect against cadmium toxicity, *Annu. Rev. Pharmacol. Toxicol. 39*, 267-294.
14. Palmiter, R. D. (2004) Protection against zinc toxicity by metallothionein and zinc transporter 1, *Proc. Natl. Acad. Sci. U. S. A. 101*, 4918-4923.
15. Kang, Y. J. (2006) Metallothionein redox cycle and function, *Exp. Biol. Med. 231*, 1459-1467.
16. Maret, W., and Vallee, B. L. (1998) Thiolate ligands in metallothionein confer redox activity on zinc clusters, *Proc. Natl. Acad. Sci. U. S. A. 95*, 3478-3482.
17. Thirumoorthy, N., Shyam Sunder, A., Manisenthil Kumar, K., Senthil kumar, M., Ganesh, G., and Chatterjee, M. (2011) A Review of Metallothionein Isoforms and their Role in Pathophysiology, *World J. Surg. Oncol. 9*, 54.
18. Robbins, A. H., McRee, D. E., Williamson, M., Collett, S. A., Xuong, N. H., Furey, W. F., Wang, B. C., and Stout, C. D. (1991) Refined crystal structure of Cd, Zn metallothionein at 2.0 Å resolution, *J. Mol. Biol. 221*, 1269-1293.
19. Sutherland, D. E. K., and Stillman, M. J. (2014) Challenging conventional wisdom: Single domain metallothioneins, *Metallomics 6*, 702-728.
20. Nielson, K. B., Atkin, C. L., and Winge, D. R. (1985) Distinct metal-binding configurations in metallothionein, *J. Biol. Chem. 260*, 5342-5350.

www.manaraa.com

21. Sutherland, D. E. K., and Stillman, M. J. (2011) The "magic numbers" of metallothionein, *Metallomics 3*, 444-463.
22. Furey, W., Robbins, A., Clancy, L., Winge, D., Wang, B., and Stout, C. (1986) Crystal structure of Cd,Zn metallothionein, *Science 231*, 704-710.
23. Chen, S.-H., Chen, L., and Russell, D. H. (2014) Metal-induced conformational changes of human metallothionein-2A: A combined theoretical and experimental study of metal-free and partially metalated intermediates, *J. Am. Chem. Soc. 136*, 9499-9508.
24. Krężel, A., and Maret, W. (2007) Dual nanomolar and picomolar Zn(II) binding properties of metallothionein, *J. Am. Chem. Soc. 129*, 10911-10921.
25. Pinter, T. B. J., and Stillman, M. J. (2014) The zinc balance: Competitive zinc metalation of carbonic anhydrase and metallothionein 1A, *Biochemistry 53*, 6276-6285.
26. Stillman, M. J., and Zelazowski, A. (1988) Domain specificity in metal binding to metallothionein. A circular dichroism and magnetic circular dichroism study of cadmium and zinc binding at temperature extremes, *J. Biol. Chem. 263*, 6128-6133.
27. Połeć Pawlak, K., Palacios, Ò., Capdevila, M., González-Duarte, P., and Łobiński, R. (2002) Monitoring of the metal displacement from the recombinant mouse liver metallothionein Zn7-complex by capillary zone electrophoresis with electrospray MS detection, *Talanta 57*, 1011-1017.
28. Stillman, M. J., and Zelazowski, A. J. (1989) Domain-specificity of Cd^{2+} and Zn^{2+} binding to rabbit liver metallothionein 2. Metal ion mobility in the formation of Cd_4-metallothionein alpha-fragment, *Biochem. J. 262*, 181-188.
29. Boulanger, Y., Armitage, I. M., Miklossy, K. A., and Winge, D. R. (1982) ^{113}Cd NMR study of a metallothionein fragment. Evidence for a two-domain structure, *J. Biol. Chem. 257*, 13717-13719.
30. Boulanger, Y., Goodman, C. M., Forte, C. P., Fesik, S. W., and Armitage, I. M. (1983) Model for mammalian metallothionein structure, *Proc. Natl. Acad. Sci. U. S. A. 80*, 1501-1505.
31. Otvos, J. D., and Armitage, I. M. (1980) Structure of the metal clusters in rabbit liver metallothionein, *Proc. Natl. Acad. Sci. U. S. A. 77*, 7094-7098.
32. Good, M., Hollenstein, R., Sadler, P. J., and Vasak, M. (1988) Cadmium-113 NMR studies on metal-thiolate cluster formation in rabbit cadmium(II) metallothionein: evidence for a pH dependence, *Biochemistry 27*, 7163-7166.
33. Vazquez, F., and Vasak, M. (1988) Comparative ^{113}Cd-NMR studies on rabbit $^{113}Cd_7$-,(Zn_1, Cd_6)-and partially metal-depleted $^{113}Cd_6$-metallothionein-2a, *Biochem. J. 253*, 611-614.
34. Otvos, J. D., Engeseth, H. R., and Wehrli, S. (1985) Preparation and cadmium-113 NMR studies of homogeneous reconstituted metallothionein: reaffirmation of the two-cluster arrangement of metals, *Biochemistry 24*, 6735-6740.
35. Nettesheim, D. G., Engeseth, H. R., and Otvos, J. D. (1985) Products of metal exchange reactions of metallothionein, *Biochemistry 24*, 6744-6751.
36. Messerle, B. A., Schäffer, A., Vašák, M., Kägi, J. H. R., and Wüthrich, K. (1990) Three-dimensional structure of human [$^{113}Cd_7$]metallothionein-2 in solution determined by nuclear magnetic resonance spectroscopy, *J. Mol. Biol. 214*, 765-779.
37. Robbins, A., McRee, D., Williamson, M., Collett, S., Xuong, N., Furey, W., Wang, B., and Stout, C. (1991) Refined crystal structure of Cd, Zn metallothionein at 2.0 Åresolution, *J. Mol. Biol. 221*, 1269-1293.
38. Byrd, J., and Winge, D. R. (1986) Cooperative cluster formation in metallothionein, *Arch. Biochem. Biophys. 250*, 233-237.

www.manaraa.com

39. Petering, D. H., and Fowler, B. A. (1986) Roles of metallothionein and related proteins in metal metabolism and toxicity: problems and perspectives, *Environ. Health Perspect. 65*, 217.
40. Vašák, M. (1991) Metal removal and substitution in vertebrate and invertebrate metallothioneins, In *Methods Enzymol.* (James F. Riordan, B. L. V., Ed.), pp 452-458, Academic Press.
41. Nielson, K. B., and Winge, D. R. (1983) Order of metal binding in metallothionein, *J. Biol. Chem. 258*, 13063-13069.
42. Sutherland, D. E. K., and Stillman, M. J. (2008) Noncooperative cadmium(II) binding to human metallothionein 1a, *Biochem. Biophys. Res. Commun. 372*, 840-844.
43. Merrifield, M. E., Huang, Z., Kille, P., and Stillman, M. J. (2002) Copper speciation in the α and β domains of recombinant human metallothionein by electrospray ionization mass spectrometry, *J. Inorg. Biochem. 88*, 153-172.
44. Ngu, T. T., Easton, A., and Stillman, M. J. (2008) Kinetic analysis of arsenic-metalation of human metallothionein: Significance of the two-domain structure, *J. Am. Chem. Soc. 130*, 17016-17028.
45. Ngu, T. T., Krecisz, S., and Stillman, M. J. (2010) Bismuth binding studies to the human metallothionein using electrospray mass spectrometry, *Biochem. Biophys. Res. Commun. 396*, 206-212.
46. Summers, K. L., Sutherland, D. E. K., and Stillman, M. J. (2013) Single-domain metallothioneins: Evidence of the onset of clustered metal binding domains in Zn-rhMT 1a, *Biochemistry 52*, 2461-2471.
47. Rigby Duncan, K. E., Kirby, C. W., and Stillman, M. J. (2008) Metal exchange in metallothioneins – a novel structurally significant Cd_5 species in the alpha domain of human metallothionein 1a, *FEBS J. 275*, 2227-2239.
48. Palumaa, P., Tammiste, I., Kruusel, K., Kangur, L., Jörnvall, H., and Sillard, R. (2005) Metal binding of metallothionein-3 versus metallothionein-2: Lower affinity and higher plasticity, *Biochim. Biophys. Acta, Proteins Proteomics 1747*, 205-211.
49. Petering, D. H., and Frank Shaw III, C. (1991) [57] Stability constants and related equilibrium properties of metallothioneins, In *Methods Enzymol.* (James F. Riordan, B. L. V., Ed.), pp 475-484, Academic Press.
50. Jacob, C., Maret, W., and Vallee, B. L. (1998) Control of zinc transfer between thionein, metallothionein, and zinc proteins, *Proc. Natl. Acad. Sci. U. S. A. 95*, 3489-3494.
51. Cols, N., Romero-Isart, N., Capdevila, M., Oliva, B., Gonzàlez-Duarte, P., Gonzàlez-Duarte, R., and Atrian, S. (1997) Binding of excess cadmium (II) to Cd_7-metallothionein from recombinant mouse Zn_7-metallothionein 1. UV-VIS absorption and circular dichroism studies and theoretical location approach by surface accessibility analysis, *J. Inorg. Biochem. 68*, 157-166.
52. Jiang, L.-J., Vašák, M., Vallee, B. L., and Maret, W. (2000) Zinc transfer potentials of the α- and β-clusters of metallothionein are affected by domain interactions in the whole molecule, *Proc. Natl. Acad. Sci. U. S. A. 97*, 2503-2508.
53. Zalewska, M., Trefon, J., and Milnerowicz, H. (2014) The role of metallothionein interactions with other proteins, *Proteomics 14*, 1343-1356.
54. Petering, D. H., Zhu, J., Krezoski, S., Meeusen, J., Kiekenbush, C., Krull, S., Specher, T., and Dughish, M. (2006) Apo-metallothionein emerging as a major player in the cellular activities of metallothionein, *Exp. Biol. Med. 231*, 1528-1534.
55. Nielson, K. B., and Winge, D. R. (1985) Independence of the domains of metallothionein in metal binding, *J. Biol. Chem. 260*, 8698-8701.

www.manaraa.com

56. Ngu, T. T., and Stillman, M. J. (2006) Arsenic binding to human metallothionein, *J. Am. Chem. Soc. 128*, 12473-12483.
57. Chen, S.-H., Russell, W. K., and Russell, D. H. (2013) Combining Chemical Labeling, Bottom-Up and Top-Down Ion-Mobility Mass Spectrometry To Identify Metal-Binding Sites of Partially Metalated Metallothionein, *Anal. Chem. 85*, 3229-3237.
58. Ngu, T. T., Dryden, M. D. M., and Stillman, M. J. (2010) Arsenic transfer between metallothionein proteins at physiological pH, *Biochem. Biophys. Res. Commun. 401*, 69-74.
59. Palacios, Ò., Pagani, A., Pérez-Rafael, S., Egg, M., Höckner, M., Brandstätter, A., Capdevila, M., Atrian, S., and Dallinger, R. (2011) Shaping mechanisms of metal specificity in a family of metazoan metallothioneins: evolutionary differentiation of mollusc metallothioneins, *BMC Biol. 9*, 4.

www.manaraa.com

Chapter 5

5 Kinetics of metal transfer reactions between zinc metallothioneins and carbonic anhydrase*

5.1 Introduction

Mammalian metallothioneins (MT) are small, multiple-metal binding proteins with roles in zinc homeostasis, cadmium detoxification, and cellular redox chemistry.[1-4] Using the 20 thiols of the cysteine residues, MTs bind up to seven divalent metals into two peptide-wrapped metal-thiolate clusters.[5] This rather unusual, highly flexible metal coordination system permits metal binding with variable coordination geometries and stoichiometries. Metals bound can be readily donated in exchange reactions depending on the relative metal binding affinities. For example, MTs have a higher affinity for cadmium than for zinc. This allows for exchange with and release of zinc from Zn-MTs concomitant with cadmium binding and sequestration.[6]

Cadmium enters cells adventitiously via essential metal ion transport channels where it associates with proteins containing metal-binding residues.[7] These associations may disrupt the protein structure or displace legitimate metals, rendering the protein non-functional. MTs scavenge cadmium with an exceptionally high average binding affinity [$\log_{10}(K_F) > 10^{16}$] and sequester the toxic cadmium into relatively inert binding sites, potentially protecting the cell against possible toxicological effects.[8] Cellular cadmium exposure also upregulates MT gene synthesis, creating new apoMT and restoring metal homeostasis.[9]

Relatively few details of the mechanisms involved in these metal exchange processes are currently available. Scavenging by apoMT for cadmium weakly associated with metal binding functionalities on the surfaces of proteins (and other cellular macromolecules), occurs rapidly.[10] The scavenging ability of Zn-MTs is slightly slower due to the occupied

* A version of this Chapter has been submitted:

T.B.J. Pinter and M.J. Stillman (2015).

www.manaraa.com

binding sites; however, the high binding affinity difference between zinc and cadmium would also result in relatively fast exchange reactions as is the case for free cadmium added to Zn-MTs *in vitro*.[11]

A more interesting situation arises when cadmium is bound into a traditional metal binding site of a metalloenzyme having, normally, a catalytically active metal in the active site. These active sites are usually not solvent-exposed because they are often buried within the protein fold, a requirement for the activity and specificity of the reaction being catalyzed.[12] Thus, these metal sites are much less accessible and are sterically hindered towards ligand exchange of the bound metal. This means that removal of a toxic metal, such as a cadmium bound to a zinc binding site, would be more difficult. Therefore, the reactions between cadmium substituted zinc-dependent enzymes and Zn-MTs are expected to be slower and would likely require involvement of protein-protein interactions (PPIs).

To provide more details on the metal exchange mechanisms that may occur between MT and a zinc-dependent enzyme, as in the function of MTs *in vivo*, we have in this Chapter, investigated the kinetics of metal exchanges between various MTs and Cd- and Zn-carbonic anhydrase (CA). Three experimental situations have been studied kinetically using electrospray ionization mass spectrometry (ESI-MS): (i) determination of the kinetics of zinc donation from Zn_7-MT to apoCA under MT limiting conditions, such that the donating species are Zn_n-MTs ($n < 7$); (ii) determination of the kinetics of metal exchange between zinc saturated MTs, with no open binding sites, Zn_7-MT and Cd-CA; and, (iii) determination of the kinetics of metal exchange in the presence of open binding sites in the MT between Zn_n-MT (where n = 3-6) and Cd-CA.

5.2 Methods

5.2.1 Purification of recombinant MT1A.

Recombinant human MT1A was purified following previously published procedures (Appendix A).[13] The DNA sequence corresponding to the human MT1A amino acid sequence, which contains additional tetra-alanine repeats at the termini and domain-linker region compared to WT human MT1A: MGKAAAACSC ATGGSCTCTG

www.manaraa.com

SCKCKECKCN SCKKAAAACC SCCPMSCAKC AQGCVCKGAS EKCSCCKKAA AA, was inserted as an N-terminal S-tag fusion into a pET29a plasmids and transformed into BL21(DE3) competent *E. coli* cells and stored as glycerol stocks at -80°C.

Briefly, cells were cultured into 4 L batches of cadmium-spiked LB (Miller) broth, MT expression was induced when $OD_{600} \approx 0.5$ and cells harvested following ~4 h induction period. MT was purified as the cadmium-saturated form using SP anion exchange columns. The S-tag was removed with thrombin CleanCleave kits (Sigma) and separated from the MT using SP cartridges. The protein was concentrated and stored in aliquots at -80°C.

5.2.2 Preparation of zinc metallothionein.

All solutions were vacuum-degassed and argon-saturated to impede cysteine oxidation. Reducing agents were not added as these affect the kinetics of metal exchange. Samples of Cd-MT were thawed under vacuum and acidified to pH 2.5 with formic acid. The released cadmium was separated from the apoprotein using Sephadex G-25 (fine) size exclusion media (GE Lifesciences) equilibrated and eluted with argon-saturated, formic acid in water, pH 2.8. Protein was eluted using a Cary 50 equipped with a flow-cell cuvette monitoring the 200-300 nm range. The apoMT was concentrated and buffer exchanged to 5 mM ammonium formate, pH 7.4 buffer under argon using 3K MWCO Amicon Ultra-4 (Millipore) filter units. A small fraction of the concentrated apoMT was remetallated with cadmium and the concentration determined using ε_{250nm} = 89,000 $M^{-1}cm^{-1}$.

Excess zinc acetate was added to the apoMT and allowed to react for 30 mins. The excess zinc was separated from the Zn_7-MT by centrifugation in 3K MWCO (Amicon Ultra-4 centrifugal filter unit filters), exchanged with 5 mM ammonium formate, pH 7.4 under argon. The final concentration of the Zn_7-MT was determined spectrometrically by adding excess cadmium to a small fraction of the Zn_7-MT, as cadmium displaces zinc stoichiometrically. The complete replacement of cadmium for zinc and zinc saturation for the Zn-MT was confirmed by ESI-MS.

www.manaraa.com

5.2.3 Preparation of apocarbonic anhydrase and cadmium-carbonic anhydrase.

10 mg of bovine erythrocyte Zn-CA (Sigma) was dissolved in 4 mL of 5 mM ammonium formate, pH 5.5 buffer containing 50 mM pyridine-2,6-dicarboxylic acid zinc chelator. This was loaded into a prewashed 10K MWCO and concentrated to 500 µL. Approximately 4 mL of fresh PDC containing buffer was added to the concentrated protein and again centrifuged. This process was repeated until all of the zinc was removed from the CA and no zinc was detected in the filtrate. In general, approximately 25 mL (6 additions of fresh PDC) were required to remove all of the zinc. The PDC was then removed from the protein by adding 5 mM ammonium formate, pH 7.4 buffer to the filter unit and spinning out the low molecular weight PDC. This process was repeated until no PDC was detected in the filtrate. In total, approximately 50 mL of PDC-free buffer were required to remove all of the PDC from the protein.

Cd-CA was made by adding 3x excess cadmium acetate to the apoCA stock and incubating for 1 h at room temperature. The excess cadmium was removed by centrifugation in a 10K MWCO filter exchanged with 5 mM ammonium formate, pH 7.4. The Cd-CA concentrations were determined by UV spectroscopy using ε_{280nm} = 54,000 $M^{-1}cm^{-1}$. The metal content of the Cd-CA was verified by ESI-MS prior to experiments and generally showed greater than 95% replacement of zinc for cadmium.

5.2.4 Reactions between Zn-MT and apoCA or Cd-CA and ESI-MS parameterization.

Zn-MT was added to apoCA or Cd-CA in 5 mM ammonium formate, pH 7.0 buffer under argon and loaded into a gastight syringe (Hamilton) and the reaction followed by ESI-MS. The solution was infused at 10 µL/min for continuous data collection using a modified, temperature-controlled syringe pump thermostated to the desired temperature (± 0.5°C). ESI mass spectral data were collected on a Bruker Micro-TOF II (Bruker Daltonics) operated in the positive ion mode calibrated with NaI as an external calibrant. The following settings were used: scan = 500-4000 m/z; rolling average = 2; nebulizer = 2 Bar; dry gas = 80°C @ 8.0 L/min; capillary = 4000 V; end plate offset = -500 V; capillary exit = 175 V; Skimmer 1 = 30.0 V; Skimmer 2 = 23.5 V; Hexapole RF = 800 V.

www.manaraa.com

5.2.5 Data treatment and kinetic analyses.

ESI mass spectra were averaged for a minimum of two minutes to ensure good signal-to-noise ratios then deconvoluted using the Maximum Entropy algorithm of the Compass DataAnalysis software package (Bruker Daltonics). Relative peak intensities were extracted from these deconvoluted spectra and plotted as a function of reaction times. These data were fit to lines using either linear regression or the ExpDecay2 equation:

$$y = y_0 + A_1 e^{-(x-x_0)/t_1} + A_2 e^{-(x-x_0)/t_2} \qquad (1)$$

in Origin 7 SR2 (OriginLab, Northhampton, MA) as guides.

The kinetic data were fit to pseudo-second order reaction mechanisms, assuming that all zinc came from the Zn-MT species and all cadmium from the Cd-CA and also that [Cd-CA] = [Zn-MT] at t = 0. Under these assumptions, the second order rate law for Cd-CA reacting with Zn-MT:

$$\text{Cd-CA + Zn-MT} \rightarrow \text{Zn-CA + Cd-MT} \qquad (2), \text{ is}$$

$$\text{Rate} = -\frac{d(CdCA)}{dt} = -\frac{d(ZnMT)}{dt} = \frac{d(ZnCA)}{dt} = \frac{d(CdMT)}{dt} \qquad (3), \text{ and, rearranging}$$

$$\frac{d(CdCA)}{dt} = -\,k\,[CdCA]^2 \qquad (4), \text{ integrated, gives}$$

$$\frac{1}{[A]_t} = kt + \frac{1}{[A]_0} \qquad (5)$$

Thus, a plot of $\frac{1}{[A]_t}$ is linear with slope = k and intercept = $\frac{1}{[A]_0}$. Eq 5 was plotted for each of the three reactions and used to determine the apparent second order rate constants.

www.manaraa.com

5.3 Results

5.3.1 Kinetics of the reaction between Zn-MT and apoCA under MT-limiting conditions

We devised an experiment where excess apoCA could compete with Zn-MT for its bound zinc to evaluate the zinc donation properties of Zn_n-MT (n < 7). The zinc exchange between Zn-MT and apoCA in a 0.75:1.0 ratio (protein:protein) was followed continuously via ESI-MS. Figure 5.1 shows the time course for the metallation by Zn-MT of apoCA. The charge states of the mass spectral data are shown on the left, and the corresponding reconstructed deconvoluted masses on the right. At the start of the reaction, the CA was almost completely in the apo form, with no detected Zn-CA in either the charge states or the deconvoluted spectra (Figure 5.1A), demonstrating the near complete extraction of zinc from Zn-CA by the zinc removal procedure. Figure 5.1B-E show an increase in Zn-CA levels as the apoCA is metallated by the Zn-MT. The apoCA is only approximately 50% metallated after 12 h of reaction time (Figure 5.1D) and is still not complete by 24 h (Figure 5.1E).

The complimentary data for MT are shown in Figure 5.2. The speciation of the MT is complicated by the multiple metallation states that coexist in solution. At the start of the experiment, the MT was mostly Zn_7-MT with a small amount of Zn_6-MT and approximately 0.5 equiv (per binding site) of cadmium remaining from the purification and metal exchange procedures (Figure 5.2A). As the reaction proceeded, the Zn_6-MT signal intensified and Zn_5-MT appeared after 1.5 h (Figure 5.2B). There was a general buildup of signal intensity for Zn_{4-6}-MT over the duration of the experiment, with a corresponding decrease in Zn_7-MT. Significantly, no Zn_3-MT was detected in either the charge state or deconvoluted spectra.

www.manaraa.com

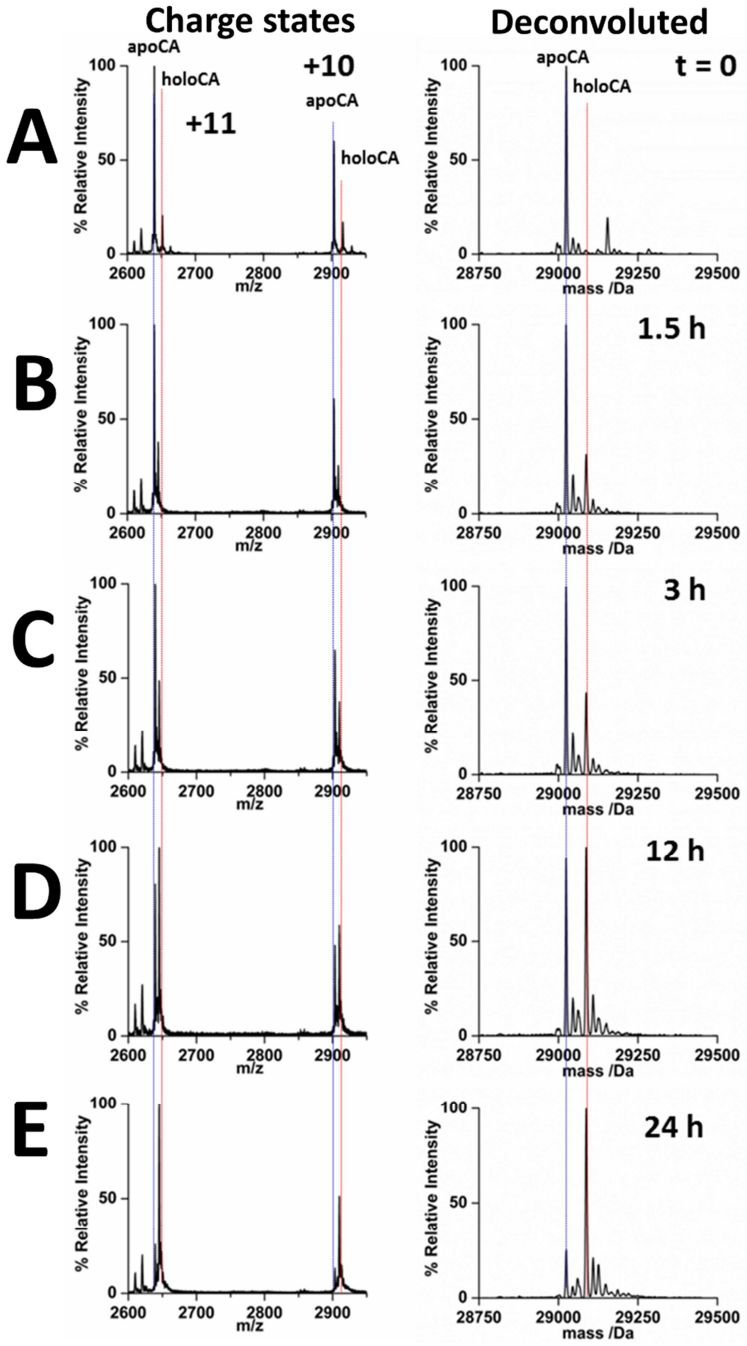

Figure 5.1: Time dependence of the CA metallation by Zn-MT. Representative ESI mass spectral data measured during the reaction between 15 µM apoCA and 12 µM Zn_7-MT are shown. The +10 and +11 charge states are shown on the left, and the corresponding deconvoluted mass on the right. The conditions of the reaction were: 5 mM ammonium formate, pH 7.0 buffer, 25°C.

www.manaraa.com

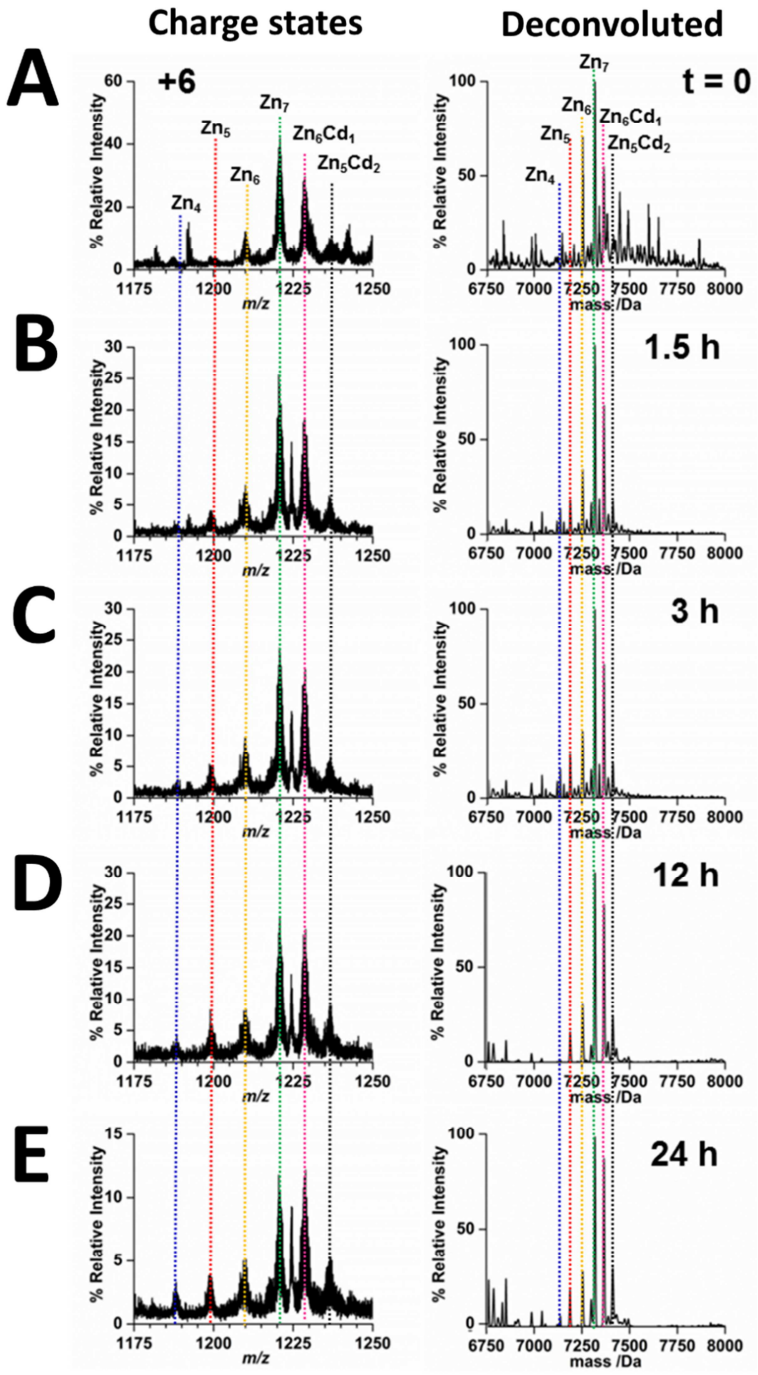

Figure 5.2: Time dependence of the MT demetallation by apoCA. Representative ESI mass spectral data measured during the reaction between 15 µM apoCA and 12 µM Zn_7-MT. The +6 charge state is shown on the left, and the corresponding deconvoluted mass on the right. The conditions of the reaction were: 5 mM ammonium formate, pH 7.0 buffer, 25°C.

www.manaraa.com

To compare the changes in speciation as a function of time, the relative peak intensities were extracted from the deconvoluted data and plotted as a function of time for the MT (Figure 5.3A) and CA (Figure 5.3B) species. The change in MT speciation over time shows that there was fast transfer from Zn_7-MT, followed by much slower release from Zn_6- and Zn_5-MT. In fact, the Zn_6- and Zn_5-MT speciation traces reached steady states only after 10,000 s. Figure 5.3A shows the extracted individual populations of the four key MT species. The overall reaction is Zn_7-MT → Zn_6-M → Zn_5-MT → Zn_4-MT, with each step donating a zinc to the apoCA. The equilibrium data in Chapter 2, showed that, at this metallation point, these three partially demetallated species would coexist (recall that the data in Chapter 2 started from apoMT and apoCA whereas the data here start with Zn_7-MT and apoCA). Figure 5.3A then, shows the change in speciation population as each of these partially metallated species equilibrates over time. The complexity in the figure arises from the presence of all four MT species in the mass spectral data.

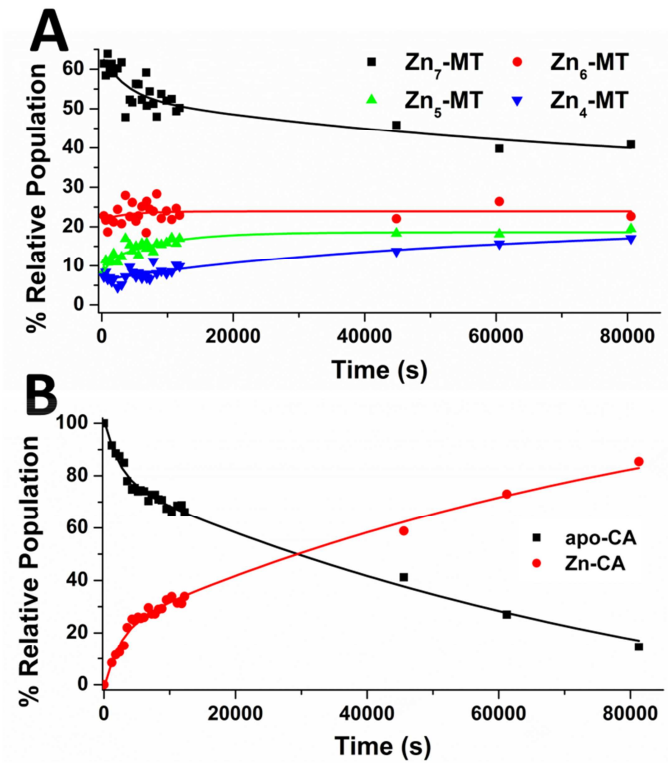

Figure 5.3: Time courses of the demetallation of (A) Zn-MT and the metallation of (B) apoCA extracted from the ESI mass spectral data. The lines have been fit to the data using the ExpDecay 2 equation as described in Section 5.2.5.

www.manaraa.com

Figure 5.3B shows the corresponding time course for the CA speciation. Because there is only one zinc bound, the data are significantly less complicated. At the 80,000 s data point only 80% of the CA had metallated, despite the fact that there were still significant amounts of Zn_7-MT and Zn_6-MT in solution.

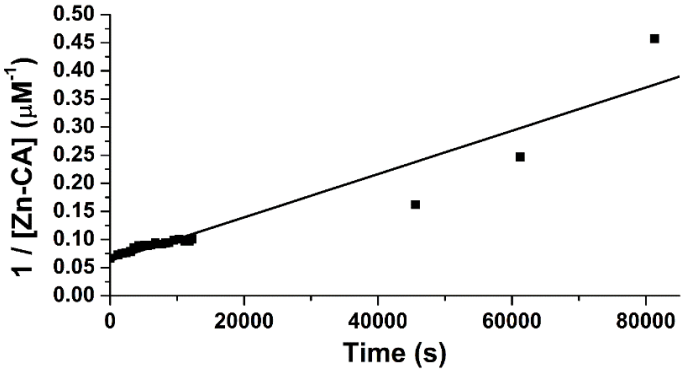

Figure 5.4: Second order kinetic analysis of the zinc metallation of apoCA under MT limiting conditions. The line is based on the speciation trace shown in Figure 5.3 and $[apoCA]_{t=0}$ = 15 µM. The apparent second order rate constant for the reaction under these conditions, as determined from a linear regression of the data, is 3.8(5) ± 0.5(8) $M^{-1}s^{-1}$.

Pseudo-second order kinetic analysis, based on the assumption that all of the zinc that was bound by the apoCA was originally bound in Zn-MT, is shown in Figure 5.4. The plot shows a strong correlation to the linear fit of the data, especially for the early phase of the reaction. The second order rate constant, first order in apoCA and first order in Zn-MT, determined from the slope was 3.8 ± 0.6 $M^{-1}s^{-1}$. Linear regression of the data for the first 12,500 s of the reaction (analysis not shown) gave a slower second order rate constant of 2.5 ± 0.5 $M^{-1}s^{-1}$.

5.3.2 Kinetics of the reaction between Zn_7-MT and Cd-CA

Metal exchange between 30 µM Zn_7-MT and 30 µM Cd-CA was measured continuously using ESI-MS. The peak intensities were extracted from the deconvoluted spectra of the data as described in the Section 5.2.5. The speciation time course curves of MT show the successive reactions of Zn_7-MT with Cd-CA forming Zn_6Cd_1-MT, which can react with

www.manaraa.com

another equivalent of Cd-CA to give Zn_5Cd_2-MT. The time course for these reactions, from the ESI mass spectral data measured over 30,000 s, are shown in Figure 5.5A and B, respectively.

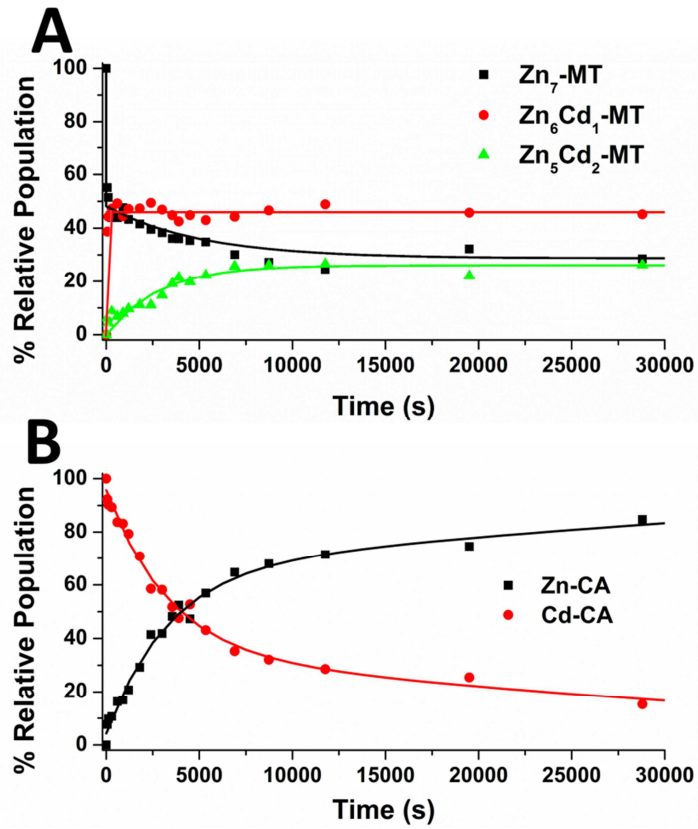

Figure 5.5: Time course of the metal exchange between Zn_7-MT and Cd-CA. (A) MT and (B) CA. Species were extracted from the ESI mass spectral data of the reaction between an equimolar (30 µM) mixture of Cd-CA and Zn_7-MT. The lines have been fit to the data using the ExpDecay 2 equation as described in Section 5.2.5. Conditions: 5 mM ammonium formate, pH 7.0, 37°C.

The only MT species that were detected in the ESI mass spectral data were the metal saturated forms [$(M^{II})_7$-MTs], as mixtures of zinc and cadmium. Initially, the reaction began with zinc saturated Zn_7-MT, which exchanged one zinc for a cadmium bound in Cd-CA to form Cd_1Zn_6-MT. This species reacted with another Cd-CA to form Cd_2Zn_5-MT. No other cadmium containing species were observed in either the charge state or deconvoluted mass spectra. The trend in the Zn_6Cd_1-MT population reflects the

www.manaraa.com

equilibrium between Zn_7-MT and Zn_5Cd_2-MT, where the trafficking of the zinc to the CA in response to the change due to cadmium binding to the MT results in a near constant population for Zn_6Cd_1-MT.

The corresponding CA metallation time course is more straightforward which is reflective of the simpler one-for-one exchange of cadmium for zinc over the course of the reaction, where the zinc from the Zn-MT is exchanging with the cadmium initially bound as Cd-CA. Again, only 80% of the Cd-CA exchanged with Zn-MT by 30,000 s despite the fact that significant amounts of exchangeable zinc (Zn_7-MT) were available.

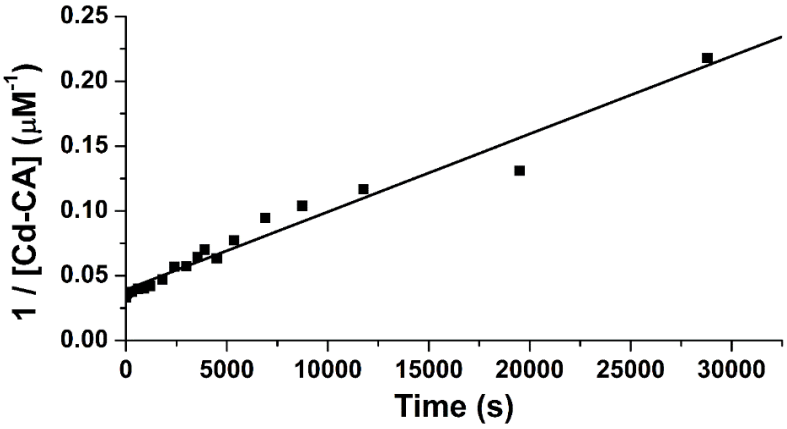

Figure 5.6: Second order kinetic analysis of the reaction of Cd-CA with Zn_7-MT. The line is based on the speciation trace shown in Figure 5.5 and $[Cd\text{-}CA]_{t=0}$ = 30 μM. The apparent second order rate constant for the reaction under these conditions, as determined from the linear regression of the data, is 6.0(0) ± 0.5(8) $M^{-1}s^{-1}$.

The integrated, pseudo-second order rate plot of 1/[Cd-CA] vs. t, for the reaction between Zn_7-MT and Cd-CA and based on assumptions regarding the kinetics of the reaction described in detail in the Section 5.2.4 and 5.2.5, shows a good correlation to the linear fit of the data (Figure 5.6). We determined the second order rate constant (first order in Cd-CA and first order in Zn-MT) for the reaction of Cd-CA with Zn-MT at 37°C to be approximately 6.0 $M^{-1}s^{-1}$.

www.manaraa.com

5.3.3 Kinetics of the reaction between partially metallated MTs and Cd-CA

We have investigated the effects of unoccupied metal binding sites in the MT on the reaction between partially metallated Zn-MT and Cd-CA. 30 µM Cd-CA was reacted with 30 µM unsaturated Zn-MT (protein concentrations) at 37°C and the cadmium-zinc exchange reaction monitored continuously using ESI-MS. The mass spectral data (not shown) indicated that the MT initially existed as a mixture of $Zn_{3\text{-}6}$MT, with Zn_4- and Zn_5- being the most populated MT metallated states. Thus, at the start of the reaction there was a mixture of between one and four unoccupied metal binding sites, with an average of between two and three unoccupied binding sites per MT protein.

The time course for the change in the population of all of the MT species extracted from the deconvoluted ESI mass spectral data for this reaction is shown in Figure 5.7A. This figure shows the change in the relative speciation of all of the detected MT species as a function of reaction time and highlights the complexity of these reactions involving multiple species. The Zn_4-MT species remains approximately constant as a result of the net balance of all of the reactions that consume or produce Zn_4-MT: Zn_5-MT → Zn_4-MT + Zn^{2+}; Zn_4-MT → Zn_3-MT + Zn^{2+}; Zn_4-MT + Cd^{2+} → Zn_4Cd_1-MT. The change in the populations for each of the other MT species shown in Figure 5.7A is also the net sum of the set of reactions involving that species.

Overall, the cadmium content of the MT species increase over the course of the reaction and the zinc content decreases. This trend is more easily observed in Figure 5.7B, where the ratio of Zn_n-MT / Cd_1Zn_{n-1}-MT has been plotted as a function of reaction time in order to compare the change in cadmium content per metallation state [i.e. each line represents the change in cadmium content for $(M^{II})_{4\text{-}6}$-MT]. For example, the positive slope of the blue line (Zn_5Cd_1-MT / Zn_6-MT) shows that the Zn_5Cd_1-MT population is increasing relative to the population of Zn_6-MT.

www.manaraa.com

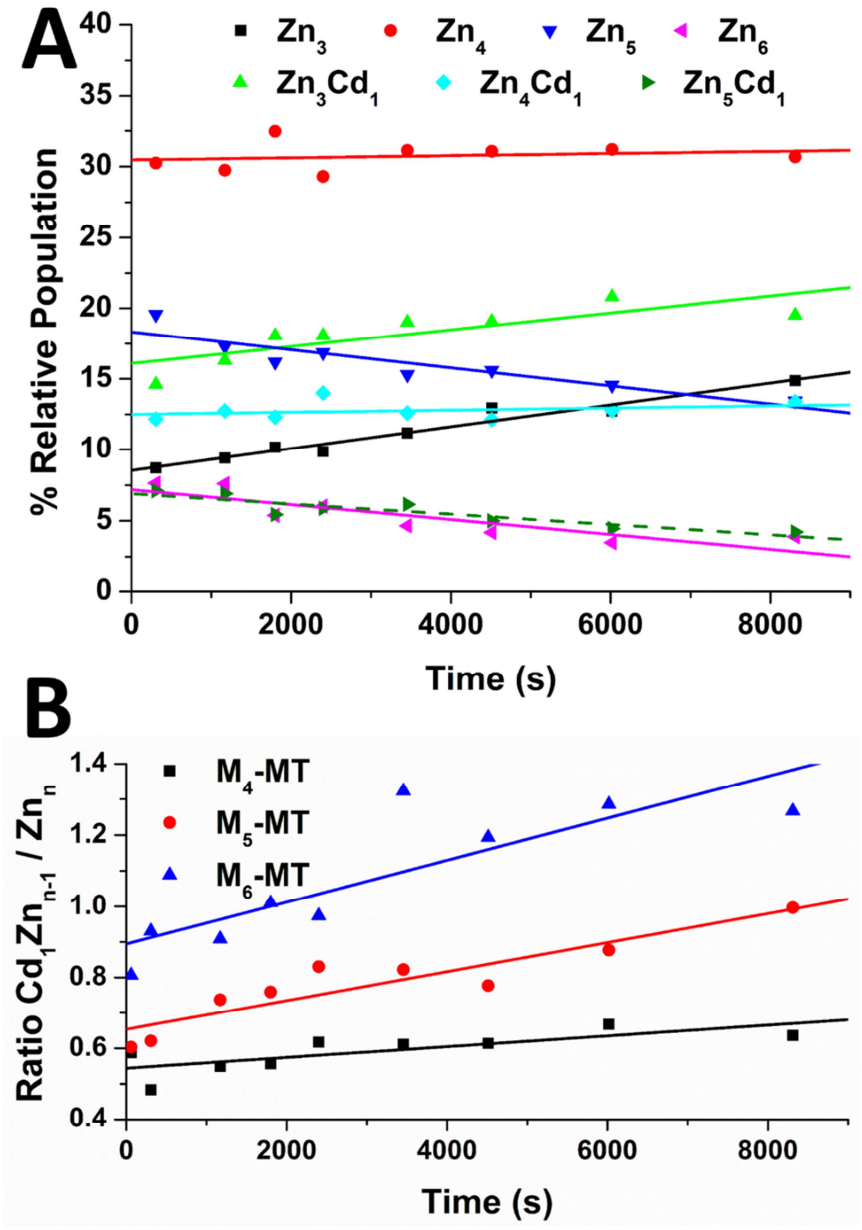

Figure 5.7: Time dependence of the populations of metallothionein species for the reaction between partially metallated Zn-MT and Cd-CA. (A) Experimentally determined time courses of MT species extracted from the ESI mass spectral data of the reaction between an equimolar (30 µM) mixture of Cd-CA and $Zn_{(3-6)}$-MT. Conditions: 5 mM ammonium formate, pH 7.0, 37°C. (B) Change in the ratio of $CdZn_{(n-1)}$-MT / Zn_n-MT for the values of n = 4, 5, and 6. The change in cadmium occupancy shown for each of the detected species as a function of time. The lines are based on linear fits to the data.

www.manaraa.com

The corresponding time course for the CA speciation during the reaction with the partially metallated Zn-MT is shown in Figure 5.8. Initially, all of the CA was of the cadmium bound form. Notably the apoCA did not extract the zinc from the partially metallated Zn-MT presumably because the zinc loading of the MT was only Zn_{3-6}-MT to begin with. Thus, the formation of the apoCA, formed from extraction of cadmium by the unoccupied MT sites, which have larger cadmium affinity values, occurs at a faster rate than does formation of the Zn-CA.

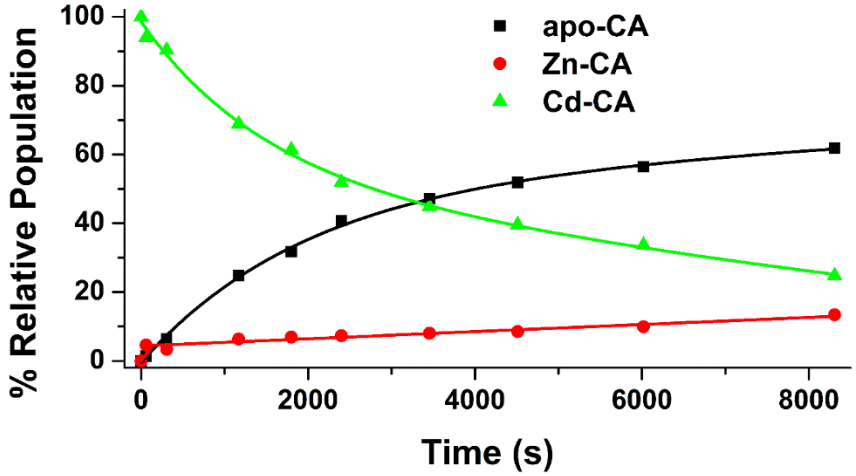

Figure 5.8: Experimentally determined time courses of CA species extracted from the ESI mass spectral data of the reaction between an equimolar (30 µM) mixture of Cd-CA and $Zn_{(3-6)}$-MT. Conditions: 5 mM ammonium formate, pH 7.0, 37°C. The lines have been fit to the data using the ExpDecay 2 equation as described in the methods sections.

The disappearance of Cd-CA was plotted as a pseudo-second order reaction (first order with respect to CA and to MT) and is shown in Figure 5.9. The data show strong correlation to a linear fit that determined the second order rate constant as approximately 11.7 $M^{-1}s^{-1}$, from the slope of the line in Figure 5.9. This rate is approximately twice as that determined for the reaction between zinc-saturated MT and Cd-CA at the same temperature (Figure 5.6).

www.manaraa.com

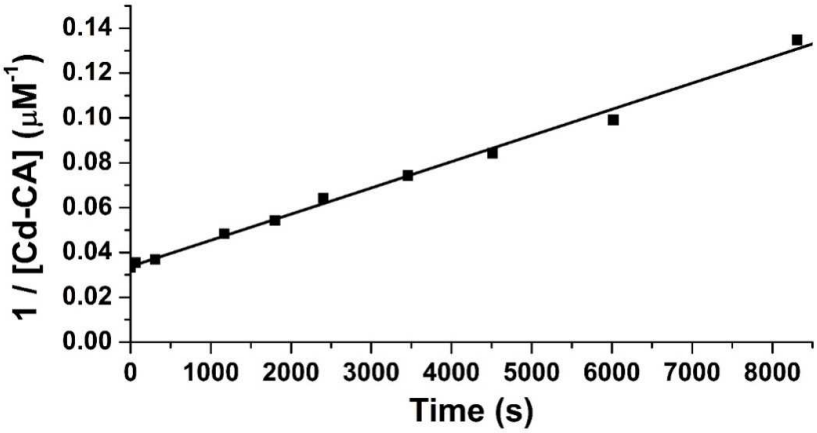

Figure 5.9: Second order kinetic analysis of the reaction of Cd-CA with partially zinc metallated MT. The line is based on the speciation trace shown in Figure 5.8 and $[Cd\text{-}CA]_{t=0}$ = 30 μM. The apparent second order rate constant for the reaction under these conditions, as determined from the linear regression of the data, is 11.6(8) ± 0.7(2) $M^{-1}s^{-1}$.

5.4 Discussion

5.4.1 Protein-protein interactions between metallothionein and other metal binding sites

Evidence of PPIs between MTs and metalloenzymes comes mostly from reports of the zinc donation properties of Zn_7-MT to apo-zinc-dependent proteins.[14-16] There have been two reports of metal substitution between MTs and cadmium-substituted zinc-dependent enzymes. In the first report, Zn_7-MT was shown to exchange a single zinc for the cadmium bound to the zinc finger domain of the Tramtrack transcriptional repressor protein.[17] The second report investigated the kinetics of the metal exchange between apo and Zn_7-MT and cadmium-substituted bovine carbonic anhydrase (Cd-CA) where the apoMT extracted the cadmium from Cd-CA over 20x faster than the Zn_7-MT exchange reaction.[18]

Most reported studies between Zn-MT and zinc binding proteins use an excess of Zn-MT as the zinc source. Therefore, those results are largely descriptive of the reactions involving Zn_7-MT only, since it is in excess, and not the partially metallated species. Previously, our group and others have demonstrated that there are seven different zinc

www.manaraa.com

binding affinities of MTs; thus, the metal affinity for an incoming metal depends on the metal loading.[19, 20] Each of the reactions of Zn_n-MTs (where n = 0-6) for either zinc donation or cadmium exchange is controlled by different reaction parameters. This is important because there is evidence of substantial pools of partially metallated MTs *in vivo*, which means that these partially metallated MTs play a key role in MT's function.[21]

5.4.2 Metal binding to carbonic anhydrase

Zinc and cadmium are bound in CA tetrahedrally by 3 HIS and a labile water molecule. Significantly, CA binds zinc and cadmium with similar affinities of approximately ($\log_{10}(K_F)$) 12.0 and 11.1, respectively at pH 7.0.[22] Thus, the ratio of the binding constants K_F^{Cd}/K_F^{Zn} is small compared to the same ratio for MT and there is, therefore, no significant driving force for metal exchange in CA. This means that CA with an existing cadmium or zinc in its binding site is resistant to exchange with free metal in solution, as has been demonstrated for many metals where similar exchanges involving free metals were shown to take from days to weeks.[23, 24]

Free metals added to the apoCA protein bind rapidly. For example, in both zinc and cadmium titration experiments of apoCA, metal binding occurs within the time of ESI mass spectral data acquisition (< 10 s) following stoichiometric mixing (data not shown). However, *in vivo*, metal concentrations are tightly regulated and the concentrations of free metals are far below that which would support free metal association to apoenzymes following their transcriptional synthesis. Therefore, other zinc sources and chaperones must deliver and insert the zinc into these active sites, as suggested as a function of Zn-MTs.[16]

With the goal of obtaining more details regarding the role of Zn-MTs in reactions with metalloenzymes, we have investigated a series of metal exchange reactions between Zn-MTs and CA. We used CA as a putative zinc-binding protein. The above results describe the metallation statuses of both the MT and CA species as a function of time. We have shown mass spectral data for only the first set of reactions as a guide to aid in interpretation of the speciation plots that follow.

www.manaraa.com

5.4.3 Are the zinc donation kinetics different for partially metallated MTs?

In the latter stages of the metal transfer reaction between Zn-MTs and apoCA, when a significant fraction of the apoCA is metallated and there is less apoCA to accept a donation, the Zn_7-MT → Zn_6-MT → Zn_5-MT → Zn_4-MT reactions occur at approximately the same rate such that the rate of formation of Zn_4-MT approximately matches the rate of loss of Zn_7-MT. We interpret this result as due to the redistribution of zinc in the MT species, restoring the thermodynamically preferred zinc occupancy based on the zinc affinities of the different Zn_n-MT species following a zinc donation event from $Zn_{5\text{-}7}$-MT to apoCA.

These data match the results from the competitive titration between apoMT and apoCA for added zinc under equilibrium conditions.[19] The apoCA was shown to compete effectively only with $Zn_{5\text{-}7}$-MT, and not with $Zn_{1\text{-}4}$-MT. In another set of experiments, where the ratio of apoCA:Zn_3Cd_4-MT was 7:1, only 1.4 zinc ions were released by the MT, though further zinc donation was initiated by incubation in the presence of GSH and GSSG.[25]

Other experiments, where the Zn_7-MT was in excess, meaning that the majority of the donated zinc species would be from Zn_7-MT → Zn_6-MT, usually showed faster zinc donation kinetics. For example, in time course experiments between excess Zn_7-MT and apoCA, also studied by ESI-MS, the apoCA was 50% metallated within 2,400 s (conditions: 10 mM ammonium acetate, pH 7.5, unknown temp.).[15] This is over 10x faster than the reaction shown here where the apoCA is 50% metallated after 25,000 s.

In conclusion, the zinc donation properties of Zn-MTs are modulated by the binding affinity differences between the zinc donor and the zinc acceptor. The thermodynamics (and kinetics) favour donation more strongly the greater the binding affinity difference is between the donor and acceptor, and the reaction occurs faster as well. We now know that the zinc are bound to MT with differing affinities (Chapter 2) and we thus expected to see slower zinc donation kinetics for Zn_n-MTs ($n < 7$). Comparing these new data to those available in the literature, we have shown that Zn_5- and Zn_6-MTs donate much

www.manaraa.com

more slowly than Zn_7-MTs. These results support the model of Zn_7-MT and Zn_6-MT as the most probable source of MT zinc donation.

5.4.4 How readily does zinc saturated MT exchange with Cd-CA?

Cadmium detoxification is another commonly described *in vivo* function of Zn-MTs. Several studies have shown that cadmium binds to MTs via very fast reaction, often within the dead-time of stopped-flow instruments (< 10 ms), using free cadmium as the Cd-source.[10, 26] These reactions are significantly slowed when the cadmium is bound by another chelator, such as another protein.[27] The metal exchange reactions are reflective of the relative binding affinities for cadmium and zinc between the two binding sites, i.e., the difference between the metal preferences of one site vs. another. For example, in the case of Cd-CA mixed with Zn-MT, the metal exchange will depend on the magnitude of $\frac{K_{CA_{Zn}}}{K_{CA_{Cd}}} \bullet \frac{K_{MT_{Cd}}}{K_{MT_{Zn}}}$. CA binds zinc with a higher affinity than cadmium, and MT binds cadmium with a higher affinity than zinc. This ratio is largely positive and a favourable exchange is thermodynamically predicted to occur.

The population time course data for the MT species (Figure 5.5A) show that there is an initial rapid Zn_7-MT to Cd_1Zn_6-MT reaction, most likely due to a small excess of cadmium that was non-specifically bound to the exterior of the Cd-CA protein. This is followed by a slower reaction of Cd_1Zn_6-MT forming Cd_2Zn_5-MT. The intermediate Cd_1Zn_6-MT reaches approximately a steady state within the first 2,000 s, after which, formation from Zn_7-MT matches the rate of the reaction that forms Cd_2Zn_5-MT.

The CA (Figure 5.5B) shows a similar change in speciation over the reaction time. The initial zinc exchange for the bound cadmium, from primarily Zn_7-MT (up to 2,000 s), appears to occurs at a faster rate than later in the reaction (where the pool of MT contains more cadmium and the Cd-CA would also encounter Cd_1Zn_6-MT). Interestingly, even up to almost 30,000 s, a significant fraction of the Cd-CA remains, despite the fact that there are zinc ions available for donation from the MT (Zn_7-MT and Cd_1Zn_6-MT). We interpret this to indicate that the reaction is approaching equilibrium, where the average relative

www.manaraa.com

affinity constants for zinc and cadmium binding to MT are approaching equality to those for CA, with respect to the concentrations of each of the species in solution.

This second order rate constant determined here of 6.0 $M^{-1}s^{-1}$ at 37°C is faster than the reported value of 2.3 $M^{-1}s^{-1}$ at the same temperature by Ejnik *et. al.*[18] The approximate agreement between these two values, however, verifies that the experimental design and data analysis procedures are accurately reflecting the kinetics of these (and similar) reactions. We also attempted to measure the kinetics at 25°C, but we observed no metal exchange reaction, up to 18 h (~65,000 s). This result also agree with those reported by Ejnik *et al*. where the second order reaction rate constant (0.33 $M^{-1}s^{-1}$) was almost 7x slower at the colder temperature.[18]

In conclusion, Zn_7-MT is able to efficiently exchange bound zinc for bound cadmium from Cd-CA. Because the rate of the reaction between the Zn-MT and Cd-CA occurs much more rapidly than is possible for a dissociative-associative metal exchange mechanism, these results support the PPI model of metal exchange between MT and enzymes. Cadmium and zinc each bind to MT and CA with relatively high affinities and therefore small dissociation constants, $K_d < 10^{-11}$. Thus, only very small concentrations of free cadmium or free zinc would be in a solution containing MT and CA, and the rate of the exchange, for a dissociative-associative metal exchange mechanism would be extremely slow.

5.4.5 Are the metal exchange kinetics between Cd-CA and $Zn_{(3-5)}$-MTs faster or slower compared to those for Zn_7-MT?

The results from the previous set of experiments raise an interesting question: if all of the metal binding sites in the MT-CA complex are occupied, how does the metal exchange take place? Since there are no obvious metal binding ligands that are free in the MT, and the CA active site is prefilled with cadmium, the exchange must somehow take place within the MT-CA complex. With open metal binding sites in either the CA or MT, the metal exchange may become easier because the lability of the metals allows for the use of a transient metal binding site to facilitate the exchange process.

www.manaraa.com

The speciation time courses in Figure 5.7 are complicated by the overlap of two competing processes: the binding of cadmium, which increases the metal load per MT, is competing against the zinc donation to the apoCA, which decreases the metal loading. The metal donation properties of partially metallated MTs differs significantly depending on the number of zincs bound. Thus, the time courses in Figure 5.7 are each the sum of the reactions that bind cadmium and donate zinc. Looking only at the zinc metallation species, we see a decrease in the Zn_6- and Zn_5-MT speciation over the course of the reaction and a significant increase in Zn_3-MT population.

The time course data corresponding to the CA species (Figure 5.8) clearly show how, under these conditions, the metal exchange between Cd-CA and Zn_n-MT occurs via a two-step mechanism. The first step is the relatively fast extraction of cadmium from the Cd-CA into the empty metal binding sites in the partially metallated Zn-MTs. The second step is the relative slow release of zinc from the partially metallated Zn-MTs to the now available apoCA from the previous step. It is important to note that the rates of these two steps will depend on the metal loading status of the MT; more empty metal binding sites will extract cadmium faster while MTs with more zinc will donate zinc faster.

These results support the hypothesis that an open coordination site results in faster cadmium extraction from a cadmium-substituted zinc enzyme. The second order rate constant obtained here (11.2 $M^{-1}s^{-1}$) is slower than that reported by Ejnik *et. al* of 18.2 $M^{-1}s^{-1}$ for the reaction between apoMT and CdCA also measured at 37°C.[18] Significantly, the second order rate constant for the partially metallated MTs (~11 $M^{-1}s^{-1}$) falls between that of zinc saturated MT (~6 $M^{-1}s^{-1}$) and apoMTs (~18 $M^{-1}s^{-1}$), which is a reflection of the cadmium-extraction abilities of each of the MT species.

5.4.6 The structure of CA and relevance to PPIs with MT

The crystal structure of carbonic anhydrase II shows that the 3 His active site sits at the bottom of a cavity that is approximately 10 – 20 Å across and 15 – 20 Å deep (Figure 5.10). This cavity is large enough to allow amino acid side chains from the MT to approach the metal binding site, especially for a Cys side chain within a flexible loop.

www.manaraa.com

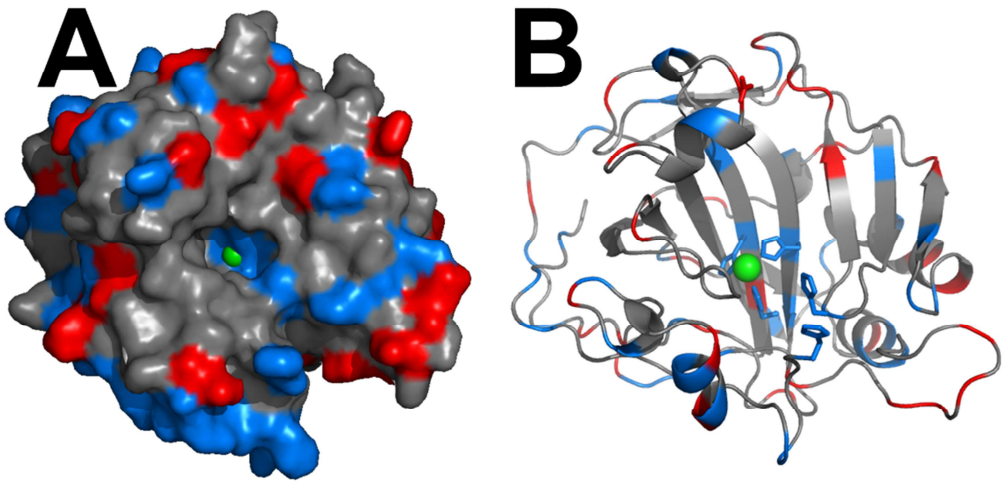

Figure 5.10: X-ray crystal structure of CA and metal binding residues that could facilitate metal transfers. Structure of human erythrocyte carbonic anhydrase II (1CA2)[28] showing (A) the surface and active site and (B) the cartoon representation. The residues have been coloured according to charge: red = negatively charged, blue = positively charged. The zinc in the active site is shown as a green sphere.

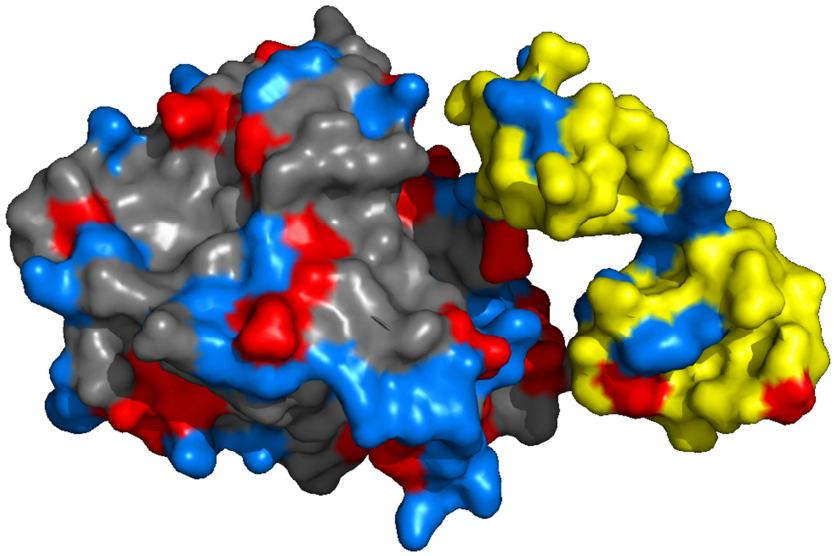

Figure 5.11: Manual docking of the crystal structures of CA and MT. CA (1CA2)[28] and MT (4MT2)[29] electrostatic contacts near the active site of the CA are able to align with complimentary charged residues of MT. The cavity size outside of the active site also permits close approach of the MT protein.

www.manaraa.com

In the MT-CA complex, nearby metal binding residues along the metal exchange pathway may facilitate the metal exchange process. The structure of CA shows that there are two histidine that would be well suited to assist in the zinc delivery or cadmium removal as intermediate metal binding residues in the exchange process. His4 sits on the rim of the active site funnel and His64 sits approximately halfway down the length of the funnel (Figure 5.10B, right of the zinc binding site). Other features of the CA protein that would be favourable to PPIs with MT are the presence of multiple surface charges that could form electrostatic interactions with the MT as shown in Figure 5.11.

5.5 Conclusions

The metal donation properties of metallothioneins have been well studied, yet many questions remain. Initially MTs were identified as having solely toxicological action from the reports of binding toxic metal ions. More recently, MTs have been suggested to play roles in the essential metal ion homeostasis of zinc and copper. The true function of MTs *in vivo* are likely a combination of the toxic metal detoxification and essential metal homeostasis, depending on the cellular metallation status (a role in cellular redox chemistry has also been suggested).

In this work, we have investigated the role of partially metallated MTs in zinc donation to an apo zinc-dependent enzyme, carbonic anhydrase. We showed that partially metallated MTs donate zinc with different propensities as a direct result of the relative binding affinities of each Zn_n-MT species for its bound zinc ions. These results support our current model where Zn_7- and Zn_6-MT are the primary zinc donating species for Zn-MTs.

We have also shown that partially metallated MTs are able to extract cadmium at rates intermediate to apoMT (fastest) and zinc-saturated MT (slowest) as a function of the number of open metal binding sites. These results suggest that metal exchange occurs in two separate steps where cadmium removal from Cd-CA occurs first, followed by a slow binding of zinc from the Zn-MT. Taken together, the results from this work support a model for metal transfers between MT and other proteins that is via protein-protein interactions which permit the essential metal homeostatic and toxic metal sequestration roles of MTs *in vivo*.

www.manaraa.com

5.6 References

1. Kang, Y. J. (2006) Metallothionein redox cycle and function, *Exp. Biol. Med. 231*, 1459-1467.
2. Maret, W., and Vallee, B. L. (1998) Thiolate ligands in metallothionein confer redox activity on zinc clusters, *Proc. Natl. Acad. Sci. U. S. A. 95*, 3478-3482.
3. Sabolić, I., Breljak, D., Škarica, M., and Herak-Kramberger, C. M. (2010) Role of metallothionein in cadmium traffic and toxicity in kidneys and other mammalian organs, *Biometals 23*, 897-926.
4. Maret, W. (2000) The function of zinc metallothionein: a link between cellular zinc and redox state, *J. Nutr. 130*, 1455S-1458S.
5. Braun, W., Vasak, M., Robbins, A., Stout, C., Wagner, G., Kägi, J., and Wüthrich, K. (1992) Comparison of the NMR solution structure and the X-ray crystal structure of rat metallothionein-2, *Proceedings of the National Academy of Sciences 89*, 10124-10128.
6. Nielson, K. B., Atkin, C., and Winge, D. (1985) Distinct metal-binding configurations in metallothionein, *J. Biol. Chem. 260*, 5342-5350.
7. Hinkle, P. M., Kinsella, P., and Osterhoudt, K. (1987) Cadmium uptake and toxicity via voltage-sensitive calcium channels, *J. Biol. Chem. 262*, 16333-16337.
8. Waalkes, M. P., and Goering, P. L. (1990) Metallothionein and other cadmium-binding proteins: recent developments, *Chem. Res. Toxicol. 3*, 281-288.
9. Bertin, G., and Averbeck, D. (2006) Cadmium: Cellular effects, modifications of biomolecules, modulation of DNA repair and genotoxic consequences (a review), *Biochimie 88*, 1549-1559.
10. Ejnik, J., Robinson, J., Zhu, J., Försterling, H., Shaw, C. F., and Petering, D. H. (2002) Folding pathway of apo-metallothionein induced by Zn 2+, Cd 2+ and Co 2+, *J. Inorg. Biochem. 88*, 144-152.
11. Ejnik, J., Shaw III, C. F., and Petering, D. H. (2010) Mechanism of Cadmium Ion Substitution in Mammalian Zinc Metallothionein and Metallothionein α Domain: Kinetic and Structural Studies, *Inorg. Chem. 49*, 6525-6534.
12. Laskowski, R. A., Luscombe, N. M., Swindells, M. B., and Thornton, J. M. (1996) Protein clefts in molecular recognition and function, *Protein Sci. 5*, 2438.
13. Chan, J., Huang, Z., Watt, I., Kille, P., and Stillman, M. J. (2007) Characterization of the conformational changes in recombinant human metallothioneins using ESI-MS and molecular modeling, *Can. J. Chem. 85*, 898-912.
14. Mason, A. Z., Moeller, R., Thrippleton, K. A., and Lloyd, D. (2007) Use of stable isotopically enriched proteins and directly coupled high-performance liquid chromatography inductively coupled plasma mass spectrometry for quantitatively monitoring the transfer of metals between proteins, *Anal. Biochem. 369*, 87-104.
15. Zaia, J., Fabris, D., Wei, D., Karpel, R. L., and Fenselau, C. (1998) Monitoring metal ion flux in reactions of metallothionein and drug-modified metallothionein by electrospray mass spectrometry, *Protein Sci. 7*, 2398-2404.
16. Zalewska, M., Trefon, J., and Milnerowicz, H. (2014) The role of metallothionein interactions with other proteins, *Proteomics 14*, 1343-1356.
17. Roesijadi, G., Bogumil, R., Vasák, M., and Kägi, J. H. (1998) Modulation of DNA binding of a tramtrack zinc finger peptide by the metallothionein-thionein conjugate pair, *J. Biol. Chem. 273*, 17425-17432.

www.manaraa.com

18. Ejnik, J., Muñoz, A., Gan, T., Shaw III, C. F., and Petering, D. (1999) Interprotein metal ion exchange between cadmium-carbonic anhydrase and apo-or zinc-metallothionein, *J. Biol. Inorg. Chem. 4*, 784-790.
19. Pinter, T. B., and Stillman, M. J. (2014) The Zinc Balance: Competitive Zinc Metalation of Carbonic Anhydrase and Metallothionein 1A, *Biochemistry 53*, 6276-6285.
20. Krężel, A., and Maret, W. (2007) Dual nanomolar and picomolar Zn (II) binding properties of metallothionein, *J. Am. Chem. Soc. 129*, 10911-10921.
21. Petering, D. H., Zhu, J., Krezoski, S., Meeusen, J., Kiekenbush, C., Krull, S., Specher, T., and Dughish, M. (2006) Apo-metallothionein emerging as a major player in the cellular activities of metallothionein, *Exp. Biol. Med. 231*, 1528-1534.
22. Lindskog, S., and Nyman, P. O. (1964) Metal-binding properties of human erythrocyte carbonic anhydrases, *Biochim. Biophys. Acta, Spec. Sect. Biophys. Subj. 85*, 462-474.
23. Kidani, Y., and Hirose, J. (1977) Coordination Chemical Studies on Metalloenzymes II. Kinetic Behavior of Various Types of Chelating Agents towards Bovine Carbonic Anhydrase, *J. Biochem. (Tokyo) 81*, 1383-1391.
24. Coleman, J. E. (1965) Human Carbonic Anhydrase. Protein Conformation and Metal Ion Binding*, *Biochemistry 4*, 2644-2655.
25. Mason, A. Z., Perico, N., Moeller, R., Thrippleton, K., Potter, T., and Lloyd, D. (2004) Metal donation and apo-metalloenzyme activation by stable isotopically labeled metallothionein, *Mar. Environ. Res. 58*, 371-375.
26. Irvine, G. W., Duncan, K. E., Gullons, M., and Stillman, M. J. (2015) Metalation Kinetics of the Human α-Metallothionein 1a Fragment Is Dependent on the Fluxional Structure of the apo-Protein, *Chem.--Eur. J. 21*, 1269-1279.
27. Li, T.-Y., Kraker, A. J., Shaw, C. F., and Petering, D. H. (1980) Ligand substitution reactions of metallothioneins with EDTA and apo-carbonic anhydrase, *Proceedings of the National Academy of Sciences 77*, 6334-6338.
28. Eriksson, A. E., Jones, T. A., and Liljas, A. (1988) Refined structure of human carbonic anhydrase II at 2.0 Å resolution, *Proteins: Struct., Funct., Bioinf. 4*, 274-282.
29. Braun, W., Vasak, M., Robbins, A., Stout, C., Wagner, G., Kägi, J., and Wüthrich, K. (1992) Comparison of the NMR solution structure and the X-ray crystal structure of rat metallothionein-2, *Proc. Natl. Acad. Sci. U. S. A. 89*, 10124-10128.

www.manaraa.com

Chapter 6

6 Conclusion*

6.1 The metal binding affinities of MT

Metallothioneins (MTs) were initially discovered by the repeated purification of cadmium-containing fractions of samples from equine kidney cortex.[1] For many years the main function of MTs was thought to be protection against the actions of toxic metals through sequestration of those metals. More recently, MTs have been suggested to play key roles in cellular zinc and copper homeostasis and, in addition, it has been suggested that they are involved in cellular redox chemistries.[2-4] The interaction of metals with MTs has therefore been at the forefront of this field of research as these suggested functions involve metal binding and release reactions. These reactions are then intricately tied to the metal binding affinities of MTs for the metal ions and determining toxic metal binding affinities of metallothioneins (MTs) has been a significant research goal since this family of metal binding proteins was first discovered.[5, 6]

Since MTs bind multiple metals, there are two values that can be assigned to the metal binding affinity: (i) the average binding affinity (across all metals bound) and (ii) the per metal or per binding site affinity. Historically, metals were thought to bind to MTs with approximately the same affinity, where the first metal was bound to the apoMT with approximately the same affinity as the last metal in forming the metal-saturated MT.[7] More recent results have shown that metal binding to MTs occurs over a range of affinities.[8, 9]

Accurately and precisely determining the metal affinities on a per site basis has been complicated by the unique properties of the MT protein family such as the ability to bind numerous metal ions per protein strand, lack of protein secondary structural elements or preformed metal binding sites, high fluxionality, and metal lability within and between

* A version of this Chapter is in preparation:
T.B.J. Pinter and M.J. Stillman (2015).

www.manaraa.com

MTs. The focus of the research carried out for this thesis was to determine accurate metal binding affinities per site and understand how these affinities control the homeostatic functions of MTs.

6.2 Metal affinities from competition experiments

At the outset of this research, it was thought that MTs had four very high affinity sites with similar affinities, and 3 weaker affinity sites with significantly decreasing affinities.[8] One of our initial goals was the development of methods to resolve the individual binding affinities of all seven sites and assign them real apparent formation constants under biologically relevant conditions.

Using competition experiments between apoMT and apoCA for zinc monitored by ESI-MS, we showed that each of zinc ions was bound to MT with a distinct affinity. Eight zinc binding events were observed as distinct, separate reactions. These experiments formed the basis of Chapter 2. Modelling the sequential, competitive, reversible bimolecular reactions that describe formation of Zn_7-MT from apoMT and Zn-CA from apoCA, allowed us to determine the relative zinc binding affinities for each of the eight reactions. Optimization of the parameters that describe all eight reactions in one simultaneous fitting procedure ensured the data were accurately reflected in the models and that the modelled parameters were fundamentally sound for all of the reactions.

The binding affinities of the MT were directly reflected in the change in metal occupation of the CA throughout the titration. The most significant result from Chapter 2 was the locking of the relative binding affinity of each of the seven independent MT metallation reactions to the known, experimentally determined value for zinc binding to apoCA. These apparent binding affinities demonstrate that the MT metal affinities span a range that simultaneously permits zinc storage, for the low occupancy, high affinity sites (Zn_{0-4}-MTs), and also zinc donation to zinc enzymes for the higher occupancy, low affinity sties (Zn_{5-7}-MTs).

We have summarized the overall scheme of binding affinities in a cartoon (Figure 6.1). This figure illustrates our current model of the “ladder” of binding affinities for the

www.manaraa.com

homeostatic roles of MT. At low concentrations of zinc, the predominant species will be low occupancy Zn_{1-4}-MTs, which act as deep zinc sinks. These high affinity sites remove zinc from zinc sensors that turn on zinc importation, increasing cellular zinc content. As the concentration of zinc increases, the weaker affinity Zn_{5-7}-MTs donate the weakly coordinated zinc to zinc enzymes and other zinc binding sties. When the concentration of zinc exceeds all available MT binding sites, zinc responsive elements turn on zinc export and upregulation of MT.

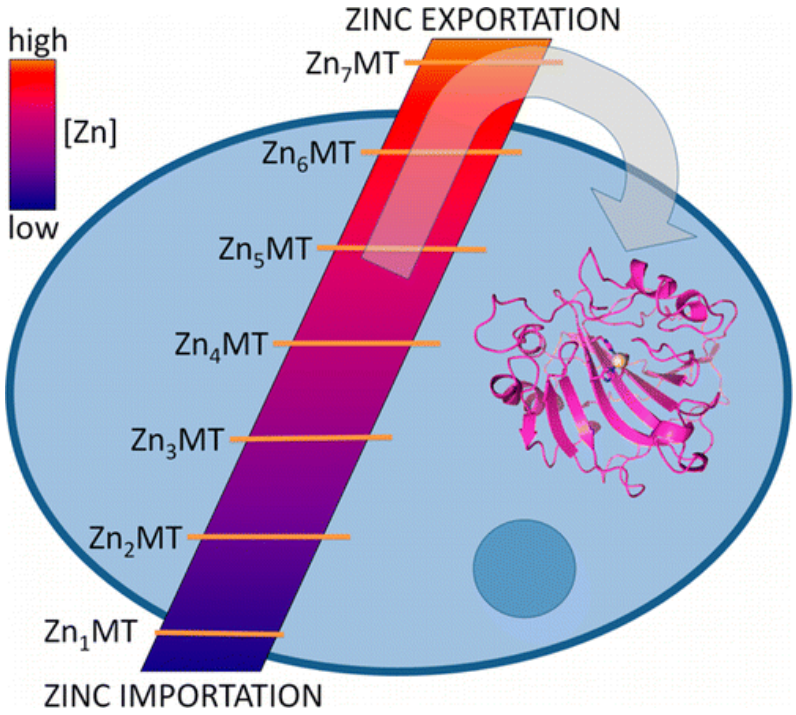

Figure 6.1: The "ladder" of zinc affinities in MTs. Reproduced with permission of ref.[10] copyright (2014) American Chemical Society.

6.3 The location of the strong and weak affinity binding sites

In the work described in Chapter 2 we were unable to determine the location of the mostly weakly bound zinc. In that report, we had also suggested that suppression of the first two, and largest, zinc binding constants was due to tangling of the apoMT peptide backbone (pink triangles, Figure 3.7). We therefore next studied the competitive metallation reactions of the domain fragments of the MT with apoCA in order to observe

www.manaraa.com

the effect of a reduced chain length on the metal donation properties and those results were described in Chapter 3.

Using the ESI-MS we were able to show the zinc occupancy between all species in solution. Modelling the ESI mass spectral data allowed us to accurately determine the individual zinc binding constants for each of the three and four zinc ions in the N-terminal β-domain and C-terminal α domain fragments, respectively. We proposed that the strongest zinc binding site was located in the C-terminus of the apoMT and that the weakest metal, the one being donated from Zn_7-MTs was located in the β-domain, N-terminal fragment.

In contrast to the trend in the full two-domain protein, the zinc binding affinities of the separated domain fragments, relative to those reported for the connected domains in the intact protein did not show the same suppression for the first zinc bound (Figure 3.7, red circles and black squares). We suggested that this was due to the fact that the apo fragments were too short to significantly tangle.

From a combination of the results presented in Chapter 2 and 3, it is apparent that the increased affinity for the intact βα-MT protein, relative to the sum of the separated β and α domains, was due to presence of the 20 cysteines that allow more binding mode options. This is important in the homeostatic role of MT with respect to zinc based on the model of Zn_5-MT ↔ Zn_6-MT ↔ Zn_7-MT as shown in the model of zinc homeostasis in Figure 6.2.

6.4 Metal selectivity between separated α and β domains

The studies described above assume pure zinc occupancy. However, cadmium is commonly bound to MT, especially in the liver and kidneys.[11] With seven (M^{II}) binding sites the question arises: Does the cadmium bind to specific regions of the peptide chain? In the saturated protein, as noted in Chapter 1, MT exhibits two-domains, and the question may be refined to ask: Is there thermodynamic control over the binding sites of

www.manaraa.com

cadmium in the presence of zinc for a specific domain? As a result, discussion of domain specificity has been a common theme in MT research.

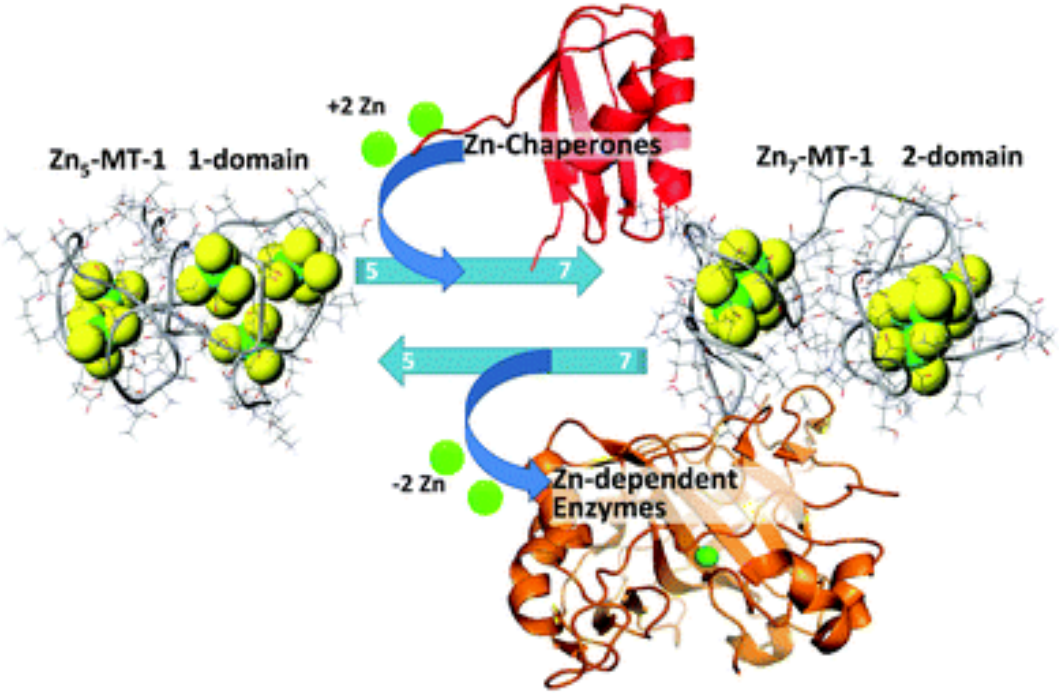

Figure 6.2: The model of homeostatic control of zinc by MT. Reproduced with permission of ref.[9] copyright (2013) American Chemical Society.

For domain specificity to be apparent, the competing metal binding affinities in specific sites must be significantly different. The metallation simulations in Chapters 1 and 2, showed that these differences should be larger than one log unit to generate a mechanism where metals distribute selectively to the higher affinity sites, as would be required for MT domain specificity. The relative zinc affinity constants reported in Chapter 3 revealed that there was some separation in the zinc affinity constants between the separated α and β-domain fragments and we questioned whether this separation was sufficiently large enough to generate a domain specific metal binding mechanism for either zinc binding to apoMTs or cadmium exchange into Zn-MTs as shown in Figure 6.3. In the intact protein, there are two models for zinc binding. Either the zinc binds randomly across both domains or zinc preferentially binds in the N-terminus region or the C-terminus region. The second model could result in domain specificity if subsequent zinc binding formed a

www.manaraa.com

clustered domain. A more complicated model involves the binding of cadmium in the presence of Zn_7-MT. Again, there are two possible models. Either cadmium distributes randomly between the sites, or the cadmium selectively binds to one of the (filled) clustered domains.

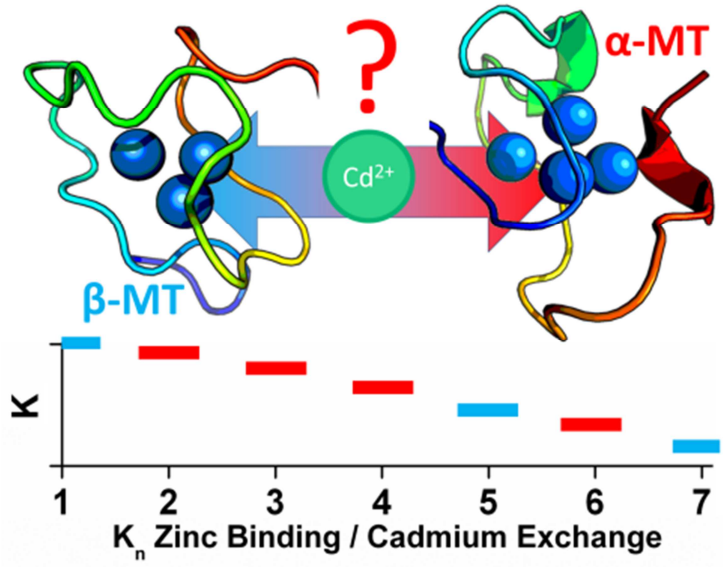

Figure 6.3: Model of cadmium exchange with Zn-MT domain fragments. The relative affinity constants of the two-domains controls the metal distributions between the two separated fragments and, therefore, within the intact protein.

The experiments described in Chapter 4 challenged the zinc domain selectivity between the apo-βMT and apo-αMT domain fragments followed by the cadmium domain selectivity between the zinc saturated Zn_3-βMT and Zn_4-αMT domain clusters. This chapter introduced the concept of competing affinity ratios between two metal binding species (e.g. K_F^1 / K_F^2) that ultimately determine where metals will bind. Modeling of the data from the ESI-MS experiments showed that there was no significant domain specificity for either cadmium binding to Zn-MTs or zinc binding to apoMTs. We also showed that selectivity for the α domain fragment was enhanced at lower pH. These results suggest that, while the apparent binding affinities are separated as shown in Chapter 3, the ratios between the competing species are not significantly different enough to generate the domain-specific mechanism of metal binding. These results

www.manaraa.com

fundamentally challenge our current understanding of zinc binding to apoMTs and cadmium exchange with Zn-MTs as these reactions have previously been suggested to occur in a completely α domain specific manner.

6.5 Kinetics of the metal exchange reactions between MTs and CA

The results discussed thus far have mostly been descriptions of the equilibrium reactions between apoMTs and apoCA in competition for added metals. Under physiological conditions, these proteins will largely be premetallated with either zinc or cadmium depending on the relative cellular loading of each of those metals. A frequently cited concern regarding cadmium toxicity is its ability to displace zinc ions from metal binding sites that require zinc for function, forming non-functional cadmium-substituted zinc binding proteins.[12]

MTs are considered to be a key component in the cellular defense mechanism against cadmium toxicity.[13] The high cadmium affinities of MTs leads to tight coordination and sequestration of any cadmium the protein encounters, preventing other potentially disruptive binding interactions from occurring.[14] MTs are also considered to be active in the rescue of cadmium-poisoned zinc binding proteins, by extracting the erroneously bound cadmium and subsequently donating one of the MT-coordinated zinc. This process of cadmium sequestration and zinc donation form the basis of MT function, *in vivo*.

In Chapter 5, we described three reactions studied kinetically that challenge the zinc donation and cadmium sequestration functions of Zn-MTs. Using kinetic ESI-MS experiments, we showed that the kinetics of zinc donation from partially metallated MTs was significantly slower than the zinc donation from zinc-saturated MTs (Zn_7-MTs). These results reinforced our model of zinc donation from Zn-MT to apo-zinc dependent enzymes, where the primary zinc donors are the high occupancy, weak affinity Zn_7- and Zn_6-MTs.

The exchange of cadmium for zinc in Cd-CA using Zn-MTs as the zinc donor was also studied kinetically. These results showed that Zn-MTs were able to restore the Cd-CA to

www.manaraa.com

the native Zn-CA. The rates of the cadmium extraction were dependent on the number of unfilled metal binding sites in MT, where more available binding sites extracted the cadmium faster. The rate of zinc donation was dependent on the total zinc loading of the MT, where higher zinc loading showed faster zinc donation kinetics.

The rates of the metal exchange reactions between MT and CA all occurred faster than would be possible if a dissociative mechanism was operative. Therefore, these results also provide support for the model whereby MT and metalloenzymes exchange metals via protein-protein interactions. These interactions are likely formed through favourable electrostatic contacts between the surface residues of the MT and CA and stabilized by the relative fluxtionality of the MT peptide chain. Metal exchange can then occur via translocation across transient metal binding residues, shuttling the metals from one binding site to the other along the affinity gradient for the metal in question.

6.6 Final Word

This work was carried out using novel applications of competition reactions for the study of metal binding affinity constants. A key feature of the experimental methodology was the extensive use of semi-quantitative data from electrospray-ionization mass spectrometry, supported by modelling of the equilibrium reactions involved. We have challenged the conventional understanding of how MT acts in its homeostatic role, particularly with respect to the zinc donation to a metalloenzyme. These results have fundamental significance in interpreting the homeostatic roles of metallothionein proteins. Of the several experiments reported, the one that illustrates the power of the techniques reported in this thesis, concern the competitive binding of zinc by ßα-MT and CA (Figures 2.2 and 2.3). The remarkable clarity of the distribution of the ten species involved in the metallation of the ßα-MT and the CA is only observable by mass spectrometry. The fact that the distribution of the species indicates the relative binding constants without the need for sophisticated analysis underlines the significance of the experimental data which directly reflect the series of linked binding constants.

www.manaraa.com

6.7 References

1. Margoshes, M., and Vallee, B. L. (1957) A cadmium protein from equine kidney cortex, *J. Am. Chem. Soc. 79*, 4813-4814.
2. Nordberg, M. (1998) Metallothioneins: historical review and state of knowledge, *Talanta 46*, 243-254.
3. Sutherland, D. E., and Stillman, M. J. (2014) Challenging conventional wisdom: single domain metallothioneins, *Metallomics 6*, 702-728.
4. Blindauer, C. A. (2015) Advances in the molecular understanding of biological zinc transport, *Chem. Commun. 51*, 4544-4563.
5. Pulido, P., Kägi, J. H., and Vallee, B. L. (1966) Isolation and Some Properties of Human Metallothionein*, *Biochemistry 5*, 1768-1777.
6. Chen, R., and Ganther, H. (1974) Relative cadmium-binding capacity of metallothionein and other cytosolic fractions in various tissues of the rat, *Environ. Physiol. Biochem. 5*, 378-388.
7. Kägi, J. H. R. (1993) Metallothionein III, (Suzuki, K. Y., Imura, N., and Kimura, M., Eds.), pp 29-35, Birkhäuser, Basel.
8. Krężel, A., and Maret, W. (2007) Dual nanomolar and picomolar Zn (II) binding properties of metallothionein, *J. Am. Chem. Soc. 129*, 10911-10921.
9. Summers, K. L., Sutherland, D. E. K., and Stillman, M. J. (2013) Single-domain metallothioneins: Evidence of the onset of clustered metal binding domains in Zn-rhMT 1a, *Biochemistry 52*, 2461-2471.
10. Pinter, T. B., and Stillman, M. J. (2014) The Zinc Balance: Competitive Zinc Metalation of Carbonic Anhydrase and Metallothionein 1A, *Biochemistry 53*, 6276-6285.
11. Dudley, R. E., Gammal, L. M., and Klaassen, C. D. (1985) Cadmium-induced hepatic and renal injury in chronically exposed rats: likely role of hepatic cadmium-metallothionein in nephrotoxicity, *Toxicol. Appl. Pharmacol. 77*, 414-426.
12. Vallee, B. L., and Ulmer, D. D. (1972) Biochemical effects of mercury, cadmium, and lead, *Annu. Rev. Biochem. 41*, 91-128.
13. Goering, P. L., and Klaassen, C. D. (1984) Tolerance to cadmium-induced hepatotoxicity following cadmium pretreatment, *Toxicol. Appl. Pharmacol. 74*, 308-313.
14. Klaassen, C. D., Liu, J., and Diwan, B. A. (2009) Metallothionein protection of cadmium toxicity, *Toxicol. Appl. Pharmacol. 238*, 215-220.

www.manaraa.com

Appendix A: Protein purification details

Table C-1: Chemical inventory

Chemical Name	Supplier
B-Isopropylthioglactoside (IPTG)	Fisher
Kanamycin A, monosulphate (>5% Kanamycin B)	Fisher
Cadmium Sulphate	Fisher
Sodium Chloride	ACP
Formic Acid	J. T. Baker
Ammonium Formate	Fisher
Ammonium Hydroxide	Fisher
Tris (hydroxymethyl) aminomethane	Caledon
Hydrochloric Acid	Caledon
18 MΩ Deionized (dI) water	Branstead
1,4-dithiothreitol (DTT)	Chemalog
L.B. (Luria Bertani). Broth, Miller (0.5% lactose)	Fisher
L.B. (Luria Bertani). Agar, Miller (0.5% lactose)	Difco
Zinc Acetate Dihydrate	Fisher
Cadmium Acetate Dihydrate	Acros Organics

The recombinant human MT1A genes were engineered in the laboratory of Dr. Peter Kille at Cardiff University, Wales. The MT genes were inserted into pET-29a plasmids that contain a kanamycin resistance marker, a transcriptase and, a Lac I repressor. Kanamycin resistance is used as a means of selection as the cells are grown on and in media that contain kanamycin. The transcriptase is required for the biosynthesis and amplification of the protein. IPTG binds to the Lac I repressor, resulting in the expression of the MT gene. This plasmid results in the addition of a short peptide called an S-tag appended onto the N-terminus of the protein, which increases protein stability during the purification process. The plasmids containing the S-tagged-MT gene, kanamycin resistance marker and *Lac I* repressor were transformed into E. coli BL21(DE3) cells.

Scheme C-1 shows the protocol used to synthesize and isolate MT. Transformed cells stored at -80^{o}C as glycerol stocks were plated onto agar containing 50 mg/L kanamycin. The cells were grown at 37^{o}C overnight. These cells were inoculated into 4 x 1 L liquid

www.manaraa.com

cultures containing 50 mg/L kanamycin and 50 μM $CdSO_4$. The liquid cultures were shaken at 37 ^oC and the absorbance of the cell culture was monitored at 600 nm until the absorbance was in the range of 0.4 to 0.6. MT expression was then induced by addition of 0.7 mL of 1M IPTG. After 30 min, an additional 150 μL of 1M $CdSO_4$ was added to metallate the expressing MT. The cells were harvested 4 h after induction by centrifugation at 6,000 rpm for 15 min at 4 °C with an Avanti J-series centrifuge (Beckman-Coulter, Canada) and JLA-9.1000 rotor. The supernatant was decanted and the cell pellet was resuspended in a solution of argon-saturated 10 mM Tris-HCl pH 7.4.

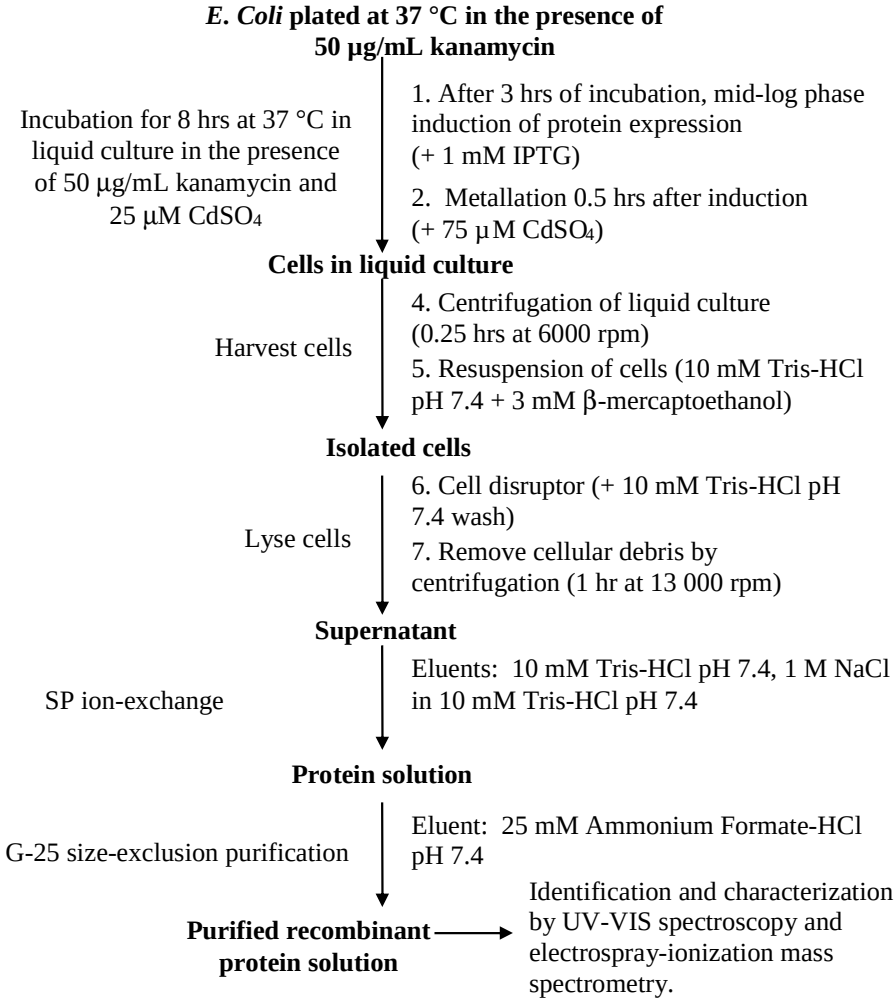

Scheme C-1: Protein preparation protocol for the synthesis of recombinant human metallothionein.

www.manaraa.com

The cell pellet was stored at -80^{o}C, thawed, and lysed using the cell disruptor (Constant Systems, UK). Cellular debris was removed by centrifugation at 13,000 rpm for 1 h at 4^{o}C with an Avanti J-series centrifuge (Beckman-Coulter, Mississauga, ON, Canada) and JLA-25.50 rotor.

A Dionex Ultimate 3000 LC pump (Thermo Scientific, Canada) was used in combination with a Hi Trap^{TM} SP Sepharose^{TM} cation exchange cartridge (Amersham Biosciences/GE Healthcare, Piscataway, NJ, USA) to purify the MT. The protein was eluted from the column using a salt (NaCl) gradient. Eluent content was monitored using UV-visible spectroscopy and the eluted fractions containing MT were collected, pooled and concentrated using a stirred ultrafiltration cell (Amicon Bioseparations/Millipore) with a YM-3 membrane, which has a molecular weight cut-off of 3000 Da. Approximately 3.5 mL deoxygenated aliquots of the protein solutions were sealed under Ar and stored at -20^{o}C.

G25 gel filtration was used to further purify the MT after the SP ion-exchange. Following SP ion-exchange, the protein solution contains large amounts of salt which must be removed in order to analyze the protein samples by mass spectroscopy. G25 was also used to demetallate the recombinant MT to generate salt-free and metal-free, apoMT. Concentrated salty Cd-MT was added to a column containing G25 media and eluted using 25 mM ammonium formate at pH 2.7 resulting in apoMT. The elution of the protein was monitored by UV-visible spectroscopy and the MT species were verified by ESI-MS.

Cadmium-bound MT was expressed as the fusion protein with a 34 residue S-tag attached to the N-terminus of the protein. Recovery of the native MT was achieved through cleavage of the S-tag with the enzyme thrombin using Thrombin CleanCleave^{TM} Kits (Sigma). Cleavage of the S-tag followed manufacturer's instructions.

Briefly, the protocol for cleaving the S-tag was as follows: the thrombin beads were suspended in a 90% (v/v) mixture of 10x cleavage buffer (500 mM Tris-HCl pH 8.0, 100 mM $CaCl_2$) and protein solution and were constantly agitated overnight at 4 ^{o}C under Ar. The beads were pelleted using centrifugation and protein was separated from the

www.manaraa.com

thrombin beads following the included instructions. The supernatant containing the MT was collected, diluted (to reduce salt concentration so the MT would stick to the SP ion exchange column) and loaded onto a Hi-trap SP cartridge. The S-tag peptide now cleaved from the MT only binds to the Hi-trap SP cation exchange column with a very weak affinity, and the S-tag elutes from the column first. Cleaved MT protein fractions were then pooled and concentrated using a stirred ultrafiltration cell (Amicon Bioseparations/Millipore) with a YM-3 membrane. 3.5 mL aliquots of the protein solutions were sealed under Ar and stored at -20^{o}C.

www.manaraa.com

Appendices

Appendix B: Supplementary figures for Chapter 2

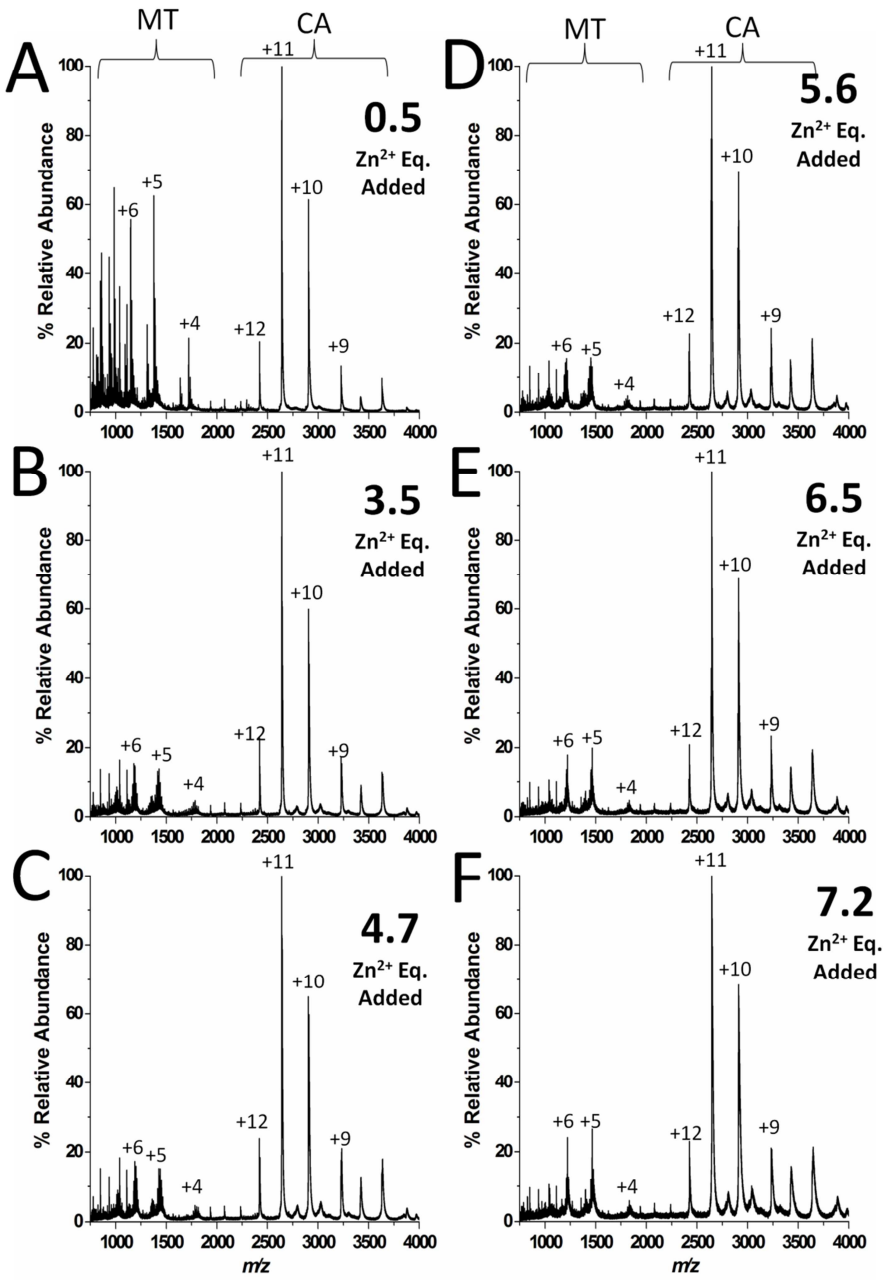

Figure A-1: Charge state ESI mass spectral data of the competitive zinc titration used to generate the deconvoluted data from Figure 2.1.

www.manaraa.com

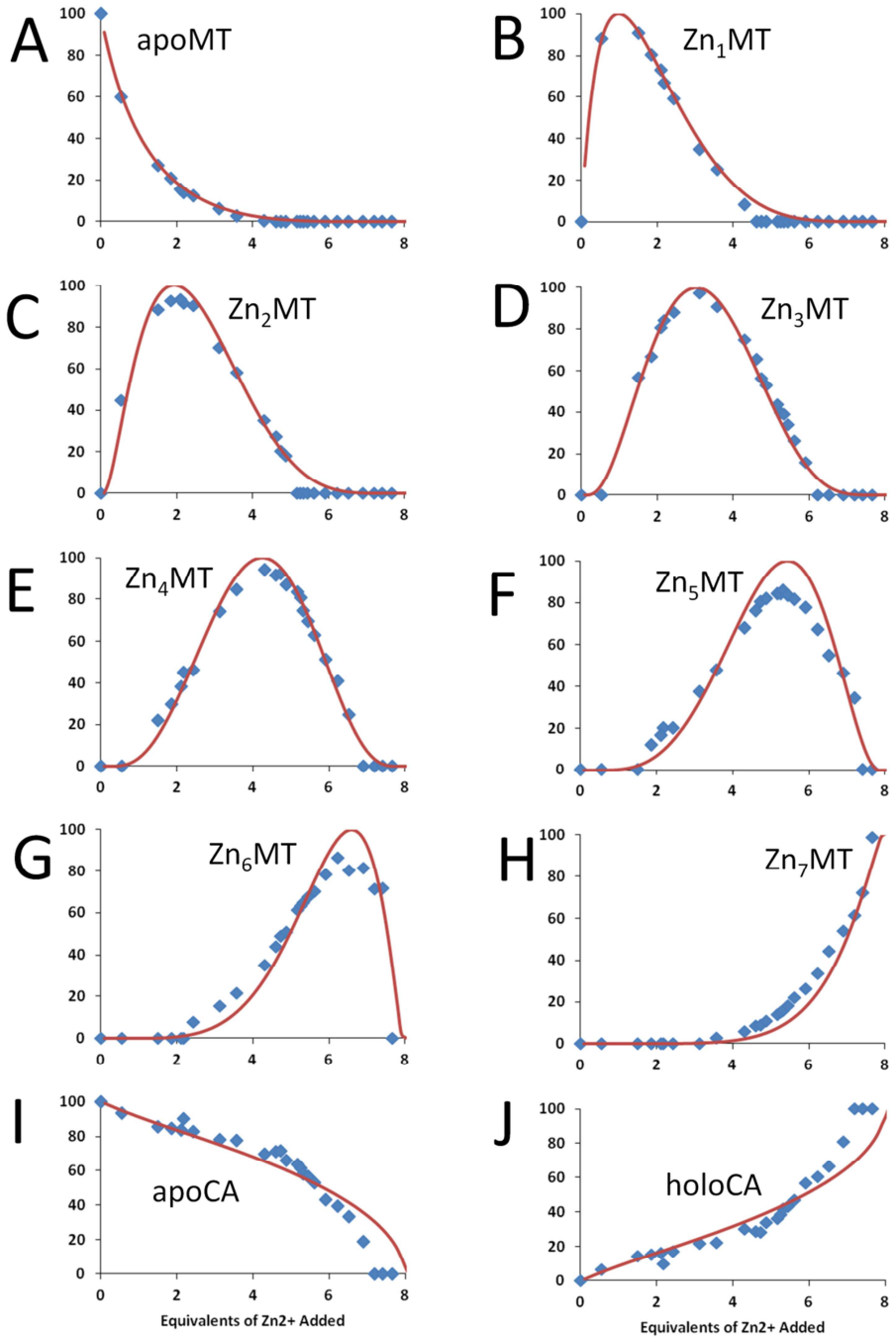

Figure A-2: Overlaid fits of experimental and modeled data sets of the competitive titration shown in Figure 2.2 and 2. 3. The experimental data sets are each shown as blue diamonds. The simulation of the best fit modelled Ks shown in Figure 2.4.

www.manaraa.com

Appendix C: Supplementary figures for Chapter 3

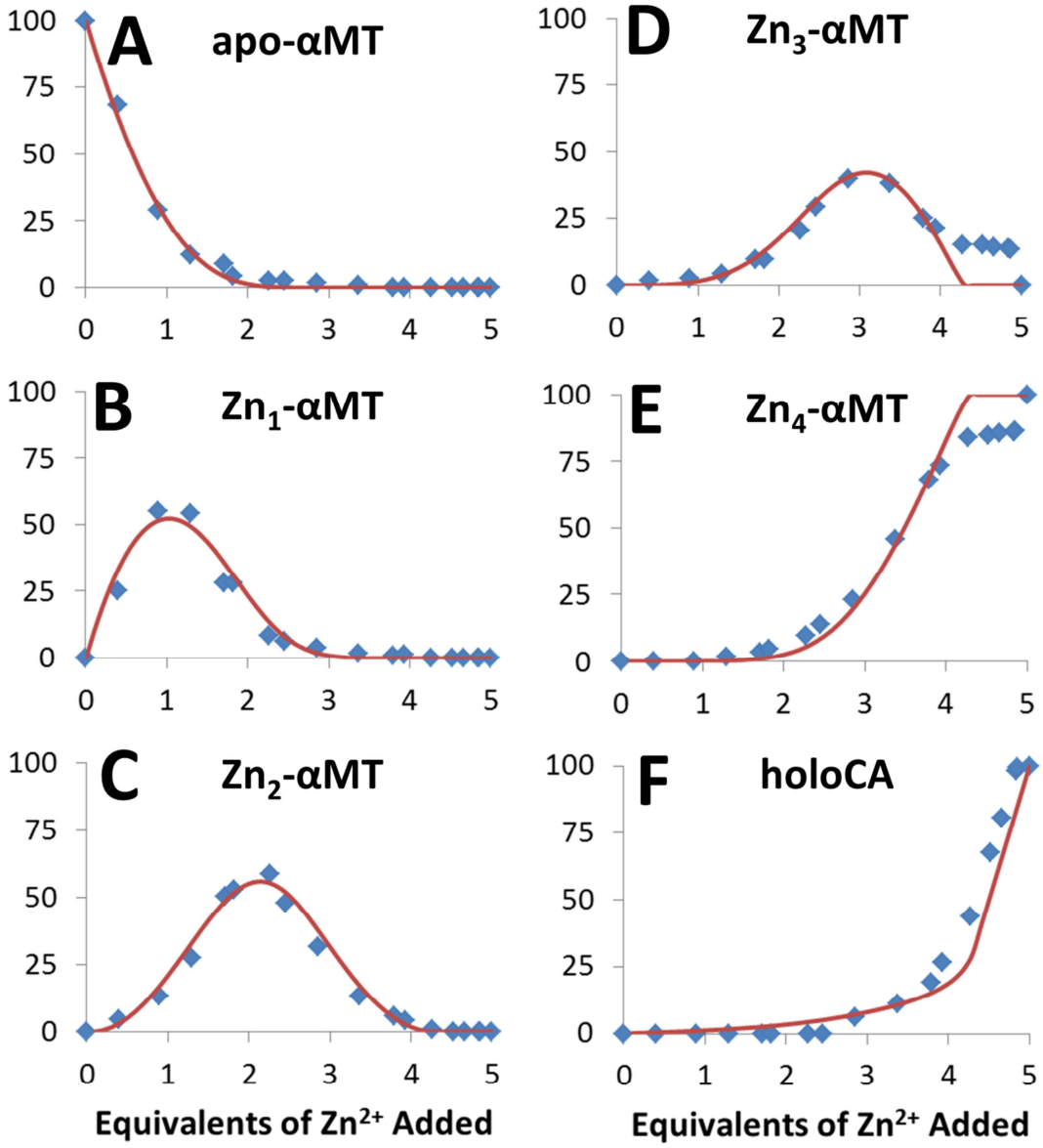

Figure B-1: Overlaid fits of experimental and modeled data sets of the competitive titration of apo-αMT and apoCA shown in Figure 3.1 and 3.2. The experimental data sets are shown as blue diamonds. The lines are the simulation of the data based on the calculated zinc binding affinities of the αMT fragment in competition with the CA shown in Figure 3.3 and Scheme 3.1.

www.manaraa.com

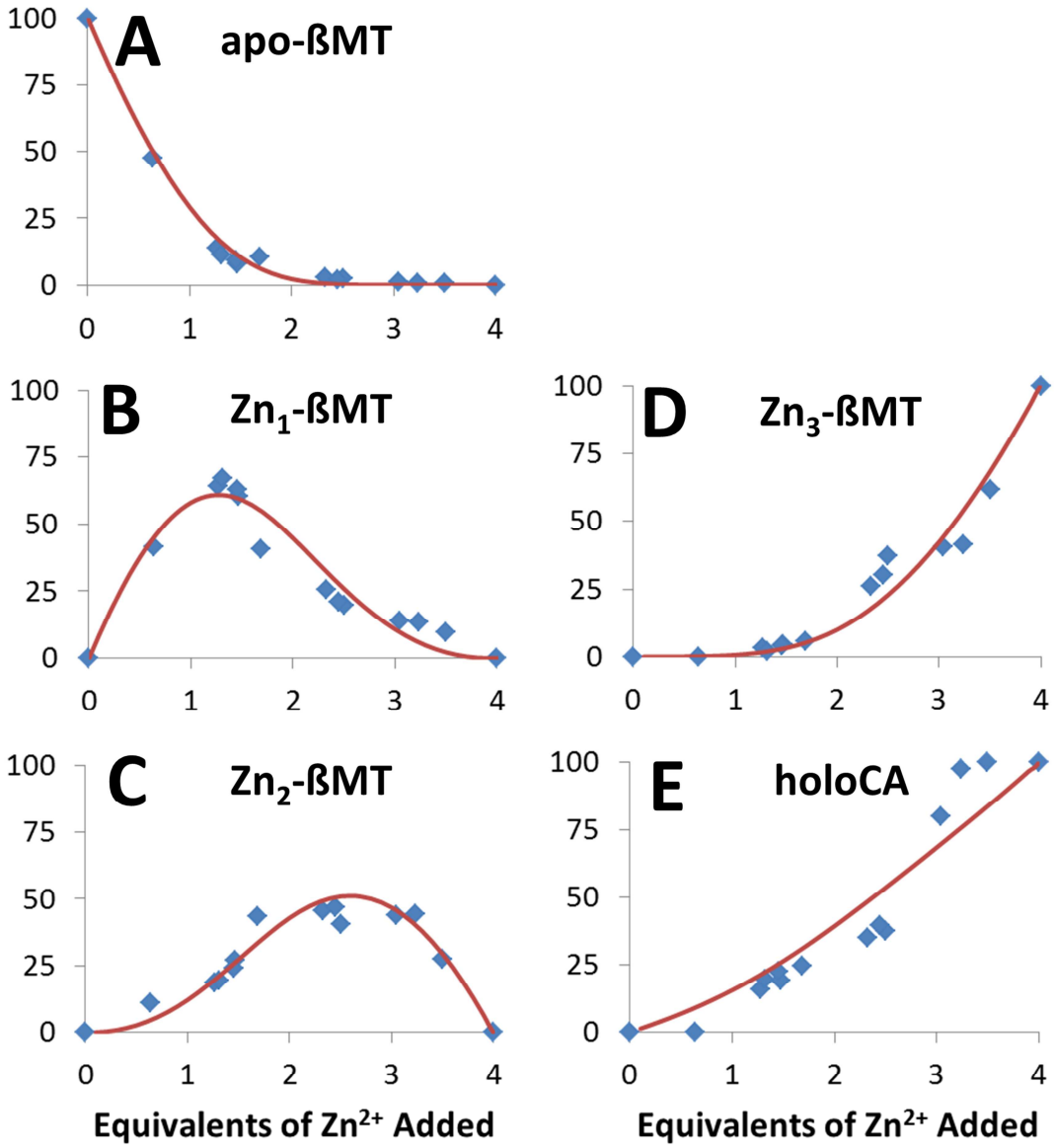

Figure B-2: Overlaid fits of experimental and modeled data sets of the competitive titration of apo-βMT and apoCA shown in Figure 3.4 and 3.5. The experimental data sets are shown as blue diamonds. The lines are the simulation of the data based on the calculated zinc binding affinities of the βMT fragment in competition with the CA shown in Figure 3.6 and Scheme 3.2.

www.manaraa.com

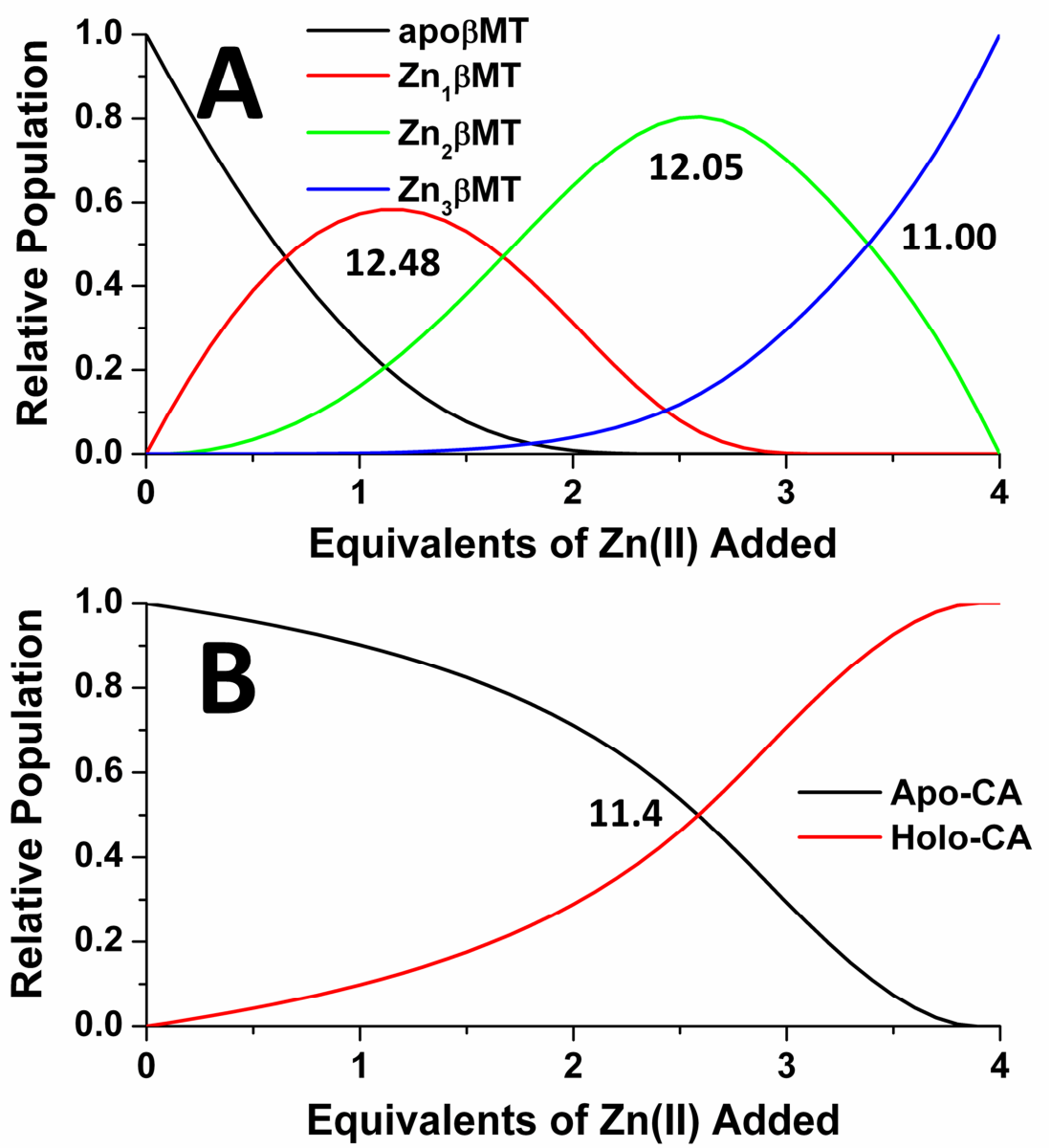

Figure B-3: Alternative modeled simulation of the competitive zinc metallation of apo-βMT (A) in the presence of apoCA (B). This simulation uses $\log_{10}K_F$ of 12.48, 12.05, and 11.00 for the βMT affinity constants. These affinities were determined by minimization of the RMSD between the simulated data and the experimental data with the relative affinities anchored to the known affinity of CA (11.4).

www.manaraa.com

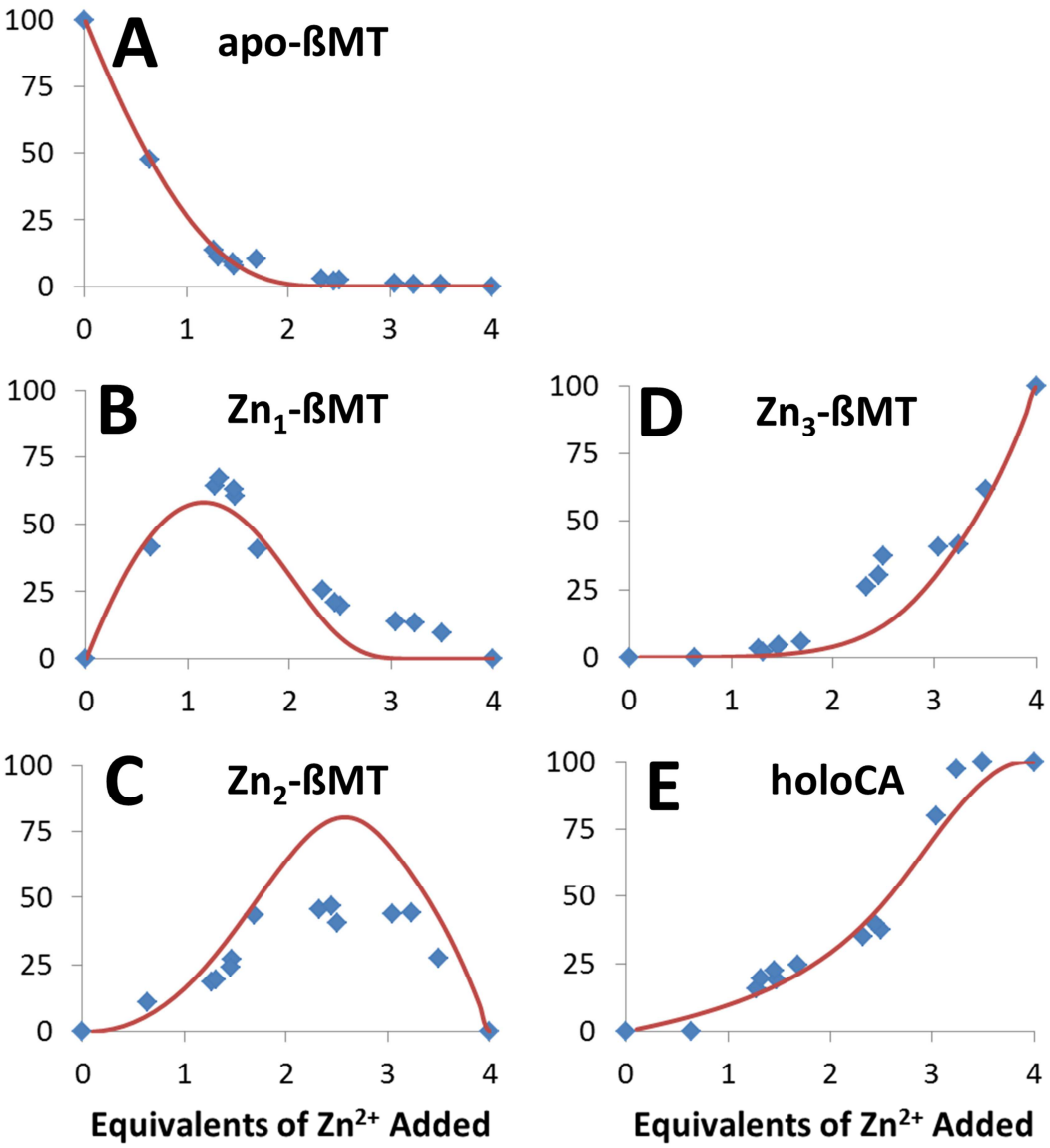

Figure B-4: Overlaid fits of experimental and the alternatively modeled data sets of the competitive titration of apo-βMT and apoCA shown in Figure 3.1 and 3.2. The experimental data sets are shown as blue diamonds. The lines are the simulation of the data based on the calculated zinc binding affinities of the βMT fragment in competition with the CA shown in Figure B-3 and Scheme 3.2.

www.manaraa.com

Appendix D: Permissions

Title:	The Zinc Balance: Competitive Zinc Metalation of Carbonic Anhydrase and Metallothionein 1A
Author:	Tyler B. J. Pinter, Martin J. Stillman
Publication:	Biochemistry
Publisher:	American Chemical Society
Date:	Oct 1, 2014

Copyright © 2014, American Chemical Society

PERMISSION/LICENSE IS GRANTED FOR YOUR ORDER AT NO CHARGE

This type of permission/license, instead of the standard Terms & Conditions, is sent to you because no fee is being charged for your order. Please note the following:

- Permission is granted for your request in both print and electronic formats, and translations.
- If figures and/or tables were requested, they may be adapted or used in part.
- Please print this page for your records and send a copy of it to your publisher/graduate school.
- Appropriate credit for the requested material should be given as follows: "Reprinted (adapted) with permission from (COMPLETE REFERENCE CITATION). Copyright (YEAR) American Chemical Society." Insert appropriate information in place of the capitalized words.
- One-time permission is granted only for the use specified in your request. No additional uses are granted (such as derivative works or other editions). For any other uses, please submit a new request.

Figure D-1: ACS Copyright Permission for Chapter 2.

www.manaraa.com

Title:	Domain selection in metallothionein 1A: Affinity controlled mechanisms of zinc binding and cadmium exchange
Author:	Tyler B. J. Pinter, Gordon W Irvine, Martin J. Stillman
Publication:	Biochemistry
Publisher:	American Chemical Society
Date:	Jul 1, 2015

Copyright © 2015, American Chemical Society

PERMISSION/LICENSE IS GRANTED FOR YOUR ORDER AT NO CHARGE

This type of permission/license, instead of the standard Terms & Conditions, is sent to you because no fee is being charged for your order. Please note the following:

- Permission is granted for your request in both print and electronic formats, and translations.
- If figures and/or tables were requested, they may be adapted or used in part.
- Please print this page for your records and send a copy of it to your publisher/graduate school.
- Appropriate credit for the requested material should be given as follows: "Reprinted (adapted) with permission from (COMPLETE REFERENCE CITATION). Copyright (YEAR) American Chemical Society." Insert appropriate information in place of the capitalized words.
- One-time permission is granted only for the use specified in your request. No additional uses are granted (such as derivative works or other editions). For any other uses, please submit a new request.

Figure D-2: ACS Copyright permission for Chapter 4.

www.manaraa.com

Curriculum Vitae

Name: Tyler B.J. Pinter

Post-secondary Education and Degrees:

University of Western Ontario
London, Ontario, Canada
2006-2010 B.Sc.
Honors Specialization in Biochemistry and Chemistry

The University of Western Ontario
London, Ontario, Canada
2010-2015 Ph.D.
Bioinorganic Chemistry

Peer-Reviewed Publications:

1. **Pinter, T.B.J.** and Stillman, M.J. (**2015**) Modelling reactions between metallothionein and carbonic anhydrase: A review. In preparation.

2. **Pinter, T.B.J.** and Stillman, M.J. (**2015**) Kinetics of metal transfers between metallothionein and carbonic anhydrase. Submitted.

3. Irvine, G.W., **Pinter, T.B.J.**, and Stillman, M.J. (**2015**) Redefining the metal binding pathways of human metallothionein 1a: Balancing zinc availability and cadmium seclusion. *Metallomics.,* Submitted.

4. **Pinter, T.B.J.** and Stillman, M.J. (**2015**) It takes two to tangle: Properties of intact MT1A derived from interaction of its isolated domains with carbonic anhydrase. *Biochem. J.,* in press, DOI: 10.1042/BJ20150676.

5. **Pinter, T.B.J.**, Irvine, G.W., and Stillman, M.J. (**2015**) Domain selection in metallothionein 1A: Affinity controlled mechanisms of zinc binding and cadmium exchange. *Biochemistry,* 54: 5006-5016.

6. **Pinter, T.B.J.** and M.J. Stillman (**2014**) The Zinc Balance: Competitive zinc metallation of carbonic anhydrase and metallothionein 1A. *Biochemistry.*, 53: 6276–6285.

7. Bohle, D.S., Dodd, E.L., **Pinter, T.B.J.**, and Stillman, M.J. (**2012**) Soluble diamagnetic model for malaria pigment: Coordination chemistry of Gallium(III)protoporphyrin-IX. *Inorg. Chem.*, 51: 10747–10761.

www.manaraa.com

8. Tiedemann, M.T., **Pinter T.B.J.**, and Stillman, M.J. (**2012**) Insight into blocking heme transfer by exploiting molecular interactions in the core Isd heme transporters IsdA-NEAT, IsdC-NEAT, and IsdE of *Staphylococcus aureus*. *Metallomics*, 4: 751 – 760.

9. **Pinter, T.B.J.**, Dodd, E.L., Bohle, D.S., and Stillman, M.J. (**2012**) Spectroscopic and theoretical studies of Ga(III)protoporphyrin-IX and its reactions with myoglobin. *Inorg. Chem.*, 51:3743–3753.

10. Ngu, T.T., Lee, J.A., **Pinter, T.B.J.**, and Stillman, M.J. (**2010**) Arsenic-metallation of triple domain human metallothioneins: Support for the evolutionary advantage and interdomain metallation of multiple-metal-binding domains. *J. Inorg. Biochem.*, 104: 232–244.

Conference Presentations:

1. Irvine, G.W., **Pinter, T.B.J.** and Stillman, M.J. (July 20–24, **2015**) Redefining the metal binding pathways of human metallothionein 1a: Balancing zinc availability and cadmium seclusion. 17th International Conference on Bioinorganic Chemistry. Beijing, China. Poster presentation by Irvine, G.W.

2. **Pinter, T.B.J.** and Stillman, M.J. (May 19–22, **2015**) Dissecting domain specificity through modeling of domain-domain interactions in metallothionein 1A. 5th Georgian Bay International Conference on Bioinorganic Chemistry. Parry Sound, ON, Canada. Oral presentation by **Pinter, T.B.J.**

3. Laakso, H.A., Marolda, C., **Pinter, T.B.J.**, Stillman, M.J., and Heinrichs, D.E. (April 1, **2015**) SbnI is a novel transcriptional regulator in *Staphylococcus aureus*. 4th London Health Research Day Conference. London, ON, Canada. Poster presentation by Laakso, H.A.

4. **Pinter, T.B.J.**, Jeen, T.Y., and Stillman, M.J. (January 31–February 2, **2015**) Challenging domain specificity in metallothionein. 19th Bioinorganic Chemistry Gordon Research Seminar. Ventura, CA, USA. Oral presentation by **Pinter, T.B.J.**

5. **Pinter, T.B.J.** and Stillman, M.J. (January 25–30, **2015**) The zinc balance: Competitive zinc metallation of carbonic anhydrase and metallothionein 1A. 53rd Metals in Biology Gordon Research Conference. Ventura, California, USA. Poster presentation by **Pinter, T.B.J.**

6. Jeen, T.Y., **Pinter, T.B.J.**, and Stillman, M.J. (August 21–22, **2014**) Challenging domain specificity: Bioinorganic metal distribution in the two-domains of metallothionein. 2014 Inorganic Chemistry Exchange Conference. St. John's, NB, Canada. Oral presentation by Jeen, T.

www.manaraa.com

7. **Pinter, T.B.J.** and Stillman, M.J. (June 1–5, **2014**) The competitive zinc metallation of metallothionein in the presence of carbonic anhydrase. 97th Canadian Chemistry Conference and Exposition. Vancouver, BC, Canada. Oral presentation by **Pinter, T.B.J.**

8. **Pinter, T.B.J.** and Stillman, M.J. (May 19–21, **2014**) Determining the zinc binding constants of metallothionein in the presence of carbonic anhydrase. 31st Chemistry Graduate Student Symposium. Buffalo, NY, USA. Oral presentation by **Pinter, T.B.J.**

9. Jeen, T.Y., **Pinter, T.B.J.,** and Stillman, M.J. (May 19–21, **2014**) Exploring the metal thiolate cluster formation of metallothionein. 31st Chemistry Graduate Student Symposium. Buffalo, NY, USA. Poster presentation by Jeen, T.Y..

10. **Pinter, T.B.J.** and Stillman, M.J. (July 22–26, **2013**) Implications of metallothionein in apoenzyme metallation. 16th International Conference on Bioinorganic Chemistry. Grenoble, France. Poster presentation by **Pinter, T.B.J.**

11. **Pinter, T.B.J.** and Stillman, M.J. (May 22–24, **2013**) Implications of metallothionein in carbonic anhydrase metallation. 4th Georgian Bay International Conference on Bioinorganic Chemistry. Parry Sound, ON, Canada. Oral presentation by **Pinter, T.B.J.**

12. **Pinter, T.B.J.** and Stillman, M.J. (January 27–29, **2012**) Exploring metal transfer between metallothioneins and metalloenzymes. 16th Bioinorganic Chemistry Gordon Research Seminar. Ventura, CA, USA. Poster presentation by **Pinter, T.B.J.**

13. **Pinter, T.B.J.** and Stillman, M.J. (January 22–27, **2012**) Exploring metal transfer between metallothioneins and metalloenzymes. 50th Metals in Biology Gordon Research Conference. Ventura, CA, USA. Poster presentation by **Pinter, T.B.J.**

14. **Pinter, T.B.J.**, Dodd, E.L., Bohle, D.S., and Stillman, M.J. (June 2, **2011**) Spectroscopic and theoretical studies of GaPPIX binding to myoglobin. 3rd Georgian Bay International Conference on Bioinorganic Chemistry. Parry Sound, ON, Canada. Poster presentation by **Pinter, T.B.J.**

15. Tiedemann, M.T., **Pinter, T.B.J.**, Heinrichs, D.E., and Stillman, M.J. (July 4–9, **2010**) Mechanistic studies of the Iron Regulated Surface Determinant (Isd) heme transfer pathway in *Staphylococcus aureus.* 6th International Conference on Porphyrins and Phthalocyanines. Bernalillo, NM, USA. Poster presentation by Tiedemann, M.T.

16. **Pinter, T.B.J.**, Tiedemann, M.T., and Stillman, M.J. (March 20, **2010**) The role of the porphyrin ring in the Iron Regulated Surface Determinant heme transfer pathway in *Staphylococcus aureus.* . London, ON, Canada. Oral presentation by **Pinter, T.B.J.**

www.manaraa.com

17. **Pinter, T.B.J.**, Lee, J.A., Ngu, T.T., and Stillman, M.J. (May 26–29, **2009**) Domain dependence of the arsenic metallation of metallothionein. 2nd Georgian Bay International Conference on Bioinorganic Chemistry. Parry Sound, ON, Canada. Poster presentation by **Pinter, T.B.J.**

Grants and Awards:

Western Chemistry CSC Travel Award The University of Western Ontario	2014
NSERC PGS-D Scholarship The University of Western Ontario	2013–2015
ICBIC-16 Poster Prize International Conference on Bioinorganic Chemistry	2013
Western Graduate Thesis Research Award The University of Western Ontario	2013
Western Graduate Research Scholarship The University of Western Ontario	2012
Ontario Graduate Scholarship The University of Western Ontario	2011
Dr. Joseph Soltys Graduate Award in Chemistry The University of Western Ontario	2011
Gold Medalist: Honors Specialization in Chemistry and Biochemistry The University of Western Ontario	2010
NSERC-USRA Recipient The University of Western Ontario	2008
Queen Elizabeth II – Aiming for the Top Scholarship The University of Western Ontario	2006–2010
Western Scholarship of Distinction Entrance Award The University of Western Ontario	2006

Research Experience:

The University of Western Ontario Graduate Researcher; Supervisor: Martin J. Stillman	London, ON 2010 – Present

www.manaraa.com

Mechanism of metalloenzyme metallation by metallothionein

The University of Western Ontario — London, ON
4490 Thesis Researcher; Supervisor: Martin J. Stillman — 2010
Mechanistic studies of the Iron Regulated Surface Determinant (Isd) heme transfer pathway in *Staphylococcus aureus*

The University of Western Ontario — London, ON
Undergraduate Research Assistant; Supervisor: Martin J. Stillman — 2008–2010
The evolutionary advantage of multi-domain metallothionein

Related Professional Experience:

Bioinorganic Chemistry (Chem2211) – Poster Day — The University of Western Ontario
Volunteer Poster Judge — London, ON
2009 –Present

Society of Graduate Students (SOGS) — The University of Western Ontario
Chemistry Councillor — London, ON
2014–Present

Chemistry Outreach Volunteer — The University of Western Ontario
Laboratory Demonstrator — London, ON
2012–Present

Georgian Bay International Conference on Bioinorganic Chemistry (CANBIC-3/4/5)
Programme Editor, Scheduling — Parry Sound, ON
2011 / 2013 / 2015

2nd Georgian Bay International Conference on Bioinorganic Chemistry (CANBIC-2)
Technical Support Lead — Parry Sound, ON

www.manaraa.com